Numerical modelling and validation of Hydrothermal liquefaction of Lignin.

Rukshan Madhawa Jayathilake

Numerical modelling and validation of Hydrothermal liquefaction of Lignin.

Shrinking core approach on particle decomposition and a comparative analysis of biocrude and HTL char

Doctoral Dissertation for the degree *Philosophiae Doctor* (PhD) at
the Faculty of Engineering and Science, Specialization in Renewable Energy

University of Agder
Faculty of Engineering and Science
2021

Doctoral dissertations at the University of Agder 362
ISSN: 1504-9272
ISBN: 978-82-8427-071-5

Print: 07 Media
Kristiansand

Dedication

To,
Loving mom and dad

Preface

The foundation for this research was initially triggered by my passion for investigation and development sustainable energy sources to counter the CO_2 emissions. As the world moves further into the industrial age and beyond, energy demand is growing, and with that, the need to reduce carbon emissions will rise. As the sole reason for the problem, the human being is responsible for developing better solutions to mitigate the carbon emissions. Biofuels will not solve the whole problem. Nevertheless, this is how I can do my part to help solve the problem.

Acknowledgments

A Ph.D. is primarily based on the contributions of a single person. Nonetheless, numerous people, directly and indirectly, contribute to improving the product's value. This treasured contribution is expressed in several ways, most of the time not evident but so crucial during the research. I would like to acknowledge whomever, for a reason or another, supported during this process. The following list might look extended, but it is certainly not comprehensive. Please apologize for that. I would have loved to thank you all!

First, thank you to Souman Rudra and Lasse Rosendahl for guiding me along with my project, providing good answers and guidance whenever I asked for your help. You have been severe as well as collaborative supervisors. Work aside, thank you, Souman, for all our discussions about cricket, life, and families. They have always been exciting and relaxing. Further, thank you for being a mentor, motivator, and even a good friend. The help and flexibility I were offered were incredible, and I was fortunate to have a supervisor like you.

Thank you, Saqib Sohail Toor, for your continued help and ideas during the initial phase of our reactor system development. Thank you for offering support whenever we asked for help. I express my gratitude to Lorenzo Riva for being patient enough to share the lab with me, and having those friendly discussions helped mold my research along the way. Thank you very much, Alfred Christy, Naureen Akhtar, and Giulia Ravenni. The contribution and experience you brought into this research work upgraded the quality of my work. Thank you very much, Odin Kvam, for your continued helps. Thank you very much, Henrik K. Nielsen, for lending me the combustion lab to make all the mess in the world. Thank you very much, James Godwin, for your contributions along the path. The assistance I received from Johan Olav, Nils R. Kristiansen, and Steve Shading was immense, and without your support, this could have been a much more demanding task.

In general, I acknowledge the assistance of Harald Sveier of Lerøy ocean harvest for lending seaweed and Gudbrand Rødsrud of Borregaard for lending the lignosulphonate. Thank you, Emma Horneman, for all the bits of help and

guidance throughout and especially when it mattered to take leave to take care of my family.

I cannot forget Basant, Saba, Werner, and Oscar. You have been incredible office mates possibly one can have. I have simply enjoyed every single chat we had. Thank you to all the remarkable friends/colleagues with whom I was fortunate enough to meet and share experiences and ideas. Darshana, Antoine, Salem, Arvind, Milad, Sissel, Sinziana, Themis, Bilal, and Dimitris. All the discussions and the Friday evening gatherings were more important than you think. Further, I would like to thank the Sri Lankan Community in Grimstad. Thank you very much, Sherami Vennerød and family, Gunhild, Mr. Pandey, and Hisøy cricket team. The impact you had was more than you imagined. Further, I would like to mention every nice person I shared my time in UiA. You may be a bit too many to mention. Nevertheless, you have supported me more than you may think.

My deepest gratitude goes to my mom, dad, brother, and sister. Having idols and role models at home is not a luxury every person experience in their lives. Thank you for everything. Moreover, thank you Kalpanie, and Lyanna, for being unbelievably patient, supportive and giving me the time throughout this journey for helping me with your loving engagement in contributing to a sustainable future.

Sammendrag

Basert på den teoretiske forståelsen av både fysiske og kjemiske mekanismer, tas det opp behovet for å utvikle en grundig matematisk modell for flytendegjøring av lignin. Dermed produseres en modell for flytendegjøring ved subkritiske temperaturer ved å bruke en 'krympende kjerne'-metode som partikkelnedbrytningsmekanisme. Konseptet med en krympende kjerne gir en relativt mindre kompleks, men likevel effektiv måte å modellere flytendegjøring på partikkelnivå.

Som første trinn brukes en mer grunnleggende versjon av modellen for å beskrive flytendegjøringen av en trepartikkel, der treflyten regnes som den kumulative flytende effekten av tremodellforbindelsene (cellulose, hemicellulose og lignin). Grunnmodellen ledet studien mot mer tiltalende modifikasjoner og forbedringer som oljeaktig film og askelagsdannelse under flytendegjøringen. Lærdommen fra den grunnleggende versjonen av modellen informerte nullhypotesen om likhet mellom kumulativ flytende effekt av modellforbindelser til flytende trevirke under de samme driftsforholdene. Modellens begrensninger førte forskningen omkring utviklingen av modellen til neste nivå.

Den foreslåtte modellen er basert på eksperimentell validering av resultatene fra en serie batch-eksperimenter. Modellen består av flytendegjøring av ligninpartikler, oljeaktig film, uorganisk (aske) lagdannelse, kinetisk modellering av sekundære derivater, og lagmodellen for intrapartikkelprosessmodellering. Det krympende kjernekonseptet brukes til å modellere hydrolysen av ligninpartikkelen. Dannelsen av oljeaktig film og et uorganisk lag rundt ligninpartikkelen og deres oppførsel er modellert med tanke på vanntransport gjennom lag, diffusjon av produkter og oppløsning av produkter i vann. Dessuten måles partikkelens overflate- og senterpunkttemperaturer ved hjelp av en lagmodell gjennom masseoverføring. Modellen viste seg å være både rask og robust. Flere relevante tilfeller med ulike driftsforhold ble testet på den anvendte model-

len for å se hvordan den fungerte. Noen svakheter ble funnet. Disse var relatert til varmeoverføring, innledende kinetiske data og andre kinetiske parametere som hastighetskonstanter. Det er fortsatt noe rom for å forbedre og for å kunne adressere industrielt relevant. Den foreslåtte modellen kan likevel støtte videre arbeid og vurderinger i emnet.

Videre er utviklingen av biokull fremstilling og oppførsel også studert i denne studien. Biokull er testet kjemisk, termisk og morfologisk for å forstå dens egenskaper. Til slutt foreslås en mulig formasjonsvei for HTL-biokull under undersøkelsen. Både høyere driftstemperaturer og lengre oppholdstid økte nitrogeninnholdet i røyene. I følge FTIR-analyse ble biokull mer aromatisk, og alifatiske grupper som finnes i biokull reduseres drastisk når temperaturen øker. Oppholdstiden påvirket ikke like mye som temperaturen når man vurderer eliminering av funksjonell gruppe. En økning i driftstemperaturer og oppholdstider ga termisk stabile forkullinger. HTL-kull ble laget ved laveste driftstemperatur og viste høyeste overflateareal og porevolum. Mer polyaromatisk kull produseres når temperatur og oppholdstid øker på grunn av karbonisering.

Så i neste fase blir den synergistiske effekten av ko-flytendegjøring av lignin med *Saccharina latissima* utforsket for å se muligheten for at lignin kan brukes som et råmateriale for ko-likvefisering. De krevende prosessforholdene med mer *Saccharina latissima* viste en positiv synergistisk effekt på bioråutbyttet men en negativ synergistisk effekt på kullproduksjon. Videre påvirket temperaturen og blandingsforholdet både utbytte av bioråolje og den kjemiske sammensetningen til bioråolje. Interessant nok viste oppholdstiden en klar innvirkning på den kjemiske sammensetningen av bioråolje, selv om det var en ubetydelig påvirkning på bioråoljeutbyttet. Temperaturvariasjonen hjalp for det meste til produksjon av alkohol og fenolforbindelser der C-O-bindingene forbrukes med økt oppholdstid. Ikke desto mindre vil samflytning av råmaterialene bidra til å forbedre bioråoljeblandingen ved å produsere flere fenoliske forbindelser, langkjedede alifatiske hydrokarboner, karboksylsyrer og ketonaldehyder og estere.

Abstract / sammendrag

Based on the theoretical understanding of both physical and chemical mechanisms, the need to develop a comprehensive mathematical model for the liquefaction of lignin is raised. Thus, a model for liquefaction at subcritical temperatures is produced using a shrinking core method as the particle decomposition mechanism. The shrinking core concept provides a relatively less complex, nonetheless effective way to model liquefaction at the particle level.

Therefore, as the first step, a more basic version of the model is used to model the liquefaction of a wood particle where the wood liquefaction is considered the cumulative liquefaction effect of the wood model compounds (cellulose, hemicellulose, and lignin). The basic model guided the study towards more appealing modifications and improvements such as the oily film and ash layer formation during the liquefaction process. The main takeaway from the basic version of the model was the null hypothesis of the equality of cumulative liquefaction effect of model compounds to the wood liquefaction in the same operating conditions. The model's shortcomings lead the research towards the development of the model to the next level.

Then the proposed model is based on the experimental validation of the results of a series of batch experiments. The model consists of liquefaction of lignin particle, oily film, inorganic (ash) layer formation, kinetic modeling of secondary derivatives, and the layer model for the intraparticle processes modeling. The shrinking core concept is used to model the hydrolysis of the lignin particle. The formation of oily film and an inorganic layer around the lignin particle and their behavior is modeled considering water transport through layers, diffusion of products, and dissolution of products in water. Moreover, the particle's surface and center point temperatures are measured using a layer model through mass transfer. The model proved to be both quick and robust. Several relevant cases with different operating conditions were tested on the applied model to see how it worked. Some weaknesses were found. These were related to heat transfer, initial kinetic data, and other kinetic parameters such as rate constants. There still exists some space to improve and to be able to address industrially relevant. Nonetheless, the proposed model can support further work and decisions on the matter.

Further, the evolution of char production and behavior is also studied in this study. The char is tested chemically, thermally, and morphologically to under-

stand its characteristics. Finally, a possible formation pathway for HTL char is proposed during the investigation. Both higher operating temperatures and longer residence times increased the nitrogen content of the chars. According to FTIR analysis, char became more aromatic, and aliphatic groups present in char are diminished drastically when the temperature increases. Residence time did not influence as much as the temperature when considering the functional group elimination. An increase in operating temperatures and residence times produced thermally stable chars. HTL char was made at the lowest operating temperature and showed the highest surface area and pore volume. More polyaromatic char is produced when temperature and residence time increase due to carbonization.

Then at the next phase, the synergistic effect of co-liquefaction of lignin with laminaria saccharina is explored to see the possibility of lignin being used as a co-liquefaction feedstock. The severe process conditions with more laminaria saccharina showed a positive synergistic effect on the biocrude yield while a negative synergistic effect on char production. Further, the temperature and blending ratio impacted both biocrude yields and the chemical composition of biocrude. Interestingly, residence time showed a clear impact on the chemical composition of the biocrude, although there was a negligible impact on the biocrude yield. The temperature variation mostly helped alcohol and phenolic compounds production where the C-O bonds are consumed with increased residence time. Nevertheless, co-liquefaction of the feedstocks would help improve the biocrude composition by producing more phenolic compounds, long-chain aliphatic hydrocarbons, carboxylic acids, and ketones aldehydes, and esters.

List of publications

A. Jayathilake M, Rudra S, Rosendahl LA. Hydrothermal liquefaction of wood using a modified multistage shrinking-core model. Fuel.2020;280:118616.https://doi.org/10.1016/j.fuel.2020.118616

B. Jayathilake M, Rudra S, Rosendahl LA. Numerical modeling and validation of hydrothermal liquefaction of a lignin particle for biocrude production. Fuel, 2021;305:121498. https://doi.org/10.1016/j.fuel.2021.121498.

C. Madhawa Jayathilake, Souman Rudra, Naureen Akhtar, Alfred A. Christy, Characterization and evaluation of char from hydrothermal liquefaction of alkali lignin in subcritical temperatures. Materials 2021, 14(11), 3024; https://doi.org/10.3390/ma14113024.

D. Jayathilake KGRM, Rudra S, Christy AA. Effect of co-liquefaction of lignin and laminaria saccharina on optimization of bio-oil yield. Energy Convers Manag X 2022;13:100151. https://doi.org/10.1016/j.ecmx.2021.100151.

List of supplementary publications

A. Rudra S, Jayathilake M. Hydrothermal Liquefaction of Biomass for Biofuel Production. Ref. Module Earth Syst. Environ. Sci., Elsevier; 2021. https://doi.org/10.1016/B978-0-12-819727-1.00043-1.

B. Jayathilake, Rukshan; Rudra, Souman (2020). Char Phase Behavior of Hydrothermal Conversion of Alkali Lignin in Subcritical Temperatures, European Biomass Conference 2020, Marseille, France.

C. Jayathilake, Madhawa; Rudra, Souman (2019). Hydrothermal Liquefaction modeling of lignin Using A Modified Multistage Shrinking-Core Model. Building a sustainable European biofuel industry. Gothenburg, Sweden.

Contents

List of figures

List of tables

1 Introduction

The rapid increase of environmental pollution, global warming, and the depletion of the available fossil fuels, as well as the increasing energy demand, have urged the modern world to move on to sustainable and renewable energy sources [1,2]. Despite these developments, diesel has been the preferred fuel in the transportation and aviation industry. Due to the high energy content, ease of use, availability, and performance [3]. With this background replacing Petro-diesel with a more environmentally friendly and sustainable option has become a current issue. For example, the projected aviation emissions will be 70% higher than in 2040 than in 2005 [4]. Therefore, addressing this issue is an important aspect. In doing that, liquid fuels derived from biomass have recently been increasingly used in global transportation. Replicating that, the contribution of biofuel to the global transportation fuel mix has grown to 2% by 2008 [5]. The following figure shows the global renewable aviation fuel market size by product[6].

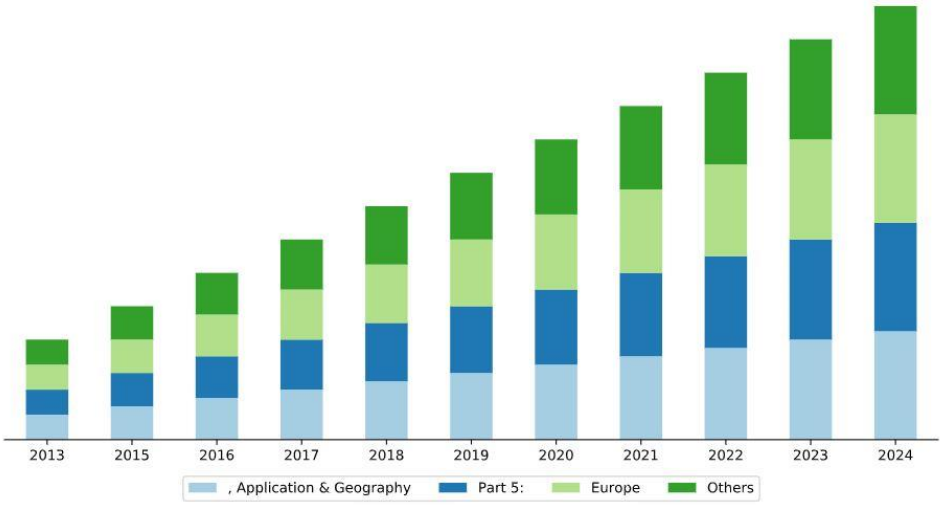

Figure 1-1: Global renewable aviation fuel market size by product[6]

Moreover, feedstock availability, conversion technology, and biofuel range are the real challenge to meet the desired goal. More importantly, after numerous test flights, various airlines have concluded that alternate biofuels can be mixed with existing jet fuel, and different fuel blends could give different out-

comes. Beyond the test levels, several leading European airlines have started using the mix of jet fuel-biofuel in the commercial routes to date [7].

In hydrothermal liquefaction (HTL), most of the available biomass can be used as feedstocks. The literature shows that the 5–35% dry solid percentages are used in the slurry making [8,9]. Nevertheless, certain biomass types might need dewatering before being pumped into the reactor due to the moisture content variation. Due to their high-water content, Algae are getting immense consideration as a better feedstock. Also, woody biomass, sewage sludge, and certain manure types are gaining attention. Although woody biomass is well suited for gasification, to use it for HTL, it must be grounded to make the slurry.

Microalgae are photosynthetic organisms characterized by being adapted to live in a comprehensive spectrum of environments. Microalgae uses carbon dioxide (CO_2) to grow photo autotrophically and produce atmospheric oxygen. Microalgae are used to produce third-generation biofuel[10–12]. Furthermore, due to the high photosynthesis efficiency, ease of availability, and higher CO_2 mitigation than the woody biomass, microalgae have a higher potential in becoming a better feedstock for HTL [13].

Moreover, algae being microscopic organisms, can grow in freshwater or saltwater, giving more space to find cultivation problems. Also, microalgae do not need to be dried to be used as a feedstock. Once it is dewatered and washed to get rid of salts, it is about making a slurry of the microalgae before it is pumped into the system for HTL [12].

Macroalgae is recognized as a better option as a feedstock for HTL than other thermochemical conversion methods. Macroalgae is not examined as much as microalgae yet. Nonetheless, macroalgae are on the verge of becoming a much better feedstock for HTL attributable to the superior photosynthesis efficiency and higher growth rate [13–15]. Also, due to the 3-dimensional growth, it significantly reduces surface use [16]. Macroalgae have high biomass productivity of $2 kgCm^{-2} year^{-1}$. Besides that, macroalgae can help clean the water contaminated by heavy metals [17].

In the meantime, macroalgae can absorb a high CO_2 amount, about 8–10 tons ha^{-1} $year^{-1,}$ than the temperate woodlands[18]. Additionally, Macroalgae can be subdivided into a few categories, such as red algae, blue algae, brown algae, and green algae [13], rich in lipids, proteins, and carbohydrates[16,19]. Apart

from the algal biomass, some other feedstocks are tested as HTL feedstocks, such as lignocellulosic biomass, sewage sludge, and different types of manure [20–22].

Straw is a by-product of cereal and grain production. The use of fertilizers and pesticides remains unchanged since straw is taken out at the latter phase of the cycle. When solely comment about straw, unless used for biofuel production, it is left for decomposition in most cases. Given that straw utilized to produce biofuel remains a by-product of conventional farming, no adverse effects or increased biodiversity threats should be expected. Additionally, grain production will be unaffected by presuming no changes in the seeds used and standard harvesting methods. It is a general assumption that removing extra biomass from cereal fields can negatively impact the soil carbon stock, so other straw should not be harvested from areas with a high Dexter-index (organic matter in the soil)[23]. Therefore, depending on the location of a potential biofuel plant, the amount of locally available straw can fluctuate depending on the Dexter index of the neighboring areas. Straw is one of the abandoned agricultural wastes. It should be noticed that carbon can be returned to fields after energy and fuel production. The straw produced from different sources holds the potential of millions of tons of bio-oil if utilized. Straw, in general, is capable of producing a biocrude yield of 30–37% of the output[24,25].

Meanwhile, straw produces char for about 25–27%, which is on par with other lignocellulosic feedstocks. The produced oil has a calorific value of about 25.5 MJ/Kg, which is slightly lower than the other considered feedstocks. Therefore, the potential of straw as a feedstock for bio-oil production is immense.

Woody biomass consists of cellulose, hemicellulose, and lignin. Cellulose and hemicellulose produce sugars, and then with further reactions, they provide a wide range of products such as phenolic compounds, glycerol [26]. Lignin liquefaction produces more char and aromatic hydrocarbons, phenols, guaiacol, and cresols in the biocrude [27]. In Europe, forests have mainly consisted of birch, spruce, aspen, pine, willow, and oak, but the rest has many different species. These types have slightly different percentages of cellulose, hemicellulose, and lignin. Woody biomass generally has a biocrude yield of 25–40 % with a heating value of around 35 MJ/Kg[20,28]. Generally, the nitrogen content of the biocrude produced from woody biomass is comparably low to the biocrude produced from marine feedstocks. When it comes to woody biomass,

feedstock pre-treatment plays a huge role since the woody biomass is rigid and robust. Therefore, before adding water to the biomass before the HTL process, physical treatments such as chipping and powdering are required.

Forest residues are a mix of trees, consisting of leaves, barks, pieces of the trunk, and branches. Mainly these are remains of cut-down trees. In the case of a mega type of reactor availability of forest, the residue could be a problem since the production of forest residues would not be from the same area or in a continuous manner. Despite the inconvenience of availability, it should produce biocrude as consistent as the woody biomass. Meanwhile, the pre-treatment required for forest residues could slightly change from what woody biomass is required due to the residues' various parts. Therefore, chipping and powdering, as well as grinding of certain parts, are required.

Generally, forest residue's water content could be slightly higher than the woody biomass, and bark would significantly differ from the total weight[29]. Forest residues have reported a biocrude yield of 22% in the literature, which is comparably a lower value to straw and woody biomass.

In recent years, much research has been reported on the HTL of lignin to obtain various products [30–33]. Mainly the discussion has been the phenolic compounds produced in lignin liquefaction. In the process of lignin to produce phenolic compounds, hydrolysis and cleavage of the ether bond and C-C bond, demethoxylation, alkylation, and condensation reactions appear, and these reactions seem to compete with each other at different phases of the process. Alternatively, hydrothermal reactions do not affect the aromatic rings [34]. The phenolic compounds from the demethoxylation and alkylation seem to be intensified as the temperature increases. Thus, due to the numerous functionalities of phenolic compounds, lignin offers the potential of producing many valuable chemicals [34].

1.1 Biofuels

Biofuels are renewable liquid fuels that are primarily produced from biomass. The biofuels produced from biomass have numerous benefits. Biofuels can be applied for several purposes, including in the transportation sector. The concept of using biofuels as a transportation fuel is first demonstrated in 1912 when Rudolf Diesel first ran a diesel engine with raw peanut oil [35]. Nevertheless, the concept of biofuels was abandoned later due to abundant and

cheap fossil fuels. Today, they have been revisited to meet the demand for energy and environmental concerns about drastic climate change.

Biofuels are broadly classified into four generations depending on the carbon source of biomass feedstock. The first-generation biofuels include bioethanol and biodiesel derived from starch, sugar crops, and vegetable oils. In recent years, first-generation biofuels have been considered controversial due to competition with food. For ethical reasons, they are not promising in fuel and energy production. The second-generation biofuels include biohydrogen and biomethane derived from non-edible lignocellulosic biomasses such as straw, wood, and forest residues. This generation of biofuels provides several advantages but still needs pre-processing and a more substantial land requirement. Pre-processing/pre-treatment is essential due to the rigid structure of lignocellulosic biomass, making it challenging to convert biomass into biofuels. Third-generation biofuels are produced from the algae biomass, such as microalgae and macroalgae. It is also known as advanced generation biofuels or algae biofuels. Fourth-generation biofuels are produced from genetically re-engineered biomass. It is based on genetically modified microscopic organisms such as microbes, yeast, fungi, microalgae, and cyanobacteria. It could involve artificial photosynthesis that can convert directly to fuel or modify the oil-storing capabilities of organisms [36]. Among the various alternative liquid fuels, algae-based biofuel has drawn much attention because of the possibility of replacing fossil fuels.

1.2 Hydrothermal Liquefaction of Biomass for Biofuel Production

Thermochemical conversion means biomass decomposition by a series of reactions under elevated conditions. These conversion techniques are not new for fuel production pathways, as they have been widely investigated since 1788 for biomass to biocrude products [37]. Many methods and processes convert biomass into usable fuel, such as gasification, pyrolysis, torrefaction, steam reforming, and hydrothermal liquefaction. It can be easily distinguished by the amount of oxygen supplied. However, the conversion process is affected by numerous factors such as biomass composition, reaction time, process economics, operating conditions, and desired products.

Among the technologies mentioned above, hydrothermal liquefaction (HTL) has shown many capabilities in providing bio-oil, which can be developed to replace transportation fuel. HTL is a high-pressure, medium-temperature thermochemical process at 553K–643K and between 10–25 MPa [21,38]**.** Therefore, hydrothermal liquefaction is the thermochemical conversion of biomass into liquid fuels by processing in a pressurized and hot water environment for adequate time to break down the concrete structure to mainly liquid components. High moisture biomass feedstocks such as microalgae and macroalgae are often used in this process. The chemistry and the mechanism of the HTL process are complicated and advanced. The products of the process are bio-crude, gas, char, and water-soluble substances [21]. HTL is successfully carried out in subcritical and supercritical conditions [21,39,40]. In this process, water acts as both a catalyst and reactant. As technology does not need drying, unlike other technologies such as pyrolysis, it has many advantages over other technologies[41]. Both batch and continuous processes are recorded in literature with similar process conditions[41].

1.2.1 Evaluation and available HTL technologies

When the HTL process's operating conditions are lowered to 473K and 2–10 MPa, the process is called hydrothermal carbonization (HTC) [42]. This process is exothermic and spontaneous. This process produces an aqueous phase and an insoluble charry product as the outputs [43,44]. Later, this method is suggested as an intermediate step towards biodiesel production from lipid-rich microalgae by Levine et al. [45]. When the operating conditions of the HTL process are changed to over 374 °C and over 25 MPa, the process produces more gas yields, and the process is called hydrothermal Gasification (HTG). Even though the method possesses a higher efficiency of around 75 %, it is not widespread due to higher capital and energy costs [43]. A summary of HTC, HTL, and HTG is shown in figure1-2**.**

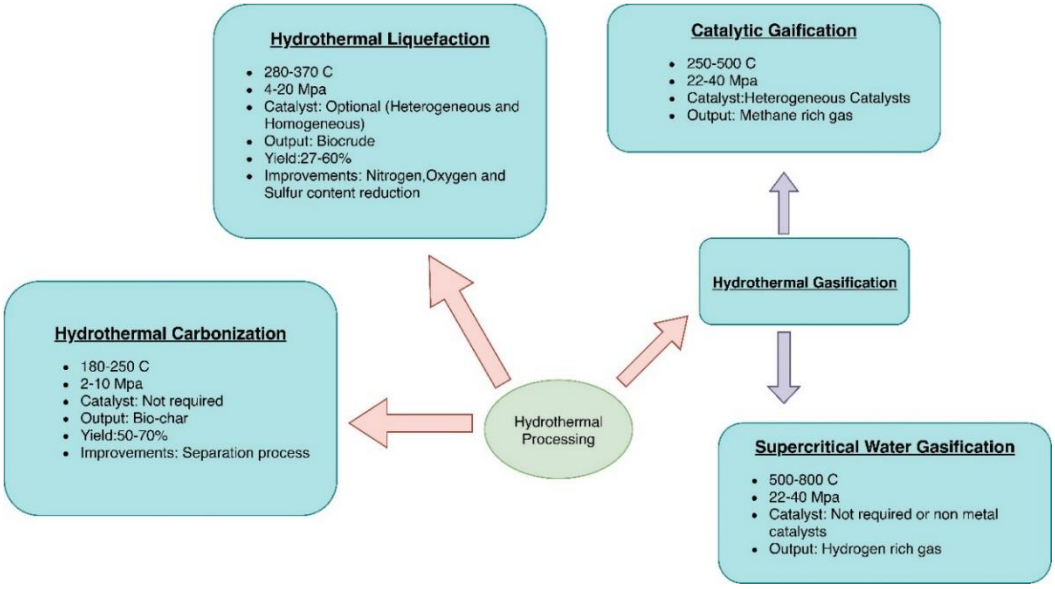

Figure 1-2: An overview of existing hydrothermal processing technologies

HTL is found to be the way to process wet biomass to obtain bio-oil, and it has been getting famous for the last few decades. However, the history of HTL goes back to the 1930s. Beckman and Elliot[46] tried to compare the properties and the yields of oil outputs from the immediate HTL process. After the analysis, governing parameters such as temperature, pressure, catalyst, and time are crucial in defining the output bio-oil quality. Behrendt et al. [47] used the HTL for lignocellulose with supercritical and subcritical solvents. This research area took gradual worldwide attention since 2009, especially in the laboratories where researchers were working on the reaction parameters such as reaction temperature, retention time, type of catalyst, and loading conditions. After that, several researchers recently backed up a brief but in-depth overview of Savage [47] on the HTL of microalgae.

Further, the studies incorporated with the reaction mechanism of HTL are pivotal as the improvement of reactor design and process optimization is directly dependent on the reaction mechanism [48–50]. First, hydrolysis breaks the biomass into fragments where dehydration, dehydrogenation, deoxygenation, and decarboxylation help break it into tiny compounds. Later, more complex chemicals are created, containing alcohol, esters, phenols, ketones, and acids by repolymerization. The new kinetic model introduced by Hietala et al.

[51] opens up new dimensions to the fast HTL technology. The process was operated at 400 °C, and the yield was at 41 % with a short retention time.
The HTL technology is in a transition position, where the technology is improving from a batch process to a continuous process. Hence, recent research has been done widely on improving the quality of bio-oil and the optimized HTL process. Further, the liquefaction process has been simulated differently, implementing new insights and improved models [52,53].
Recent research shows the encouraging pathways of improving HTL biocrude into a replacement for the Petro-diesel. Costanzo et al. [54] extracted bio-oil from HTL, which has similar gasoline properties from wet biomass after hydrodenitrogenation by catalytic treatment. Meanwhile, Pedersen et al. [20] have also obtained biocrude with (oxygenated) precursors to compounds in the gasoline boiling range with aspen wood. Moreover, the authors introduced a continuous flow reactor that resulted in higher heating yields. Some others used wet and dry biomass with a conventional process temperature to significantly obtain higher yields of phenolics [55]

1.3 Modeling of HTL process

Reaction mechanisms, chemical conversions, phase behaviors, thermodynamic properties, and the properties of the products must be considered to model the HTL process. Thermodynamic property variation and the phase behavior of the HTL process are rather complex and challenging to predict [21]. The available water in the wet biomass works as both a solvent and a reactant in the liquefaction process [56]. Moreover, Hydrolysis and repolymerization reactions are much accountable in the HTL process [19,21,57]. Therefore, special attention and models must be implemented to process the HTL process successfully. Different research groups use various approaches and numerous modeling pathways to model the process[4,52,53,58–62]. Some groups have used kinetic modeling approaches[53,56,63,64], while others have used CFD[52,58–62] and other simulations.
A review by Ederer and Gilles[65] on a comparison of thermodynamic kinetic modeling with other approaches gave an in-depth insight into thermodynamic kinetic modeling. The comprehensive thermodynamic modeling of a reactor carried out by Lu et al. [66] considered gas-liquid equilibrium, chemical equi-

librium, exergy, and energy for supercritical water. The results are used to predict the hydrogen purification of an online gas separator. The general kinetic model for HTL of microalgae by Valdez et al.[56] demonstrated the contribution of lipids and proteins of biomass for the biocrude. They created a model that facilitated different reaction rates for carbohydrate, lipid, and protein fractions. Recently, Vo et al.[63][64] developed a quantitative kinetic model with a general reaction network and studied the yields of various microalgae in various temperatures and residence times. Supporting the conclusions of Valdez et al.[56] Vo et al. [63,64] articulated that the reaction pathways of producing bio-oil and aqueous phase from lipids, proteins, and carbohydrates dominate the HTL process. Meanwhile, the kinetic model developed by Sheehan and Savage[53] managed to predict biocrude yields as many as 70 from 12 reported studies to a 5wt% accuracy. Together with the high accuracy of the model, this study managed to support the conclusions of Vo et al. [64] and Valdez et al. [56] as well. One of the highlights of this model was the ability to handle the different biochemical compositions of different feedstocks and under different process conditions such as fast liquefaction.

Few research groups have developed CFD models to predict HTL or HTG processes. Compared to other thermochemical processes, the number of CFD models developed to give predictions on HTL is deficient. Yoshida and Matsumura [58] are one of the first ones to develop a reliable CFD model to give predictions on either HTL or HTG. The developed CFD model predicts yields and improves the reactor in supercritical water gasification. After validating the CFD model, the reactor is improved using the simulation data to obtain a carbon gasification efficiency of 0.94 with a 4.9 wt % glucose solution in supercritical conditions. Mosteiro-Romero et al. [52] used a shrinking core model to simulate the dissolution of a wood particle in subcritical water.

Furthermore, the process parameters are investigated using the model. A comprehensive mathematical model to model reaction pathways for hydrolysis and pyrolysis is developed. Kinetic data are taken from the literature due to the lack of experimental data where the model can predict the number of solid residues produced and final product distribution. Recently, Ranganathan and Savithri [59] used a two-dimensional unsteady CFD model to investigate the heat transfer, fluid dynamics, and reaction kinetics of the HTL process using Nannochloropsis sp lab-scale plug flow continues reactor. Unlike Yoshida and

Matsumura[58], the model should be further developed to predict the yields more accurately. Even though the model must be further developed, several predictions are given by the model after validating the existing experimental data. CFD is used to model hexadecane's kinetics, a heavy oil model compound by Alshammari and Hellgardt [60]. Most of their work is based on the isothermal conditions and the residence times. Although more data are yet to be included in the data for better predictions, valuable conclusions are made with the results of the CFD model, such as reducing the reactor diameter for better conversion rates. Tran et al. [67] recently suggested suitable process parameters for fast HTL process using a three-dimensional CFD model of a nozzle reactor considering both steady-state and transient analysis methods. Their work is based on achieving high heating rates in the reactor, where they achieved the best mass flow rate of 60:20 (hot: cold flows mil/min) to obtain the best mixing and heating rates.

Goodwin et al.[68] developed a CFD model to simulate a microchannel reactor to investigate the supercritical water gasification of Xylose. They mainly concentrated on Hydrogen-rich gas production. Comparatively, short residence times of less than 1 second are simulated and studied with the CFD model. With this study, microchannel reactors are proven to be very effective in improving supercritical water gasification of biomass. Caputo et al.[69] conducted another CFD study of supercritical water gasification of glucose, where they studied a continuous process. The complex flow regimes and fluid dynamics are studied using the CFD simulations. With the optimization process performed using the simulations, they managed to achieve a 74% of H_2 yield in the syngas. When the CFD results and experimental studies are coupled, interesting conclusions are made on the reactor behavior where certain parts behave as mixed reactors and plug flow reactors. Furthermore, the numerical investigation carried out by Jin et al.[70] on glycerol gasification in supercritical water with a 3-D CFD model exposed several optimized parameters. While using a tabular reactor, side reactions, reactor length, preheating of water, and feeding angle for water are extensively studied. To conclude their work, a multi-injection feeding method for water is proposed, decreasing carbon gasification efficiency.

More recently, Yukananto et al.[71] used CFD modeling to study SCWG of glycerol in a tee junction-shaped cylindrical reactor. The model proved to be

going along well with the experimental data besides the slight differences in predicting outlet temperatures and carbon gasification efficiencies. Nevertheless, the model's flow behaviors are well explained, while the impacts of gravity force and velocity ratio between two inlets are influential inflow patterns and heating process, respectively. Extending their work from SCWG to char formation in SCWG, Yukananto et al. [62] suggested char yield can be increased up to 87% when the reactor size is increased close to a pilot-scale using a CFD model. Char formation during supercritical gasification is specially investigated in their work, while the model proved to be reliable with only a 13% prediction different from the experimental studies.

Modeling the HTL process has been a challenge due to the complex chemistry and lack of kinetic data. Despite the complexity of the modeling process, recent studies demonstrate an eagerness to develop more models and an improvement in predictions as most of the work mentioned above can predict process, flow dynamics, and process parameters to a satisfactory level. Nonetheless, more simulation models must be developed with newer approaches and more details with fewer simulated data error percentages than experimental data. In this case, simulations can study more profound aspects of HTL with shorter time consumption and fewer expenses.

1.4 Motivation

The need for a comprehensive and descriptive HTL model is a need. Many studies and models have been developed with only kinetic schemes, but there is a void in modeling HTL as a comprehensive process incorporating particle decomposition, intraparticle behavior, and further reactions such as repolymerization and condensation reactions. In addition, research hinted at a possible oily film development through the liquefaction process around the biomass particle, which boosts the importance of modeling such an oily film.[52,72]. Moreover, the development of oily film and ash layers has yet been experimentally studied and proven. Hence, modeling the formation of these layers could further clarify the liquefaction behavior and give better explanations on particle decomposition behaviors at different process conditions.

In literature, different approaches and concepts are used for the modeling procedures. In that case, the shrinking core concept is easy to use, a practical concept nevertheless. Further, the less complexity of the shrinking core concept

allows other details and phenomena to be attached without compromises. The shrinking core concept is used for gas-solid reaction models abundantly[73–76]. Further, it has been used by researchers to model wood and cellulose liquefaction at different extents[52,77]. The shrinking core concept has characteristics that can easily model phenomena such as liquefaction. When the decomposition is considered, the placement of the particle's surface is changed only in the radial direction. Due to this, detecting the particle surface at different time frames is accessible where it gives a better base for modeling the oily film and ash layers. Nevertheless, to use the shrinking core concept, the particle is assumed to be non-porous, and only the resultant layers are considered porous. Although the porous particles can be handled with grain models, The modeling process is far more complex and challenging to integrate oily films and ash layers since the placement of the actual particle surface is a complex scenario[74].

Lignin is a waste from the paper industry. Although lignin is a well-studied feedstock with HTL, the chemicals produced by HTL of lignin and the abundant availability are appealing. Therefore, lignin is an appropriate choice for an HTL feedstock. In addition, the possibility of using lignin as a co feedstock with other feedstocks to obtain better results in HTL is another motive. The char formation and the char formation mechanism during the HTL process are also essential to check. Although HTL of lignin and biocrude from lignin HTL is well studied chemically already, the char formation and the mechanism have not been studied thoroughly. A proper study on char formation would help learn the possible uses of HTL char as a helpful material or a precursor to a valuable output.

1.5 Objective and research question

This research aims to develop a comprehensive HTL model using a new version of the shrinking core model for a set of solid-liquid reactions that will depend on the thickness of the oily film and ash layer produced from the resultants of the solid-liquid reactions. The diffusion of water governs the thickness of the product layers, the reaction rates through the product layers, and the counter diffusion of products through those newly created product layers. Further, the feedstock used is a waste from the paper industry, produced in vast amounts and only used to produce heat by combustion. Further, this thesis

discusses the char formation and char formation mechanism of lignin HTL by stepping outside the model. In that process, a mechanism for char formation is proposed using the structural, chemical, thermal, and physical behavior of char produced at different operating temperatures and residence times. In the next phase, the performance of lignin in co-liquefaction with laminaria saccharina is studied statistically, where the chemical behavior of biocrude and the yields are optimized. Further, the synergistic effect of co-liquefaction is studied mainly because laminaria saccharina is a widely available feedstock in this part of the world, specifically in Norway. Overall, the main research objective, which constitutes the thread along with this thesis, is:

Developing a robust and comprehensive liquefaction model using the shrinking core concept with lignin as a feedstock.

Furthermore, the research questions which have been answered are:

1. How does the shrinking core model respond to different operating parameters?
2. How does the oily film and ash layer form and behave during the liquefaction process?
3. How does the particle surface temperature change during liquefaction?
4. How does char formation occur and the char formation mechanism of liquefaction?
5. How does the char behave according to operating temperature and residence time?
6. Does co-liquefaction of lignin with seaweed have a synergistic effect, and how to optimize the biocrude yield of co-liquefaction Statistically?

1.6 Thesis structure

The thesis structure is arranged upon the research questions to give a better fluidity to the evolution of the thesis. The structure is as follows.

Chapter 1- A brief introduction on the motivation, objectives, research questions, and a basic structure of the thesis.

Chapter 2- The information required to understand the materials and the developed process in each article is described. The chapter starts by describing different types of materials used in work. Then the methods followed in each article, the experimental procedures, and the extraction of biocrude is described. Further, the different types of analysis methods and instruments are described. Finally, the statistical methods used in the articles are discussed

Chapter 3- After explaining materials and methods, chapter 3 discusses the contributions of each article produced during the Ph.D. Each subsection of the chapter briefly discusses each article's motivation, method, results, and research findings. Article A and B discuss the mathematical model developed using a single particle system using a shrinking core concept. Article C discusses the evaluation and characterization of char produced during the HTL of alkali lignin. The structure and chemistry of the char are discussed, where a formation pathway for the char is proposed. Article D is based on synergetic effects of co-liquefaction of lignin with laminaria saccharina (sugar kelp). Surface response methodology is used to optimize the biocrude and char yields.

Chapter 4- The main results and findings are assembled in Chapter 4, where a discussion is formed.

Chapter 5- The challenges and limitations, results, and conclusions from the findings are presented in chapter 5. Moreover, the future work planned during the Ph.D. is summarized at the end of this chapter.

The thesis concludes with the bibliography and the appendices. The visual representation of the research papers with the primary investigated process is shown below in Figure 1-3.

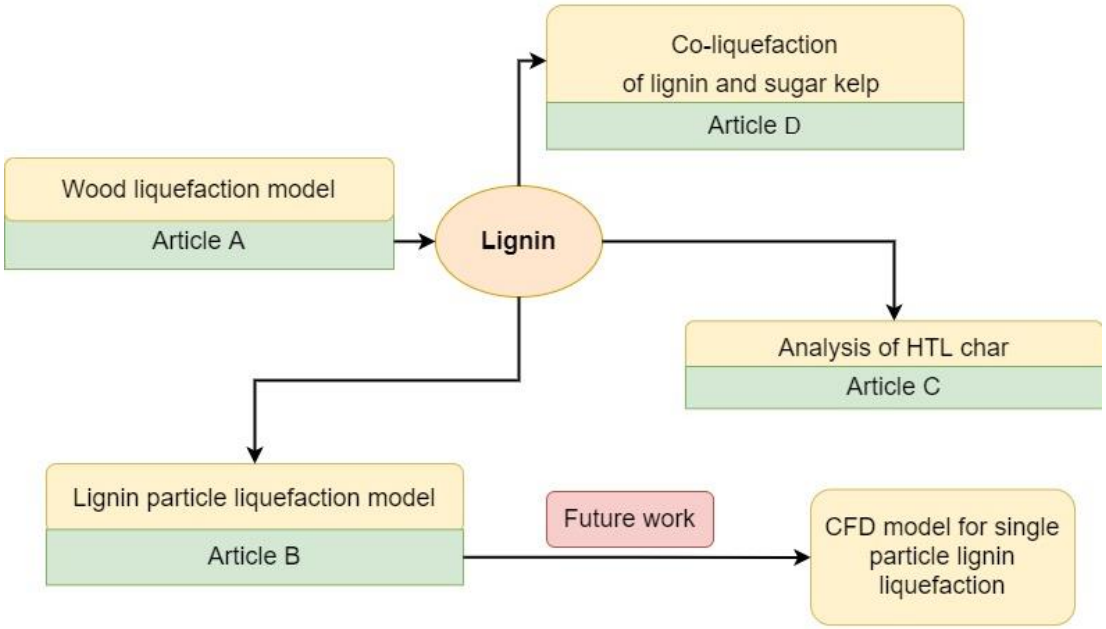

Figure 1-3:Visual representation of the research papers with the main investigated process

2 Materials and methods

2.1 Materials

In this research, the primary feedstock used is alkali lignin, obtained from Sigma-Aldrich, Norway. Article B and C are based on HTL of lignin. In Article D, co-liquefaction of lignin with laminaria saccharina (sugar kelp) is studied. Laminaria saccharina for the experiments is obtained from Lerøy ocean harvest. Before the experiments, laminaria saccharina is washed and air dried to get rid of the salt.

2.1.1 Lignin

Lignin comprises phenylpropanoid chains, linked mainly by carbon-carbon and ether bonds. Further, it is the second most abundant biopolymer observed in the plant cell wall. Identifying a complete structure of a lignin polymer is difficult due to the complex nature and characteristic difficulties in categorizing lignin polymers. Figure 2-1 below shows a model structure of softwood lignin.

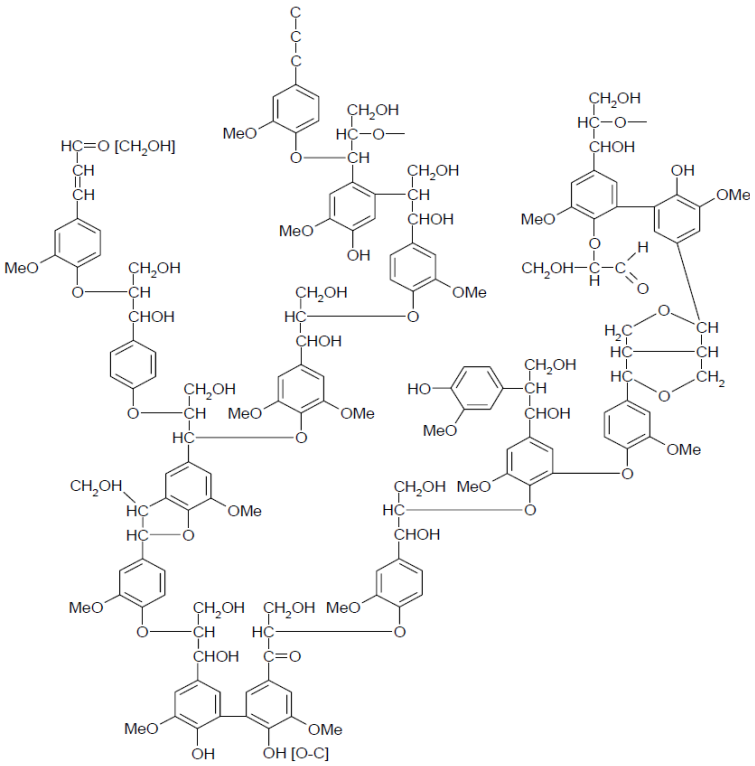

Figure 2-1:A model structure of lignin from softwood [78]

The plant species, age, soil condition, climate, and cultivation practices determine the moieties present in the lignin polymer. p-hydroxyphenyl (H) moieties (p-coumaryl alcohol), coniferyl alcohol (G) moieties(guaiacyl), and sinapyl alcohol (S) (Syringyl) moieties are the essential phenolic monomers which are the building blocks of lignin as shown in Figure 2-2 [79–84]. The propane side chains link the phenolic monomers to the lignin polymeric structure. Different pre-treatment processes are utilized to determine the lignin available on the lignocellulosic biomass. In addition, various lignin characterization methods are applied to determine the phenylpropanoid moieties in the polymer. Softwood lignin comprises guaiacyl (G) moieties, while hardwoods consist of guaiacyl and syringyl moieties[79]. Lignin from grasses is primarily *p*-hydroxyphenyl (H) moieties with guaiacyl (G) and syringyl (S) moieties in smaller percentages.

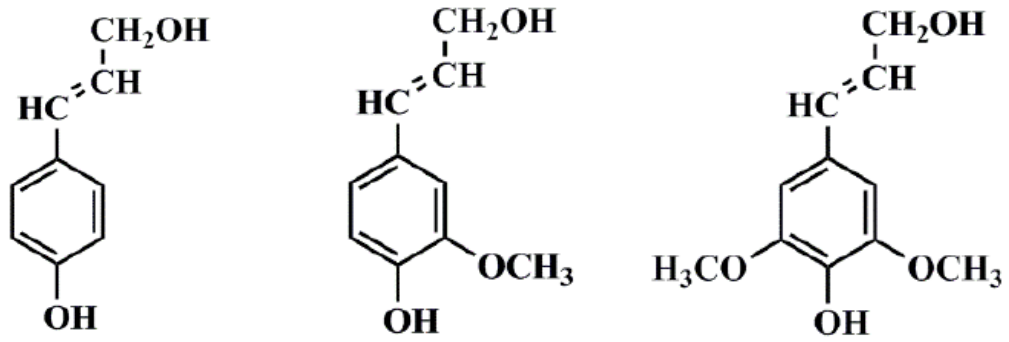

a) b) c)

Figure 2-2:Structures of three basic phenolic monomers that from lignin. a) p-coumaryl alcohol or p-hydroxyphenyl (H) b) Coniferyl alcohol or guaiacyl (G) c) Sinapyl alcohol or Syringyl (S) [79]

Figure 2-3 below shows the alkali used in the experiments in this study

Figure 2-3:Alkali lignin used for the experiments

Proximate and ultimate analysis data for the alkali lignin used for the research is shown below in table 2-1.

Table 2-1: Proximate and Ultimate Analysis of Alkali lignin

Proximate Analysis (Wt%)			**Ultimate Analysis (Wt%, Ash free)**			
VM	ASH	FC	C	H	N	O
69.11	16.84	14.05	47.18	6.19	3.61	43.02

VM= Volatile matter, FC=Fixed Carbon, d. b= dry base

2.1.2 Laminaria saccharina

Sugar kelp laminaria saccharina (saccharina latissima) is a cold water seaweed species distributed mainly in the northern hemisphere[85]. Being one of the fastest-growing seaweeds in the European waters and having produced relatively good biocrude yields, laminaria saccharina holds a potent ability to be a promising feedstock for HTL[86,87]. Like the other seaweed, L. saccharina holds a very high moisture content (75-90%) where the dry matter consists of nutritional components such as carbohydrates, lipids, proteins, vitamins, and minerals in variable amounts depending on the cultivation site and the time of the harvest[88]. Like other seaweed types, L. Saccharina contains substantial polysaccharides (up to 70% of dry matter), particularly alginate, cellulose, fucoidan, laminarin, and mannitol[86,88,89]. In contrast, lipids account for a small portion of 0.6–3.4% of the dry matter depending on the harvest season [90]. Nevertheless, sugar kelp is abundantly found in Norwegian waters,

where it becomes an excellent candidate to be tested with HTL. Figure 2-4 below shows the laminaria saccharina used in the laboratory.

Figure 2-4: Laminaria saccharina used for the experiments

Proximate and ultimate analysis data for the laminaria saccharina used for the research is shown below in table 2-2.

Table 2-2: Proximate and Ultimate Analysis of laminaria saccharina

Proximate Analysis (Wt%)			**Ultimate Analysis (Wt%, Ash free)**			
VM	ASH	FC	C	H	N	O
69.11	16.84	14.05	47.18	6.19	3.61	43.02

2.2 Hydrothermal Liquefaction experiments

The hydrothermal liquefaction experiments are performed with an in-house HTL reactor rig designed and fabricated during this Ph.D. work. The batch process performed for this work is without catalyst, and water is used as the solvent. In articles B and C, only lignin is used as the feedstock, wherein in article D, sugar kelp is used along with lignin as the feedstock.

The HTL reactor rig consists of several different parts. Below, figure 2-5 shows a schematic diagram of the rig, whereas figure 2-6 shows an actual rig image.

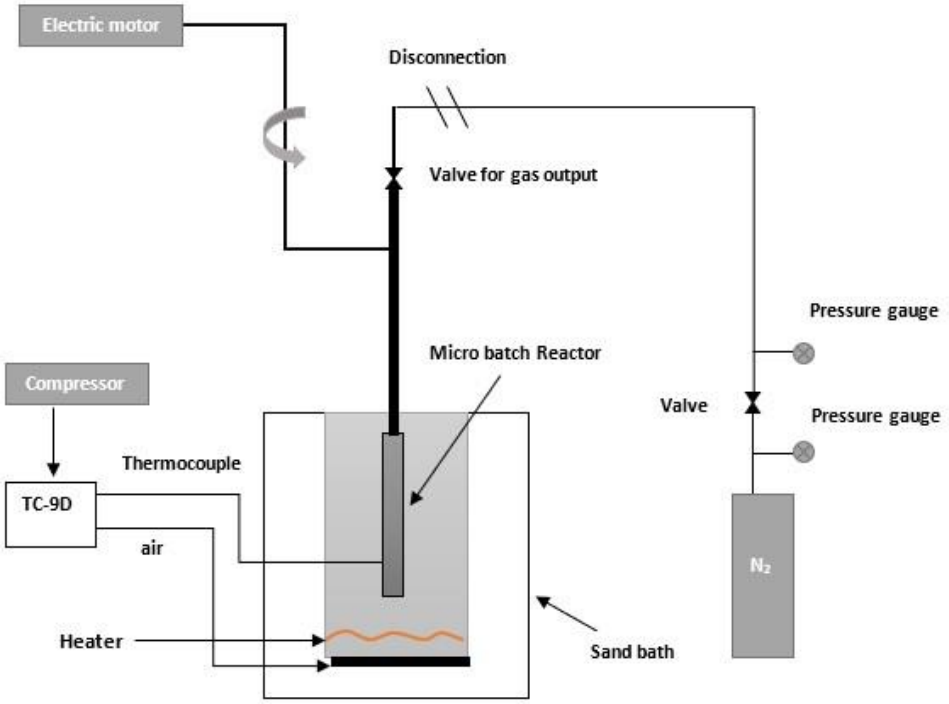

Figure 2-5:Schematic diagram of the HTL rig

The microreactor from Graco High-Pressure Equipment Inc (HiP) is connected to a shaker device run by an electrical motor. The rod connecting the reactor is connected to the motor shaft through an eccentric to output a reciprocating movement. The motor has a max frequency of 35Hz, where for the shaking effect, only 32Hz frequency is used to obtain an rpm of about 7-8.

Figure 2-6:Actual figure of the reactor system

The reactor is submerged in Al_2O_3 sand, placed in an SBD-2L sandbath produced by Keison. A TC-9D temperature controller by Techne controls the temperature of the sandbath. A compressor connected to the sandbath through the TC-9D controller produces the airflow through the sand bath. An actual figure of the reactor used for the experiment is shown in Figure 2-7 below.

Figure 2-7:A figure of the actual reactor used for the experiments

2.2.1 Experimental method

The lignin slurry of 10% of lignin is used for article B and article C. Distilled water is used as the solvent for all the cases. A tabular steel reactor produced by Graco High-Pressure Equipment Inc (HiP) with a volume of 24ml is used for the experiments. In all the experiments, to keep space for produced gasses and expansions, an 8ml dead volume is kept. A fluidized sandbath is used to heat the reactor. The sand bath is heated up to the required temperature value during the experiments. After being loaded with the required feed slurry, the reactor is sealed and checked for leakages by purging N_2. Once the reactor is cleared from the leakages and kept inside the sandbath for the required residence time. Then it is taken out and put into cold water at once. Then the reactor is kept there for 30 mins until it cools down to room temperature. An external shaking mechanism is used to shake the reactor during the experiments. In articles, B and C, three temperature values and three residence times are used. The temperatures used are 573 K, 603 K, and 623 K, while the residence times range 10 min, 15 min, and 20 min. Therefore, every temperature value is studied with three residence times. For the experiments' consistency, every experiment is repeated five times, and average values are used for analysis.

For article D, the temperatures used are 573 K, 603 K, and 633 K, while the exact residence times as articles B and C are used.

2.2.2 The extraction process of biocrude

In the downstream HTL process, four different outputs can be obtained (biocrude, gas, aqueous phase, and char). According to the literature, it is a known fact that HTL produces a gas phase rich in CO_2, CO, CH_4, and H_2[91,92]. In this study, gas and aqueous phases are not analyzed since the study is based on the behavior of the biocrude and char phases.

In the extraction process, acetone is used as the extracting agent. The reactor is washed with acetone four times after every experiment to extract all the products. Moreover, the solution is filtered, and the solid product is separated. The liquid phase from the HTL is taken to the centrifuge to ensure no remaining solid residue in the liquid phase. It is then added to the solid phase if the solid residue is found. To ensure solid and liquid phases are appropriately separated, solid residue (char phase) is again washed with acetone before filtering for a second time. After the char phase is separated, it is dried at 378 K for 24 hours before quantifying.

The liquid phase is then evaporated using a rotary evaporator to divide the biocrude phase from the aqueous phase and the remaining acetone (added in the extraction process). Below, figure 2-8 shows the extraction process used during the study.

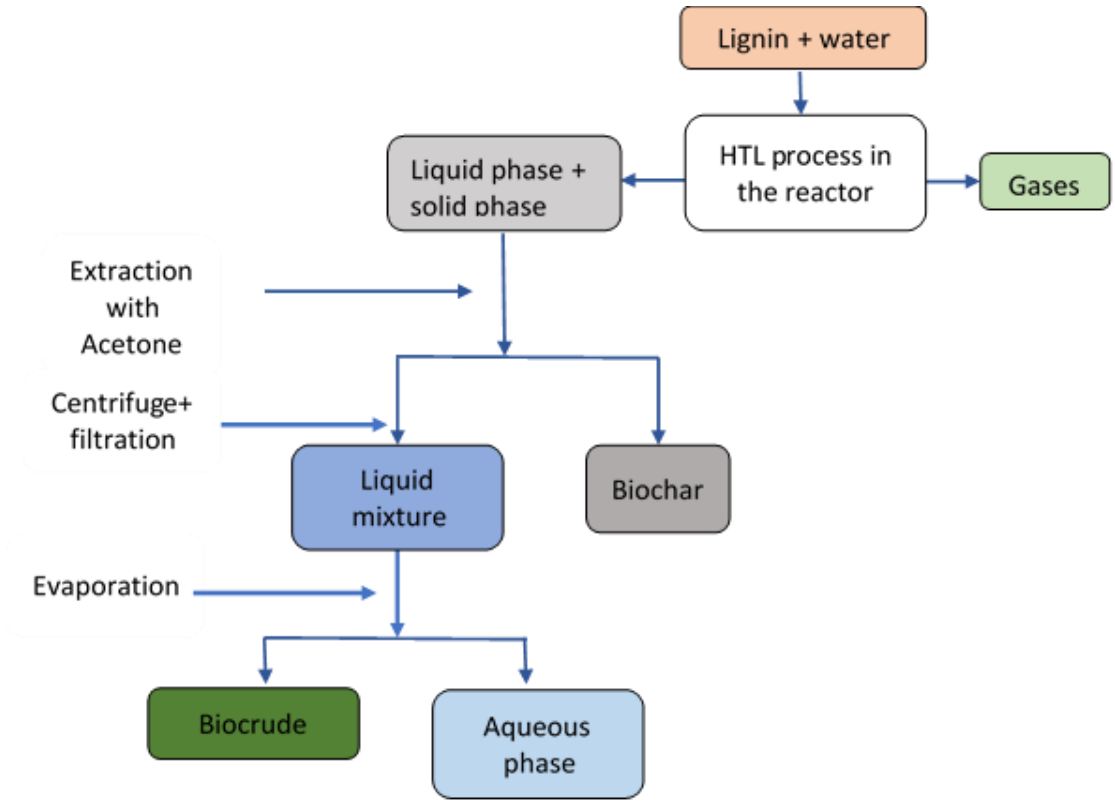

Figure 2-8: Extraction method used in the study

2.3 Characterization

After the separation process is completed, each phase is quantified before sending to the analysis and characterization. Below eq 1 and 2 are used to quantify the biocrude and char yield, respectively.

$$Biocrude\ yield(wt\%) = \frac{Mass\ of\ biocrude\ recoverd\ after\ the\ extraction\ (g)}{Initial\ amount\ of\ feedstock\ used\ for\ the\ experiment\ (g)} \times 100\%$$

Eq 1

$$Char\ yield\ (wt\%) = \frac{Mass\ of\ char\ recoverd\ after\ the\ extraction\ (g)}{Initial\ mass\ of\ feedstock\ used\ for\ the\ experiment\ (g)} \times 100\%$$

Eq 2

2.3.1 Ultimate analysis

C-H-N/O ultimate analysis is performed at the University of Agder in all instances. (Article B and C). In article B and article C, a 2400 Series II CHNS/O Elemental Analyzer (PerkinElmer, USA) is used in-house, according to the standard EN ISO 16948:2015. Sulfur content is assumed negligible in all cases, although a shallow sulfur content is present in lignin. The difference between the other elements calculates oxygen. All the measurements are taken in triplicates.

2.3.2 Proximate analysis

According to EN standard techniques, a proximate analysis is performed in a muffle furnace LT 40/11/P330 (Nabertherm, Germany). EN 15148, EN 14774-2, and EN 14775 standards are used, respectively, for volatile matter, moisture content, and ash content of biomass.

2.3.3 Surface area and porosity

In article C, the surface area and porosity of the HTL char are studied. The test is performed with nitrogen adsorption at 77 K (NovaTouch, Quantachrome, USA). The Brunauer- Emmett-Teller (BET) model is then employed to calculate the surface area. Pore volume is calculated with the quenched solid density functional theory (QSDFT), using the calculation model for slits and cylindrical pores on the adsorption branch. Before performing each surface area measurement and porosity, samples are degassed at 423 K for six hours. The total pore volume is defined from the amount of N_2 adsorbed at a p/p_0 value of 0.99.

2.3.4 Scanning electron microscopy

Scanning electron microscopy (SEM) has to be used to study a material's morphology and microstructure. A morphological study is performed for char samples produced in article C. For that study presented in article C, the samples' scanning electron microscope (SEM) images are obtained using a JSM-7200F scanning electron microscope (JEOL, Tokyo, Japan).

2.3.5 Fourier transform infrared spectroscopy

In article C and article D, FTIR analysis is carried out to study the functional groups of HTL char and biocrude. The sample's infrared spectrum is measured using a Perkin Elmer FTIR spectrometer (Perkin-Elmer Ltd., Cambridge, UK) equipped with a nitrogen-cooled mercury-cadmium telluride detector. In article C, each dried sample dispersed in KBr as a 10% mixture is placed in a sample cup of a Perkin Elmer diffuse reflectance accessory, and the surface of the sample is carefully leveled flat. The spectrum of finely ground KBr is used as the background. The spectrum is measured in the range 4000–600 cm^{-1}, and a total of 32 scans are made at a resolution of 4 cm^{-1}. After that, the resulting average reflectance spectrum is transformed into the Kubelka–Munk format and saved as the final spectrum.
In article D, The FTIR instrument is equipped with a Harrick single reflectance attenuated total internal reflectance (ATR) accessory and liquid nitrogen cooled MCT detector. Each sample is placed on the ATR crystal using a blunt glass rod. The sample is made to spread on the crystal, and the spectrum is measured in the range of 4000- 600 cm^{-1}. A background is measured with the ATR crystal before applying the sample. A total of 32 scans at a resolution of 4 cm^{-1} are made on each sample. The infrared spectra in absorbance format are used to compare the functional groups in the samples.

2.3.6 Thermogravimetric analysis

In article C, thermogravimetric analysis of the HTL char samples and lignin is carried out. Mettler-Toledo Thermal Analyzer (TGA, Mettler-Toledo, Columbus, OH, USA) is used for the analysis. TGA and derivative thermogravimetry

(DTG) graphs are used in this research to examine the thermal behavior of char. The temperature is raised from 303 to 1273 K with a heating rate of 20 K/min with nitrogen as the purging gas with a 25 mL/min constant flow rate.

2.4 Unreacted Shrinking core model

This study uses a modified shrinking core model in Article A and Article B. In the unreacted shrinking core model, the decomposition of the biomass particle is assumed to be only in the radial direction. Therefore, it is assumed that the reactions occur only on the particle surface. Due to the mass transfer from the reactions, the mass reduction occurred in the radial direction of the particle.

2.4.1 Shrinking core model for spherical particles

A simple way of describing the reaction of a solid particle with a liquid or specific water is by using the shrinking core model [52,77,93]. The shrinking core model's primary assumption is that the reaction develops topochemical, only on a single surface that distinguishes two zones within the solid particle. The shrinking core system consists of an unreacted core consist of a solid chemical mixture and an already reacted outer layer made of liquid/solid product. The outer layer is porous, and the gas/liquid diffuses through the outer layer. Nevertheless, it can be either reacting or not reacting with liquid/gas diffuses depending on the material the outer layer is made. Besides, if it is not reacting, that is due to its inert nature. When the surface reactions occur, the core is available to consume the core-outer shell interface shifts inward.

In the proposed model, the core -outer shell interface is a spherical surface concentrical to the unreacted external core. Further, when the surface reactions are happening, the outer shell grows thicker. Nevertheless, with the dissolve of the outer shell into the water, the thickness changes. This theory can be employed in various particle geometries were in this model for spherical particles.

Article A assumes that the particle is decomposed with surface reactions, and all the products are dissolved in water instantly without forming any layer around the biomass particle. Figure 2-9 below shows a graphical interpretation of the assumed shrinking core concept applied for the proposed model[52,73,77].

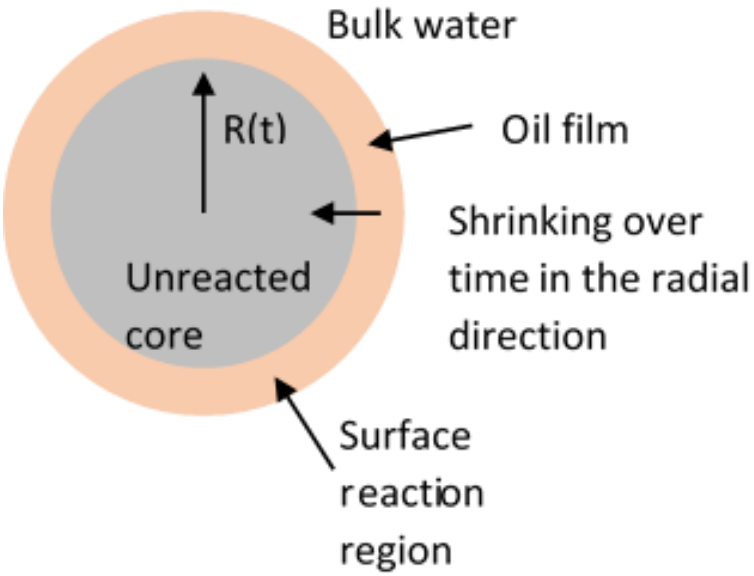

Figure 2-9: Shrinking core model assumed for the hydrolysis of the biomass particle submerged in water.

In the proposed model in Article A, the particle has initially been deemed a combination of cellulose, hemicellulose, and lignin. At different temperatures and with corresponding reaction kinetics, each component is hydrolyzed. A custom reaction rate constant is developed to determine the hydrolysis of each component (shown later in the modeling process). The biomass particle decomposition is believed to be a cumulative effect of the liquefaction of each component. According to Kamio et al.[77], diffusion of the water monomer through the aqueous film surrounding the biomass particle is modeled using the mass transfer of water.

$$M_w = 4\pi r^2 k_A (C_b - C_S) \qquad \text{Eq 3}$$

M_w correspond to the mass transfer rate of the water monomer, r is the radial position of the particle, k_A is the mass transfer coefficient, C_B represents the bulk water monomer concentration, and C_S is the water concentration at the surface.

Hydrolysis of the spherical particle is stated below, where M_B is the hydrolysis reaction rate at the surface of each model component and $k_H$is the hydrolysis rate constant.

$$M_B = 4\pi r^2 k_H C_S \quad \text{Eq 4}$$

The overall rate constant of hydrolysis of the biomass particle k_H is assumed to be the sum of hydrolysis rate constants of three model components. Below, eq 5 shows the overall hydrolysis rate constant of the biomass particle.

$$k_H = k_{cellulose} + k_{hemicellulose} + k_{lignin} \quad \text{Eq 5}$$

(k_H becomes a different value according to the model component, which is hydrolyzed. As an example, if only Cellulose is being hydrolyzed $k_H = k_{cellulose}$ while, if both Cellulose and hemicellulose are being hydrolyzed $k_H = k_{cellulose} + k_{hemicellulose}$. Therefore, the particle decomposes at different rates.)

Mass transfer between water and biomass particles should be equal at steady-state conditions. Therefore, from (3) and (4),

$$r_w = \frac{4\pi r^2 C_B}{\frac{1}{k_A} + \frac{1}{k_H}} \quad \text{Eq 6}$$

r_w represents the reaction rate of the water monomer for one biomass particle. When the decomposition rate is described with the mass balance and when the radius of the particle is *r*,

$$\frac{d\,(4\pi r^3 \rho/3)}{dx} = -r_B \quad \text{Eq 7}$$

Here r_B is the reaction rate of the biomass molecule for a unit biomass particle, and ρ is the molar density of the biomass particle. (ρ changes according to each wood component) Therefore, with stoichiometry,

$$-r_w = \beta r_B \quad \text{Eq 8}$$

Where β represents the stoichiometry value of water in the hydrolysis reaction.

(In the proposed model, initially, it is assumed that the biomass particle is consist of 45% of Cellulose, 25% Hemicellulose, and 30% of Lignin). Substituting (6) and (8) to (7),

$$4\pi r^2 \rho \frac{dr}{dt} = \frac{4\pi r^2 C_B}{\frac{1}{k_A}+\frac{1}{k_H}} \quad \text{Eq 9}$$

When the radial position of the surface becomes *r*, the decomposition ratio of the biomass particle can be written as,

$$1 - x = \frac{\frac{4}{3}\pi r^3 \rho}{\frac{4}{3}\pi {r_0}^3 \rho} = (\frac{r}{r_0})^3 \quad \text{Eq 10}$$

Where x is the decomposition ratio of a unit biomass particle. After derivation over time,

$$-\frac{dx}{dt} = \frac{3r^2}{r_0^3}\frac{dr}{dt} \quad \text{Eq 11}$$

By substituting from (10) and (11) to (9),

$$\frac{4\pi {r_0}^3}{3}\rho \frac{dx}{dt} = \frac{4\pi {r_0}^2 C_B (1-x)^{\frac{2}{3}}}{\beta(\frac{1}{k_A}+\frac{1}{k_H})} \quad \text{Eq 12}$$

When the decomposition of the biomass particle is expressed by the concentration of each wood component molecule, x can be expressed, as shown below in equation 13.

$$x = \frac{\sum(C_{mod\ i,0} - C_{mod\ i})}{\sum C_{mod\ i,0}} \quad \text{Eq 13}$$

Where $C_{mod\ i,0}$ is the concentration of each wood component molecule at t=0, and $C_{mod\ i}$ is the concentration of each wood component molecule at t=t.

$$r_B = \frac{dx}{dt} = \frac{3C_b(1-x)^{\frac{2}{3}}}{r_0 \beta \rho(\frac{1}{k_A}+\frac{1}{k_H})} \quad \text{Eq 14}$$

Therefore substituting (13) into (14),

$$r_d = \frac{dC_{bio}}{dt} = -k_x \sum C_{mod\ i}^{\frac{2}{3}} \quad \text{Eq 15}$$

Where i = 1,2,3

Here, r_d is the decomposition rate of the biomass particle, $k_x$is the rate coefficient of biomass decomposition and $C_{mod\ i}$ is the concentration of each wood component. Therefore,

$$k_x = \frac{3C_b \sum C_{mod\ i,0}^{\frac{1}{3}}}{r_0 \beta \rho (\frac{1}{k_A} + \frac{1}{k_H})} \quad \text{Eq 16}$$

According to the wood model component or components, which are being hydrolyzed within a given moment, k_x turn into a different rate constant due to the change in k_H.

Every rate constant is temperature dependent. As the temperature is changed during the process, the Arrhenius equation can calculate the changing rate constants.

$$k_{i,t} = k_{0,i}\, e^{\frac{-E_a}{RT}} \quad \text{Eq 17}$$

Where, $k_{i,t}$ is the calculated rate constant, $k_{o,i}$ is the frequency factor and,E_a is the Activation energy for each component. Arrhenius law can be applied to all the reactions since the rate constants are changed with temperature. Moreover, the heating process can be expressed by the following equation 18.

Heating process; $T = \vartheta_T\, t + T_{ini}$ Eq 18

Where, ϑ_T is the heating rate, *t* represents time and, T_{ini} is the initial temperature.

By substituting (15) from (16), (17), and (18), an equation for biomass decomposition can be created.

2.4.2 Unreacted Shrinking core model with an outer shell

During the liquefaction process, the ash component available in lignin might form as a separate layer around the lignin particle. Thus, a limiting factor is introduced to define the amount of lignin particle's convertible part. A similar limiting factor can be found in the literature [52,94]. With such a background, a limiting factor is introduced such as follows,

$$k_{con} = \frac{m_0 - m_{(t)}}{m_0 - m_{ash}} \qquad \text{Eq 19}$$

Where, m_0 is the initial weight of lignin, $m_{(t)}$ is the weight of the sample at a given time t, and m_{ash} is the ash weight in the sample.
Due to the formation of the inorganic layer, the diffusion of water to the particle surface is limited. After adding the limiting factor, the overall decomposition of the lignin particle is shown as follows.

$$r_d = -k_x k_{con} C_{lig}^{\frac{2}{3}} \qquad \text{Eq 20}$$

Decomposition of the lignin particle depends on the water's concentration on the particle's surface and the unreacted lignin remaining in the system. When the oily film and ash layer are formed around the lignin particle, the water concentration on the lignin particle's surface depends on the water diffused through the oily film and ash layer. Therefore, when an oily film of thickness $'w'$ and an ash layer of thickness $'w_{Ash}'$ are formed, decomposition of the lignin particle depends on the formation of the oily film and ash layer, diffusion of water through the formed layers, and the dissolution of the oily film in water. According to Eq 20, when the oily film is not present, decomposition of the lignin particle can be written as

$$r_d = -\frac{3C_B C_{lig\ i,0}^{\frac{1}{3}}}{r_0 \beta \rho \left(\frac{1}{k_A} + \frac{1}{k_H}\right)} k_{con} C_{lig}^{\frac{2}{3}} \qquad \text{Eq 21}$$

When the oily film is present, if the water concentration at the lignin particle surface is C_S, then.

$$k_x = \frac{3C_S C_{lig\ i,0}^{\frac{1}{3}}}{r_0 \beta \rho (\frac{1}{k_A} + \frac{1}{k_H})} \quad \text{Eq 22}$$

Therefore by Eq 21 and Eq 22,

$$r_d = -\frac{3C_S C_{lig\ i,0}^{\frac{1}{3}}}{r_0 \beta \rho (\frac{1}{k_A} + \frac{1}{k_H})} k_{con}\, C_{lig}^{\frac{2}{3}} \quad \text{Eq 23}$$

In the presence of the oily film and ash layer, the decomposition of the lignin particle depends on the concentration of water (C_S) on the particle surface and water consumption by the hydrolysis reaction on the particle surface.
The rate of water diffusion through the oily film when the ash layer is present can be written as follows in Eq 24. The modeling of the oily film is influenced by the method used [52].

$$r_{diffusion} = 4\pi(r + w_{Ash} + w)^2 k_M (C_B - C_{S1}) \quad \text{Eq 24}$$

Where $(r + w_{Ash} + w)$ is the radius of the oily film, C_{S1} is the water concentration in between oily film and the ash layer, and k_M is the mass transfer coefficient through the oily film. If the ash layer is not formed, then the oily film radius becomes $(r + w)$.

$$k_M = \frac{k_{Diff}}{w} \quad \text{Eq 25}$$

k_{Diff} represent the diffusion coefficient of the oily film, which is calculated by the Stokes-Einstein equation.

$$k_{Diff} = \frac{k_B T}{6\pi r_{H_2O} \mu_{Oil}} \quad \text{Eq 26}$$

Where, k_B is the Boltzmann's constant, T is the temperature (K), r_{H_2O} is the radius of the water molecule and μ_{Oil} is the viscosity of the oily film.

The rate of diffusion of water through the ash layer can be written as follows in Eq 27.

$$r_{diffusion\_ash} = 4\pi(r + w_{Ash})^2 k_{M\_ash}(C_{S1} - C_S) \quad \text{Eq 27}$$

Where $(r + w_{Ash})$ is the radius of the ash layer, and C_S is the water concentration at the surface of the lignin particle. k_{M_ash} is the mass transfer coefficient through the ash layer, which depends on the ash layer's diffusion coefficient. (Calculated by Fick's law). The rate of change of water concentration at the particle surface can be written according to the formations of oily film and ash layer. There are four different scenarios considered as follows.

$$\frac{dC_S}{dt} = rate\ wate\ of\ water\ diffusion\ through\ the\ ash\ layer - rate\ of\ water\ consumed\ by\ the\ hydrolys \quad \text{Eq 28}$$

Therefore, when

$$w > 0\ and\ w_{Ash} = 0\ ;\ \frac{dC_S}{dt} = 4\pi(r + w)^2 k_M(C_B - C_S) - 4\pi r^2 k_H C_S k_{con} \quad \text{Eq 29}$$

$$w > 0\ and\ w_{Ash} > 0\ ;\ \frac{dC_S}{dt} = r_{diffusion\_ash} - 4\pi r^2 k_H C_S k_{con} \quad \text{Eq 30}$$

$$w = 0\ and\ w_{Ash} > 0\ ;\ \frac{dC_S}{dt} = 4\pi(r + w_{Ash})^2 k_{M\_ash}(C_B - C_S) - 4\pi r^2 k_H C_S k_{con} \quad \text{Eq 31}$$

$$w = 0\ and\ w_{Ash} = 0;\ \frac{dC_S}{dt} = -4\pi r^2 k_H C_S k_{con} \quad \text{Eq 32}$$

The undissolved volume of the oily film at a given time (V_{oil})can be written as below in Eq 33,

$$V_{oil} = \frac{4}{3}(\pi(r + w_{Ash} + w)^3 - (r + w_{Ash})^3) = \frac{m_{oil}}{\rho_{oil}} \quad \text{Eq 33}$$

Here, m_{oil} is the mass of the oily film at a given time and ρ_{oil} is the density of the oily film.

When both sides are differentiated and rearranged,

$$\frac{dw}{dt} = \frac{1}{4\pi\rho_{oil}}\left(\frac{1}{r+w_{Ash}+w}\right)^2 . \frac{dm_{oil}}{dt} - \left[1 - \left(\frac{r+w_{Ash}}{r+w_{Ash}+w}\right)^2\right]\left[\frac{dr}{dt} + \frac{dw_{Ash}}{dt}\right] \quad \text{Eq 34}$$

The rate of change of mass of the oily film equals the difference in the formation and the dissolution of the oily film.

$$\frac{dm_{oil}}{dt} = r_{oil} - r_{dissolve} \quad \text{Eq 35}$$

Here, r_{oil} is the rate of formation of the oily film and $r_{dissolve}$ is the rate of dissolution of the oily film in water.
From Fick's first law,

$$r_{dissolve} = k_{M2}\ 4\pi(r + w_{Ash} + w)^2\ (C_{Sat} - C_{\infty}) \quad \text{Eq 36}$$

k_{M2} is the mass transfer coefficient to the water from the oily film. Here C_{∞} is assumed to be zero assuming that the hydrolysis products' solubility is equal to their concentration at the oily film's surface. Moreover, at some distance, the dissolution of the hydrolysis products in water is infinite.

$$k_{M2} = \frac{k_{Diff1}}{r+w_{Ash}+w} \quad \text{Eq 37}$$

The diffusivity of oily film to water (k_{Diff1}) is calculated by the Stokes-Einstein equation. Using the same method used in Eq 20, the ash layer volume can be written in Eq 38 below.

$$V_{ash} = \frac{4}{3}(\pi(r + w_{Ash})^3 - (r)^3) = \frac{m_{ash}}{\rho_{ash}} \quad \text{Eq 38}$$

Here, m_{ash} is the mass of the ash layer at a given time and ρ_{ash} is the density of the ash. When both sides are differentiated and rearranged,

$$\frac{dw_{Ash}}{dt} = \frac{1}{4\pi\rho_{ash}}\left(\frac{1}{r+w_{Ash}}\right)^2 . \frac{dm_{ash}}{dt} - \left[1 - \left(\frac{r}{r+w_{Ash}}\right)^2\right]\left[\frac{dr}{dt}\right] \quad \text{Eq 39}$$

The radius of the lignin particle at each time can be calculated by the following Eq 40.

$$r(t) = \sqrt[3]{\frac{3m_{lig}}{4\pi.\rho_{lig}}} \quad \text{Eq 40}$$

Each chemical component's theoretical values are calculated using differential equations using the backward Euler method. From the differential equations, the variation of each chemical compound's concentrations is obtained in *mol/m*^{3}. Then, each chemical compound or resultant phase is presented as a percentage of the total input.

2.4.3 Applications and limitations of the shrinking core model

A common approach to model gas-solid reactions or liquid-solid reactions is using Shrinking Core Model. Generally, a shrinking core concept can be preferred, mainly because it is relatively easy to pair with a reactor model. Nevertheless, it is not assured of replicating any experimental data reliably. The main drawback is that the number of assumptions related to the core-shell structure is not always coherent with the real-world behavior of the particle. Due to the lack of literature, particularly on the heating and fast reaction kinetics, some of the kinetic data is modified to fit reaction equations to obtain the literature's yield values. Possibly this could cause the differences in the model predictions and the experimental values.

Several assumptions are put up during the cause of the modeling sequence to reach the final results.

- The liquid-solid reaction is limited to a single interface (outer surface of the biomass particle) separating the solid substance and the product.
- A uniform particle porosity is assumed in each layer.
- Constant temperature and pressure are considered inside the particle (Article A).
- In article A, the products dissolve in water at once without forming a layer around the particle.
- The dynamic of the change of the water concentration profile is very fast compared to the change of the reaction interface position.
- Kinetics are the first-order dependent on the concentration of the water

The above assumptions can lead to some constraints of applicability of the model in a real-world scenario. The following issues must be pointed out particularly.

a) The assumption of surface reaction on the particle is the most critical assumption of the model. This assumption is not always correct in reality. Initially, suppose the particle is already porous. In that case, it does not decompose according to the shrinking core concept unless the controlling regime is diffusion: If the particle is porous, the liquid (water) reactant concentration could fall close to zero (even zero) close to the unreacted core-outer shell interface. Therefore, the water monomers cannot diffuse (and react) into the unreacted core as it is instantly consumed before approaching the core. When it comes to fast reactions relative to diffusion, water diffuses in regions where the core is already consumed. Conversely, if the kinetics overshadows intraparticle diffusion, a particle with porous properties could react homogeneously due to the radially uniform gas composition. Therefore, the shrinking core model is valid in the case of the kinetic regimes when the considered particle is initially not porous.

b) Although first-order kinetics is primarily correct, adsorption is a vital phenomenon, too: these typically reduce the apparent kinetic order.

c) Thermal homogeneity of the biomass particle is an important aspect too. For most small particles, thermal homogeneity may be a correct assumption. Nevertheless, it is also linked to the value of heat of reaction.

e) Reversible gas-solid and liquid-solid reactions are extremely common. The basis of a reversible reaction happening at the interface of the unreacted core

and the outer shell is that dependent on the relative amount of liquid component and product existing at the interface, and the interface can move towards the particle center or to the external surface depending on the reaction rate (globally positive or negative). In reality, the proposed model always believes that the water only diffuses through the solid and oil layer without reacting. Besides, this can be true for water, not the solid product, if the reaction is reversible. The solid product and the oil layer are reagents for incoming water. Therefore, there must be reactions in the layers too.

f) In Article A, no cross-reactions among chemicals produced from different model compounds are considered. Most of these chemicals exist simultaneously, so there could be several reactions among them. Nevertheless, the authors understand and accept the existence of these reactions, and the assumption of not happening these reactions are only to reduce the complexity of the calculations.

Regardless of the mentioned limitations, the shrinking core model is extensively used even for the more critical cases. Further, numerous works with reversible and even multi-step reactions can be observed in the literature. Due to its simplicity and more straightforward applicability, the shrinking core model can still be used in complex reactor and particle-related problems.

2.5 Layer model

Article B employs a layer model to investigate the intra-particle transport and sub-processes of the thermally thick spherical lignin particle. As learned from the model results, the ash layer and oily film thickness are relatively small (10^{-7}mm and 10^{-12} mm, respectively), to the lignin particle diameter (10^{-5}mm). The lignin particle is considered a single homogenous particle. The layer model is based on the pyrolysis model developed by Mehrabian et al., 2012[95]. Figure 2-10 below shows the proposed layer model for the model.

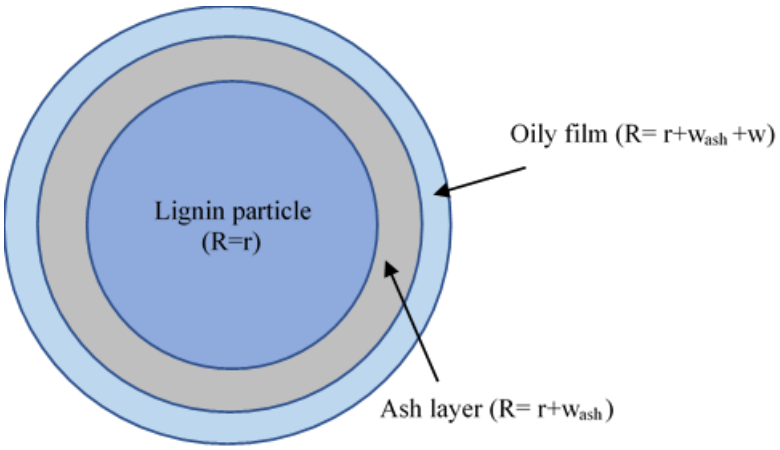

Figure 2-10:Layer model is considered for the intraparticle process.

The shrinkage of the three layers is assumed to be in the radial direction, and this is done to avoid model complexities. Further, homogeneous particle boundary conditions are assumed. Further, it is assumed that any point at a certain distance from the surface at a radial direction has the same conversion rates and temperatures[96].

During the conversion process, the mass of the particle and layer thickness are changed. When the lignin particle is being decomposed, the oily film changes its thickness according to the diffusion of water to the lignin particle surface, rate of hydrolysis, and dilution of the oily film in water. Meanwhile, the boundaries are being moved towards the center of the particle. Consequently, the density and the particle radius may change throughout the thermal conversion process of the particle.

For the lignin particle, thermal energy conversion is expressed in the following Eq 41.

$$\frac{\partial}{\partial t}\rho H = -\nabla.\rho v H - \nabla.q \qquad \text{Eq 41}$$

Where, $\frac{\partial}{\partial t}\rho H$ is the accumulation rate of enthalpy per unit volume, $\nabla.\rho v H$ represents enthalpy change by advection per unit volume, and $\nabla.q$ is the conductive heat transfer per unit volume.

For simplification, the thermal energy per unit volume is replaced by the thermal energy per layer. After that, the energy equation can be written as follows in Eq 42

$$\frac{\partial}{\partial t}\sum_c m_i H_i = \sum_{c=in} \dot{m}_{in} H_{in} - \sum_{c=out} \dot{m}_{out} H_{out} + k_{L_i} \Delta x_{0Li} \left(T_{B(i-1)} - T_{Li}\right) - k_{L_i} \Delta x_{1Li} \left(T_{Li} - T_{Bi}\right) \quad \text{Eq 42}$$

Where, $m_i H_i$ are the multiplication of mass and specific enthalpy of each component present in the layer i, $\dot{m}_{in} H_{in}$ is the multiplication of mass flow rate and specific enthalpy respectively of each component at the boundary, k_{L_i} is the thermal conductivity of layer i, Δx_{0Li} is the ratio of the area of the boundary $B(i-1)$ to half of the layer i thickness, and Δx_{1Li} is the ratio of the boundary Bi to half of the layer i thickness. Moreover T_{Li} and T_{Bi} are temperatures of the center of layer i and the temperature at the boundary Bi, respectively. (Since three layers are considered here, $i = 1,2,3$)

The equation for mass conservation of each layer is written as follows in Eq 14,

$$\frac{\partial}{\partial t}\sum_c m_i = \sum_{in} \dot{m}_{Bi-1} - \sum_{out} \dot{m}_{Bi} \quad \text{Eq 43}$$

Furthermore, from the specific heat at constant pressure,

$$dH = c_p dT \quad \text{Eq 44}$$

From Eq 42, Eq 43 and Eq 44, below Eq 45 can be obtained.

$$\sum_c m_i c_i \frac{dT_i}{dt} = \sum_{in}\left[\dot{m}_{Bi-1}(H_{B(i-1)} - H_i)\right] - \sum_{out}[\dot{m}_{Bi}(H_i - H_{Bi})] + k_{L_i} \Delta x_{0Li} \left(T_{B(i-1)} - T_{Li}\right) - k_{L_i} \Delta x_{1Li} \left(T_{Li} - T_{Bi}\right) \quad \text{Eq 45}$$

Enthalpy of each component at each boundary and each layer is estimated by the following Eq 46,

$$H_i(T) = \Delta H_f^{\circ} + \int_{T_{ref}}^{T} c_p dT \quad \text{Eq 46}$$

In this equation, ΔH_f° signify the Standard enthalpy of formation and c_p denotes specific heat capacity.
The boundary temperatures are computed by utilizing the energy balance at each boundary.

$$k_{L_i}\Delta x_{1Li}\,(\,T_{Li} - T_{Bi}) - k_{L_{i+1}}\Delta x_{0Li+1}\,(T_{Bi} - T_{L(i+1)}\,) = \sum_{c=in}\dot{m}_{Bi}H_{Bi} - \sum_{c=out}\dot{m}_{Bi}H_{Bi} \quad \text{Eq 47}$$

In the proposed model, reactions are taken place on the particle surface. Thus a resultant component could leave boundary instead of the components which entered a specific boundary. The right-hand side of Eq 47 corresponds to the enthalpy difference of products and reactants of the reactions. The mass flow rate (Eq 48) of each component is dependent on the reaction rates $(r)_i$ and stoichiometry (η_i) of each reaction.

$$\dot{m}_{Bi} = \sum_{c=out} r_i \eta_i \quad \text{Eq 48}$$

2.6 Kinetic models

In Article A, cellulose, lignin, and hemicellulose are treated differently in three different kinetic reaction schemes, whereas is in Article B, an improved version of the lignin kinetic reaction scheme from Article A is used. This section discusses the three kinetic reaction schemes used in Articles A and B.

The reaction mechanism used in Article A for Cellulose liquefaction is inspired by the reaction mechanisms proposed by Cantero et al. [97], Minowa et al. [91], and Kamio et al. [77]. According to Kamio et al. [77], Cantero et al. [97], Sasaki et al. [98–100], and Minowa et al. [91], water-soluble intermediates are formed from the hydrolysis of cellulose. Then the end products of the

liquefaction (water-soluble products (aqueous phase), biocrude, gas, and char.) are formed through further hydrolysis, polymerization, dehydration, and decomposition of the intermediates. The secondary and primary char is challenging to differentiate and quantify experimentally, both char components are taken as a lump component in the model. Below figure 2-11 shows the reaction mechanism used for the cellulose liquefaction process.

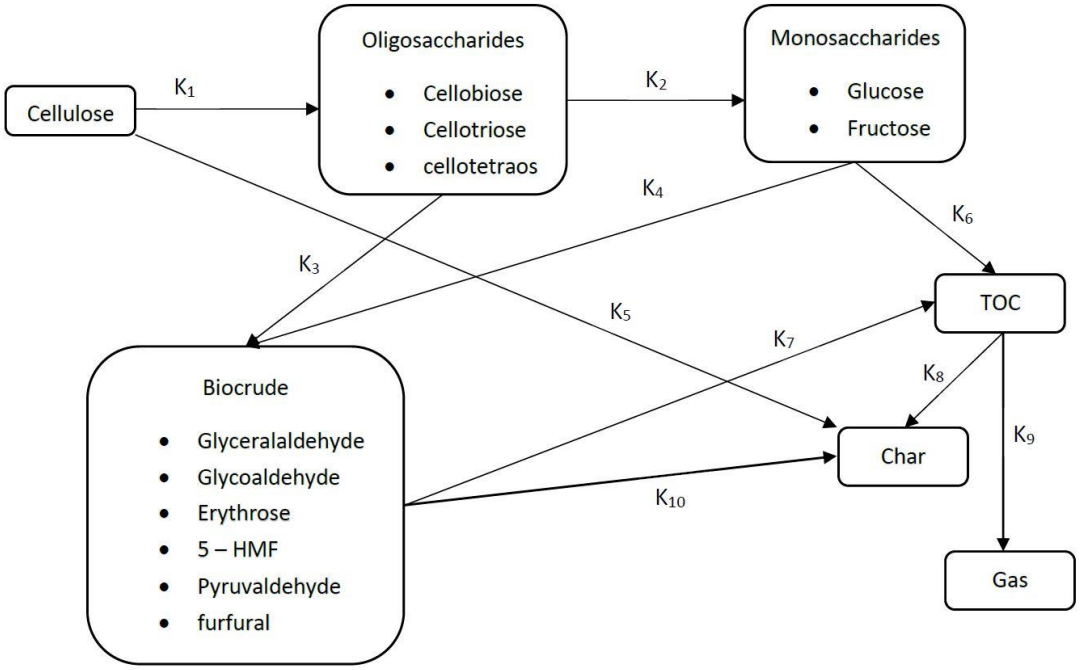

Figure 2-11: Reaction mechanism used for cellulose liquefaction

The lignin reaction mechanism is centered around the kinetic study and reaction mechanism proposed by Yong and Matsumara [92] and Fang et al.[101], Zhang et al.[102], Forchheim et al.[103], and Arturi et al.[104]. The proposed reaction scheme consists of a gas phase, char, an aqueous phase with TOC, and a biocrude phase consisting of phenols, Aromatics, Guaiacol. Some hydrolysis products decomposed into tertiary components with further reactions, which then contributed to the model.

The shrinking core model relates to the initial phase's primary or heterogeneous hydrolysis reactions. Then the secondary decomposition, polymerization, and dehydration reactions are modeled using a conventional kinetic model, which is not observed with other models using the shrinking core concept. Below, figure 2-12 shows the proposed reaction scheme for lignin during the liq-

uefaction process. The required kinetic parameters for the lignin liquefaction model are taken from the literature[92,102,103,105,106].

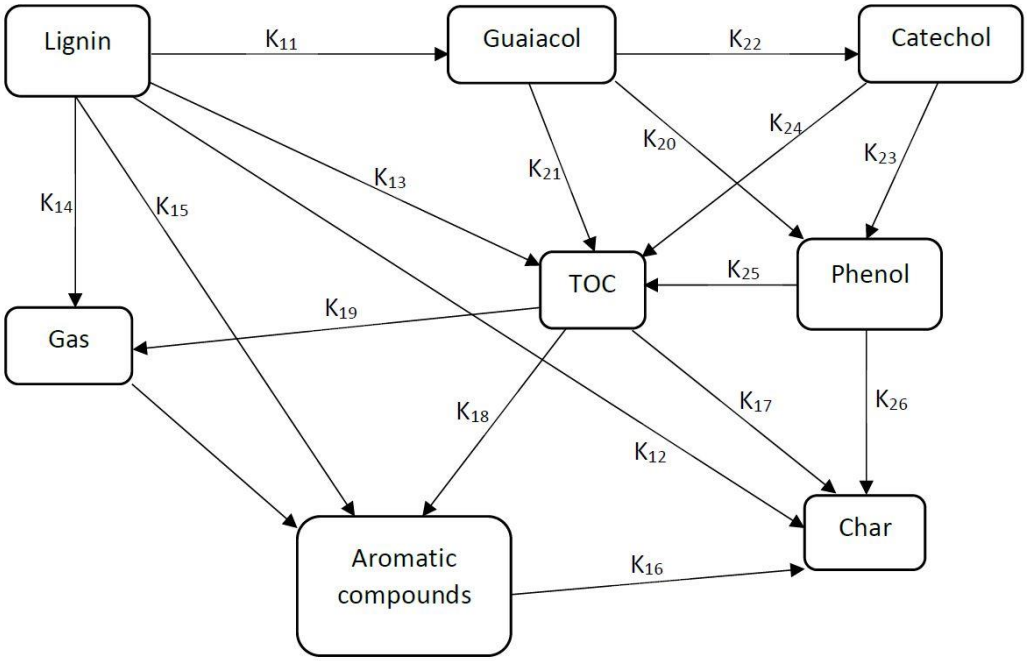

Figure 2-12: Reaction mechanism used for lignin liquefaction in Article A

For Article B, the lignin liquefaction model developed for Article A is used with added chemicals and reactions. In article B, M-cresol, O-cresol, and related reactions are added as components of the biocrude phase. Figure 2-13 shows the reaction scheme used to model the lignin liquefaction process in Article B.

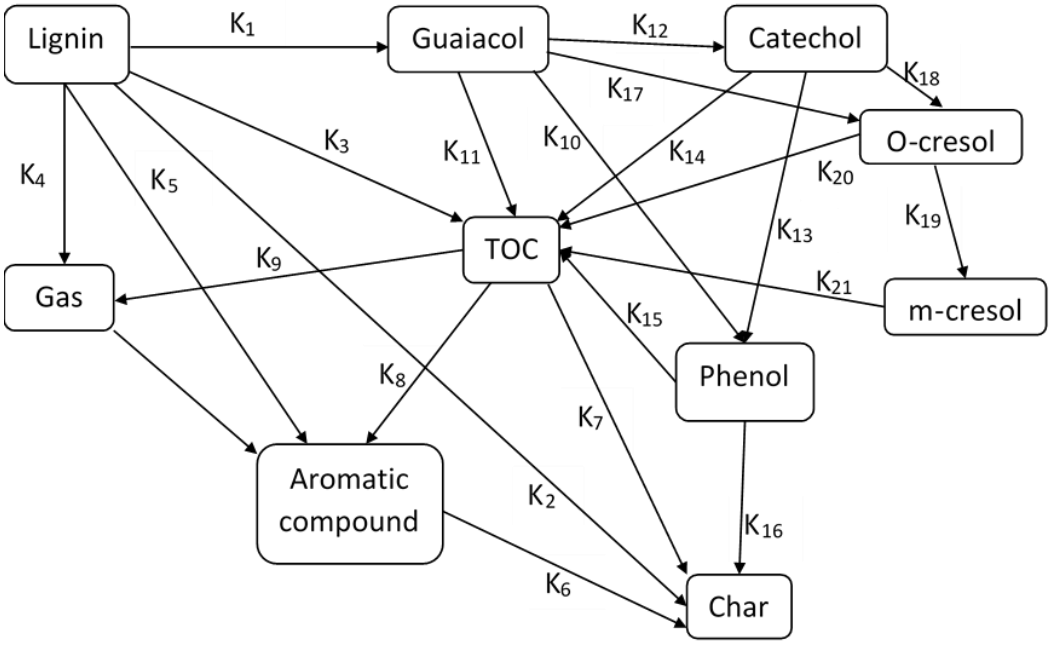

Figure 2-13: Reaction mechanism used for lignin liquefaction in Article B

The proposed hemicellulose liquefaction model is mainly built on the work done by Pronyk and Mazza and Pinkowska et al.[107,108]. The monophasic reaction mechanism for hemicellulose hydrolysis proposed by Pronyk and Mazza[107] is used to develop this model. According to the proposed model, hemicellulose is hydrolyzed into the intermittent product of Xylo-oligomers and then to xylose. Figure 2-14 shows that the hydrolysis products are decomposed into derivatives, such as furfural. In this model, furfural is used as the final derivative from the liquefaction due to the lack of kinetic data on other chemicals produced in hemicellulose liquefaction. Required kinetic parameters are taken from the literature[107–110,110].

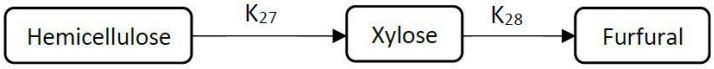

Figure 2-14: Reaction mechanism used for hemicellulose liquefaction in Article A

2.7 Statistical methods

Articles A and B are based on a mathematical model of hydrothermal liquefaction of a single particle wood particle and a lignin particle. The model code is written in MATLAB, and the differential equations developed in the mathematical model are solved and discretized in MATLAB using the backward Euler method. The model predictions are validated using the experimental data and coefficient of determination (R^2).

Article D is based on a statistical analysis of co-liquefaction yields of lignin and laminaria saccharina. The interconnections illustrating the relationships between the main independent parameters and the yields of the products are investigated. The response surface methodology (RSM) is used in the article where the Box Behnken Design (BBD) strategy is used to optimize the biocrude yield and minimize the char yield. BBD is a multi-level and multifactorial design where in this study, three levels (-1, 0, 1) and three factors (X_1, X_2, X_3) are used with three replicates. The BBD consists of a set of points that are spread at the midpoint of each edge of the multidimensional cube specified by the levels and a center point at the cube's center, as shown in figures 2-15 below.

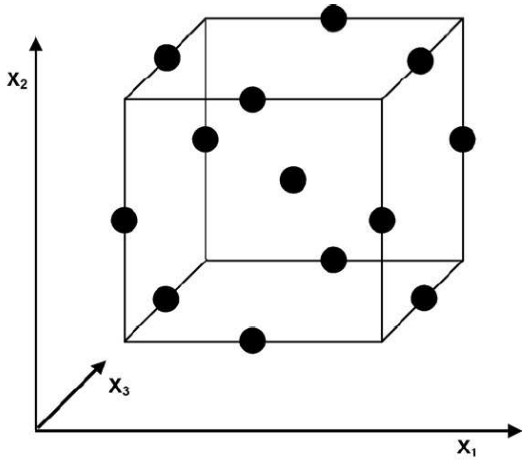

Figure 2-15:Box-Behnken experimental design with three factors[111]

In the experimental phase, three independent variables are selected as factors, while two yield values from the experiments are chosen as responses. The independent variables are prescribed into three different levels as +1, 0, and -1,

which correspond to the minimum level, medium level, and maximum level. These levels are generally decided according to initial experiments and tests. Fifteen runs (different combinations of independent variables) are then designated randomly by the Minitab 17.1.0 software (Minitab Ltd., Coventry, UK) with a minimum bias as mentioned before, and the center point is triplicated to be able to approximate the pure error. The yield value of each response for the designated runs is experimentally acquired. Independent variables and responses are then analyzed using the software. A polynomial quadratic equation is used in Eq 49 to fit the relationship between the variables and the responses.

$$Y = a_0 + \sum_{i=1}^{4} a_i X_i + \sum_{i=1}^{4} a_{ii} X_i^2 + \sum_{i=1}^{4} \sum_{i=j} a_{ij} X_i X_j + \varepsilon \qquad \text{Eq 49}$$

Where Y is the measured response value related to each factor level combination, α_0 is the intercept coefficient, α_i, αii, and α_{ij} are the regression coefficients calculated from the obtained experimental values of Y, X_i and X_j are the levels of independent variables and ε represent the error of the model. The regression analysis and the analysis of variance (ANOVA) are performed. A Fisher`s F-test at a confidence level of 95% is completed to inspect the statistical significance of the regression coefficients. The lack of fit test, coefficient of determination (R^2), and adjusted coefficients of determination (R^2_{adj}) are examined to evaluate the suitability of the quadratic models. Derringer's desirability function is accompanied to perform the RSM. When optimizing a few responses simultaneously, Derringer's desirability function is reliable and valuable. In Derringer's desirability function, each response (Y_i) is transformed into a dimensionless function (individual desirability function) (d_i). This newly produced dimensionless function ranges from 0 to 1, depending on the degree of optimization of the response (Y_i). In the most desirable scenario, d_i goes close to 1 and 0 at the least desirable case.

3 Research contributions

This chapter introduces the main contributions that characterize this thesis work. They can be categorized into three clear sections based on the results acquired from the experiments in many published and submitted articles. These research articles are discussed and presented briefly, underlining their relevance and significance regarding the associated topic. The sequence, which the topics and articles are presented, follows a logical sequence formed to improve the understanding of the overall research process. Furthermore, the components necessary to follow through the Discussion chapter (see Chapter 4) are supplied. The complete versions of the articles are accessible in the Appendices. Figure 3-1 below shows a visual representation of the research papers and the book chapter with the primary investigations and their weight percentage to the total Ph.D. work.

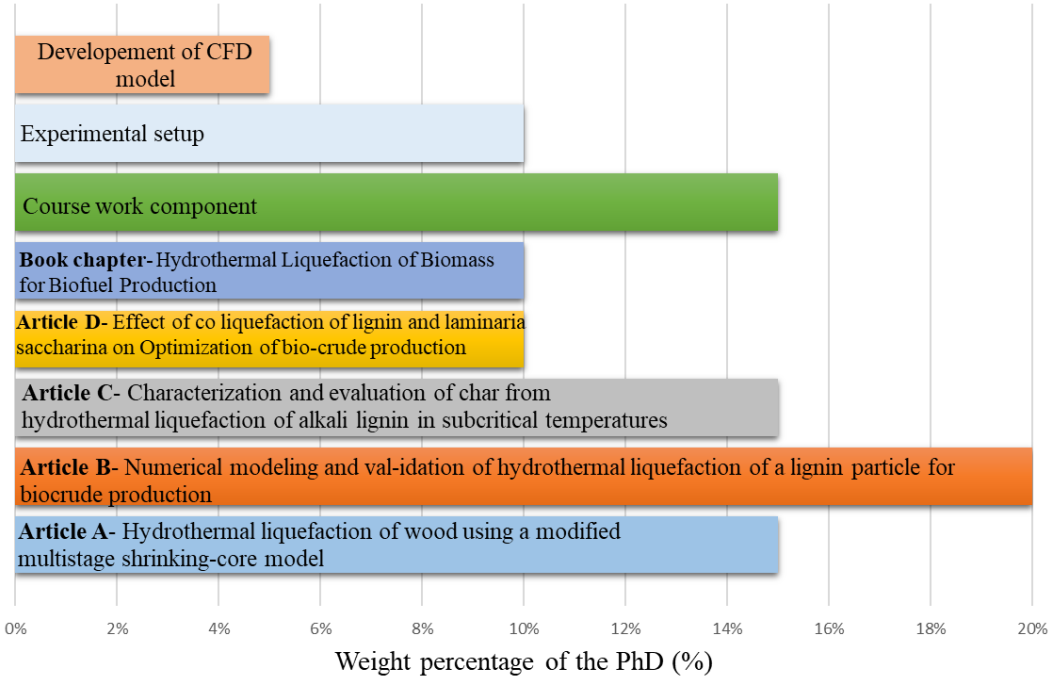

Figure 3-1 Visual representation of the research papers with the main investigation

3.1 Single-particle decomposition mechanism

The first stage of the research explored the possibility of modeling the decomposition of biomass particles during the HTL process. The shrinking core mechanism is used as the preferred decomposition mechanism. Therefore, the decomposition is assumed to have happened only in the radial direction. Further, the reactions are supposed to happen only on the particle surface. In addition to the hydrolysis reaction and drying of the particle, a kinetic model is employed to model the secondary and tertiary reaction scheme taking part in the water phase. The models are developed only to work in the subcritical temperatures close to the critical point. Therefore, the temperature values from 573K to 647 K are considered.

In article A, a wood particle is used as the biomass particle. The basis of the model is the radial decomposition of the particle and the cumulative liquefaction effect of each model compound (cellulose, hemicellulose, and lignin) on the overall liquefaction effect. The variation of biocrude, char, aqueous, and gas phases are investigated against several independent variables. During this work, it was observed that the liquefaction of the hemicellulose occurred at lower temperatures than the considered temperature range. Further, the cumulative liquefaction effect of the model compounds could not match the liquefaction results of wood liquefaction. The model displayed many paths to improving, and new concepts can be added. Nevertheless, the model showed numerous positives towards showing a credible path for developing a reliable mathematical model for liquefaction.

With the findings of Article A, Article B is developed assuming a lignin particle. Nevertheless, the modeling process addressed more profound attributes of the liquefaction mechanism by modeling the formation of an oily film and an inorganic layer (ash) around the particle during the liquefaction process. These layers are supposed to affect the overall liquefaction mechanism considerably. Further, the intraparticle behavior during the liquefaction is also simulated, and the actual particle surface temperatures and particle center temperatures are investigated. The kinetic model attached to the decomposition model simulated the further repolymerization, condensation, and decomposition reactions in the water phase.

Additionally, variation of selected main chemicals in the biocrude phase of lignin liquefaction is studied with several independent variables. The model displayed some fascinating results on the behavior of the oily film and the inorganic film around the particle and their possible impact on the liquefaction process. Most of these findings are difficult to measure practically due to the extreme conditions and fast kinetics of the HTL process.

3.1.1 Article A

This work is focused on developing a particle decomposition model using the shrinking core method. Then the different decomposition behaviors are investigated with different operating conditions to find better conditions for better biocrude yields. Further, the motivation is to investigate the different behaviors of each model compound and their contribution towards the widespread liquefaction at different conditions.

The decomposition is assumed to happen only in the radial direction, and the hydrolysis reaction is considered to happen on the particle surface. Apart from the particle decomposition mechanism, a kinetic model is employed to model the repolymerization, condensation, and decomposition reactions outside the particle. The wood particle is considered a mix of cellulose, hemicellulose, and lignin, where each model compound is treated separately in three different decomposition and drying reaction regimes. Then the cumulative liquefaction effect of the model compounds is taken to develop the overall liquefaction model.

No inter reactions are considered among chemicals produced from different model compounds in this model. Further, it is assumed, the distribution of model compounds in wood continues. Variation of the behavior of four phases from liquefaction (biocrude, char, aqueous, and gas) are investigated against several independent variables. The validation of the model is carried out using data available in the literature. The graphical abstract of the article is shown in figure 3-2 below.

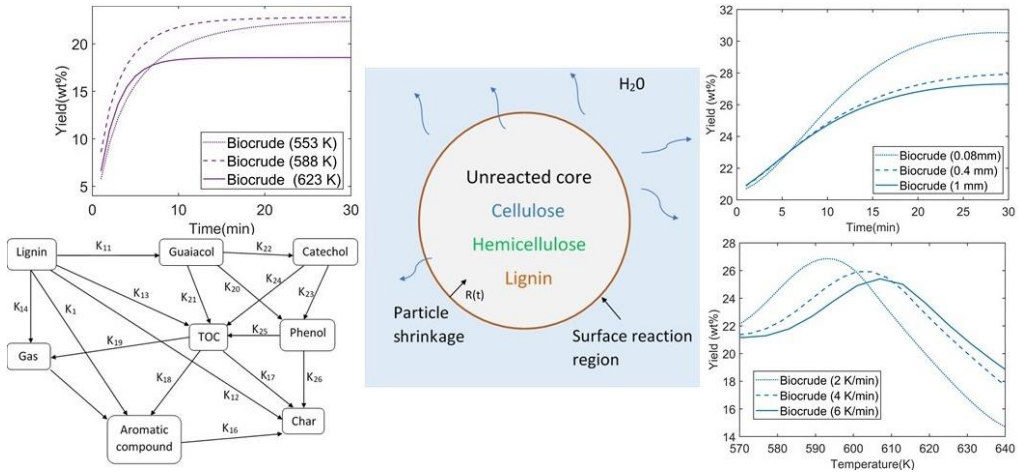

Figure 3-2:Graphical abstract of Article A Top left shows the biocrude phase variation at different operating temperatures, bottom left shows the reaction scheme used, the middle figure shows the particle decomposition mechanism, top right biocrude phase variation with different particle size and bottom-right biocrude phase variation with different heating rates.

During the model development phase, it is understood that the hemicellulose hydrolyses at a lower temperature than the considered temperature range in the study. When the system is heated up to the considered temperature, hemicellulose is already hydrolyzed and added to the system. Therefore, in the presented model, the hemicellulose liquefaction model is briefly modeled, and it was decided to work on it separately due to the complex characteristics of the hemicellulose liquefaction process. Nevertheless, cellulose and lignin liquefaction are modeled and studied in the considered temperature range.

The single-particle system is modeled and then tested with different independent variables. First, the variation of yield values is investigated with different operating temperature values, and 553 K, 588 K, and 623 K are used as the operating temperature values. Both Cellulose and lignin showed decreased biocrude yield with increasing operating temperature, while char and gas phases showed the opposite.

Three different heating rates (2 K/min,4 K/min,6 K/min) are used for the analysis.

Lignin showed a relatively different behavior to cellulose in this regard. Although the decomposition of lignin and evaluation of yield values showed

similar behavior to cellulose at the lower temperature range, yield values became almost similar close to the critical point for all the heating rates.
Cellulose hydrolysis shows a significant impact on the overall wood liquefaction behavior. Char yields of the cellulose hydrolysis are not affected significantly by the heating rates. After 600K, wood liquefaction shows higher char and gas yields of 47% and 20%, respectively, with lower heating rates. For maximum operating temperatures, over 600K TOC and biocrude yields tend to increase. Therefore, it could be observed that the heating rates produce higher biocrude yields at shorter residence times. This is an interesting observation of fast liquefaction where shorter residence times are used. The diameter of the biomass particle has shown a definite impact on the hydrolysis rate of both Cellulose and Lignin.

A limited number of reactions and chemical compounds are employed in the model. Furthermore, kinetic data used in the model are obtained from the literature from various studies under various process conditions. The experimental studies used for validation are operated with various process conditions and different workup methods. Therefore, in the validation plots, the model predictions for wood are underpredicted or over predicted most of the time. Furthermore, one of the main ideas of developing this model is to observe the difference in the cumulative liquefaction effect of main wood components against actual wood liquefaction. Thus, it is evident that there is an enormous gap between wood liquefaction and modeling wood liquefaction as a cumulative effect of the wood component liquefaction.

3.1.2 Article B

Article B is an extension of Article A. Besides, here, the focus is given to lignin liquefaction and developing a comprehensive model to simulate liquefaction. Therefore, several aspects are given more profound attention. The particle decomposition is modeled similarly to Article A, where a shrinking core model is used. Further, a similar kinetic model to Article A is used here, with precise kinetic data for six different components of the biocrude phase (Aromatic hydrocarbons, guaiacol, catechol, phenol, O-cresol, and M-cresol). In this model, the formation of an oily film and an inorganic layer (ash) around

the particle surface during liquefaction is modeled. Formation of such layers are proposed in the literature[52,72]

Despite having much research and many models developed with only kinetic schemes, there is a void in modeling liquefaction as a complete process. Thus, it is scarce to find details on the shrinkage of the particle, mass transfer from the particle, and the temperature behavior inside the particle during the liquefaction process. Furthermore, the formation of oily film and ash layer is yet to be experimentally studied. Therefore, modeling the formation of the oily film and ash layer could clarify the liquefaction behavior and produce better explanations for particle decomposition behaviors at different process conditions. Below, figure 3-3 shows a sequential diagram of the modeling process of the mathematical model.

The model presented in Article B consists of four main sections. They are liquefaction of lignin particle, oily film, ash layer formation behavior during the liquefaction, kinetic model to model other liquefaction processes of initial products, and the layer model for the intraparticle processes.

In the proposed model, several aspects such as transport of water to the surface of the particle, diffusion through the ash layer and oily film, adsorption on the particle surface, heterogeneous reaction, desorption of the products from the particle, diffusion of the products through the ash layer, and transport of products back to ambient through the dissolution of products in water are considered.

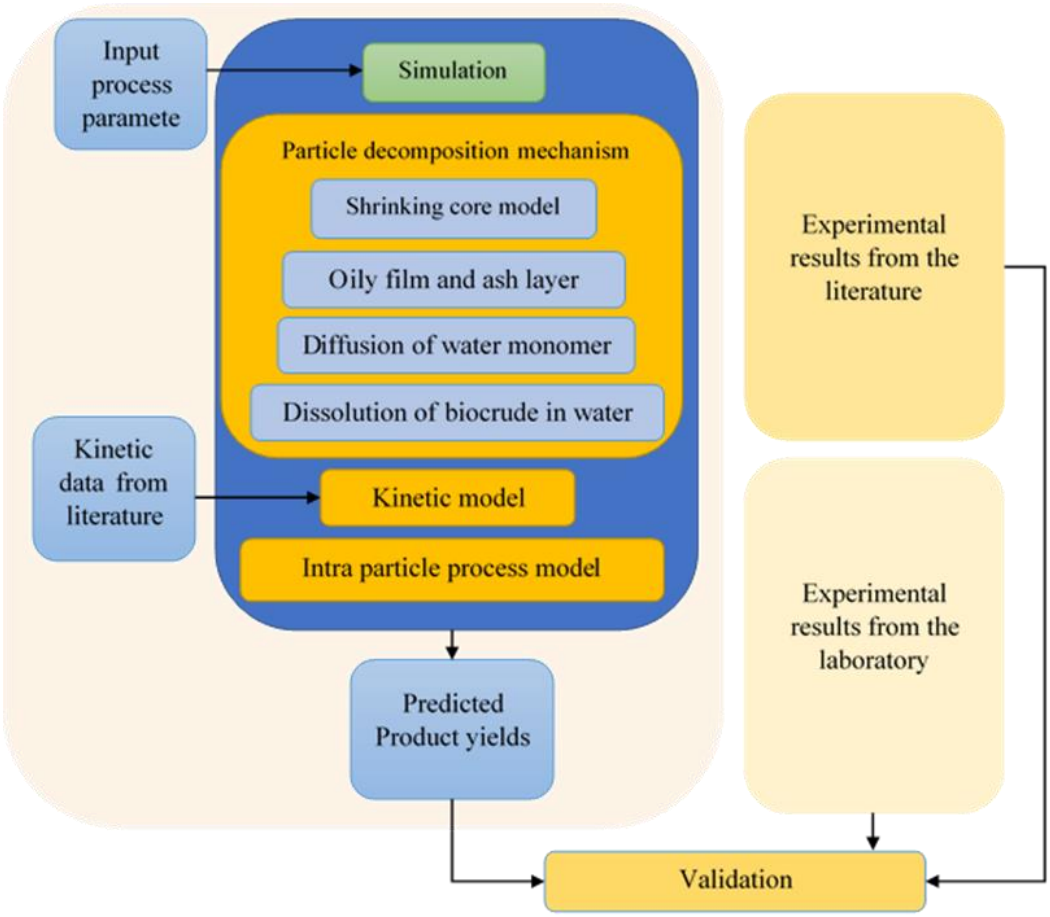

Figure 3-3:Schematic diagram of the method used for developing the model

With the layer model, the intraparticle process is modeled. Therefore, the particle's temperature behavior at the particle's surface and the mass transport from the particle to the system are investigated. Besides, the biocrude phase is vital as it is considered a mix of six different chemicals. With this model, each chemical component's variation can be investigated. Therefore, this model gives a better insight into lignin liquefaction. Figure 3-4 shows the Layer model considered for the intraparticle process.

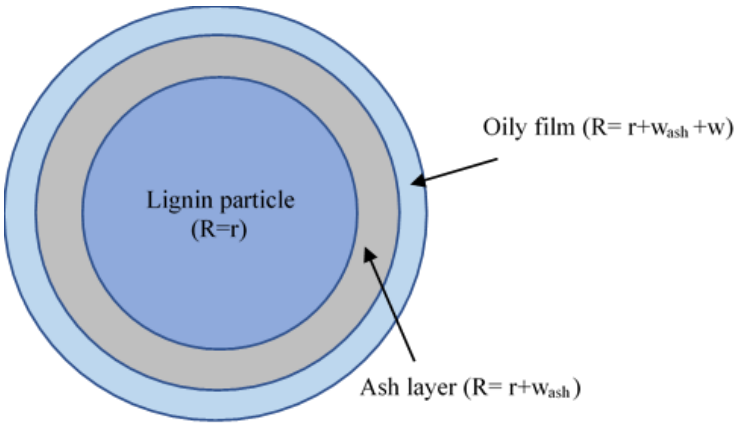

Figure 3-4:Layer model is considered for the intraparticle process.

At 573K with a particle size of 0.08 mm, aromatic hydrocarbons show the maximum yield of 0.23 w/w_0. Slower heating rates have produced better yields with all the chemical components. For longer residence times and close to the critical point, heating rates reduce the yields. The oily film and ash layer shows a similar formation process and behavior at different process conditions. Oily film and inorganic (ash) layer behavior at different operating temperatures is shown below in Figures 3-5.

According to Figures 3-5, oily film thickness increases dramatically with higher operating temperatures and dissolves quickly. The rapid increase of the oily film can be justified by the initial rapid growth of aromatic hydrocarbons with higher temperatures. In another way, the oily film's behavior might impact the product yields too. Similarly, the initial rapid increase with the ash layer could be due to the fast initial hydrolysis of lignin under unobstructed water monomer arrival to the particle surface. Both the oily film and the ash layer are relatively thinner with lower temperatures, which helps both water and the products quickly diffuse through them. More water goes through to the lignin particle surface, which allows hydrolysis.

The dissolution of the ash layer depends on the oily film thickness. Moreover, thinner oily film and ash layer could allow guaiacol to quickly come out to the water to complete the secondary decomposition and produce more secondary products. With higher operating temperatures, due to the rapid increase of the oily film and the ash layer, water diffusion is hampered, leading to reduced

lignin's initial hydrolysis. Potentially, this could impact reduced yields of bi-ocrude at higher operating temperatures. Therefore, a further study of the formation of oily film and the ash layer can be significant.

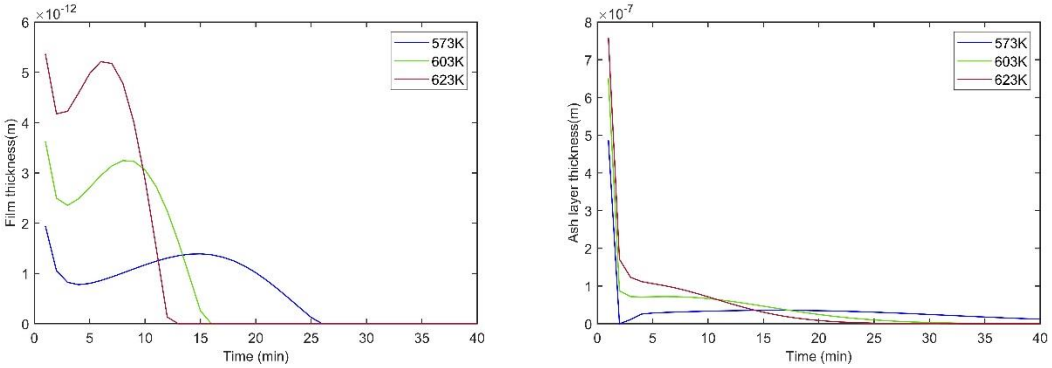

a) b)

Figure 3-5:Impact of temperature on oily film and ash layer formation with a lignin particle radius of 0.08mm at 573K, 603K, and 623Ka) Oily film b) Ash layer

According to the model predictions, when a particle radius is of the power of 10^{-5} m is utilized, the oily film thickness and ash layer thickness are of the power of 10^{-12} m and 10^{-7} m, respectively. Hence, there might not be a significant impact of oily film and ash layer thickness on the liquefaction. Nevertheless, the actual impact of the thickness of the oily film and ash layer is yet to be tested experimentally.

Some of the model input values can differ from actual liquefaction conditions and could change the results since the availability of data used for this model is limited and bears a high uncertainty in the yields due to the different workup processes.

3.2 Characterization and evolution of HTL char

This article focuses on the characterization and the evolution of char produced from HTL of alkali lignin in subcritical temperatures. The motivation of this article is to figure out how the char phase is progressed chemically, structurally, thermally, and physically through the temperature and residence time in-

crease. The char is examined for chemical, structural, thermal, and surface changes.

3.2.1 Article C

The motivation to study char broadly is to explore the possibility of utilizing HTL char effectively. It could be either in porous carbon production, as a fertilizer for agricultural purposes, or using it as a carbon capture material. Nevertheless, this study evaluates HTL char properties and characteristics with different operating temperatures and residence times. Further, the secondary motivation is to understand the char production mechanism through different characterizations. This study investigates the morphological, surface, thermal, and chemical characteristics of HTL char from lignin liquefaction. The functional groups present in char are studied with Fourier transform infrared spectroscopy (FTIR), where the structural and surface behavior is studied with scanning electron microscopy (SEM). Thermogravimetric (TGA) analysis is used to study the thermal characteristics, while char's surface and pore distribution are determined using the nitrogen adsorption/desorption method. The chars are produced with different HTL operating temperatures and residence times to study and understand the different char-derived attributes with varying process parameters.

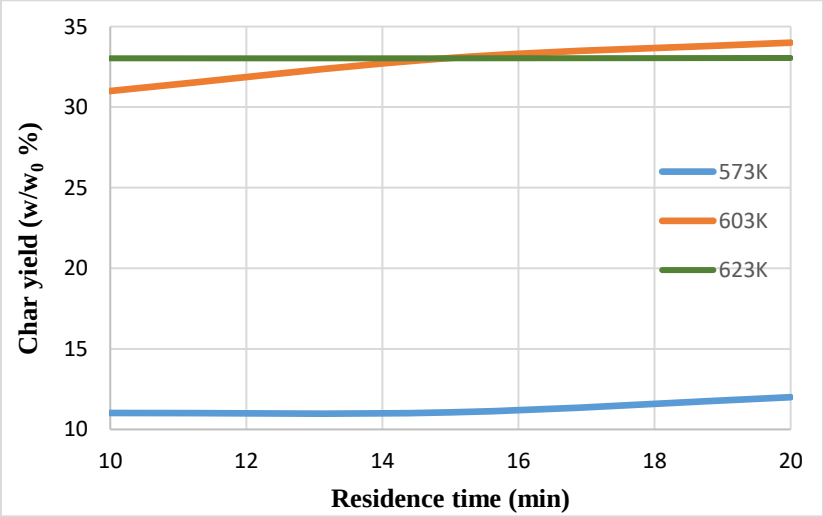

Figure 3-6:Char yield variation

Char yield seemed to be impacted by the operating temperature, where the impact of the residence time is almost negligible in the range of temperature and residence time values used. Nevertheless, both increasing operating temperature and residence time positively impacted the nitrogen content of the chars. The char yield variation with different temperatures and residence times are shown above in figure 3-6

The FTIR analysis brought out several interesting observations. Chars became aromatic with an increased operating temperature, significantly improving the aromatic ring and the carbonyl group. Meanwhile, the aliphatic groups are seen to vanish gradually. Residence times seemed to have the same effect as temperature even though the impact is considerably low. However, the carbonyl group demonstrated a contradictive behavior with temperature and residence time, where it indicated an increase with increasing operating temperature, while a decrease is shown with the longer residence times. Figure 3-7 below shows the FTIR spectra of char from different operating temperatures and residence times.

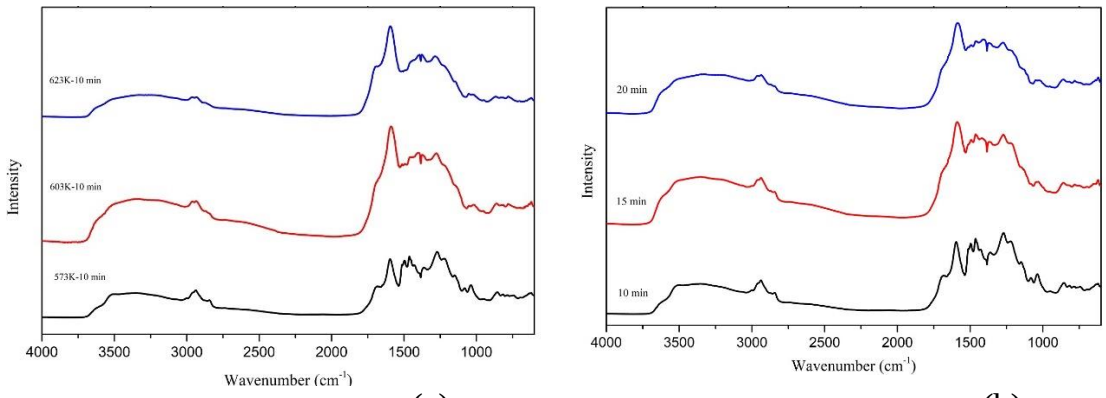

Figure 3-7: FTIR spectra of chars from (a) different temperatures with a 10 min residence time (b) different residence times at 573 K.

Increasing operating temperatures and longer residence times formed char with higher thermal stability, where at 573K, the residence time significantly affected the thermal stability. Interesting conclusions can be made when FTIR analysis conclusions are mapped with the thermal behavior. Chars become

aromatic with increasing temperature and residence time. Therefore, the bonds in the chemicals in the char get strengthened due to the aromatic rings. Ultimately these aromatic bonds could bolster the stability of the chars. Therefore, the creation of more stable structures at higher operating temperatures and longer residence times can be detected through these observations. A possible reaction pathway of char formation is suggested with all the characterizations. The cleavage of the weak bonds can be seen at lower operating temperatures, where polymerization is detected at both higher temperatures and longer residence times. Char is mainly created due to the carbonization process, and longer residence time creates more polyaromatic rings by aiding further carbonization. Figure 3-8 below demonstrates the proposed reaction mechanism for char formation from lignin HTL.

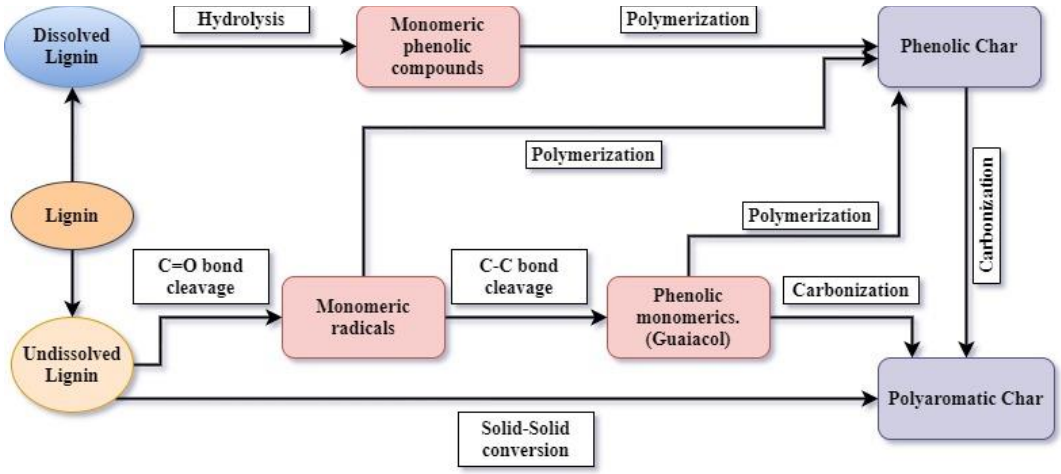

Figure 3-8: Reaction mechanism for char formation from lignin HTL.

3.3 Co-liquefaction of lignin and laminaria saccharina

Lignin is the foremost natural source of aromatic compounds[104]. Process lignin can be used effectively for producing biocrude or biofuel with hydrothermal liquefaction, and it has been studied numerous times. Lignin is a significant by-product of the paper and pulp industry, and therefore lignin is mainly used for energy recovery in the mills [112]. Primarily, lignin-based research focuses on value-added chemicals and high-performance materi-

als[113–115] production. Nevertheless, lignin is studied as a source for biofuel production through HTL, showing promising signs [27,92,106,116].
Macroalgae is a promising feedstock for biofuel production mainly due to their high conversion rate, flexibility, and environmental friendliness[15,86,117,118]. According to many studies, macroalgae can produce relatively high biocrude yields[86]. Macroalgae produce high biocrude yields when it has high lipid content. Due to the high protein content of macroalgae, high nitrogen content in biocrude is observed where can be turned into a disadvantage for the fuels. Further, in general, HTL of lignin produced relatively high amounts of char than seaweed.

This study aims to optimize the liquid fuel production of co-liquefaction of laminaria saccharina and lignin. The statistical method response surface method with a Box Behnken Design (BBD) is employed to design, verify the model, and perform the surface analysis. Additionally, the operating parameters that produce better bio-oil yields and lower char yields of HTL of blended feedstocks are optimized. The FTIR analysis is used to analyze the functional groups of the biocrude.

3.3.1 Article D

In this study, the independent variables of the HTL process, such as operating temperature (X_1), residence time (X_2), and feedstock blending ratio (X_3), are considered the independent factors of the Box Behnken Design (BBD) where biocrude yield (Y_1) and char yield (Y_2) from co-liquefaction of lignin and laminaria saccharina are considered the responses. The design of experiment (DOE) software-Minitab 17.1.0. is used to optimize the factors. Using the theories of BBD, factors, levels, and responses and the experimental scheme are specified. . In all the studies, each independent factor is set into three levels (+1, 0, and −1) which correspond to the minimum level, medium level, and maximum level respectively. The considered independent factors and their preferred levels are shown below in table 3-1.

Table 3-1:Independant factors used in the experimental design and their levels

Independent factors	Levels		
	-1	0	1
Operating temperature (X_1)	573K	603K	633K
Residence time (X_2)	10min	15min	20min
Blending ratio (X_3)	0.2	0.4	0.6

The RSM is completed in three different stages. Initially, the yields are optimized when the feedstocks are used separately. First, the behavior of biocrude and char yields from HTL of lignin is studied where the same method is followed with laminaria saccharina. Then, the optimization of co-liquefaction of two feedstocks is performed. The levels of all process factors are presumed based on results obtained from preliminary tests and studies. The optimized bio-oil yields of HTL of lignin and laminaria saccharina as different feedstocks based are shown in table 3-2.

Table 3-2:The optimized bio-oil yield of HTL of lignin and laminaria saccharina based on the DOE

Feedstock	Residence time (min)	Temperature (K)	Oil yield (w/w_0)
Lignin	17.27	573	0.2801
Laminaria Saccharina	10	627.55	0.2782

The following polynomial quadratic equations (Eq 50 and Eq 51) are developed and fitted to correlate the connection between the selected three variables and the two responses, respectively.

$$Biocrude = -5.599 + 0.02048\ X_1 + 0.01677\ X_2 - 1.530\ X_3 - 0.000018\ X_1^2 + 0.000006\ X_2^2 - 0.1929\ X_3^2 - 0.000025\ X_1 * X_2 + 0.003042\ X_1 * X_3 - 0.00721\ X_2 * X_3 \quad \text{Eq 50}$$

$$Char = -22.58 + 0.0713\ X_1 + 0.0342\ X_2 + 4.672\ X_3 - 0.000056\ X_1^2 - 0.000453\ X_2^2 - 0.082\ X_3^2 - 0.000028\ X_1 * X_2 - 0.00755\ X_1 * X_3 - 0.01396\ X_2 * X_3 \quad \text{Eq 51}$$

In this study, two different responses are being monitored. Thus, multi-response optimization is employed to evaluate the optimal values of the responses to the three independent factors. Derringer's desirability function-based method for multiparameter optimization is used[119].

Per Derringer's desirability function approach, the optimum process conditions are the temperature of 573K, the residence time of 20min, and the blending ratio of 0.2. Under the optimum process conditions, the predicted bio-oil yield and char yield are 0.2513w/w_0 and 0.1791w/w_0, respectively. The composite desirability value close to 1 (0.8959) is observed, demonstrating that all responses achieve good results. Below, figure 3-9 shows the Plots for simultaneous optimization of operating variables (Temperature, residence time, and blending ratio).

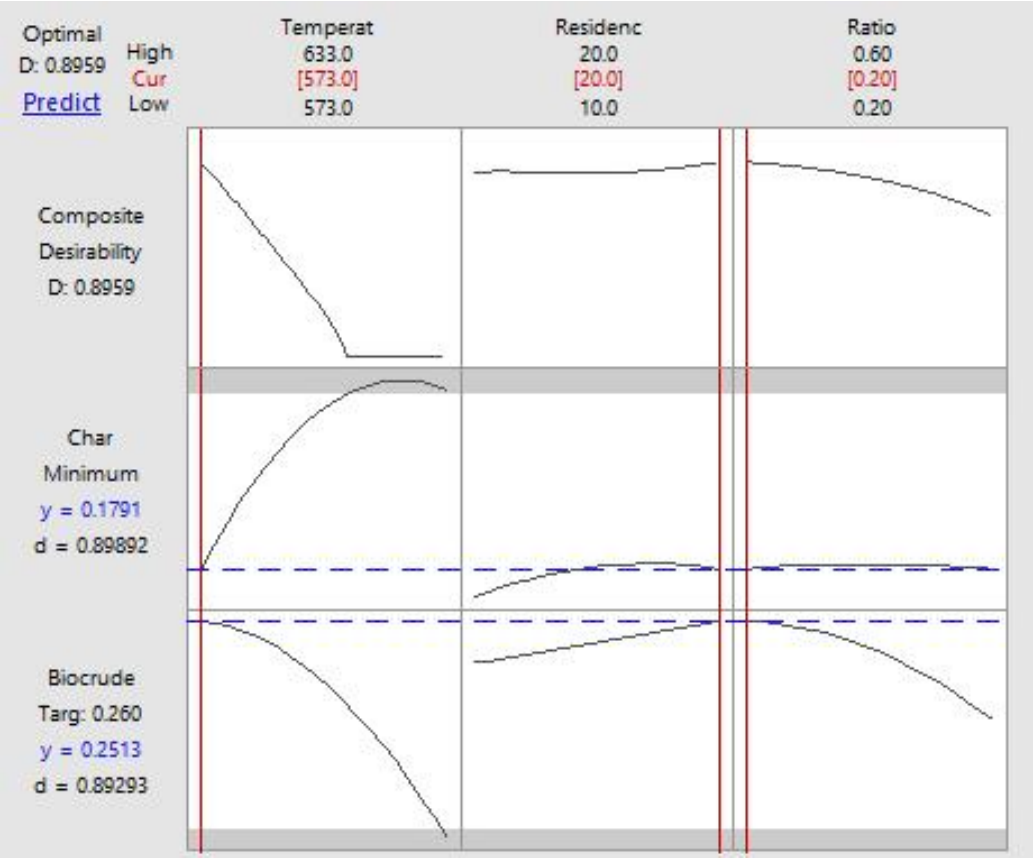

Figure 3-9:Plots for simultaneous optimization of operating variables (Temperature, residence time, and blending ratio)

Once the optimum values are obtained, the predicted and experimental values are compared to examine the actual deviation of the yield values and determine the model's accuracy. Table 3-3 shows the predicted and experimental values at the optimum process conditions.

Table 3-3:The predicted and the experimental values of the responses under the optimum process conditions.

Response	Predicted value (w/w_0)	Experimental value	Deviation
Bio-oil yield	0.2513	0.26 ± 0.03	3.34%
Char yield	0.1791	0.19 ± 0.07	5.73%

In this study, one of the motivations is to investigate the positive effect of the co-liquefaction itself on the yield values. Therefore to determine that the synergistic effect (SE) is measured. The principle of SE is to compare the actual and the theoretical yields of co-liquefaction. For the SE analysis, biocrude yields obtained at 45 different operating conditions are used. Five different blends of lignin and laminaria saccharina (Laminaria saccharina blending ratio of 0, 0.2, 0.4, 0.6, and 1) are used for the analysis.

With a blending ratio of 0.2 and at 603K and with 10 min residence time, the biocrude yield is higher than the theoretical bio-oil yield value. The recorded positive synergistic effect is 0.019 w/w_0. Although 0.019 w/w_0 is not a significant positive synergistic value numerically, this is proof that the synergistic effect is visible even at milder operating conditions. Furthermore, according to the SE values variation shown in Figure 3-10 below, the strengthening of the synergistic effect continues to be reinforced as the operating conditions get harsher. This fact clearly emphasizes the positive impact of co-liquefaction on increasing the biocrude yield. Nevertheless, the results show that the co-liquefaction represses the biocrude yield at milder conditions.

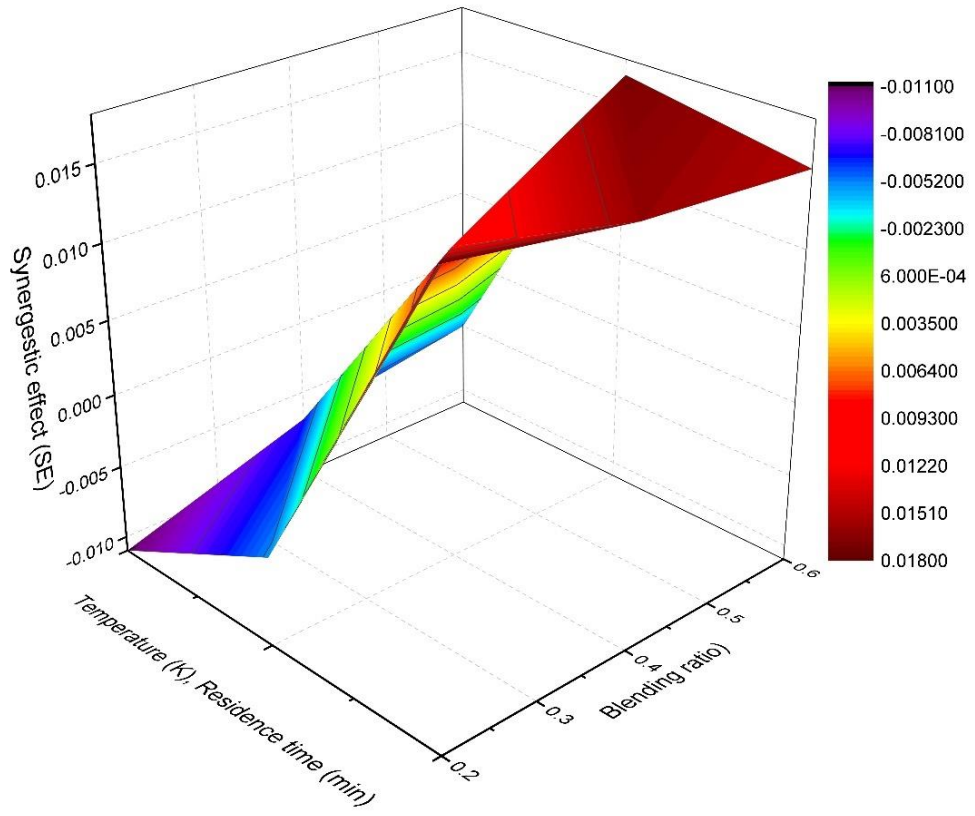

Figure 3-10:Synergistic effect variation

The FTIR analysis is performed to study the variation of the functional groups in the biocrude with different operating conditions. Furthermore, residence time increase showed a more substantial impact on the chemical components of the biocrude.

When the operating temperature increases, more compounds that consist of C-H bonds and probably the C-O bonds are created and increased. With the increase of residence time, compounds like water, fatty acid amides, phenols, and N-containing heterocyclic compounds are reduced from the biocrude due to the breakdown of the carbohydrates and the proteins available unreacted macroalgae (laminaria saccharina)[120]. When the blending ratio has increased, a gradual decline in water, fatty acid amides, phenols, and N-containing heterocyclic compounds from the system is identified.

At the end of the study, it is found that the residence time influenced the functional groups present in the biocrude, although statistically, it has a negligible effect on the biocrude yield. Besides, the temperature and blending ratio are

the controlling factors of biocrude yield. The negative synergetic effect is observed at milder process conditions and lignin-rich environments, while harsher process conditions and increase in laminaria saccharina mass ratio brought positive synergetic effect to the yields. Moreover, the co-liquefaction showed a positive synergetic effect on reducing the char yield. According to the multiparameter optimization, the best biocrude yield of 0.2513 w/w_0 with a minimum char yield of 0.1791w/w_0 can be produced at 573K, 20 min residence time, and a blending ratio of 0.2 where still it is at a negative synergetic phase. According to the FTIR results, independent variables showed different impacts on the variation of functional groups available in the biocrude. The temperature variation mostly helped Alcohol and phenolic compounds production, mainly where the C-O bonds are consumed with the increase of residence time. Nevertheless, co-liquefaction of the feedstocks would help improve the biocrude composition by producing more phenolic compounds, long-chain aliphatic hydrocarbons, carboxylic acids, and ketones aldehydes, and esters.

4 Discussion and the thesis findings

The scope and the motivation of this thesis are to explore the applicability of shrinking core model to model particle (lignin) decomposition in liquefaction and investigate the behavior and the use of lignin in liquefaction in different ways. The research articles presented in this thesis cover a few sub-topics, which describe the main objective from several perspectives. Nevertheless, the focus is primarily on the impact of the shrinking core model on describing particle decomposition in the liquefaction process and then the behavior of lignin in liquefaction in different perspectives. According to the thesis findings, it is possible to build up a discussion over the results of this research.

In the investigation process, the performance of the models and experimental results are assessed concerning several independent parameters. Those parameters are operating temperature, residence time, and blending ratio. Meanwhile, the addressed responses can be listed mainly as biocrude yield and char yield, while functional groups behavior and synergetic effect in Article C and D, respectively. The impacts of the mentioned parameters on the mentioned responses are further investigated and discussed in the following sections.

4.1 Impact of the operating temperature

The variation of the liquefaction temperature is observed to affect several properties of the liquefaction results. According to the literature, an increase in operating temperature has resulted in different feedstocks [26,28,86,91,92,121]. Nonetheless, in general, an increase in operating temperature has reduced the biocrude yield while increasing the char yield.

Cellulose showed a gradual increase at 573K, whereas when the temperature increased to 603K, it showed a relatively faster decomposition and a faster growth of biocrude yield. Then the yield values started going down where the char yield started to pick up showed a steady increment. Meanwhile, at 623K, the biocrude yield only reduced from where it started, while char yield showed the exact opposite behavior to the biocrude behavior. The behavior of total organic carbon (TOC) is very similar to the biocrude behavior in this case. One of the main conclusions here is the assistance of higher temperature to polymerization, where more char is created from the chemicals available in the

biocrude and aqueous phases. Similar variations are observed from previous studies [77,91,93,97–100].

Lignin decomposition does not show much of a relation to the operating temperature. The biocrude yield shows a very similar yield value variation throughout all the temperature values but only a tiny decrement of the yield value with the temperature increase after showing a maximum at 603K. Meanwhile, char yield only increased with the increase of the operating temperature. Like cellulose, the conclusion here is the higher strengthening of secondary reactions to help polymerization produce more char at higher temperatures. Some of the previous studies reported similar behaviors [26,32,103,106].

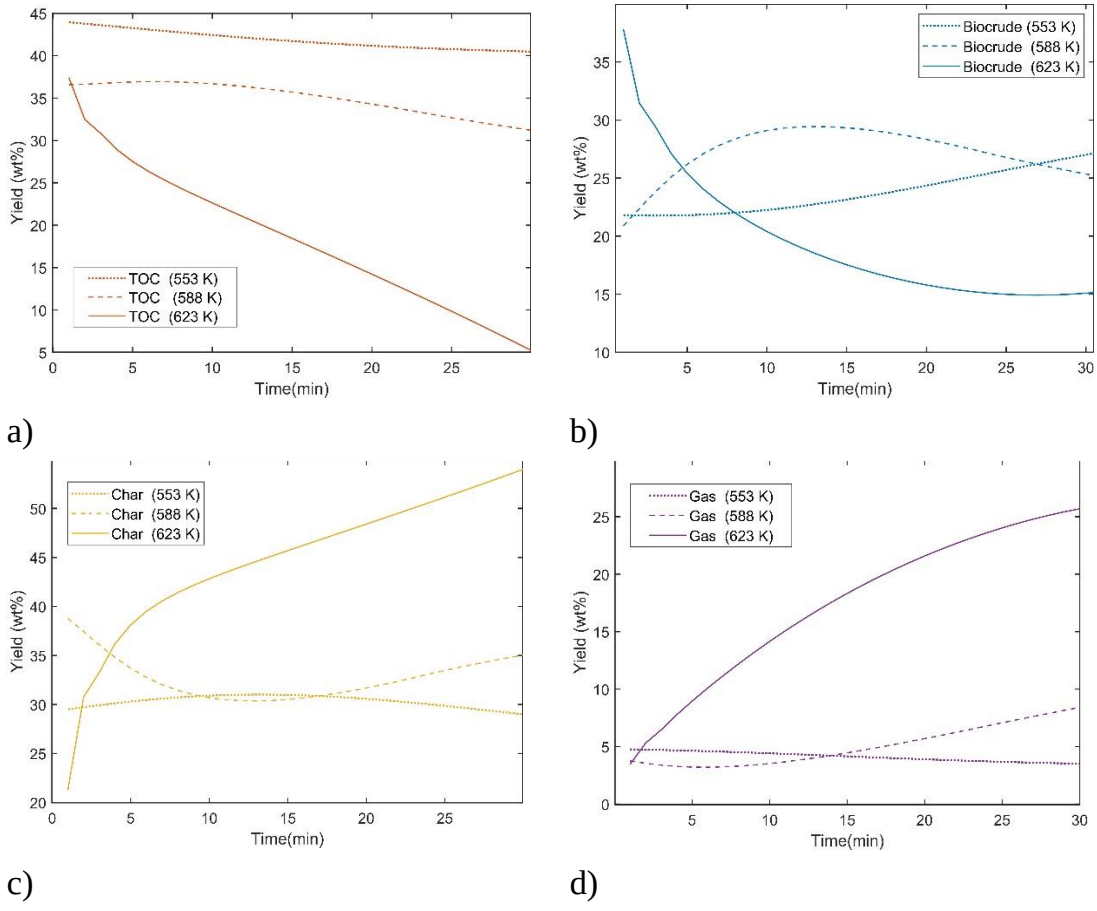

Figure 4-1:Effect of temperature on wood as a cumulative effect of hydrolysis of Cellulose, hemicellulose, and lignin-derived outputs at 553K, 588K and 623K a) TOC b) Biocrude c) Char d) Gas

Wood liquefaction showed very similar behavior to cellulose liquefaction behavior with the temperature increase. Therefore, the higher biocrude yield from wood liquefaction is obtained around 603K. Temperature tends to impact cellulose liquefaction significantly, which can be visible on the wood liquefaction graphs. This is one of the critical findings of Article A. The liquefaction behavior of wood as a cumulative effect of liquefaction of model compounds are shown in above figure 4-1

In article B, the temperature dependence of different chemicals in the biocrude phase, oily film, ash layer behavior, and the surface temperature of the lignin particle is investigated. The temperature of the considered six chemicals are shown in below figure 4-2

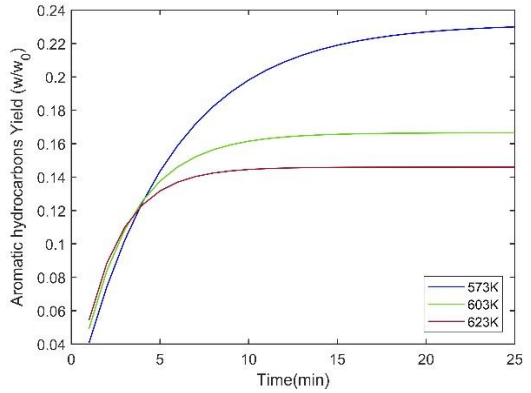

a)

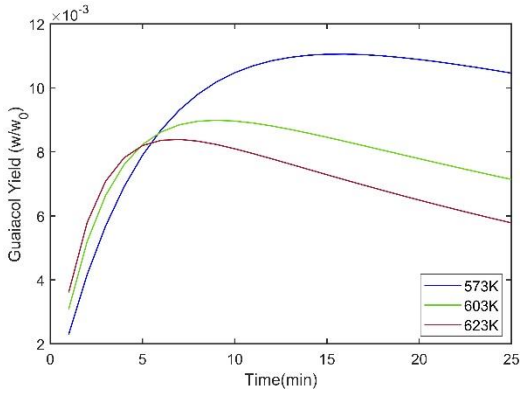

b)

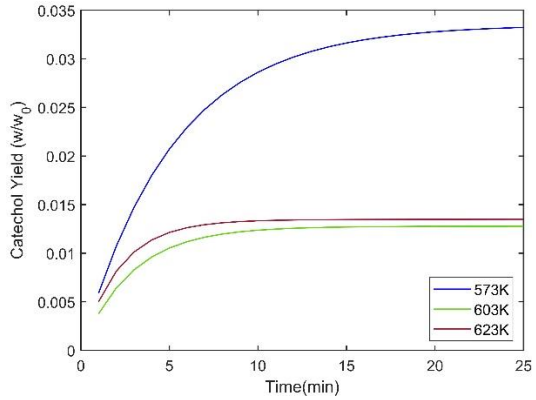

c)

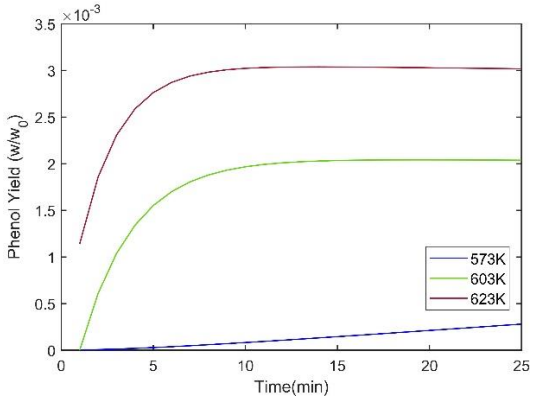

d)

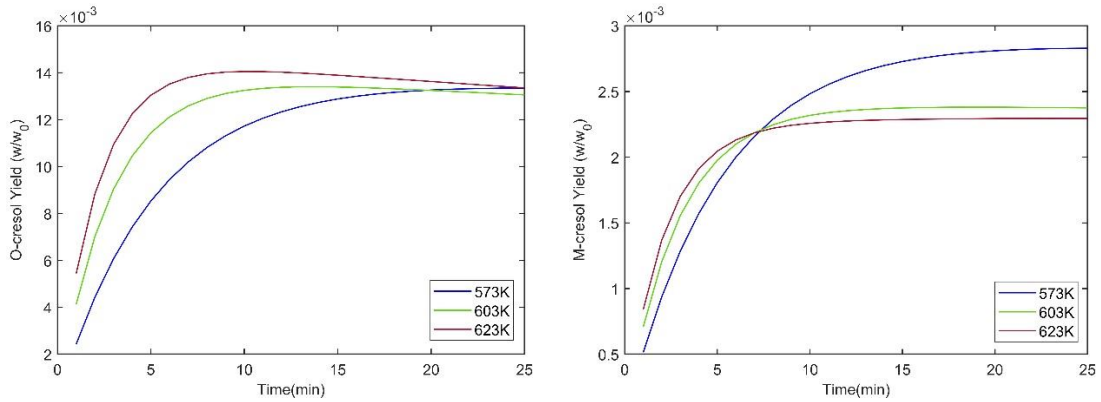

e) f)

Figure 4-2: Effect of temperature on production of components of bi-ocrude at 573K, 603K and 623K with a lignin particle radius of 0.08 mm a) Aromatic hydrocarbons b) Guaiacol c) Catechol d) Phenol e) O-cresol f) M-cresol

Generally, lignin is hydrolyzed faster and produces various products by de-composition[32,92,103,104]. As the temperature increases, yields of aromatic hydrocarbons, guaiacol, and m-cresol are reduced while the phenol is in-creased. In the model, aromatic hydrocarbons represent benzene, toluene, and naphthalene, nonphenolic aromatic compounds. Therefore the reported high aromatic hydrocarbons at lower temperatures are due to ionic reactions rather than free radical reactions [92].

Meanwhile, catechol yield shows a dip at 603K and increases again slightly at 623K. A similar variation of catechol is observed by Yong and Matsumara [92]. Most of the components show a decrease in the yields with increasing temperature. The reason could be improved secondary reactions with a higher ionic water product and decomposition or repolymerization of these chemicals into char. Specially guaiacol is an intermediate degradation component in the lignin decomposition process[112]. With increasing temperature and residence time, guaiacol decreases in the system, mainly due to its high reactivity and decomposition into catechol and phenols[106]. Since the bond energy of the aliphatic $C-O$ bond is lesser than the aromatic $C-O$ bond it is prone to be more reactive[92].

Moreover, the high ionic product and dielectric constant of water could impact the fast decomposition of guaiacol into phenol. Similar variation is shown by both guaiacol and catechol. Guaiacol is the main structure of softwood lignin.

Catechol, o-cresol, and phenol are not natural lignin and are only produced by guaiacol's secondary decomposition or hydrolysis [92,112,122–124]. Therefore, the variation of catechol, o-cresol, and phenol is dependent on guaiacol. Similar behavior of phenol and guaiacol is observed by Pińkowska et al.2012, [103,106]. M-cresol is a direct derivate from o-cresol, where m-cresol is possibly created through alkyl rearrangement [122].

Oily film and the ash layer demonstrated an exciting behavior when the operating temperature was changed. The variation of oily film thickness and the ash layer thickness at different operating temperatures are shown below in Figures 4-3.

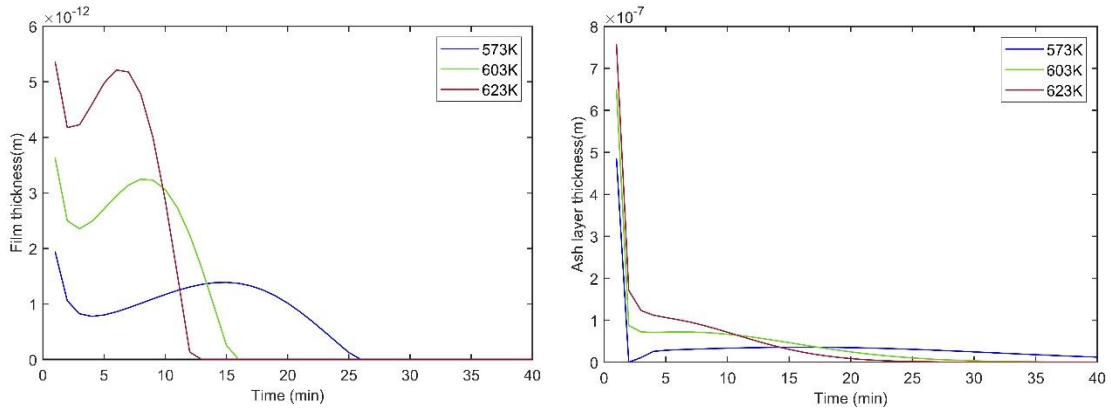

a) b)

Figure 4-3:Impact of temperature on oily film and ash layer formation with a lignin particle radius of 0.08mm at 573K, 603K, and 623K a) Oily film b) Ash layer

The initial high thickness of the oily film and the ash layer can be the initial fast decomposition of lignin. When the particle is submerged in the water, no oily film or ash layer exists. Therefore, there is no resistance for water to reach the lignin particle surface. Nevertheless, the oily film and ash layer is formed with the reactions progressing, and the water monomer's movement to the particle surface is impeded. As time increases, the oily film and ash layer become equilibrium and dissolve into the system.

Both the oily film and the ash layer are relatively thinner with lower temperatures, which helps both water and the products quickly diffuse through them.

However, oily film thickness increases dramatically with higher operating temperatures before it dissolves quickly. The rapid increase of the oily film can be justified by the initial rapid growth of aromatic hydrocarbons and guaiacol with higher temperatures. In another way, the oily film's behavior could impact the product yields too. Similarly, the initial rapid increase with the ash layer could be due to the fast initial hydrolysis of lignin under unobstructed water monomer arrival to the particle surface. More water goes through to the lignin particle surface, which allows hydrolysis.
The dissolution of the ash layer depends on the oily film thickness. Moreover, thinner oily film and ash layer could allow guaiacol to quickly come out to the water to complete the secondary decomposition and produce more secondary products. With higher operating temperatures, due to the rapid increase of the oily film and the ash layer, water diffusion is hampered, leading to reduced lignin's initial hydrolysis. Potentially, this could impact reduced yields of biocrude at higher operating temperatures. Therefore, further study of the formation of oily film and the ash layer can be significant.

In Article C, a reduction in pore volume is noted with the increasing temperature, where the surface area showed the minimum at 603 K. According to the SEM analysis, the char formed at 573 K comprises large particles (>10 um) with a smooth surface.

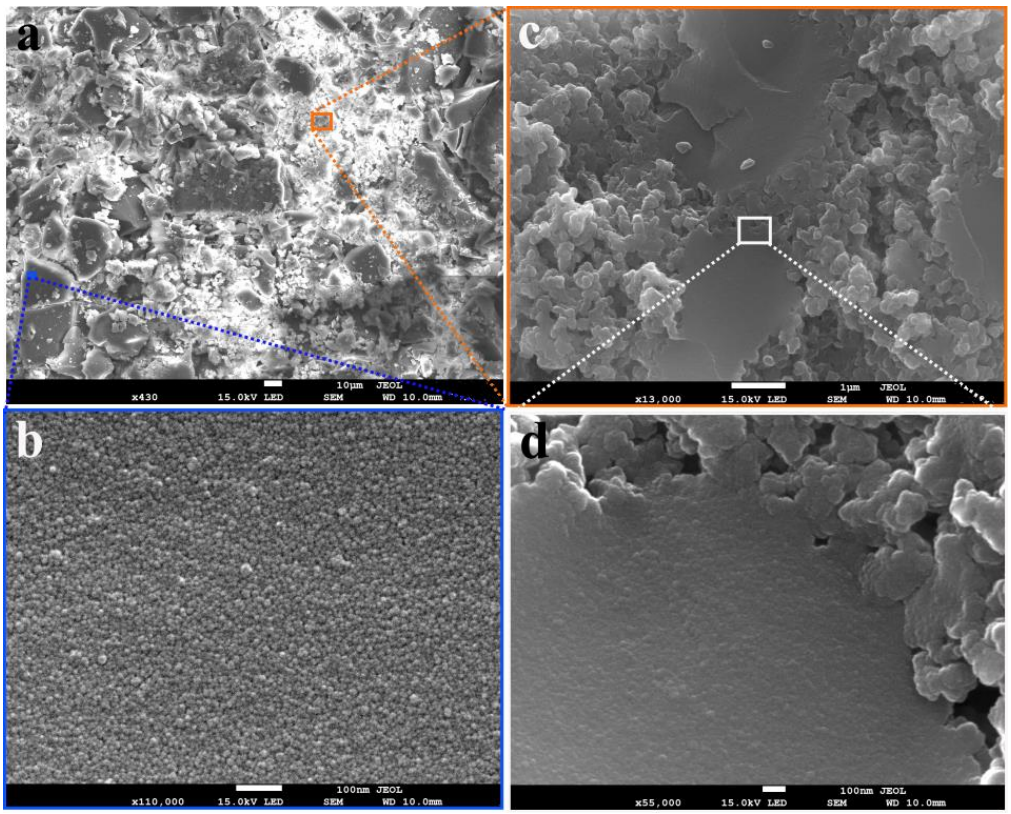

Figure 4-4: (a) SEM image taken at low magnification for the char produced at 573 K and 10 min residence time; (b). high magnification (x110000) image of the area indicated as a blue color small square in part (a); (c) high magnification (x13000) image of the area

A high-resolution SEM image (Figure 4-4) showed the presence of pores distributed all over the surface of these particles.

At low operational temperatures (<603 K), the hydrothermal char is reported to exhibit minimum vesicle formation compared to the pyrolysis char, and this inhibition is suggested to be due to the permeation of water into the pores [125]. A significantly higher surface area and pore volume were observed compared to the pyrolysis char. These findings are consistent with the N2 adsorption studies presented in the previous section.

HTL char produced at 603 K exhibited small particles with many vesicles adhered to the surface. With the high-resolution images, the presence of pores on the surface of these particles is observed. An increase in vesicle formation with the increase in operating temperature could be due to the bolstering of the

degradation process and intense release of gaseous materials that did not fully diffuse out and then condensed during the cooling process. A further increase of the operating temperature to 623 K aids the release of gaseous materials to some extent so that volatiles have sufficient energy to escape the lignin matrix timely [125].

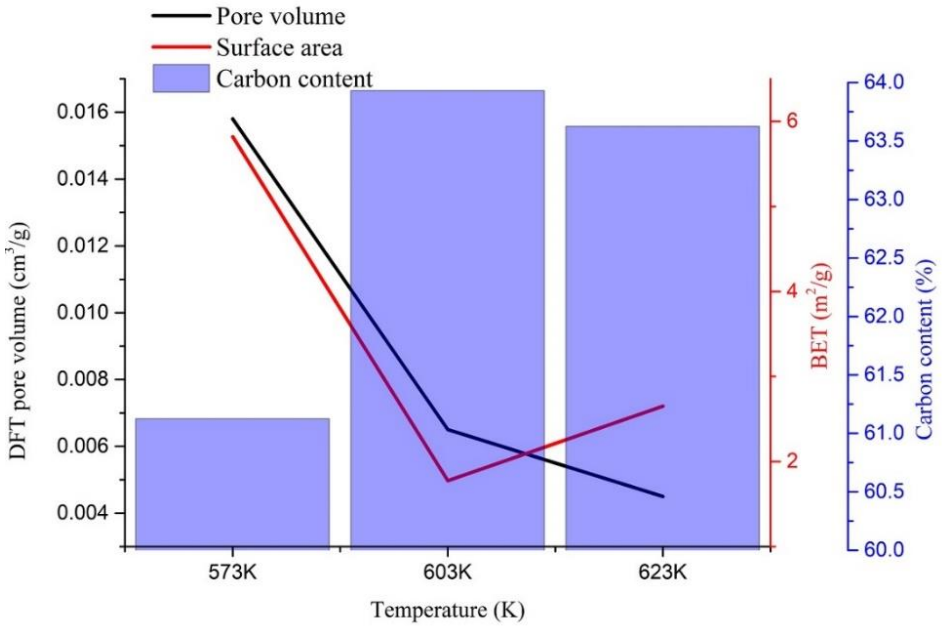

Figure 4-5: Relationship of carbon content surface area and the pore volume.

The lowest operating temperature of 573K yielded both the highest pore volume and surface area, where the pore volume declined with the increasing operating temperature. The surface area showed the behavior of inverse dependability to the carbon content of the sample. Figure 4-5 above illustrates the relationship between pore volume, surface area, and the carbon content of the samples produced at different temperatures.

The surface area of HTL char produced at 573K (5.82 m^2/g) is considerably higher than of the lignin pyrolysis char (about 0.5 m^2/g) and pyrolysis char from wood (2.39 m^2/g) produced at the same temperature[126,127]. At 603K, both pyrolysis char (about 2 m^2/g) and HTL char (1.77 m^2/g) showed similar

surface area values, whereas the HTL char produced at 623K (2.65 m^2/g) showed a lesser value than the pyrolysis char (about $5m^2/g$) produced at the same temperature[126]. Moreover, similar pore volume adaptation is seen with hydrochar made by Hydrothermal carbonization (HTC) [128].
Polar functional groups decrease with increasing operating temperature [129]. These groups are reduced to produce an aromatic char[126,130]. Such aromatic rings would produce fused aromatic rings after losing oxygen and hydrogen. Therefore, the increasing temperatures and the longer residence times promote fused ring production, resulting in more char. Although the aliphatic groups are eliminated from the chars produced at higher temperatures, many studies have shown that those aliphatic groups can be found in the liquid phase[92,106]. The small amount of aromatic and aliphatic OH ($3415cm^{-1}$) seen vanish with the increasing operating temperature. This behavior can be mainly credited to improving the dehydration reaction[131]. The band at 1595 cm^{-1}[126,130] corresponding to the aromatic ring C=O and carbonyl group (1684 cm^{-1}) are seemed to be increased drastically with the increase of operating temperature. This means the C-C and C-H bonds are consumed throughout the hydrothermal liquefaction process. O- containing functional groups in char can be used to measure char as an adsorptive material. When the O-containing functional groups are enhanced, biochar has improved heavy metals' sorption ability [132,133]. Although aromatic ring C=O and carbonyl groups increase with operating temperature, aromatic and aliphatic OH and Guaiacyl C-O significantly decrease.

Monomeric radicals can be created by splitting weak bonds in the lower operating temperatures, and the produced radicals can potentially create new radicals by attracting hydrogen to form monomeric phenolic compounds. C-C bonds can also be broken when the operating temperature increases to create phenolic monomeric compounds. Meanwhile, these phenolic compounds can be polymerized and potentially produce more char. More fused aromatic rings could also be produced when the operating temperature increases and comes close to the critical point, leading to more polyaromatic char.

The impact of temperature in co-liquefaction and the variation of functional groups are studied in Article D. When the operating temperature increases,

more compounds that consist of C-H bonds and probably the C-O bonds are created and increased. Thus, it can be observed that the temperature increase has produced more alcohols and phenolic compounds in the biocrude. Below figure 4-6 shows the FTIR spectra of biocrude different temperatures with a 10 min residence time and 0.2 blending ratio

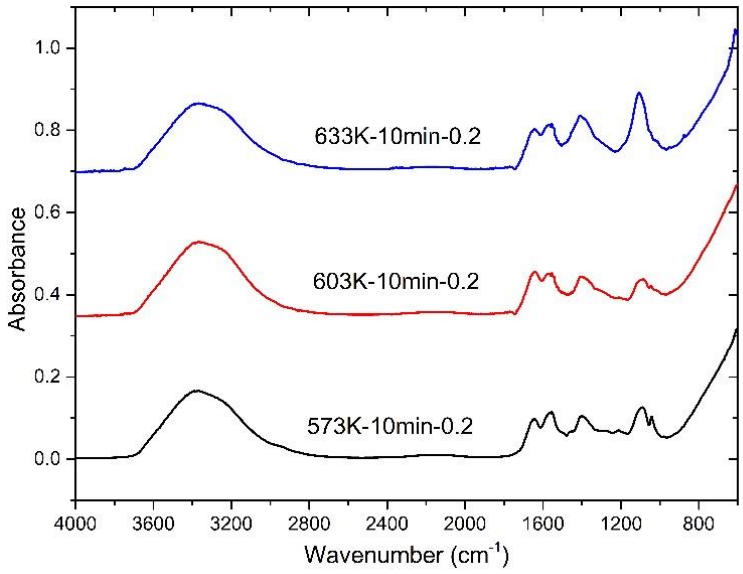

Figure 4-6:FTIR spectra of bio crudes from (a) different temperatures with a 10 min residence time and 0.2 blending ratio

4.2 Impact of the residence time

Many researchers investigated the effect of residence time on product yields [134–136]. Boocock and Sherman[137] figured out the longer residence times could reduce the biocrude yields except for the very high loading conditions. Some studies show the negative effect of higher temperatures and longer residence times on char yields [135], while others suggest longer residence times have a negligible impact on liquid yields [138]. Therefore, the model predictions tend to follow most of the observations in literature except the suggestions by Wadrzyk et al. [135] and Yj et al. [138].

Biocrude and TOC from cellulose showed a similar behavior where both came to a maximum of around 20 min of residence time and then reduced gradually. Longer residence time helped the further polymerization and increased the char yields. Lignin showed a relatively fast decomposition, and then all the components were kept at almost a constant yield value. Like the wood lique-

faction behavior at different temperatures, the yield values followed the cellulose liquefaction behavior.

In Article B, all the considered chemicals except guaiacol, yields tend to stay approximately constant with longer residence times for all the considered temperatures. Understandably, guaiacol shows a decrease with the longer residence time where it shows a maximum of $11 \times 10^{-3} w/w_0$ at 15 min residence time. With this observation, it can be determined that any factor resulting in a higher yield of monomers such as temperature (553K-643K) or longer residence times helps both repolymerization and depolymerization[139]. Therefore, the opposite trends of guaiacol and catechol to reduce and phenol to rise simultaneously are supported.

In Article C, the char yield behavior is studied with three different residence times. According to the char yield values, the residence time did not significantly impact the yield. Nevertheless, repolymerization reactions seem to become prominent with the higher operating temperatures and longer residence times, leading to the higher char yield at higher temperatures[92,102].
Although aromatic ring C=O (1595 cm^{-1}) is increased with the longer residence time, it is not as significant as the operating temperature. Further, the carbonyl group (1684 cm^{-1}) decreased with the longer residence time. A simple explanation for reducing the carbonyl group is the consumption of C-C and C-H bonds with a longer residence time. Nevertheless, longer residence times are not as effective as the temperature for consuming C=C and C-H bonds. Due to the dealkylation reaction, CH_3 and CH_2 groups are primarily removed from the chars, and this reaction could be influenced slightly by the residence time. The spectrum depicts a vanishing of the little aliphatic content with the residence time increases.
Nevertheless, the peak reduction relates to the aliphatic content, which is slower with the residence time increase than the operating temperature increase. Therefore, although it is a minor impact, longer residence times are resulted in removing the aliphatic content from the chars in HTL. In this study, the longest residence time (20 mins) could not increase the char yield significantly, even at 623K. Therefore, the impact of residence time on producing

phenolic monomeric compounds and generating more char with polymerization must be studied further with much longer residence times.

More thermal stability is seen with the char formed at longer residence times. The shortest residence time produced the char with the highest percentage mass loss at each operating temperature, while the longest residence time shows the opposite.

Nevertheless, residence time played an essential part in the quality of the biocrude produced in the co-liquefaction of lignin and laminaria saccharina. Figure 4-7 shows the behavior of functional groups when the residence times are changed at 573K and with a blending ratio of 0.2. Furthermore, residence time increase showed a more substantial impact on the functional groups in the biocrude. With the increase of residence time, compounds like water, fatty acid amides, phenols, and N-containing heterocyclic compounds are reduced from the biocrude due to the breakdown of the carbohydrates and the proteins available unreacted macroalgae (laminaria saccharina) [120]. Further, the esters such as triglyceride are reacted during the process with the increased residence time. In addition, the consumption of the C-O bonds available in the biocrude can be seen while an increase of C=O bonds, –CH2 and -CH3 groups representing the long-chain aliphatic hydrocarbons is observed. Therefore, it is understandable that the residence time helped to consume C-O bonds while producing new C=O bonds.

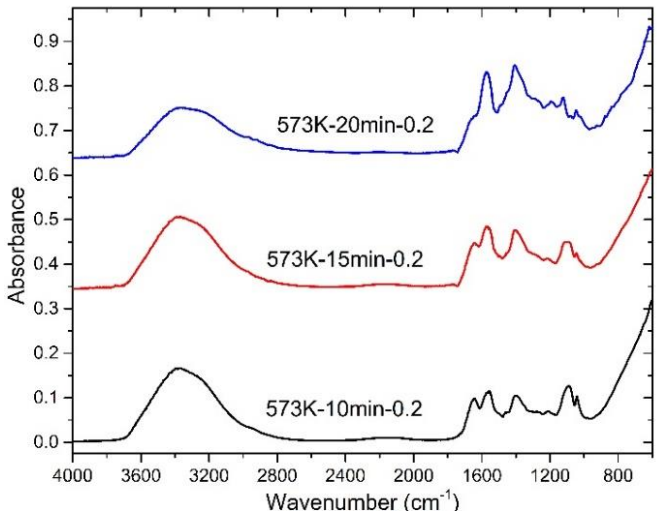

Figure 4-7: FTIR spectra of bio crudes from different residence times at 573 K and blending ratio of 0.2

4.3 Impact of heating rate

Cellulose showed producing higher char yields with higher heating rates. Thus the cellulose component got more charred with higher heating rates. At slower heating rates, the particle stays at the lower temperature values longer, giving more time for the particle to decompose. Therefore in the graphs, it is misleading to see the slower heating rates resulted in faster decomposition. When the particle stays longer in the medium, that helps the further decomposition and recombination reactions. The cellulose liquefaction results reinforce this behavior by Kamio et al.[93]. Moreover, wood liquefaction results by Mosteiro-Romero et al.[52,134].

Lignin showed a faster decomposition at lower heating rates too, and it produced maximum yields of around 620 K. Lignin did not show a significant adjustment in yields with the heating rate change. The slightly high outputs in the lower heating rates could be the longest time it takes to increase the temperature. Therefore the particle is kept under the low temperature for a longer time, and the hydrolysis takes over the drying. With the high heating rates, the particle is dried faster, and thus the charring of the particle is promoted.

The lignin component did not show much affected by the heating rate. All the yield components produced similar percentages of yields with the temperature increase. Product yields of lignin liquefaction showed similar values at all heating rates when the temperature reached the critical point. Therefore, the impact of the heating rate is essential only at shorter residence times. Thus, the heating rate can be used critically in the fast liquefaction concept. Further, the higher heating rates could promote secondary reactions and result in higher char yields. Therefore. Due to both drying and increased activity of secondary reactions, char yield is improved with the higher heating rate close to the supercritical region. When the heating rates are high, at first, the particle gets charred rapidly, and it obstructs the production of liquid yields initially due to the reduced hydrolysis of the particle. 4K/min and 6K/min heating rates enforced a negligible variance on the yields except for the gas component. Thus, these observations confirm the observations and conclusions made by Akhtar and Amin [38] on the negligible impact of heating rates on wood and its model components due to the high dissolution and stabilization of decomposed fragments in subcritical water

In Article B, six different chemicals behavior is studied under different heating rates. Other chemicals do not significantly change their yields by the heating rate change, apart from phenol production. Besides, at 640K, phenol production is reduced to $3 \times 10^{-4} w/w_0$ from $1.75 \times 10^{-3} w/w_0$ when the heating rate increases from 1K/min to 5 K/min.

Oily film and the ash layer demonstrated a thicker layer formation with higher heating rates. The main reason for this behavior is the fast production of guaiacol with higher heating rates and the quick production of ash due to the drying of the particle. The biocrude yield behavior is compared, suggesting the possible influences of the oily film and ash layer thicknesses on the biocrude components' yields.

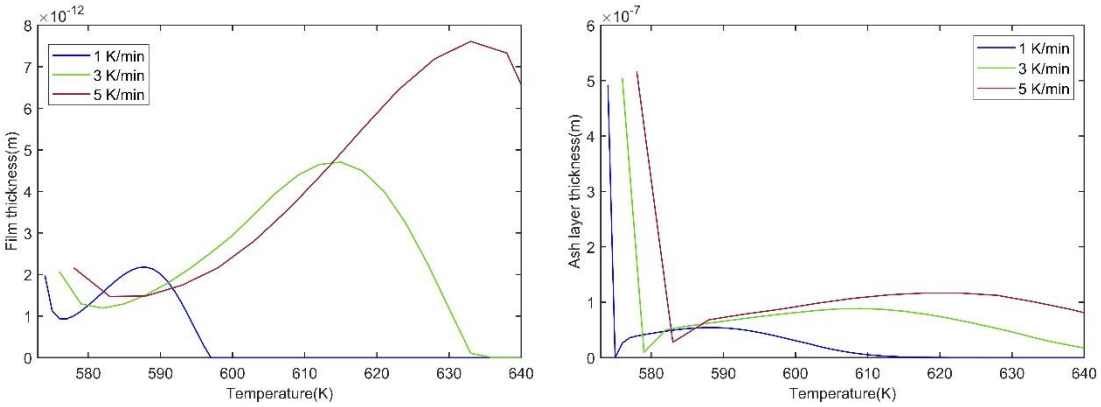

a) b)

Figure 4-8:Impact of heating rate on oily film and ash layer formation with heating rates of 1K/min, 3K/min and 5K/min with a lignin particle radius of 0.08mm a) Oily film b) Ash layer

The thickness of the oily film and ash layer results from the rate of production of those layers and the rate of dissolution of the oily film and ash layer in water. At lower heating rates, catechol, phenol, and cresols are promoted through guaiacol decomposition. Therefore, guaiacol, one of the two main components of the oily film, decomposes faster at lower heating rates. Therefore the oily film thickness reduces faster through dissolution in the water and decomposition into other chemicals. When the heating rates have increased, the produc-

tion rate of catechol, phenol, and cresols is hindered. Therefore, the oily layer thickness is reduced at a lower rate. Meanwhile, close to 640K and with higher heating rates, guaiacol yield is considerably high, depicting the larger thickness of the oily film. Figure 4-8 above shows the oily film and ash layer behavior with different heating rates

4.4 Impact of the blending ratio

In Article D laminaria saccharina blending ratio is changed from 0.2 to 0.6. The variation of the biocrude yield can be seen in Figure 4-9 below. The increase of the blending ratio at 573K has reduced the biocrude yield. Meanwhile, the increase of operating temperature at 0.2 blending ratio has also created the same effect on biocrude yield. Ultimately this observation justifies one of the main results of Article D of obtaining the optimum biocrude yield at 573K 20 min and 0.2 blending ratio.

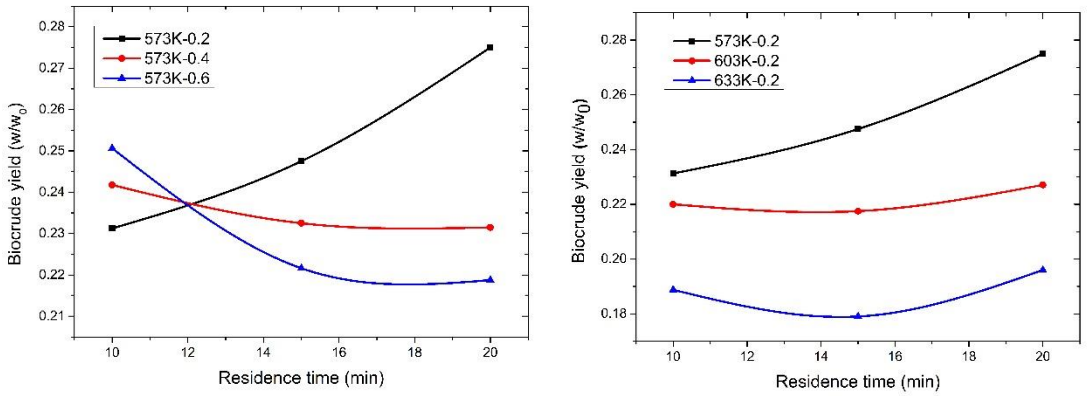

a) b)

Figure 4-9: Variation of biocrude yield a) with different blending ratios at 573K b) with different operating temperatures with 0.2 blending ratio

Figure 4-10 explains the change of functional groups in the biocrude with the change of the blending ratio of the feedstock mix. When the blending ratio is called zero, the feedstock consists of 100% lignin, where the blending ratio is referred to as one feedstock made out of 100% laminaria saccharina. When the

blending ratio increases, the peak at 3380 cm^{-1} shows a gradual decline, corresponding to the reduction of water, fatty acid amides, phenols, and N-containing heterocyclic compounds from the biocrude. An interesting finding is that the introduction of laminaria saccharina dramatically enhanced the peak at 1560cm^{-1}, 1395$cm^{-1,}$ and 1050$cm^{-1,}$ which relates to the C=O bonds, C-H bonds, and the C-O bonds. These findings prove that the feedstocks' co-liquefaction (adding laminaria saccharina) would produce more phenolic compounds, long-chain aliphatic hydrocarbons, carboxylic acids, and ketones, aldehydes, and esters.

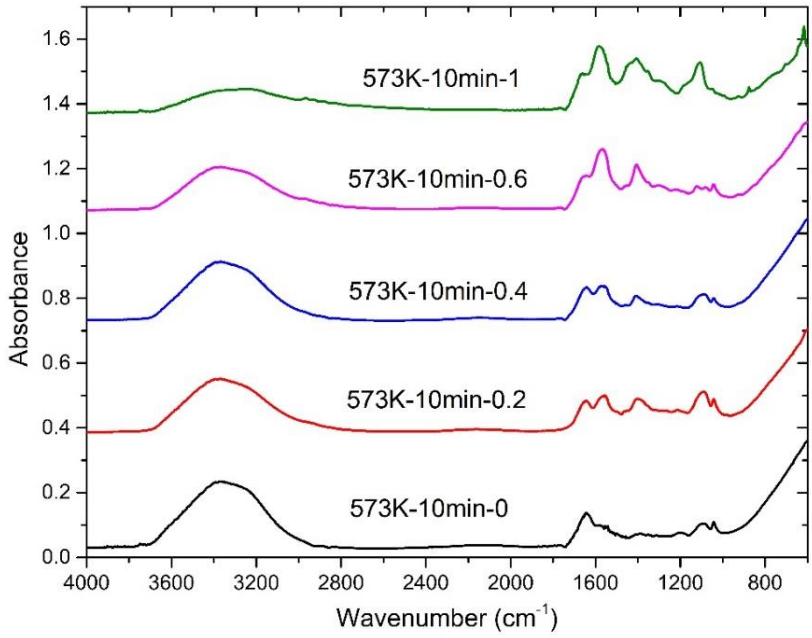

Figure 4-10:FTIR spectra of biocrude from different blending ratios at 573K and with a 10 min residence time

5 Conclusion

5.1 Remarkable outcomes

The scope of this thesis was a numerical and experimental study of lignin hydrothermal liquefaction. As described, the idea of studying the numerical modeling was to explore the simulate the actual liquefaction mechanism using a shrinking core model to model using wood and lignin as feedstocks. Then the coupling of experimental study with the model and further studying the different aspects of lignin liquefaction such as char and co-liquefaction. The proposed process was, therefore, proposed by taking into consideration a few main aspects:

- Modeling of liquefaction using a shrinking core model
- Study the formation of oily film and ash layer around the particle during liquefaction
- Modeling of the behavior of different chemicals in biocrude with different independent variables
- Study on char from lignin liquefaction
    - Structural, chemical, and thermal evolution of char
- Co-liquefaction of lignin with laminaria saccharina
    - Optimized biocrude and char yields
    - Synergistic effect of co-liquefaction
    - Evolution of the functional groups of char

The research sub-questions were put forward accordingly. Answers were described through the work discussed in the thesis and presented and described in the appended papers. The main conclusions revealed that the shrinking core model could be used effectively in modeling liquefaction where the oily film and the ash layer could play an important role. Thus, further practical study on those layers could be beneficial. Further, the char from lignin HTL presented more aromatic properties when the operating temperatures were increased. At 573K lignin, HTL char showed significantly higher surface area than lignin and wood pyrolysis char at the same temperature. Nevertheless, the use of HTL char in a possible useful product is doubtful, according to this study. The

co-liquefaction showed that more severe process conditions created the synergistic effect.

The first step of the research was to develop a basic liquefaction model using the shrinking core model. Thus, a wood particle is used as the biomass, and the impact of different model compounds on overall wood liquefaction is modeled using the shrinking core model. The model's suitability and robustness are tested with different operating temperatures, residence times, particle sizes, and heating rates. In most of the cases, the model showed an acceptable prediction capability. Moreover, it was understood that the hypothesis used for the research is null. The cumulative liquefaction effect of the model compounds could not match the overall wood liquefaction effect. The main problem could be the lack of cross-reactions between the chemicals produced from different model compounds. Further, the lack of initial kinetic data played an important role in determining the robustness of the model too.

After that, the shrinking core model-based liquefaction model is further developed using lignin as the feedstock. This model studies the formation and behavior of an oily film and an inorganic layer around the particle during the liquefaction process. The intraparticle behavior and the behavior of selected six different chemicals in the biocrude phase are investigated. The oily film and inorganic layer showed similar behaviors. At higher temperatures, the thickness grew large. Further, it could be seen that the thickness of the oily film and the ash layer directly impact the decomposition of the particle. The model showed a much better accuracy with the experimental data where it illustrates the robustness of the model.

Once the shrinking core model is finished, the study on char produced from lignin liquefaction is carried out. The motivation was to investigate the behavior of char with different operating temperatures and residence times in the perspective of the possibility of using char helpfully. The morphological study showed the formation of vesicles at 603K and their increase at 623K. The higher temperatures and longer residence times produced more thermally stable and aromatic char. Most functional groups' residence time had the same effect as the temperature on a smaller scale.

Finally, the co-liquefaction effect of lignin with laminaria saccharina is carried out to examine the synergistic effect of the co-liquefaction. The optimum biocrude yield is 573K with a 20 min residence time and 0.2 blending ratio. The synergistic effect seems to be strengthened with harsher operating conditions and a higher blending ratio of laminaria saccharina. The residence time impacted the functional groups present in the biocrude, although it did not statistically impact the biocrude yield.

Parallel to this study, a literature survey is performed on the impact of heating rates on the liquefaction process and the nitrogen content and denitrogenation of biocrude.

5.2 Challenges and limitations

For apparent reasons, section 5.1 primarily emphasized and reviewed the most relevant results acquired during the work explained in this thesis. Nevertheless, it is equally essential to take the opportunity to focus on the main challenges and limitations this research came across. It is the expectation of the author that such barriers may be explored and overcome with further research. Below mentioned is a brief list:

- The suitability of the Shrinking core model: - The reason to use the shrinking core model for the study is discussed before. Nevertheless, it is used mainly due to the less complexity of modeling the complex process with this model. Besides, the shrinking core model has few drawbacks when modeling this process.

- Kinetic model: - The number of chemicals used in the kinetic model is limited in Articles A and B. The reasons were the lack of kinetic data availability and the reduced complexity of the model. Further, in Article A, the cross-reactions between chemicals produced at different model compounds were not considered keeping in mind that it needs separate individual study, which would consume a considerable amount of time. Therefore, that is kept for future work. Nevertheless, in Article

B, many chemicals and reactions between them are considered successful.

- Experimental study on the oily film and the ash layer: - One of the main highlights in Article B is the oily film and the ash layer around the particle. The oily film and ash layer dissolution data and the water diffusion data through oily film and ash layer are taken from the literature, and some of those data are not verified at the temperatures and pressure used for the process. Furthermore, the formation of those layers and their behaviors has to be experimentally investigated to be validated, although it will be challenging.

- Economic costs: Throughout the thesis, the criticality represented in the simultaneous optimization of the quality of the product was regularly emphasized. Nevertheless, in this study, the factor of economic costs is not discussed mainly because this study is based on developing a method to optimize the yield rather than the production costs. Further, to produce biodiesel from the biocrude produced, a long and complex process has to be followed, which would cost a lot more money. Therefore, discussing the economy of the process would not be critical.

- High treatment temperature: - It was observed that both the quality and the yield of the biocrude and char are strongly linked to the high temperatures in the liquefaction process. From an economic perspective, using high temperatures and pressures would inevitably increase the production costs and generate some technological obstacles. Therefore, it is more appropriate and feasible to use operating temperatures as low as possible.

- Utilization of biocrude and char: - In this study, mainly biocrude and char production are discussed. Besides the end process, the product matters when it comes to the real-world scenario. Therefore, the possible use of char must be found out and developed. As for the biocrude, a

more feasible industry such as the heavy fuel industry must be searched upon to be used with less refining and processing.

- Utilization of aqueous and gas phases: In this study, the aqueous and gas phases are not studied mainly due to the lack of analysis instruments. Nevertheless, these products could be utilized in different ways and places. Therefore, the Same as the biocrude and char phase aqueous phase and the gas phase should be studied and utilized more efficiently.

- Lignin as a feedstock: - The thesis explained and justified why this research mainly focused on exploiting lignin. However, lignin is produced in vast amounts as a by-product in the paper industry. Hence a deeper study on the use of this type of feedstocks would have provided helpful information to generate biofuels.

- Lab-scale dependence: - In a multi-step process, described by numerous parameters simultaneously affecting each other, the up-scaled results might differ substantially from the lab ones. Therefore, the results and conclusions should not be used on continuous or upscaled system analysis.

- Laminaria saccharina as the co feedstock: - Laminaria saccharina is widely available in Norway and Europe. The liquefaction results of laminaria saccharina showed a possible positive input in the biocrude yield. Therefore, the co-liquefaction study was carried out where it showed the positive synergistic effect in the last article (Article D)

- Statistical significance: - The significant time required for the liquefaction to perform with a batch reactor with a volume of 24 ml, as well as the low amount of material (lignin), hampered the production of a significant amount of biocrude and char. The number of runs performed to complete a single sample for each configuration in each article was always enough to guarantee both the repeatability and the statistical significance. Nevertheless, a more extensive set of experiments would have certainly steered more accurate results.

- Sustainability: - The environmental impact of the process was not studied in this work too. Nonetheless, the environmental impact of this process should be assessed to improve this process. Therefore, LCA of the process, method production of feedstocks, harvesting processes, and the energy-wise process optimization should be performed. Further, the more environmentally viable products from the HTL should be found out and produced.

5.3 Future work

On the brink of the challenges and limitations, which could take action as hurdles to the develop improved models, a continuation of the related research is highly suggested. Overall, the present work pioneered and underlined the prospect of using the shrinking core concept to develop a robust liquefaction model to describe particle decomposition in the liquefaction process and the use of lignin as a liquefaction feedstock and its by-products. Nevertheless, there are still many sub-research questions to address.

CFD model: - CFD model is already being developed based on the numerical model proposed in Article B. A CFD model will help understand the temperature around and inside the particle more. Further, the flow field results could help optimize the yields and study the char formation and the behavior of oily film and the ash layer around the particle.

An improved model with machine learning techniques: -. As a future study, the model proposed in Article B will be used with different feedstocks separately and together as co-liquefaction. Further, the machine learning techniques will be used to compare the model predicted yields and experimental yield values to optimize and predict, best yields and corresponding operating parameters. Thus, the motive is to develop an artificial intelligence-driven universal liquefaction model based on a shrinking core concept that can predict optimized yields and operating conditions for given feedstocks.

Dedicated model for hemicellulose: - During the model development for Article A, it was fascinating to see the different behavior of hemicellulose in the liquefaction process to the other two model compounds. Further, a robust and reliable model has not been observed for hemicellulose liquefaction in the literature. In addition, certain studies show contradictive behaviors in hemicellulose liquefaction. These things elaborate the space to study hemicellulose liquefaction to reap its harvest. Though it is challenging, a reliable model for hemicellulose liquefaction could provide lots more information and understanding to the field. Hence it is suggested to continue studies on hemicellulose and even develop improved models for hemicellulose liquefaction.

Further study on HTL char producing useful material: - In Article C, the evolution of char from lignin liquefaction is studied having the idea of observing the possibility of utilizing HTL char helpfully. Since char accounts for a considerable mass ratio from liquefaction output, it is wise to study the possibility of observing the practical ways of using HTL char. It could be for agricultural purposes, porous carbon production, or even co-liquefaction feedstock with other feedstocks. Especially according to the functional groups available in char, it can be seen that there are a lot more chemicals that can be extracted from HTL char. Moreover, a study is proposed to observe the possibility of producing char with as few beneficial chemicals as possible. That means the valuable chemicals stay in the liquid phase, which can be extracted relatively easily. In addition, char formation is a complex mechanism, and if it can be controlled, it could vastly benefit the liquefaction technology at the industrial level.

Experimental study on oily film and ash layer formation: - There are no experimental studies on the oily film and ash layer behavior. In a process like liquefaction, studying these could be next to impossible. Nonetheless, the behavior of these two layers directly impacts the liquefaction yields according to the conclusion of Article B. Therefore, especially with fast liquefaction, these layers could play an important role, and a proper study on these layers could help improve the liquefaction yields in fast liquefaction and in continuous processes where HTL practices in a larger scale.

Techno-economic analysis on HTL: - A techno-economic analysis on hydro-thermal liquefaction will give lots of important data if it is required to develop a scaled-up reactor system. During the Ph.D., an ASPEN plus model was developed to perform a techno-economic analysis. Sensitivity analysis has been carried out with the model to study its behavior when scaled up and investigate the different yields at different operating temperatures. Nevertheless, a more robust techno-economic model with real-world data would be beneficial for bringing this technology to an industrial level.

References

[1] Gollakota ARK, Kishore N, Gu S. A review on hydrothermal liquefaction of biomass. Renew Sustain Energy Rev 2018;81:1378–92. https://doi.org/10.1016/j.rser.2017.05.178.

[2] Hoffmann J, Rudra S, Toor SS, Holm-Nielsen JB, Rosendahl LA. Conceptual design of an integrated hydrothermal liquefaction and biogas plant for sustainable bioenergy production. Bioresour Technol 2013;129:402–10. https://doi.org/10.1016/j.biortech.2012.11.051.

[3] Edenhofer DO. The IPCC Special Report on Renewable Energy Sources and Climate Change Mitigation n.d.:41.

[4] Tzanetis KF, Posada JA, Ramirez A. Analysis of biomass hydrothermal liquefaction and biocrude-oil upgrading for renewable jet fuel production: The impact of reaction conditions on production costs and GHG emissions performance. Renew Energy 2017;113:1388–98. https://doi.org/10.1016/j.renene.2017.06.104.

[5] Ramirez JA, Brown RJ, Rainey TJ. A Review of Hydrothermal Liquefaction Bio-Crude Properties and Prospects for Upgrading to Transportation Fuels. Energies 2015;8:6765–94. https://doi.org/10.3390/en8076765.

[6] Market Intellica. Mark Intellica n.d. https://marketintellica.com (accessed November 24, 2021).

[7] Kousoulidou M, Lonza L. Biofuels in aviation: Fuel demand and CO2 emissions evolution in Europe toward 2030. Transp Res Part Transp Environ 2016;46:166–81. https://doi.org/10.1016/j.trd.2016.03.018.

[8] Minowa T, Zhen F, Ogi T. Cellulose decomposition in hot-compressed water with alkali or nickel catalyst. J Supercrit Fluids 1998;13:253–9. https://doi.org/10.1016/S0896-8446(98)00059-X.

[9] Qian X, Nimlos MR, Johnson DK, Himmel ME. Acidic sugar degradation pathways. Appl Biochem Biotechnol 2005;124:989–97. https://doi.org/10.1385/ABAB:124:1-3:0989.

[10] Ross AB, Biller P, Kubacki ML, Li H, Lea-Langton A, Jones JM. Hydrothermal processing of microalgae using alkali and organic acids. Fuel 2010;89:2234–43. https://doi.org/10.1016/j.fuel.2010.01.025.

[11] Biller P, Sharma BK, Kunwar B, Ross AB. Hydroprocessing of bio-crude from continuous hydrothermal liquefaction of microalgae. Fuel 2015;159:197–205. https://doi.org/10.1016/j.fuel.2015.06.077.

[12] Jazrawi C, Biller P, Ross AB, Montoya A, Maschmeyer T, Haynes BS. Pilot plant testing of continuous hydrothermal liquefaction of microalgae. Algal Res 2013;2:268–77. https://doi.org/10.1016/j.algal.2013.04.006.

[13] Ross AB, Jones JM, Kubacki ML, Bridgeman T. Classification of macroalgae as fuel and its thermochemical behaviour. Bioresour Technol 2008;99:6494–504. https://doi.org/10.1016/j.biortech.2007.11.036.

[14] Singh R, Balagurumurthy B, Bhaskar T. Hydrothermal liquefaction of macro algae: Effect of feedstock composition. Fuel 2015;146:69–74. https://doi.org/10.1016/j.fuel.2015.01.018.

[15] Aresta M, Dibenedetto A, Barberio G. Utilization of macro-algae for enhanced CO2 fixation and biofuels production: Development of a computing software for an LCA study. Fuel Process Technol 2005;86:1679–93. https://doi.org/10.1016/j.fuproc.2005.01.016.

[16] Bach Q-V, Tran K-Q, Lystad KQ. Fast hydrothermal treatment of macroalga: characterization of products. Chem Eng Trans 2016:97–102. https://doi.org/10.3303/CET1650017.

[17] Raize O, Argaman Y, Yannai S. Mechanisms of biosorption of different heavy metals by brown marine macroalgae. Biotechnol Bioeng 2004;87:451–8. https://doi.org/10.1002/bit.20136.

[18] Chung IK, Sondak CFA, Beardall J. The future of seaweed aquaculture in a rapidly changing world. Eur J Phycol 2017;52:495–505. https://doi.org/10.1080/09670262.2017.1359678.

[19] He Y, Liang X, Jazrawi C, Montoya A, Yuen A, Cole AJ, et al. Continuous hydrothermal liquefaction of macroalgae in the presence of organic co-solvents. Algal Res 2016;17:185–95. https://doi.org/10.1016/j.algal.2016.05.010.

[20] Pedersen TH, Grigoras IF, Hoffmann J, Toor SS, Daraban IM, Jensen CU, et al. Continuous hydrothermal co-liquefaction of aspen wood and glycerol with water phase recirculation. Appl Energy 2016;162:1034–41. https://doi.org/10.1016/j.apenergy.2015.10.165.

[21] Toor S, Rosendahl L, Rudolf A. Hydrothermal liquefaction of biomass: A review of subcritical water technologies. Energy 2011;36:2328–42. https://doi.org/10.1016/j.energy.2011.03.013.

[22] Vardon DR, Sharma BK, Scott J, Yu G, Wang Z, Schideman L, et al. Chemical properties of biocrude oil from the hydrothermal liquefaction of

Spirulina algae, swine manure, and digested anaerobic sludge. Bioresour Technol 2011;102:8295–303. https://doi.org/10.1016/j.biortech.2011.06.041.

[23] Sørensen J, Antman A, Brubæk S, Andersen BH, Teerikangas J, Lindqvist K, et al. Nordic Agriculture Air and Climate. Nordic Council of Ministers; 2015.

[24] Patil PT, Armbruster U, Martin A. Hydrothermal liquefaction of wheat straw in hot compressed water and subcritical water–alcohol mixtures. J Supercrit Fluids 2014;93:121–9. https://doi.org/10.1016/j.supflu.2014.01.006.

[25] Singh R, Chaudhary K, Biswas B, Balagurumurthy B, Bhaskar T. Hydrothermal liquefaction of rice straw: Effect of reaction environment. J Supercrit Fluids 2015;104:70–5. https://doi.org/10.1016/j.supflu.2015.05.027.

[26] Promdej C, Matsumura Y. Temperature Effect on Hydrothermal Decomposition of Glucose in Sub- And Supercritical Water. Ind Eng Chem Res 2011;50:8492–7. https://doi.org/10.1021/ie200298c.

[27] Yong TL-K, Matsumura Y. Reaction Kinetics of the Lignin Conversion in Supercritical Water. Ind Eng Chem Res 2012;51:11975–88. https://doi.org/10.1021/ie300921d.

[28] de Caprariis B, De Filippis P, Petrullo A, Scarsella M. Hydrothermal liquefaction of biomass: Influence of temperature and biomass composition on the bio-oil production. Fuel 2017;208:618–25. https://doi.org/10.1016/j.fuel.2017.07.054.

[29] Magdeldin M, Kohl T, Järvinen M. Techno-economic assessment of integrated hydrothermal liquefaction and combined heat and power production from lignocellulose residues 2018. https://doi.org/10.13044/j.sdewes.d5.0177.

[30] Fache M, Boutevin B, Caillol S. Vanillin Production from Lignin and Its Use as a Renewable Chemical. ACS Sustain Chem Eng 2016;4:35–46. https://doi.org/10.1021/acssuschemeng.5b01344.

[31] Lui MY, Chan B, Yuen AKL, Masters AF, Montoya A, Maschmeyer T. Unravelling Some of the Key Transformations in the Hydrothermal Liquefaction of Lignin. ChemSusChem 2017;10:2140–4. https://doi.org/10.1002/cssc.201700528.

[32] Sauer J, Dahmen N, Hornung U, Schuler J, Kruse A. Hydrothermal Liquefaction of Lignin. J Biomater Nanobiotechnology 2017;8:720–6. https://doi.org/10.4236/jbnb.2017.81007.
[33] Kang S, Li X, Fan J, Chang J. Classified Separation of Lignin Hydrothermal Liquefied Products. Ind Eng Chem Res 2011;50:11288–96. https://doi.org/10.1021/ie2011356.
[34] Kang S, Li X, Fan J, Chang J. Hydrothermal conversion of lignin: A review. Renew Sustain Energy Rev 2013;27:546–58.
[35] King AG, Wright MW. Rudolph Diesel Meets the Soybean: "Greasing" the Wheels of Chemical Education. J Chem Educ 2007;84:202. https://doi.org/10.1021/ed084p202.
[36] Vassilev SV, Vassileva CG. Composition, properties, and challenges of algae biomass for biofuel application: An overview. Fuel 2016;181:1–33. https://doi.org/10.1016/j.fuel.2016.04.106.
[37] Dimitriadis A, Bezergianni S. Hydrothermal liquefaction of various biomass and waste feedstocks for biocrude production: A state of the art review. Renew Sustain Energy Rev 2017;68:113–25. https://doi.org/10.1016/j.rser.2016.09.120.
[38] Akhtar J, Amin NAS. A review on process conditions for optimum bio-oil yield in hydrothermal liquefaction of biomass. Renew Sustain Energy Rev 2011;15:1615–24. https://doi.org/10.1016/j.rser.2010.11.054.
[39] Minowa T, Yokoyama S, Kishimoto M, Okakura T. Oil production from algal cells of Dunaliella tertiolecta by direct thermochemical liquefaction. Fuel 1995;74:1735–8. https://doi.org/10.1016/0016-2361(95)80001-X.
[40] Faeth JL, Valdez PJ, Savage PE. Fast Hydrothermal Liquefaction of Nannochloropsis sp. To Produce Biocrude. Energy Fuels 2013;27:1391–8. https://doi.org/10.1021/ef301925d.
[41] Biller P, Ross AB. Potential yields and properties of oil from the hydrothermal liquefaction of microalgae with different biochemical content. Bioresour Technol 2011;102:215–25. https://doi.org/10.1016/j.biortech.2010.06.028.
[42] Nizamuddin S, Ahmed Baloch H, Griffin GJ, Mubarak NM, Bhutto AW, Abro R, et al. An overview of effect of process parameters on hydrothermal carbonization of biomass. Renew Sustain Energy Rev 2017;73:1289–99. https://doi.org/10.1016/j.rser.2016.12.122.

[43] López Barreiro D, Barreiro DL, Prins W, Ronsse F, Brilman W. Hydrothermal liquefaction (HTL) of microalgae for biofuel production: State of the art review and future prospects. Biomass Bioenergy n.d.;53:113–27.
[44] Heilmann SM, Davis HT, Jader LR, Lefebvre PA, Sadowsky MJ, Schendel FJ, et al. Hydrothermal carbonization of microalgae. Biomass Bioenergy 2010;34:875–82. https://doi.org/10.1016/j.biombioe.2010.01.032.
[45] Levine RB, Pinnarat T, Savage PE. Biodiesel Production from Wet Algal Biomass through in Situ Lipid Hydrolysis and Supercritical Transesterification. Energy Fuels 2010;24:5235–43. https://doi.org/10.1021/ef1008314.
[46] Beckman D, Elliott DC. Comparisons of the yields and properties of the oil products from direct thermochemical biomass liquefaction processes. Can J Chem Eng 1985;63:99–104. https://doi.org/10.1002/cjce.5450630116.
[47] Behrendt F, Neubauer Y, Oevermann M, Wilmes B, Zobel N. Direct Liquefaction of Biomass. Chem Eng Technol 2008;31:667–77. https://doi.org/10.1002/ceat.200800077.
[48] Demirbaş A. Effect of lignin content on aqueous liquefaction products of biomass. Energy Convers Manag 2000;41:1601–7. https://doi.org/10.1016/S0196-8904(00)00013-3.
[49] Yuan XZ, Tong JY, Zeng GM, Li H, Xie W. Comparative Studies of Products Obtained at Different Temperatures during Straw Liquefaction by Hot Compressed Water. Energy Fuels 2009;23:3262–7. https://doi.org/10.1021/ef900027d.
[50] Overend RP, Milne T, Mudge L, editors. Fundamentals of Thermochemical Biomass Conversion. Springer Netherlands; 1985.
[51] Hietala DC, Faeth JL, Savage PE. A quantitative kinetic model for the fast and isothermal hydrothermal liquefaction of Nannochloropsis sp. Bioresour Technol 2016;214:102–11. https://doi.org/10.1016/j.biortech.2016.04.067.
[52] Mosteiro-Romero M, Vogel F, Wokaun A. Liquefaction of wood in hot compressed water Part 2–Modeling of particle dissolution. Chem Eng Sci 2014;109:220–35. https://doi.org/10.1016/j.ces.2013.12.039.
[53] Sheehan JD, Savage PE. Modeling the effects of microalga biochemical content on the kinetics and biocrude yields from hydrothermal liquefac-

tion. Bioresour Technol 2017;239:144–50.
https://doi.org/10.1016/j.biortech.2017.05.013.
[54] Costanzo W, Hilten R, Jena U, Das KC, Kastner JR. Effect of low temperature hydrothermal liquefaction on catalytic hydrodenitrogenation of algae biocrude and model macromolecules. Algal Res 2016;13:53–68.
https://doi.org/10.1016/j.algal.2015.11.009.
[55] Zhu Z, Rosendahl L, Toor SS, Yu D, Chen G. Hydrothermal liquefaction of barley straw to bio-crude oil: Effects of reaction temperature and aqueous phase recirculation. Appl Energy 2015;137:183–92.
https://doi.org/10.1016/j.apenergy.2014.10.005.
[56] Valdez PJ, Tocco VJ, Savage PE. A general kinetic model for the hydrothermal liquefaction of microalgae. Bioresour Technol 2014;163:123–7.
https://doi.org/10.1016/j.biortech.2014.04.013.
[57] Zou S, Wu Y, Yang M, Li C, Tong J. Bio-oil production from sub- and supercritical water liquefaction of microalgae Dunaliella tertiolecta and related properties. Energy Environ Sci 2010;3:1073–8.
https://doi.org/10.1039/C002550J.
[58] Yoshida T, Matsumura Y. Reactor Development for Supercritical Water Gasification of 4.9 wt% Glucose Solution at 673 K by Using Computational Fluid Dynamics. Ind Eng Chem Res 2009;48:8381–6.
https://doi.org/10.1021/ie9002188.
[59] Ranganathan P, Savithri S. Computational Fluid Dynamics simulation of hydrothermal liquefaction of microalgae in a continuous plug-flow reactor. Bioresour Technol 2018;258:151–7.
https://doi.org/10.1016/j.biortech.2018.02.076.
[60] Alshammari YM, Hellgardt K. CFD analysis of hydrothermal conversion of heavy oil in continuous flow reactor. Chem Eng Res Des 2017;117:250–64. https://doi.org/10.1016/j.cherd.2016.10.002.
[61] Tran K-Q, Håkansson L, Trinh TT. CFD pre-study of Nozzle reactor for fast hydrothermal liquefaction. Energy Procedia 2017;142:861–6.
https://doi.org/10.1016/j.egypro.2017.12.138.
[62] Yukananto R, Pozarlik A, Bramer E, Brem G. Numerical modelling of char formation during glucose gasification in supercritical water. J Supercrit Fluids 2018;140:258–69.
https://doi.org/10.1016/j.supflu.2018.06.007.

[63] Vo TK, Lee OK, Lee EY, Kim CH, Seo J-W, Kim J, et al. Kinetics study of the hydrothermal liquefaction of the microalga Aurantiochytrium sp. KRS101. Chem Eng J 2016;306:763–71. https://doi.org/10.1016/j.cej.2016.07.104.

[64] Vo TK, Kim S-S, Ly HV, Lee EY, Lee C-G, Kim J. A general reaction network and kinetic model of the hydrothermal liquefaction of microalgae Tetraselmis sp. Bioresour Technol 2017;241:610–9. https://doi.org/10.1016/j.biortech.2017.05.186.

[65] Ederer M, Gilles ED. Thermodynamic Constraints in Kinetic Modeling: Thermodynamic-Kinetic Modeling in Comparison to Other Approaches. Eng Life Sci 2008;8:467–76. https://doi.org/10.1002/elsc.200800040.

[66] Lu Y, Guo L, Zhang X, Yan Q. Thermodynamic modeling and analysis of biomass gasification for hydrogen production in supercritical water. Chem Eng J 2007;131:233–44. https://doi.org/10.1016/j.cej.2006.11.016.

[67] Tran K-Q, Klemsdal AJ, Zhang W, Sandquist J, Wang L, Skreiberg Ø. Fast Hydrothermal Liquefaction of Native and Torrefied Wood. Energy Procedia 2017;105:218–23. https://doi.org/10.1016/j.egypro.2017.03.305.

[68] Goodwin AK, Rorrer GL. Modeling of Supercritical Water Gasification of Xylose to Hydrogen-Rich Gas in a Hastelloy Microchannel Reactor. Ind Eng Chem Res 2011;50:7172–82. https://doi.org/10.1021/ie102482y.

[69] Caputo G, Rubio P, Scargiali F, Marotta G, Brucato A. Experimental and fluid dynamic study of continuous supercritical water gasification of glucose. J Supercrit Fluids 2016;107:450–61. https://doi.org/10.1016/j.supflu.2015.09.022.

[70] Jin H, Guo S, Guo L, Cao C. A mathematical model and numerical investigation for glycerol gasification in supercritical water with a tubular reactor. J Supercrit Fluids 2016;107:526–33. https://doi.org/10.1016/j.supflu.2015.06.028.

[71] Yukananto R, Pozarlik AK, Brem G. Computational fluid dynamic model for glycerol gasification in supercritical water in a tee junction shaped cylindrical reactor. J Supercrit Fluids 2018;133:330–42. https://doi.org/10.1016/j.supflu.2017.11.001.

[72] Vogel F. Catalytic Conversion of High-Moisture Biomass to Synthetic Natural Gas in Supercritical Water. Handb. Green Chem., American Can-

cer Society; 2010, p. 281–324.
https://doi.org/10.1002/9783527628698.hgc024.
[73] Galgano A, Blasi CD. Modeling Wood Degradation by the Unreacted-Core-Shrinking Approximation. Ind Eng Chem Res 2003;42:2101–11. https://doi.org/10.1021/ie020939o.
[74] Ahn H, Choi S. A comparison of the shrinking core model and the grain model for the iron ore pellet indurator simulation. Comput Chem Eng 2017;97:13–26. https://doi.org/10.1016/j.compchemeng.2016.11.005.
[75] Peters B, Džiugys A, Navakas R. A SHRINKING MODEL FOR COMBUSTION/GASIFICATION OF CHAR BASED ON TRANSPORT AND REACTION TIME SCALES. Mechanics 2012;18:177–85. https://doi.org/10.5755/j01.mech.18.2.1564.
[76] Tudela I, Bonete P, Fullana A, Conesa JA. Parameter Sensitivity Study of the Unreacted-Core Shrinking Model: A Computer Activity for Chemical Reaction Engineering Courses. J Chem Educ 2011;88:56–8. https://doi.org/10.1021/ed100302n.
[77] Kamio E, Sato H, Takahashi S, Noda H, Fukuhara C, Okamura T. Liquefaction kinetics of cellulose treated by hot compressed water under variable temperature conditions. J Mater Sci 2008;43:2179–88. https://doi.org/10.1007/s10853-007-2043-6.
[78] Adler E. Lignin chemistry—past, present and future. Wood Sci Technol 1977;11:169–218. https://doi.org/10.1007/BF00365615.
[79] Henriksson G. 6. Lignin. De Gruyter; 2009.
[80] Pinkert A, Goeke DF, Marsh KN, Pang S. Extracting wood lignin without dissolving or degrading cellulose: investigations on the use of food additive-derived ionic liquids. Green Chem 2011;13:3124–36. https://doi.org/10.1039/C1GC15671C.
[81] Collinson SR, Thielemans W. The catalytic oxidation of biomass to new materials focusing on starch, cellulose and lignin. Coord Chem Rev 2010;254:1854–70. https://doi.org/10.1016/j.ccr.2010.04.007.
[82] Tobimatsu Y, Chen F, Nakashima J, Escamilla-Treviño LL, Jackson L, Dixon RA, et al. Coexistence but independent biosynthesis of catechyl and guaiacyl/syringyl lignin polymers in seed coats. Plant Cell 2013;25:2587–600. https://doi.org/10.1105/tpc.113.113142.

[83] Kuroda K. Analytical pyrolysis products derived from cinnamyl alcohol-end groups in lignins. J Anal Appl Pyrolysis 2000;53:123–34. https://doi.org/10.1016/S0165-2370(99)00067-4.

[84] Buranov AU, Mazza G. Lignin in straw of herbaceous crops. Ind Crops Prod 2008;28:237–59. https://doi.org/10.1016/j.indcrop.2008.03.008.

[85] Bolton JJ, Germann I, Luning K. Hybridization between Atlantic and Pacific representatives of the Simplices section of Laminaria (Phaeophyta). Phycologia 1983;22:133–40. https://doi.org/10.2216/i0031-8884-22-2-133.1.

[86] Anastasakis K, Ross AB. Hydrothermal liquefaction of the brown macroalga Laminaria saccharina: effect of reaction conditions on product distribution and composition. Bioresour Technol 2011;102:4876–83. https://doi.org/10.1016/j.biortech.2011.01.031.

[87] Broch OJ, Alver MO, Bekkby T, Gundersen H, Forbord S, Handå A, et al. The Kelp Cultivation Potential in Coastal and Offshore Regions of Norway. Front Mar Sci 2019;5. https://doi.org/10.3389/fmars.2018.00529.

[88] Holdt SL, Kraan S. Bioactive compounds in seaweed: functional food applications and legislation. J Appl Phycol 2011;23:543–97. https://doi.org/10.1007/s10811-010-9632-5.

[89] Nielsen MM, Manns D, D'Este M, Krause-Jensen D, Rasmussen MB, Larsen MM, et al. Variation in biochemical composition of Saccharina latissima and Laminaria digitata along an estuarine salinity gradient in inner Danish waters. Algal Res 2016;13:235–45. https://doi.org/10.1016/j.algal.2015.12.003.

[90] Monteiro JP, Rey F, Melo T, Moreira ASP, Arbona J-F, Skjermo J, et al. The Unique Lipidomic Signatures of Saccharina latissima Can Be Used to Pinpoint Their Geographic Origin. Biomolecules 2020;10:107. https://doi.org/10.3390/biom10010107.

[91] Minowa T, Fang Z, Ogi T, Várhegyi G. Decomposition of Cellulose and Glucose in Hot-Compressed Water under Catalyst-Free Conditions. J Chem Eng Jpn 1998;31:131–4. https://doi.org/10.1252/jcej.31.131.

[92] Yong TL-K, Matsumura Y. Kinetic Analysis of Lignin Hydrothermal Conversion in Sub- and Supercritical Water. Ind Eng Chem Res 2013;52:5626–39. https://doi.org/10.1021/ie400600x.

[93] Kamio E, Takahashi S, Noda H, Fukuhara C, Okamura T. Effect of heating rate on liquefaction of cellulose by hot compressed water. Chem Eng J 2008;137:328–38. https://doi.org/10.1016/j.cej.2007.05.007.

[94] Hu S, Jess A, Xu M. Kinetic study of Chinese biomass slow pyrolysis: Comparison of different kinetic models. Fuel 2007;86:2778–88. https://doi.org/10.1016/j.fuel.2007.02.031.

[95] Mehrabian R, Zahirovic S, Scharler R, Obernberger I, Kleditzsch S, Wirtz S, et al. A CFD model for thermal conversion of thermally thick biomass particles. Fuel Process Technol 2012;95:96–108. https://doi.org/10.1016/j.fuproc.2011.11.021.

[96] Thunman H, Leckner B, Niklasson F, Johnsson F. Combustion of wood particles—a particle model for eulerian calculations. Combust Flame 2002;129:30–46. https://doi.org/10.1016/S0010-2180(01)00371-6.

[97] Cantero DA, Bermejo MD, Cocero MJ. Kinetic analysis of cellulose depolymerization reactions in near critical water. J Supercrit Fluids 2013;75:48–57. https://doi.org/10.1016/j.supflu.2012.12.013.

[98] Sasaki M, Adschiri T, Arai K. Kinetics of cellulose conversion at 25 MPa in sub- and supercritical water. AIChE J 2004;50:192–202. https://doi.org/10.1002/aic.10018.

[99] Sasaki M, Kabyemela B, Malaluan R, Hirose S, Takeda N, Adschiri T, et al. Cellulose hydrolysis in subcritical and supercritical water. J Supercrit Fluids 1998;13:261–8. https://doi.org/10.1016/S0896-8446(98)00060-6.

[100] Sasaki M, Fang Z, Fukushima Y, Adschiri T, Arai K. Dissolution and Hydrolysis of Cellulose in Subcritical and Supercritical Water. Ind Eng Chem Res 2000;39:2883–90. https://doi.org/10.1021/ie990690j.

[101] Fang Z, Sato T, Smith RL, Inomata H, Arai K, Kozinski JA. Reaction chemistry and phase behavior of lignin in high-temperature and supercritical water. Bioresour Technol 2008;99:3424–30. https://doi.org/10.1016/j.biortech.2007.08.008.

[102] Zhang B, Huang H-J, Ramaswamy S. Reaction kinetics of the hydrothermal treatment of lignin. Appl Biochem Biotechnol 2008;147:119–31. https://doi.org/10.1007/s12010-007-8070-6.

[103] Forchheim D, Hornung U, Kruse A, Sutter T. Kinetic Modelling of Hydrothermal Lignin Depolymerisation. Waste Biomass Valorization 2014;5:985–94. https://doi.org/10.1007/s12649-014-9307-6.

[104] Arturi KR, Strandgaard M, Nielsen RP, Søgaard EG, Maschietti M. Hydrothermal liquefaction of lignin in near-critical water in a new batch reactor: Influence of phenol and temperature. J Supercrit Fluids 2017;123:28–39. https://doi.org/10.1016/j.supflu.2016.12.015.

[105] Ye Y, Zhang Y, Fan J, Chang J. Novel Method for Production of Phenolics by Combining Lignin Extraction with Lignin Depolymerization in Aqueous Ethanol. Ind Eng Chem Res 2012;51:103–10. https://doi.org/10.1021/ie202118d.

[106] Pińkowska H, Wolak P, Złocińska A. Hydrothermal decomposition of alkali lignin in sub- and supercritical water. Chem Eng J 2012;187:410–4. https://doi.org/10.1016/j.cej.2012.01.092.

[107] Pronyk C, Mazza G. Kinetic Modeling of Hemicellulose Hydrolysis from Triticale Straw in a Pressurized Low Polarity Water Flow-Through Reactor. Ind Eng Chem Res 2010;49:6367–75. https://doi.org/10.1021/ie1003625.

[108] Pińkowska H, Wolak P, Złocińska A. Hydrothermal decomposition of xylan as a model substance for plant biomass waste – Hydrothermolysis in subcritical water. Biomass Bioenergy 2011;35:3902–12. https://doi.org/10.1016/j.biombioe.2011.06.015.

[109] Delbecq F, Wang Y, Muralidhara A, El Ouardi K, Marlair G, Len C. Hydrolysis of Hemicellulose and Derivatives—A Review of Recent Advances in the Production of Furfural. Front Chem 2018;6. https://doi.org/10.3389/fchem.2018.00146.

[110] Möller M, Schröder U. Hydrothermal production of furfural from xylose and xylan as model compounds for hemicelluloses. RSC Adv 2013;3:22253–60. https://doi.org/10.1039/C3RA43108H.

[111] Ferreira SLC, Bruns RE, Ferreira HS, Matos GD, David JM, Brandão GC, et al. Box-Behnken design: An alternative for the optimization of analytical methods. Anal Chim Acta 2007;597:179–86. https://doi.org/10.1016/j.aca.2007.07.011.

[112] Brebu M, Vasile C. THERMAL DEGRADATION OF LIGNIN – A REVIEW. Cellul Chem Technol 2010;44:353–63.

[113] Stewart D. Lignin as a base material for materials applications: Chemistry, application and economics. Ind Crops Prod 2008;27:202–7. https://doi.org/10.1016/j.indcrop.2007.07.008.

[114] Thakur VK, Thakur MK, Raghavan P, Kessler MR. Progress in Green Polymer Composites from Lignin for Multifunctional Applications: A Review. ACS Sustain Chem Eng 2014;2:1072–92. https://doi.org/10.1021/sc500087z.

[115] Kadla JF, Kubo S, Venditti RA, Gilbert RD, Compere AL, Griffith W. Lignin-based carbon fibers for composite fiber applications. Carbon 2002;40:2913–20. https://doi.org/10.1016/S0008-6223(02)00248-8.

[116] Breunig M, Gebhart P, Hornung U, Kruse A, Dinjus E. Direct liquefaction of lignin and lignin rich biomasses by heterogenic catalytic hydrogenolysis. Biomass Bioenergy 2018;111:352–60. https://doi.org/10.1016/j.biombioe.2017.06.001.

[117] Elliott DC, Hart TR, Neuenschwander GG, Rotness LJ, Roesijadi G, Zacher AH, et al. Hydrothermal Processing of Macroalgal Feedstocks in Continuous-Flow Reactors. ACS Sustain Chem Eng 2014;2:207–15. https://doi.org/10.1021/sc400251p.

[118] Parsa M, Jalilzadeh H, Pazoki M, Ghasemzadeh R, Abduli M. Hydrothermal liquefaction of Gracilaria gracilis and Cladophora glomerata macro-algae for biocrude production. Bioresour Technol 2018;250:26–34. https://doi.org/10.1016/j.biortech.2017.10.059.

[119] Derringer G, Suich R. Simultaneous optimization of several response variables. J Qual Technol 1980;12:214–9.

[120] Jin B, Duan P, Xu Y, Wang F, Fan Y. Co-liquefaction of micro- and macroalgae in subcritical water. Bioresour Technol 2013;149:103–10. https://doi.org/10.1016/j.biortech.2013.09.045.

[121] Brown TM, Duan P, Savage PE. Hydrothermal Liquefaction and Gasification of Nannochloropsis sp. Energy Fuels 2010;24:3639–46. https://doi.org/10.1021/ef100203u.

[122] Wahyudiono, Sasaki M, Goto M. Thermal decomposition of guaiacol in sub- and supercritical water and its kinetic analysis. J Mater Cycles Waste Manag 2011;13:68–79. https://doi.org/10.1007/s10163-010-0309-6.

[123] Kleinert M, Barth T. Phenols from Lignin. Chem Eng Technol 2008;31:736–45. https://doi.org/10.1002/ceat.200800073.

[124] Lawson JR, Klein MT. Influence of water on guaiacol pyrolysis. Ind Eng Chem Fundam 1985;24:203–8. https://doi.org/10.1021/i100018a012.

[125] Hu J, Shen D, Wu S, Zhang H, Xiao R. Effect of temperature on structure evolution in char from hydrothermal degradation of lignin. J Anal Appl Pyrolysis 2014;106:118–24. https://doi.org/10.1016/j.jaap.2014.01.008.

[126] Sharma RK, Wooten JB, Baliga VL, Lin X, Geoffrey Chan W, Hajaligol MR. Characterization of chars from pyrolysis of lignin. Fuel 2004;83:1469–82. https://doi.org/10.1016/j.fuel.2003.11.015.

[127] Zhao S-X, Ta N, Wang X-D. Effect of Temperature on the Structural and Physicochemical Properties of Biochar with Apple Tree Branches as Feedstock Material. Energies 2017;10:1293. https://doi.org/10.3390/en10091293.

[128] Zhu X, Liu Y, Qian F, Zhou C, Zhang S, Chen J. Role of Hydrochar Properties on the Porosity of Hydrochar-based Porous Carbon for Their Sustainable Application. ACS Sustain Chem Eng 2015;3:833–40. https://doi.org/10.1021/acssuschemeng.5b00153.

[129] Zhou L, Liu Y, Liu S, Yin Y, Zeng G, Tan X, et al. Investigation of the adsorption-reduction mechanisms of hexavalent chromium by ramie biochars of different pyrolytic temperatures. Bioresour Technol 2016;218:351–9. https://doi.org/10.1016/j.biortech.2016.06.102.

[130] Wahyudiono, Sasaki M, Goto M. Recovery of phenolic compounds through the decomposition of lignin in near and supercritical water. Chem Eng Process Process Intensif 2008;47:1609–19. https://doi.org/10.1016/j.cep.2007.09.001.

[131] Chen Y, Yang H, Wang X, Zhang S, Chen H. Biomass-based pyrolytic polygeneration system on cotton stalk pyrolysis: influence of temperature. Bioresour Technol 2012;107:411–8. https://doi.org/10.1016/j.biortech.2011.10.074.

[132] Liu Z, Zhang F-S. Removal of lead from water using biochars prepared from hydrothermal liquefaction of biomass. J Hazard Mater 2009;167:933–9. https://doi.org/10.1016/j.jhazmat.2009.01.085.

[133] Chen Z, Ma L, Li S, Geng J, Song Q, Liu J, et al. Simple approach to carboxyl-rich materials through low-temperature heat treatment of hydrothermal carbon in air. Appl Surf Sci 2011;257:8686–91. https://doi.org/10.1016/j.apsusc.2011.05.048.

[134] Mosteiro-Romero M, Vogel F, Wokaun A. Liquefaction of wood in hot compressed water: Part 1 — Experimental results. Chem Eng Sci 2014;109:111–22. https://doi.org/10.1016/j.ces.2013.12.038.

[135] Wądrzyk M, Berdel M, Janus R, Brilman DWF. Hydrothermal processing of pine wood: effect of process variables on bio-oil quality and yield. E3S Web Conf 2019;108:02004. https://doi.org/10.1051/e3sconf/201910802004.

[136] Qu Y, Wei X, Zhong C. Experimental study on the direct liquefaction of Cunninghamia lanceolata in water. Energy 2003;28:597–606. https://doi.org/10.1016/S0360-5442(02)00178-0.

[137] Boocock DGB, Sherman KM. Further aspects of powdered poplar wood liquefaction by aqueous pyrolysis. Can J Chem Eng 1985;63:627–33. https://doi.org/10.1002/cjce.5450630415.

[138] Yj Y, J X, Tc L, Zw R. Liquefaction of sawdust for liquid fuel. Fuel Process Technol 1999;60:135–43.

[139] Kozliak EI, Kubátová A, Artemyeva AA, Nagel E, Zhang C, Rajappagowda RB, et al. Thermal Liquefaction of Lignin to Aromatics: Efficiency, Selectivity, and Product Analysis. ACS Sustain Chem Eng 2016;4:5106–22. https://doi.org/10.1021/acssuschemeng.6b01046.

Appendices

Article A

Hydrothermal liquefaction of wood using a modified multistage shrinking-core model. Jayathilake, Madhawa; Rudra, Souman; Rosendahl, Lasse A. (2020). Published in Fuel (2020).

The layout has been revised

Hydrothermal Liquefaction of Wood Using A Modified Multistage Shrinking-Core Model

Madhawa Jayathilake[a], Souman Rudra[a1], Lasse A. Rosendahl[b]

[a] Department of Engineering Sciences, University of Agder, Jon Lilletuns vei 9, 4879 Grimstad, Norway, Tel: +47 37233308, Email address: rukshanj@uia.no
Tel: +47 37 23 30 36, Email address: souman.rudra@uia.no

[b] Department of Energy Technology, Aalborg University, Pontoppidanstræde 101, 9220, Aalborg, Denmark, E mail address : lar@et.aau.dk

[1] corresponding author Tel: +47 37 23 30 36,
E mail address: souman.rudra@uia.no

Abstract

Wood liquefaction in hot compressed water is modelled using the hydrolysis of Cellulose, Hemicellulose, and Lignin. These three components are reacted under catalyst-free subcritical conditions in a temperature range from 553K to 640K, and the heating rate ranges from 2 K/min to 6 K/min. Using a simplified reaction scheme, water-soluble products[2] (WSP), Biocrude, char, and gas are generated through intermediates with each wood component. A modified multistage shrinking core model is employed to simulate biomass particle degradation.

The reaction and kinetic regime of the hydrothermal liquefaction[3] (HTL) process are treated separately for each wood component. Although the lack of initial fast reaction kinetic data limits the development of more accurate models, computed results displayed a generous fit to data from the literature.

At 593K for a 2K/min heating rate and particle size of 0.08 mm, biocrude shows the maximum yield of 26.87% for wood liquefaction. Although lower heating rates show fast initial lignin hydrolysis, for longer residence times, and close to the critical point, yield outputs show similar yields. Meanwhile, char and gas yields of cellulose model show maximums of 55 wt.% and 25 wt.% respectively at 640K with a 2K/min heating rate. Nevertheless, char yield values become very similar at 640K for different heating rates for the cellulose hydrolysis model. Both cellulose and lignin hydrolysis models show better hydrolysis with smaller particle sizes. Besides, lignin decomposition shows more dependence on the particle size, where it decomposes much faster with 0.08mm particle and slower than Cellulose with the 1mm particle.

Keywords*: - *Liquefaction*, *Shrinking-core, Wood, Hydrolysis

WSP	Water-soluble products
HTL	Hydrothermal liquefaction
TOC	Total organic carbon
5-HMF	5-hydroxyl-methyl-furfural

[2] WSP: - Water soluble products

[3] HTL: -Hydrothermal Liquefaction

1. Introduction

Hydrothermal liquefaction (HTL) is a thermochemical conversion method which mainly produces a liquid crude oil. In the HTL process, initially, the biomass is decomposed into smaller molecules through hydrolysis [1]. HTL process and hydrolysis of wood in subcritical and supercritical water have been widely investigated recently[2–7]. Besides, the main components of wood are also used to study the hydrolysis such as cellulose and Lignin [8–18]. Radical decomposition of Cellulose to oligosaccharides and monosaccharides at 513 K is investigated where the latter showcased heating rates below 1 K/s affected the cellulose hydrolysis[10,11]. As the most abundant component of woody biomass, Cellulose is widely used for hydrolysis studies. The increase of hydrolysis products in supercritical water and the kinetics of cellulose hydrolysis in the sub and supercritical water is also proposed successfully with a grain model by Sasaki et al.[14,15,17]. Cellulose and glucose decomposition pathways in hot compressed water under catalysts free conditions are investigated by Minowa et al. [19]. A study by Kabyemela et al. [20] observed the forward epimerization of glucose to fructose in subcritical temperatures, where backward epimerization from fructose to glucose is found to be negligible. Glucose is decomposed quickly from 573K to 623K [20]. Although the activation energies for glucose decomposition to fructose did not differ much around critical point, 5-hydroxyl-methyl-furfural (5-HMF) reaction kinetics are drastically changed around 603K due to ionic product and low density of water [21].

Yong and Matsumara [9] extensively studied the lignin decomposition in the subcritical conditions and came up with a comprehensive reaction scheme. According to Yong and Matsumara [9], most of the reaction rate constants of lignin decomposition followed the Arrhenius behavior where some of the reactions follow a non-Arrhenius behavior. Zhang et al. [22] proposed a kinetic model with kinetic data for Kraft lignin decomposition and suggested the kraft pine lignin followed a two-phase decomposition scheme. Forchheim et al. [23] successfully estimated the phenolic products from lignin hydrothermal depolymerization with another kinetic model where they discussed some tendencies of gas and solid residue behavior in variable operating conditions.

Hydrolysis studies on hemicellulose are not abundantly found. Pronyk and Mazza [13] proposed a monophasic and biphasic reaction mechanism for hemicellulose hydrolysis. The contribution from hemicellulose to biocrude is quite small as the production of furfural from hemicellulose is found to be considered insignificant after 443K [13]. A recent review by Delbecq et al. [24] extensively discussed the furfural synthesis from bio-based products where the hydrolysis of hemicellulose and derivatives are analyzed and optimized. Hemicellulose (Xylan) produced its maximum hydrolysis yield at a low-temperature value of 493 K-508 K [25] or even lower temperatures such as 473 K[26]. With higher temperatures, the hydrolysis of xylan is decreased significantly, and ultimately xylose, and then furfural production is decreased[26].

Various approaches are used to model the hydrolysis of wood and the decomposing method of the wood, while the shrinking core approach is one of the main criteria used[7,10,11,27]. Galegano and Blasi [27] and Kamio et al. [10,11] used the unreacted shrinking core concept to model pyrolysis and hydrolysis, respectively, by using the same particle decomposition concept in two different thermochemical processes. Mosteiro-Romero et al. [7] developed a mathematical model on wood hydrolysis with a shrinking core model, which was developed upon well designed experimental data. It was able to predict the hydrolysis products yields to a convincing extent, which were modeled as lump components.

1.1 Shrinking core approach and hydrolysis modeling

Hydrolysis modeling of wood with kinetic models is scarce[7]. Frequently, model compounds are abundantly used for the kinetic models of hydrolysis studies[4,5,8–11,13,22,25]. Besides, the proposed model is influenced by the model developed by Kamio et al. [11] for cellulose hydrolysis.

Kamio et al. [11] developed a single particle system in subcritical conditions for cellulose hydrolysis with a shrinking core approach for the particle, where reduction of the particle occurs only in the radial direction. Due to a surface

reaction on the particle surface, cellulose particle is hydrolyzed by the water monomer and result in producing oligosaccharides to the system. Then the oligosaccharides are further hydrolyzed into monosaccharides where it is then hydrolyzed into degradation products. Here the oligosaccharides represent the glucose units, and monosaccharides represent glucose and fructose. Degradation products represent the decomposition products from monosaccharides as overall.

In the proposed model, wood hydrolysis is modeled using the hydrolysis of three main components of wood. Each wood component has its hydrolysis reaction mechanism and will produce hydrolysis products. It is proposed to model the wood hydrolysis by using the cumulative effect of each hydrolysis model from the three wood components. The decomposition of the wood particle is assumed to be only in the radial direction. Thus, the modeling criteria used in this model are a shrinking core model. Figure 1 below shows a graphical model of the assumed shrinking core concept used for the proposed model.

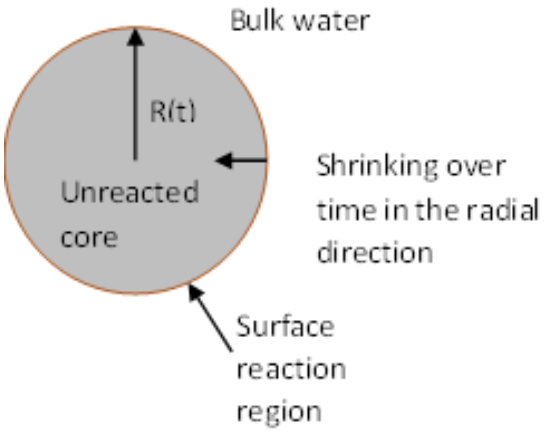

Figure 11: Shrinking core model assumed for the hydrolysis of the wood particle of model components submerged in water

The modeling criteria of the shrinking core model is based on the model proposed by Kamio et al.[11], Galegano and Blasi[27], and Mosteiro-Romeiro et al.[7]. Reactions used in this model are divided into cellulose reactions, lignin reactions, and hemicellulose reactions.

Despite the various studies on hydrolysis studies on each component of wood separately, there is a lack of models of studying the behavior and role of each wood component in the overall wood liquefaction. By developing a model with having all the three main components of wood, the effect of each component hydrolysis on wood hydrolysis can be studied. Moreover, the contribution of each component on the liquefaction outputs can be thoroughly investigated. Therefore, a mathematical model for decomposition of wood in subcritical temperature is developed using a modified shrinking core model where a custom reaction kinetic rate is developed to hydrolysis of each wood component. Wood consists of Cellulose, Lignin, and hemicellulose. Although the hydrolysis of each component is treated separately, core shrinkage is modeled as a cumulative effect of hydrolysis of each component. Hence, this model simulates wood decomposition by using three main components of wood. Furthermore, the behavior of each component and their distribution in different outputs can be studied with this model. The hydrolysis of each component is used as the initial reaction of the process. The diffusion of water monomers to the particle surface to initiate hydrolysis and dissolution of the products in water is also given importance during the modeling process. Once the degradation process is underway with heterogeneous hydrolysis, the dissolved compounds will further hydrolyze with homogeneous hydrolysis and behave according to the kinetic model. More chemical compounds are incorporated in the model, and chemical reactions of those chemical compounds are used rather than using lump components. In the developed model, the kinetic reaction rate constants vary according to the temperature. Since the temperature is changed during the process, the Arrhenius equation[28] is used to calculate the fluctuating rate constants. Additionally, kinetic parameters from the literature are used for the initial kinetic data for the mathematical model.

2. Method

2.1 Decomposition of the biomass particle

In the proposed model, initially, the particle is considered as a combination of Cellulose, hemicellulose, and Lignin. At different temperatures, according to the reaction kinetics, each component is started hydrolyzing. The hydrolysis of each component is determined by the developed reaction rate constant (Shown later in the modeling process). The overall biomass particle decomposition is assumed to be a cumulative effect of each component and in the radial direc-

tion. As Kamio et al.[11] proposed, diffusion of the water monomer through the aqueous film surrounding the biomass particle is modeled using the mass transfer of water.

$$M_w = 4\pi r^2 k_A (C_b - C_S) \quad (1)$$

M_w represent the mass transfer rate of the water monomer, r is the radial position of the particle, k_A is the mass transfer coefficient, C_B represents the bulk water monomer concentration, and C_S is the water concentration at the surface.

Hydrolysis of the biomass particle is expressed below, where M_B is the hydrolysis reaction rate at the surface of each wood component $k_H$is the hydrolysis rate constant.

$$M_B = 4\pi r^2 k_H C_S \quad (2)$$

Assuming the overall rate constant of hydrolysis of the biomass particle k_H is the sum of hydrolysis rate constants of three wood components. Below, equation 3 shows the overall hydrolysis rate constant of the biomass particle hydrolysis.

$$k_H = k_1 + k_5 + k_{10} + k_{11} + k_{12} + k_{13} + k_{14} + k_{26} \quad (3)$$

(k_H becomes a different value according to the wood component, which is being hydrolyzed. As an example, if only Cellulose is being hydrolyzed $k_H = k_1 + k_5$ while, if both Cellulose and hemicellulose are being hydrolyzed $k_H = k_1 + k_5 + k_{26}$. Therefore, at different time intervals, the particle decomposes at different rates.)

At steady-state condition, as mass transfer should be equal between water and biomass particle, from (1) and (2)

$$r_w = \frac{4\pi r^2 C_B}{\frac{1}{k_A} + \frac{1}{k_H}} \quad (4)$$

r_w represents the reaction rate of the water monomer for one biomass particle. When the decomposition rate is described in a point of view in the mass balance of a biomass particle and when the radius of the particle is *r*,

$$\frac{d\,(4\pi r^3\rho/3)}{dx} = -r_B \qquad 5$$

Here r_B is the reaction rate of the biomass molecule for a unit biomass particle, and ρ is the molar density of the biomass particle. (ρ changes according to each wood component) Therefore, with stoichiometry,

$$-r_w = \beta r_B \qquad 6$$

Where β represents the stoichiometry value of water in the hydrolysis reaction.

(In the proposed model, it is assumed that the biomass particle is consist of 45% of Cellulose, 25% Hemicellulose, and 30% of Lignin)

Substituting (4) and (6) to (5),

$$4\pi r^2\rho\frac{dr}{dt} = \frac{4\pi r^2 C_B}{\frac{1}{k_A}+\frac{1}{k_H}} \qquad 7$$

When the radial position of the surface becomes *r*, the decomposition ratio of the biomass particle can be written as,

$$1 - x = \frac{\frac{4}{3}\pi r^3\rho}{\frac{4}{3}\pi {r_0}^3\rho} = (\frac{r}{r_0})^3 \qquad 8$$

Where, x is the decomposition ratio of a unit biomass particle. After derivation over time,

$$-\frac{dx}{dt} = \frac{3r^2}{r_0^3}\frac{dr}{dt} \qquad 9$$

By substituting from (8) and (9) to (7),

$$\frac{4\pi {r_0}^3}{3}\rho\frac{dx}{dt} = \frac{4\pi {r_0}^2 C_B(1-x)^{\frac{2}{3}}}{\beta(\frac{1}{k_A}+\frac{1}{k_H})} \qquad 10$$

When the decomposition of the biomass particle is expressed by the concentration of each wood component molecules, x can be expressed, as shown below in equation 11.

$$x = \frac{\sum(C_{mod\ i,0} - C_{mod\ i})}{\sum C_{mod\ i,0}} \quad 11$$

Where $C_{mod\ i,0}$ is the concentration of each wood component molecule at t=0, and $C_{mod\ i}$ is the concentration of each wood component molecule at t=t.
From (11),

$$r_B = \frac{dx}{dt} = \frac{3C_b(1-x)^{\frac{2}{3}}}{r_0 \beta \rho (\frac{1}{k_A} + \frac{1}{k_H})} \quad 12$$

Therefore substituting (11) into (12),

$$r_d = \frac{dC_{bio}}{dt} = -k_x \sum C_{mod\ i}^{\frac{2}{3}} \quad 13$$

Where i = 1,2,3
Here, r_d is the decomposition rate of the biomass particle, $k_x$is the rate coefficient of biomass decomposition and $C_{mod\ i}$ is the concentration of each wood component. Therefore,

$$k_x = \frac{3C_b \sum C_{mod\ i,0}^{\frac{1}{3}}}{r_0 \beta \rho (\frac{1}{k_A} + \frac{1}{k_H})} \quad 14$$

According to the wood component or components, which are being hydrolysed, k_x becomes a different rate constant due to the change in k_H.
All the rate constants are changed with temperature. Since the temperature is changed during the process Arrhenius equation can be used to calculate the changing rate constants.

$$k_{i,t} = k_{0,i}\, e^{\frac{-E_a}{RT}} \quad 15$$

Where, $k_{i,t}$ is the calculated rate constant, $k_{o,i}$ is the frequency factor and,E_a is the Activation energy for each component. Arrhenius law can be applied to all the reactions in the process since the rate constants are changed with temperature. Moreover, the heating process can be expressed by the following equation 16.

Heating process; $T = \vartheta_T\, t + T_{ini}$ 16

Where, ϑ_T is the heating rate, *t* represents time and, T_{ini} is the initial temperature.

By substituting to (13) from (14), (15), and (16), an equation for biomass decomposition can be developed.

Differential equations developed to calculate the change in yield of each component in the system is listed in the appendix.

The model predicted values are compared and validated with the experimental values in literature. Theoretical values of each chemical component are calculated from differential equations A1-A18 using the backward Euler method. According to the required initial concentration of each component of wood in the system (given that different wood types have different ratios of each wood component) number of moles of each wood, component is calculated and inserted. From the differential equations, the variation of the concentrations of each chemical compound is obtained. Then for each wood component, each chemical compound or resultant phase is presented as a percentage of the input. For the calculations in the developed model, it is assumed no losses during the extraction process, as well as the carbon recovery is >99 %.

2.2. Cellulose hydrolysis model

The reaction mechanisms for Cellulose are influenced by the reaction mechanism proposed by Cantero et al. [21] Minowa et al. [19] and Kamio et al. [11]. According to Kamio et al. [11], Cantero et al. [21], Sasaki et al. [14,15,17] and Minowa et al. [19] from the hydrolysis of Cellulose, water-soluble intermediates are formed. Then the further hydrolysis, polymerization, dehydration, and decomposition creates the degradation products from the intermediates such as water-soluble products (aqueous phase), biocrude, gas, and char. As the secondary char is hard to quantify experimentally, both primary and secondary char produced is taken as a lump component. Figure 2 shows the reaction pathway used for the cellulose hydrolysis and decomposition during the liquefaction process. Table 1 shows the type of each reaction used in the cellulose hydrolysis model.

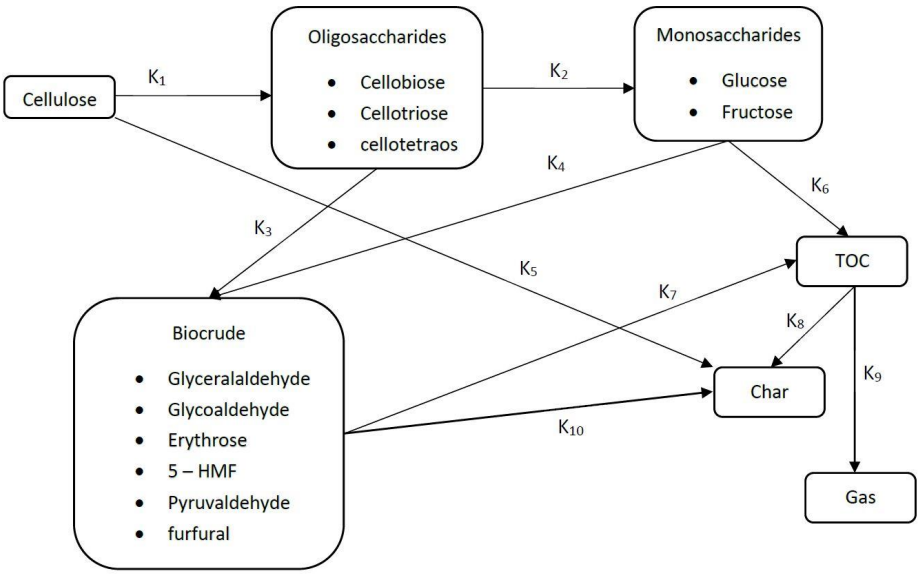

Figure 12:Reaction pathway of cellulose decomposition

Table 4:Reaction type of each reaction used in the cellulose liquefaction model

Kinetic parameter	Reaction type	Kinetic parameter	Reaction type
K_1	Hydrolysis	K_6	Decomposition
K_2	Hydrolysis	K_7	Decomposition
K_3	Dehydration	K_8	Polymerization
K_4	Dehydration	K_9	Decomposition
K_5	Dehydration	K_{10}	Polymerization

Below equations from 17 to 25 show the reactions incorporated in the cellulose liquefaction model.

$$cellulose + a_1H_2O \xrightarrow{k_1} b_1 oligosaccharides \quad 17$$

$$oligosaccharides + a_2H_2O \xrightarrow{k_2} b_2 monosaccharides \quad 18$$

$$oligosaccharides \xrightarrow{k_3} b_3(Biocrude)+H_2O \quad (19)$$

$$monosaccharides \xrightarrow{k_4} b_4(Biocrude)+H_2O \quad (20)$$

$$cellulose \xrightarrow{k_5} b_5 Char+H_2O \quad (21)$$

$$monosaccharides \xrightarrow{k_6} b_6 TOC \quad (22)$$

$$Biocrude \xrightarrow{k_7} b_7 TOC \quad (23)$$

$$TOC \xrightarrow{k_8} b_8 Char + b_9 CO_2 \quad (24)$$

$$Biocrude \xrightarrow{k_{10}} b_{10} Char \quad (25)$$

a_i is the stoichiometry value for water for each hydrolysis reaction. (where *i=1,2*)

b_i is the stoichiometry value for the reaction output for each reaction. (where *i=1,2, 3…,10*)

Micro-crystalline Cellulose, which is consisted of 230 glucose molecules, is used to model the cellulose component. Although oligosaccharides are supposed as a mix of cellobiose, cellotriose, and cellotetraose, for simplification, the kinetic data related to cellobiose is chosen for the model. Furthermore, monosaccharides are a mix of glucose and fructose, where the kinetic data for glucose decomposition is used for the model. '*Biocrude''* is supposed to be a mix of chemicals such as glycolaldehyde, glyceraldehyde, erythrose, pyruvaldehyde, dihydroxyacetone, furfural, and 5-hydroxymethyl-2-furaldehyde (5-HMF)[29]. Therefore 'Biocrude' represents the biocrude phase produced by the cellulose liquefaction. For the calculations, kinetic data for 5-HMF is used in the model for '*Biocrude*.' For the cellulose hydrolysis model, required kinetic parameters are taken from the literature[11,14,15,17,19–21,29,30]. Due to the simplified reaction scheme for cellulose hydrolysis and decomposition, some of the important conversions, such as the formation of phenolic compounds from Cellulose [18,31], are not included as separate chemical reactions.

The term 'TOC' is used to indicate the water-soluble organics in the aqueous phase from cellulose hydrolysis except for Cellulose, light aldehydes (except 5-HMF, glycolaldehyde, glyceraldehyde.) and carboxylic acids. In the cellu-

lose hydrolysis model, Cellulose is considered as the biomass. Biocrude is assumed to consist of glycolaldehyde, glyceraldehyde, erythrose, pyruvaldehyde, dihydroxyacetone, furfural, and 5-hydroxymethyl-2-furaldehyde (5-HMF). TOC is assumed to consist of water-soluble organics. Even though light aldehydes and carboxylic acids can be dissolved in water, those compounds are considered as a part of the biocrude phase.

2.3. Lignin hydrolysis model

The lignin hydrolysis mechanism is based on the kinetic study and reaction pathways proposed by Yong and Matsumara [9] and Fang et al.[32], where the kinetic data is based on Yong and Matsumara[9], Zhang et al.[22], Forchheim et al.[23], and Arturi et al.[33]. Yong and Matsumara proposed a detailed reaction scheme for lignin hydrolysis, which consists of a gas phase, char, an aqueous phase, and another phase consist of phenols, TOC, Aromatics, Guaiacol. With further secondary hydrolysis reactions, some of the hydrolysis products decompose into tertiary components, which are also included in this model. In the proposed model, the shrinking core concept relates to the primary or the heterogenous hydrolysis reactions. Secondary decomposition, polymerization, and dehydration reactions are modeled using a conventional kinetic model, which is not being observed with other models that have used the shrinking core concept. Below, figure 3 shows the used reaction pathway of hydrolysis and decomposition of Lignin during the liquefaction process. For the lignin liquefaction model, required kinetic parameters are taken from the literature[9,22,23,34,35]. Table 2 shows the type of each reaction used in the lignin hydrolysis model.

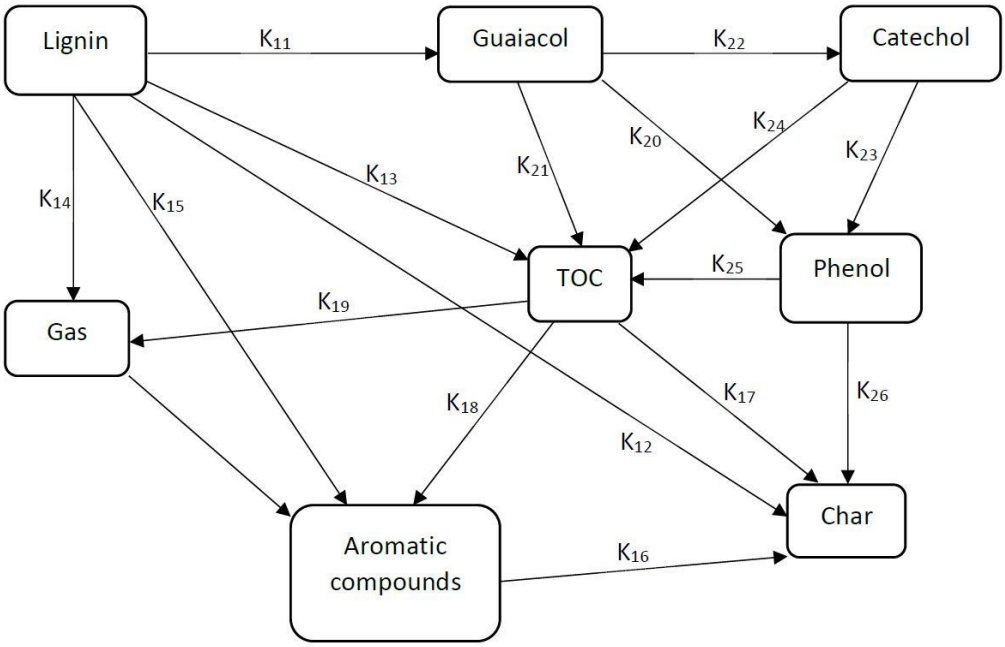

Figure 13:Reaction pathways of Lignin in hydrothermal conditions.

Table 5:Reaction type of each reaction used in the lignin liquefaction model

Kinetic parameter	Reaction type	Kinetic parame-ter	Reaction type
K_{11}	Hydrolysis	K_{19}	Gasification
K_{12}	Dehydration	K_{20}	Decomposition
K_{13}	Hydrolysis	K_{21}	Decomposition
K_{14}	Hydrolysis	K_{22}	Decomposition
K_{15}	Hydrolysis	K_{23}	Decomposition
K_{16}	Polymerization	K_{24}	Decomposition
K_{17}	Polymerization	K_{25}	Decomposition
K_{18}	Decomposition	K_{26}	Polymerization

Below equations from 26 to 34 show the reactions incorporated in the lignin liquefaction model.

$$Lignin + c_1H_2O \xrightarrow{k_i} d_1 guaiacol + d_2 Aromatics + d_3 TOC + d_4 CO_2 \quad 26$$

$$Lignin \xrightarrow{k_i} d_5\ char + H_2O \quad 27$$

$$Aromatics \xrightarrow{k_i} d_6\ char \quad 28$$

$$TOC \xrightarrow{k_i} d_7 char \quad 29$$

$$TOC \xrightarrow{k_i} d_8 Aromatics + d_9 CO_2 \quad 30$$

$$Guaiacol \xrightarrow{k_i} d_{10} Phenol + d_{11} TOC + d_{12} catechol \quad 31$$

$$Catechol \xrightarrow{k_i} d_{13} Phenol + d_{14} TOC \quad 32$$

$$Phenol \xrightarrow{k_i} d_{15} TOC \quad 33$$

$$Phenol \xrightarrow{k_i} d_{16} Char \quad 34$$

c_i is the stoichiometry value for water for each hydrolysis reaction. (where *i=1*)

d_i is the stoichiometry value for the reaction output for each reaction. (where *i=1,2, 3,…16*)

Alkali Lignin is used as the modeling compound for Lignin, which has an empirical formula of $C_{108}H_{107}0_{37}$ and an average unit molecular weight of 1996 g/mol per unit[36]. Additionally, for the modeling procedure, an average molecular weight of 10 kg/mol is used, which is the same value Matsumara et al. [8,9] used. Thus, it is assumed that the lignin structure consists of 5 Alkali lignin units. During the calculations, all the components are normalized to 1 atom 'C' per molecule for the simplification. The term 'TOC' is used to indicate the soluble organics in the aqueous phase from lignin hydrolysis except for Lignin, Aromatic hydrocarbons (includes naphthalene, benzene, toluene), catechol, guaiacol, and phenol. In the results section, the term 'biocrude' is used to refer to the cumulative value of Aromatic hydrocarbons, catechol, guaiacol, and phenol. Here Lignin is considered as the biomass. Therefore, it does not belong to TOC, although it is soluble in water. Biocrude is assumed to consist of aromatic hydrocarbons, catechol, guaiacol, benzene, toluene, and phenol. Although benzene and toluene are slightly soluble in water, in this model, they are a part of the biocrude phase. Thus, those chemicals are not included in TOC.

2.4 Hemicellulose hydrolysis model

Hemicellulose hydrolysis model is based on the work from Pronyk and Mazza and Pinkowska et al.[13,25]. Pronyk and Mazza proposed a monophasic and a biphasic mechanism for hemicellulose hydrolysis, where the monophasic mechanism is chosen to develop this model. Hemicellulose is hydrolyzed into the intermittent product of Xylo-oligomers and then again to xylose. As shown in figure 4 below, the hydrolysis products further decompose into derivatives, mainly furfural. In this model, furfural is used as the final derivative from the liquefaction, due to the lack of availability of kinetic data. For the hemicellulose hydrolysis model, required kinetic parameters are taken from the literature[13,24–26,26].

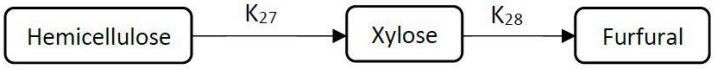

Figure 14:Reaction pathways of hemicellulose in hydrothermal conditions

Table 3 shows the reaction type of each reaction used in the hemicellulose liquefaction model.

Table 6:Reaction type of each reaction used in hemicellulose liquefaction model

Reaction	Reaction type	Reaction	Reaction type
K_{27}	Hydrolysis	K_{28}	Dehydration

Equation 35 and 36 show the reactions incorporated in the hemicellulose liquefaction model.

$$Hemicellulose + e_1 H_2O \xrightarrow{k_{27}} f_1 xylose \quad 35$$

$$xylose \xrightarrow{k_{28}} f_2(Biocrude) \quad 36$$

e_i is the stoichiometry value for water for each hydrolysis reaction. (where *i=1*)

f_i is the stoichiometry value for the reaction output for each reaction. (where $i=1,2$)

'*Biocrude''* is supposed to be a mix of chemicals such as furfural and aldehydes. Literature available on hemicellulose hydrolysis contradicts each other occasionally. According to Pronyk and Mazza [13], conversion of xylose into furfural is about 4% from potentially available xylose in the system. Moreover, the hemicellulose hydrolysis starts around 403K, and the Xylo-oligomers and monomers available in the system maximize around 443K [13]. The maximum furfural percentage recorded during the experiments is around 443K, which is still beyond the temperature range considered in this model. Meanwhile, the pentose sugar arabinose present in hemicellulose could make the hydrolysis more susceptible to the lower temperatures [13]. In the Meantime, according to Pinkowska et al. [25], the maximum yield of saccharides such as xylose is obtained around 508K. Then the increasing temperatures favored the conversion of saccharides into furfurals, aldehydes, and carboxylic acids. Möller and Schröder[26] observed a maximum furfural yield of 49 % at 473K from xylose conversion, while xylan conversion provides a maximum of around 13 % of furfural. Moreover, following the results from Pinkowska et al. [25] and Pronyk and Mazza [13], the requirement of lower temperatures(433K-453K) for the xylan hydrolysis on producing xylose is observed. From all these studies, it is evident that the hemicellulose hydrolysis occurs and gives the best furfural yields at low temperatures from 403K to 493K. During this study, lack of kinetic data, as well as the less contribution of hemicellulose degradation products to the wood hydrolysis process, are observed. Nevertheless, a simple two-stage hemicellulose hydrolysis model is developed based on the available literature. Due to the lack of kinetic data availability on char production of hemicellulose hydrolysis, char is not considered as a degradation product from hemicellulose. Although the temperatures required for better furfural yields from hemicellulose hydrolysis is not within the temperature range considered in this model, still the hemicellulose hydrolysis data is included in the model to perform the wood hydrolysis.

2.5 General assumptions and simplifications

The wood particle is considered as a spherical particle with a given radius in this model. It is submerged in an infinitely large water volume, much larger than the radius of the particle. Hence the dilution of the hydrolysis products is assumed to be infinite at a given distance from the particle center. In this model, it is assumed that there is always enough water in the system to perform all the required hydrolysis reactions. The particle decomposition is assumed only in the radial direction. Therefore, during hydrolysis, the particle is decomposed in the radial direction. Thermophysical properties are presumed to be constant throughout the process as well. The temperature of the particle is always supposed to be equals to the temperature of the fluid surrounding it. As the particle is assumed to be homogenous in properties and composition, no mass transfer is considered, and no accumulation of products from the hydrolysis in the particle is considered. Furthermore, the primary char and secondary char from the reactions are considered as one.

It is learned that an ash layer and an oily film is developed around the shrinking core during the hydrolysis process[7]. Therefore, in the next phase of this model, the effect and behavior of such an ash layer and an oil film are studied and developed. Thus, in this model, it is assumed that all the products from hydrolysis leave the particle surface and does not form a layer on the outside of the wood particle. Hence, water monomers can proceed to the particle and continue the hydrolysis reaction. Besides, wood hydrolysis is modeled as the cumulative effect of the hydrolysis of the three main components of wood. Therefore, the hydrolysis of each model component is modeled separately. Each model component starts hydrolysis at different temperatures and emits hydrolysis products to the system. When each model component hydrolyzes, the radius is assumed to be reduced in a rate that correspondent to the rate constant of hydrolysis of the specific model component.

As described in the assumption section, hydrolysis of Cellulose, Lignin, and Hemicellulose occurs only on the surface of the particle at a given time. In the model, char is produced in two different ways. For the simplification, char produced by dehydration is considered as a direct degradation product of cellulose and lignin hydrolysis. Dehydration happens throughout the particle volume, and this leads to the particle becoming more charred with time. When the

Carbon content of the particle is increased, it enforces a restriction on the capability of water to react with the wood components. Therefore, unreacted highly charred biomass could have remained in the system. The term primary char stands for this kind of highly charred unreacted biomass. Secondary char (or coke) represents the char produced through the further decomposition of the biocrude and aqueous phase [3,7]. Although char consists of these two components, the presence of secondary char in the resultant of the liquefaction process is small [7]. It is assumed that ash does not participate in reactions.

The composition of the particle is not changed with time or with the hydrolysis reaction. The particle is decomposed only in the radial direction, and the decomposition is dependent only on the biomass left in the particle and the concentration of water in the system. As the reactions proceed, the hydrolysis products are dissolved in the water, and the further hydrolysis reactions of the particle are not affected by the diluted products.

A simplified elemental balance is used for the model by using an approximation for oxygen and hydrogen balance in each compound. Therefore, only Carbon balance is given importance in the modeling process due to the simplification of the calculations. According to Yong and Matsumara [9], H_2 and CO_2 are present in the gas phase in lignin hydrolysis, with CO_2 being the major contributor. Nevertheless, the CO_2 percentage increased with increasing temperature in the subcritical region, and H_2 is decreased with time. Therefore, for the gas phase, CO_2 is used as the model compounds since CO_2 is the principal component in the gas phase.

The stoichiometry for the hydrolysis reactions is calculated based on the experimental results available in the literature. To define the stoichiometry as many as three experimental data are considered in most of the reactions. However, due to the lack of literature, the stoichiometry for some reactions is determined based on a single experimental work. To determine the stoichiometry for each reaction, a set of stoichiometric coefficients for each reaction is calculated, which has a minimum of residual sum of squares (i.e., the difference between the calculated and available experimental values). Mosteiro-Romero et al. [3] showed the product distribution in each holding temperature is the same at all temperatures from 523K -623K. Thus, it is assumed that the determined stoichiometry is the same at each holding temperature and valid throughout the temperature range, which the model is using. Then, at the con-

sidered temperature values, the experimental data is fit to the equations. As the experimental data for water is not available, different stoichiometric values for the hydrolysis reactions are calculated using hydrogen and oxygen balance.
Furthermore, due to the lack of literature, especially on the heating stage and of fast reaction kinetics, some of the kinetic data is modified and fit to reactions equations to obtain the yield values in the literature. It could be a possible reason for some of the over predictions and under predictions in the model. The differential equations developed in the mathematical model are solved and discretized in MATLAB R2019b.

3. Results and discussion

3.1 Model predictions

In this section, different predictions from the developed model are illustrated. First, the impact of temperature increase on each wood component hydrolysis and wood hydrolysis is discussed. Subsequently, the impact of residence time, the impact of heating rate on product yield, and the effect of biomass particle size are also explained.

3.1.1 Effect of temperature on the product composition

Figure 5 shows the impact of temperature variation on cellulose hydrolysis, where figures 5a, 5b,5c, and 5d show the variation of TOC, biocrude, char, and gas yield, respectively. Three temperature values (553K, 588K, and 623K) are used to observe the effect of temperature on the yields. According to figure 5, char and gas yields become much higher with the increase of temperatures while biocrude and TOC levels go down.

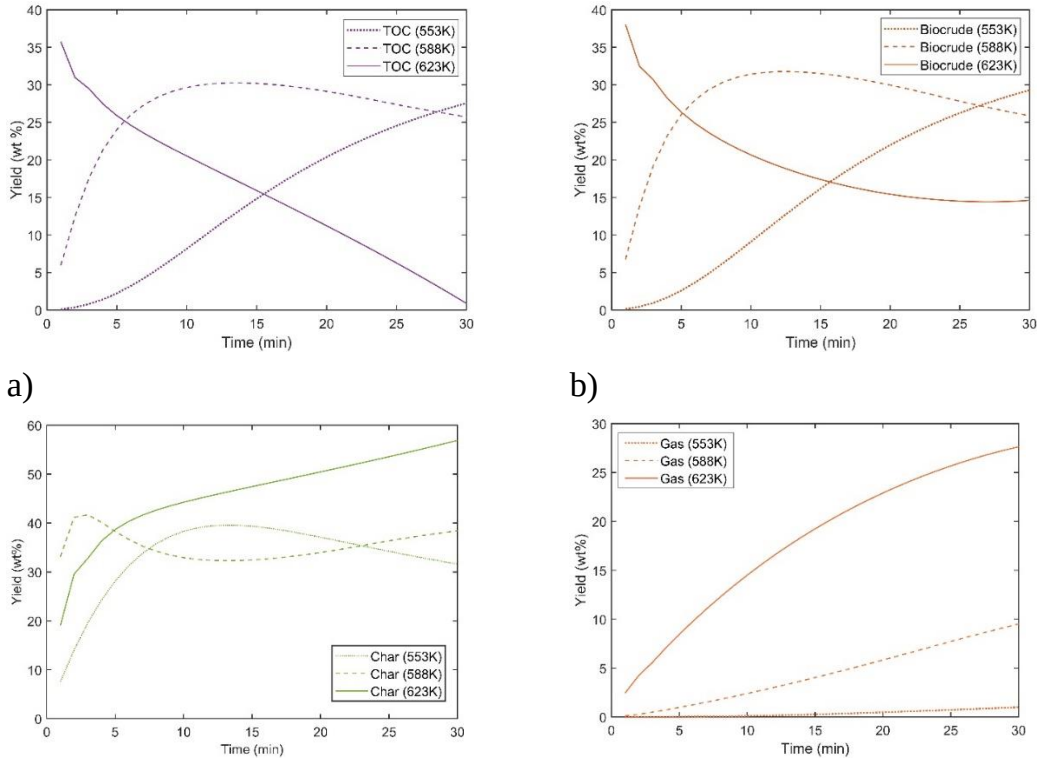

Figure 15:Effect of temperature on hydrolysis of Cellulose derived outputs at 553K, 588K, and 623K a) TOC b) Biocrude c) Char d) Gas

In this model, both primary and secondary char is considered. Therefore, with longer resident times and higher temperatures, higher char yields can be justified. These high yields can be possible, mainly due to the increase of char in secondary reactions. Subsequently, water-soluble organics and light aldehydes in the aqueous phase (TOC) could convert into char and biocrude (5-HMF and furfural, etc.) with further homogeneous hydrolysis reactions and secondary char reactions. Similar variations are observed in work done by Kamio et al. [10,11] Minowa et al.[19], Cantero et al. [21], and Sasaki et al. [14,15,17], where the gas and char yields become notably close to the supercritical region. According to Minowa et al.[19] char can be a decomposition product of further hydrolysis of soluble methanol products, which helps the observations above.

Char was not considered as an output product of the hydrolysis model by Kamio et al.[10,11]. Consequently, they managed to obtain a higher biocrude yield in their model with increasing temperature. It can be mainly due to not

having a char phase in their model. As this model has char yields incorporated, the reduction of biocrude yields with higher temperatures can be examined.

Figure 6 below shows the impact of temperature on lignin-derived product variation. Lignin hydrolyzed quickly into the hydrolysis products due to the rapid kinetics. Fast hydrolysis of Lignin is observed in the available literature [8,9,23,33,37]. Following the cellulose hydrolysis pathway, more char and gas yields are produced by higher temperatures. Sauer et al. [37] proposed that the desired liquefaction of Lignin is between 553K and 653K, which is observed with this model as well.

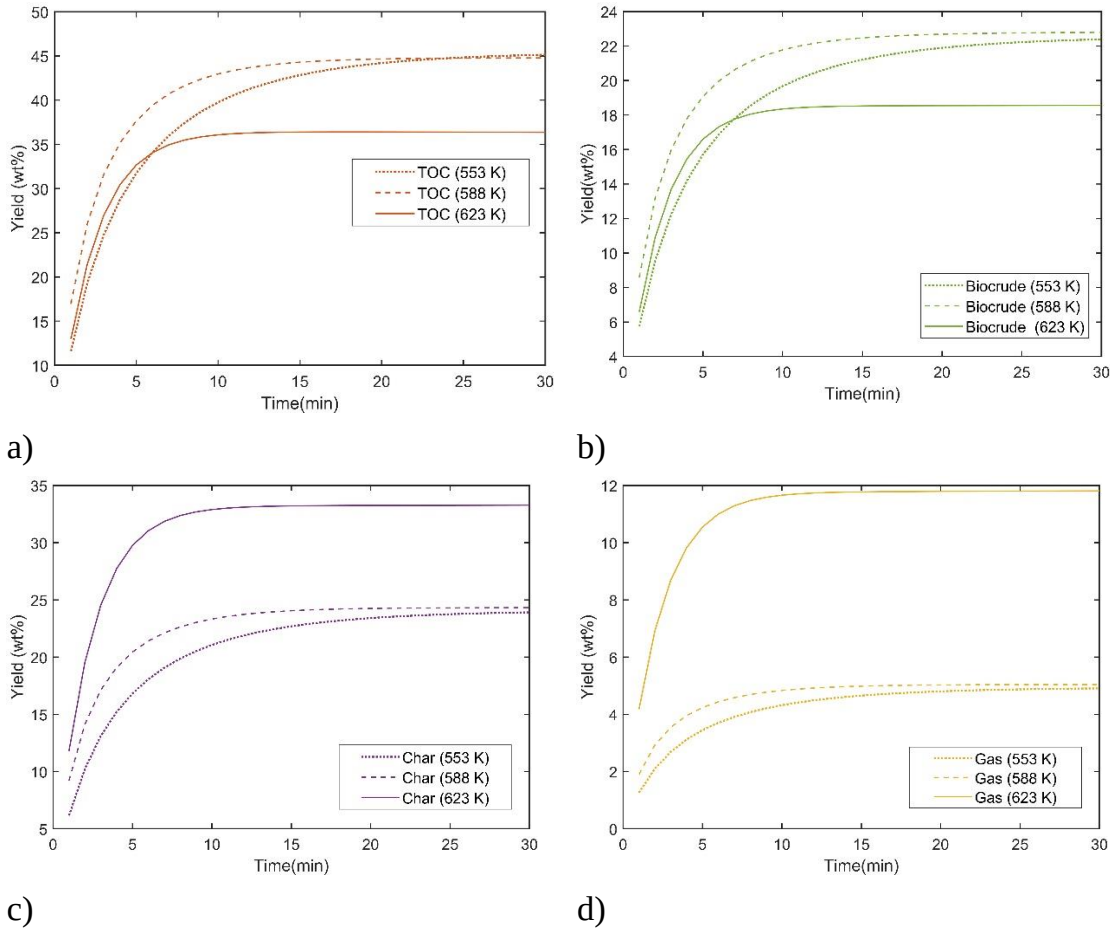

Figure 16: Effect of temperature on hydrolysis of lignin-derived outputs at 553K, 588K, and 623K a) TOC b) Biocrude c) Char d) Gas

Figure 7 below illustrates the behavior of xylose and biocrude created from hemicellulose. Hemicellulose hydrolysis reaction path follows the hydrolysis reaction pathway of Cellulose to some extent. Since only the xylose and bi-

ocrude phases are modeled, many observations cannot be made with hemicellulose hydrolysis. Nevertheless, the formation of biocrude can be understood with higher temperatures. Pronyk and Mazza [13] showed that the hydrolysis of hemicellulose could be observed at low temperatures, such as 443 K in minimal percentages.

Furthermore, a shallow conversion of xylose into biocrude at 443K is illustrated [13]. According to figure 7.b), xylose percentage comes to a maximum of around 500 K, which is within the ranges presented by Pronyk and Mazza[13] as well as Pinkowska et al. [25]. With the temperature rise following the conclusions in literature, xylose shows a maximum close to 500K. At 560K, the yield of xylose is almost zero. Therefore, the impact of hemicellulose on the cumulative result is almost zero in the temperature range of 553 K to 623 K. Since the temperature range considered in this study is from 553 K to 623 K, the impact of hemicellulose on the cumulative result is not considered.

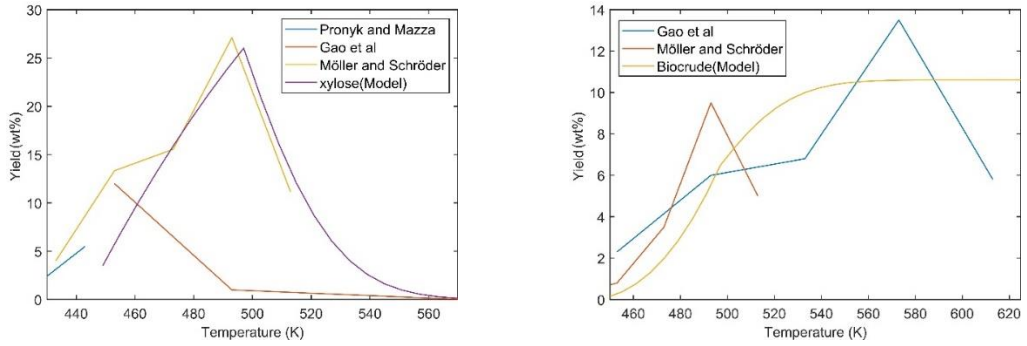

a) b)

Figure 17: Effect of temperature on hydrolysis of hemicellulose-derived outputs a) xylose c b) biocrude

With the cumulative hydrolysis effect of each wood component, the wood hydrolysis is modelled. Figure 8 shows the variation of hydrolysis product yields with the increasing temperatures. The term' TOC' is used to represent the aqueous phase in wood liquefaction. Gas and char components are increased expressively at 623K while the TOC and the biocrude phase decreased significantly. The higher temperatures close to supercritical conditions promote Hydrothermal gasification rather than liquefaction[38]. That could be the main reason for the dramatic decrease in TOC and the increase of the gas phase.

When scrutinized, overall wood hydrolysis product variation slightly follows the cellulose hydrolysis component variation. A significant increase in char yields is observed due to the higher char yields obtained at higher temperatures by cellulose hydrolysis. Shoji et al. [4,5] observed similar variations in wood hydrolysis experiments they performed, where they examined high char yields at higher temperatures. Furthermore, the improvement of biocrude yields, up to some temperature value until it is reduced again, facilitating further reactions to produce more char and gas [3–5,38].

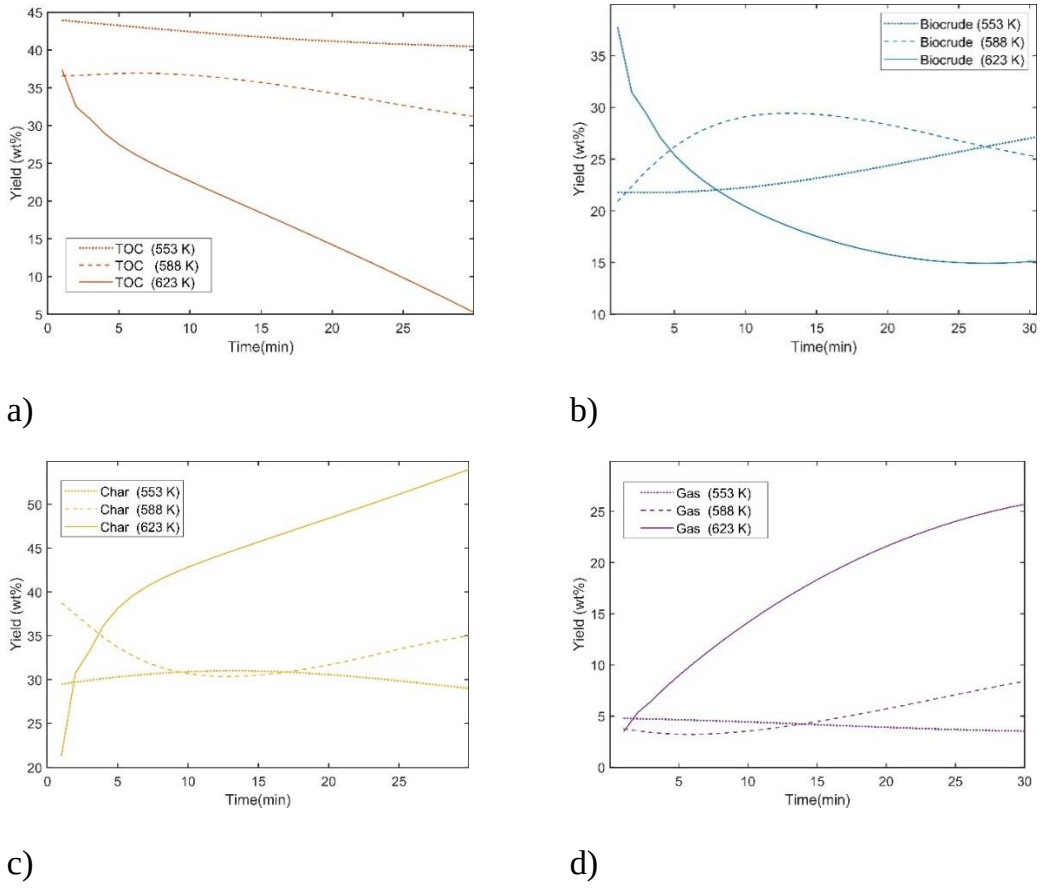

Figure 18:Effect of temperature on wood as a cumulative effect of hydrolysis of Cellulose, hemicellulose, and lignin-derived outputs at 553K, 588K and 623K a) TOC b) Biocrude c) Char d) Gas

3.1.2 Effect of residence time on the product composition

The residence time of the liquefaction process is one of the crucial parameters of the process. Figure 9 below shows the variation of products of Cellulose,

Lignin, and wood hydrolysis. In this scenario, a residence time of 100 minutes is used at 573K.

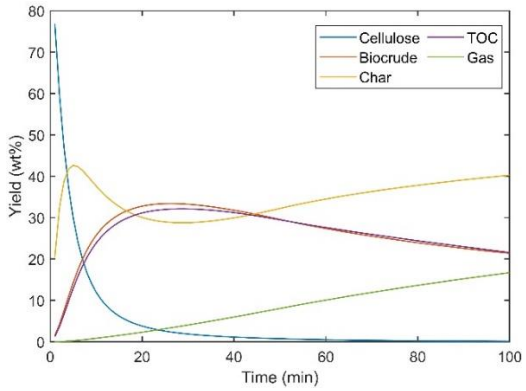

a)

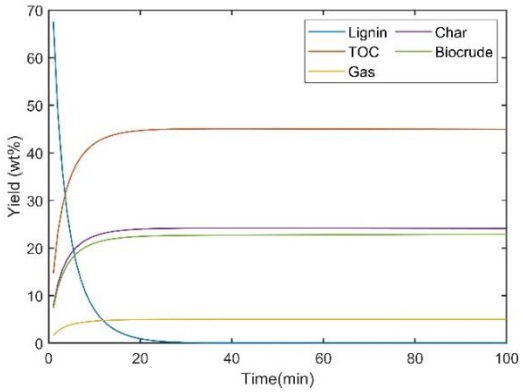

b)

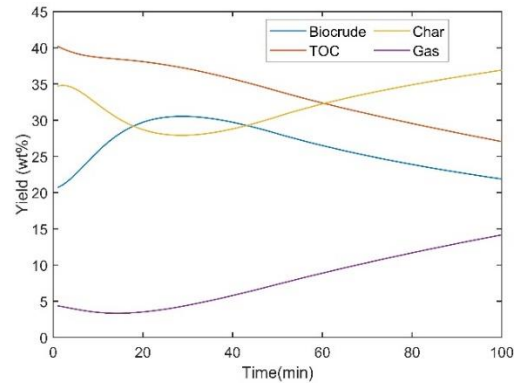

c)

Figure 19:Effect of residence time on hydrolysis at 573 K a) cellulose b) lignin c) wood

According to the above figure 9a, cellulose hydrolysis shows an increase in char and gas yields with longer residence times. Furthermore, TOC and biocrude yields show an initial rise, followed by a gradual reduction of the yields. Although lignin hydrolysis (figure 9b) does not show a significant increase in the yield percentages, the product yields rise to their maximum values much quicker due to the relatively fast decomposition of Lignin. In the end, char yields again are the primary output at longer residence times due to further chain reactions and inter reactions between hydrolysis components.

According to figure 9c, wood hydrolysis products are significantly led by the char yields with longer residence times while it shows a decrease until about 30 minutes of residence time. Meanwhile, biocrude shows a gradual reduction

at longer residence time, which can be observed in Mosteiro-Romero et al. [3,7]. Gas yields follow the behavior of char yields during the whole reaction time, showing an increase in values after 20 mins of residence time. That may be due to the higher conversion of biocrude and TOC into char and gas at longer reaction times. Showing accordance with experimental work from Boocock and Sherman[39], Cellulose and wood hydrolysis show a reduction in biocrude yields with longer residence times with this model.

Many researchers investigated the effect of residence time on product yields [3,40,41]. Boocock and Sherman[39] figured out the longer residence times could reduce the biocrude yields except for the very high loading conditions. Wadrzyk et al. [40] showed the negative effect of higher temperatures and longer residence times on char yields where Yj et al. [42] found out the improvement of liquid yields with longer residence times are negligible. Therefore, the model predictions are following all these observations in literature except the studies by Wadrzyk et al. [40] and Yj et al. [42].

3.1.3 Effect of heating rate

Three different heating rates (2 K/min, 4 K/min, and 6 K/min) are applied in the model to analyze the impact of the heating rate on the product yields. Figure 10 below shows the yield variation of cellulose-derived products with different heating rates in a temperature range of 560 K to 640K. High biocrude yields with lower heating rates are observed with cellulose hydrolysis experiments by Kamio et al. [10,11]. In the proposed model, lower heating rates promote biocrude yields up to 610K (Figure 10b) in cellulose hydrolysis, which follows the work done by Kamio et al. [10,11]. Furthermore, Brand et al.[43] obtained a higher biocrude yield with a higher heating rate (20 K/min) for the temperature range 553K-623K. The proposed model produced results which are coincided with Brand et al.[43]. Relatively smaller activation energies can be the reason for the high yields with slower heating rates. Meanwhile, with slower heating rates, the particle can be hydrolyzed longer, which ultimately provides longer residence times.

Higher heating rates tend to promote relatively higher char yields for cellulose hydrolysis. According to this observation, with higher heating rates cellulose component of the particle gets more charred. Further, it is observed that the

lower heating rates promote better and quicker hydrolysis and, as a result, helps further decomposition and recombination reactions. This trend is supported by the cellulose liquefaction results by Kamio et al.[10], and wood liquefaction results by Mosteiro-Romero et al.[3,7].

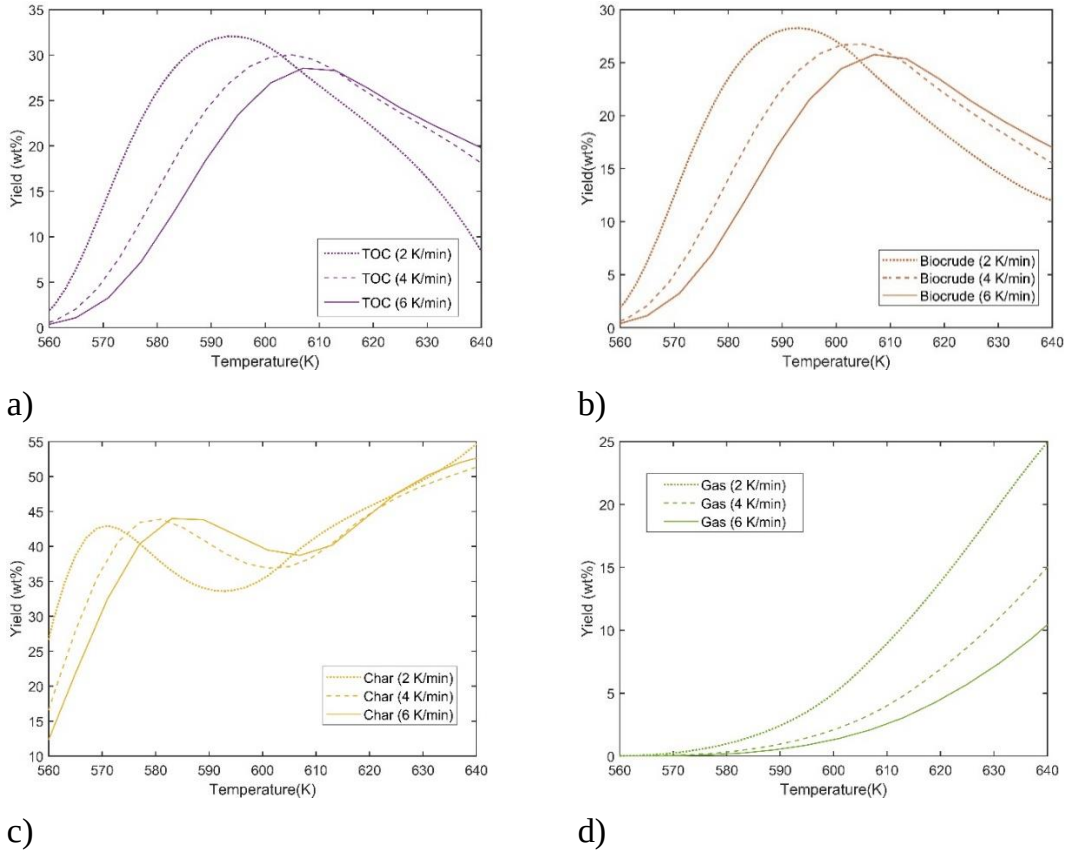

Figure 20:Effect of heating rate on cellulose hydrolysis) TOC b) biocrude c) char d) gas

Lower heating rates promote better and faster lignin decomposition (figure 11), where it produces maximum yields around 620 K. According to figure 12, Lignin does not show a significant change in yields with the heating rate variation. The reason for the slight high yields of outputs in the lower heating rates could be the better decomposition of Cellulose and Lignin in the lower heating rates, as shown in figure 11.

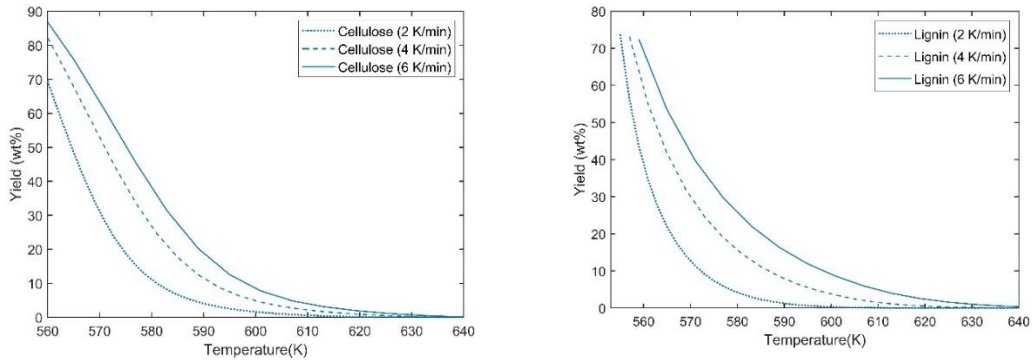

a) b)

Figure 21:Effect of heating rate on hydrolysis of a) cellulose b) lignin

Regardless of the heating rate, all the hydrolysis components produced similar percentages of yields with the temperature increase. Besides, char and gas components show an increase in the yield values around 620K. Slower heating rates have resulted in a faster product yield increase. Ultimately when the temperature value reaches 640K (the critical point is at 647 K), Product yields have become almost the same value. Therefore, the impact of heating rate is essential only at shorter residence times. Therefore, the heating rate could be a critical aspect of the fast liquefaction concept. In a review study on optimum process conditions for liquefaction, Akhtar et al.[44] showcased the higher heating rates are resulted in higher char yields mainly due to the dominance of secondary reaction. Char yield shows an increase with the higher heating rate close to the supercritical region, justifying that statement by Akhtar et al.[44].

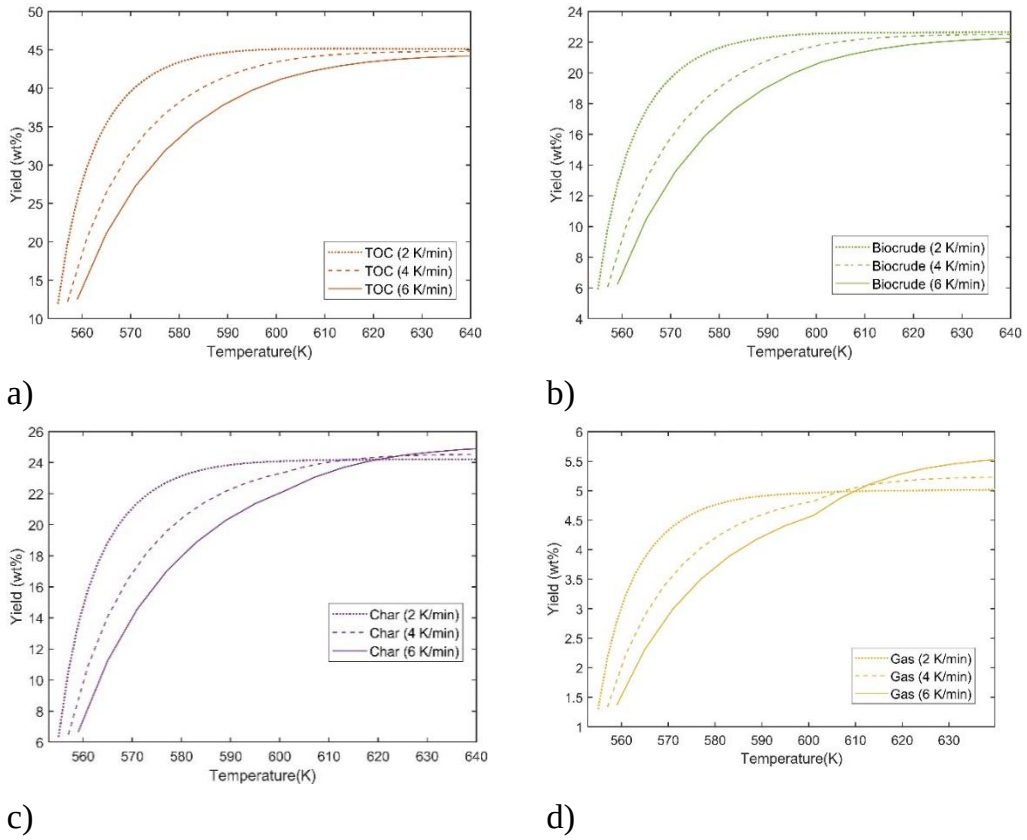

Figure 22:Effect of heating rate on lignin hydrolysis a) TOC_L b) biocrude c) char d) gas

According to the results shown in figure 13, for a given temperature value, lower heating rates produce higher biocrude yields until about 600K, where char yields and gas yields are increased dramatically after 600K. Initially, higher heating rates produce higher char yields, while after 610K, higher biocrude and TOC yields are produced. Higher biocrude and gas yields could be due to the lower activation energy of the hydrolysis reactions and longer hydrolysis time. This behavior coincides with the experimental results from Kamio et al. [10] and Mosteiro-Romero et al. [3,7].

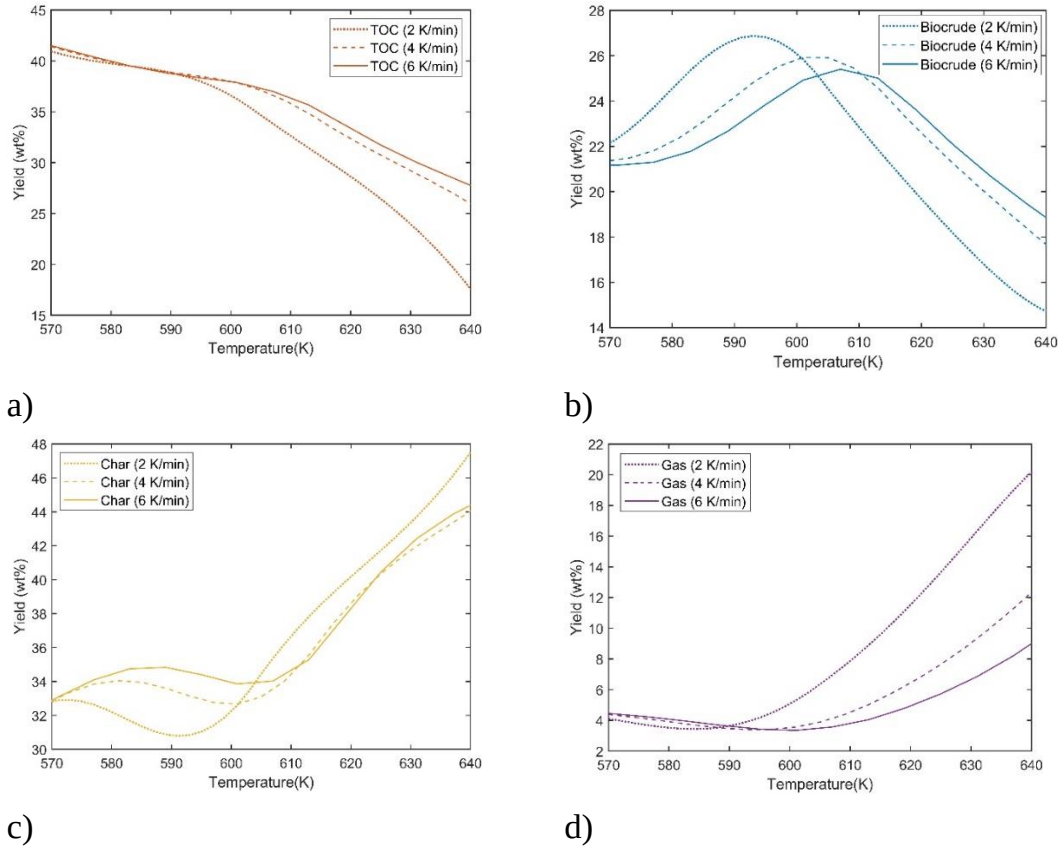

Figure 23:Effect of heating rate on wood hydrolysis a) TOC b) biocrude c) char d) gas

With higher heating rates, initially, the particle gets charred promptly, and it hinders the production of liquid yields initially due to the decreased hydrolysis effect on liquid yields. Nevertheless, at higher temperatures, higher heating rates promote liquid yields than gas and char yields. This increase is, could be due to the higher liquid yields from cellulose liquefaction at higher temperatures with higher heating rates. Besides, 4K/min and 6K/min heating rates have imposed a negligible difference on the yields except for the gas component. Therefore, the conclusions made by Akhtar and Amin [44] on the negligible impact of heating rates on wood and each wood component due to the high dissolution and stabilization of decomposed fragments in subcritical water can be justified by the model predictions.

3.1.3 Hydrolysis behavior on particle size.

The rationale of the particle size reduction is to provide better accessibility of biomass to the solvent or the liquefaction medium. Nonetheless, as both sub-critical and supercritical water are proper heat transfer mediums, change of particle radius makes a low impact on the change of yields [44]. Three sizes of particle radius (0.08mm, 0.1 mm, and 1 mm) are used as the particle radius. Figure 14 shows the particle decomposition of Cellulose and Lignin with different particle radius. It is evident with cellulose and lignin hydrolysis graphs as the decomposition of cellulose and lignin components become much slower with the increase of the radius. Besides, slightly increased char yields are shown with the larger particles. Since the reactions occur on the particle surface, the radius and of the particle could play an essential role in the hydrolysis process.

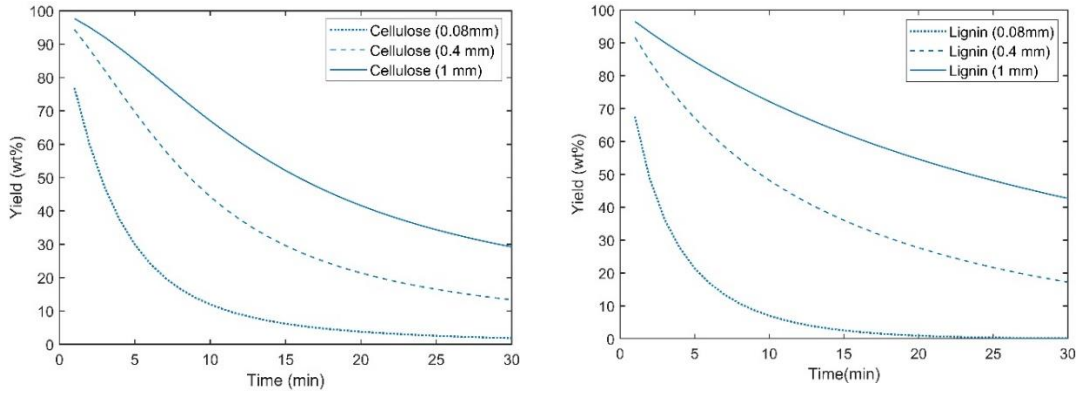

a) b)

Figure 24:Effect of particle size on hydrolysis of a) cellulose b) lignin

Figure 15 shows the cellulose hydrolysis, and the behavior of Cellulose derived components with different particle sizes. The main reason for the smaller particle size to produce more yields is the faster decomposition of the particle. All the particle sizes show the same trend, although the smaller particle size shows a dramatic increase of char yields at the initial stage. This increase could be due to fast kinetics with the smaller particle radius. Besides, the workup procedures could influence the char and bio-oil yields.

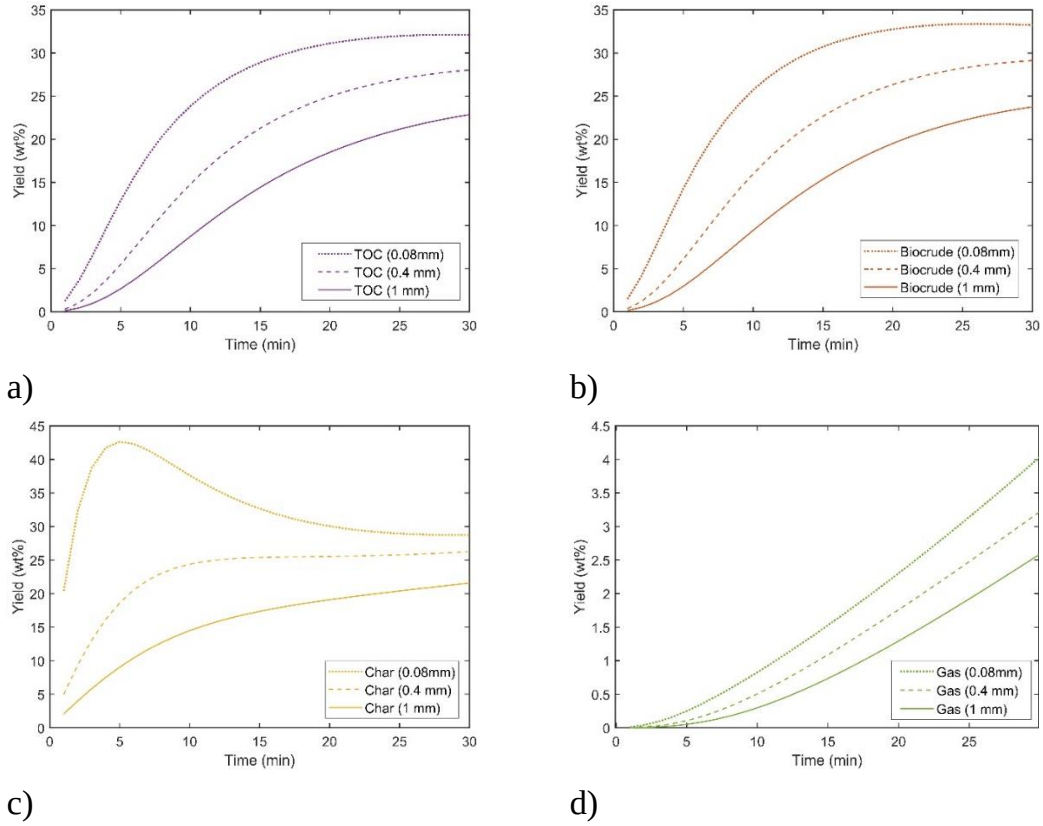

Figure 25: Effect of particle size on hydrolysis of cellulose a) TOC b) bi-ocrude c) char d) gas

According to figure 16, Lignin follows the same pattern as Cellulose, where the smaller particle decomposes quickly. Further, faster decomposition has produced higher yields quickly.

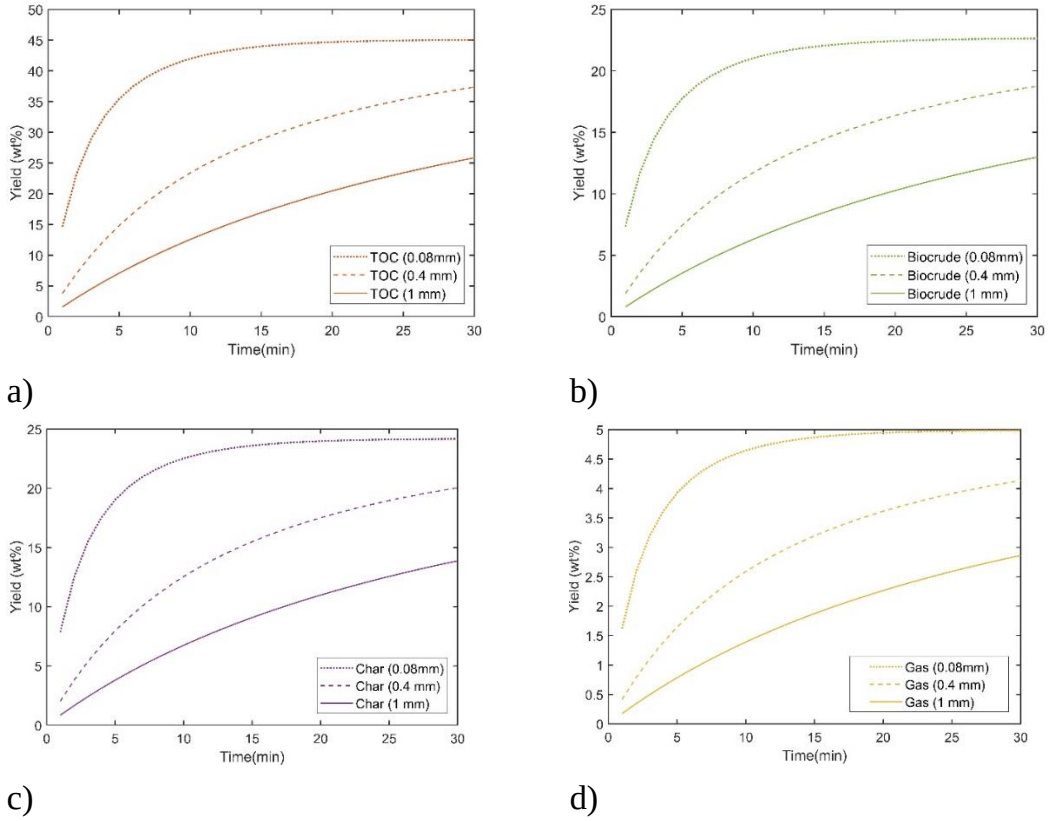

Figure 26: Effect of particle size on hydrolysis of Lignin a) TOC b) biocrude c) char d) gas

Unreacted biomass is not considered as char, and only the primary and secondary char is considered for the char phase in this model. Therefore, the amount of char produced with larger wood particle size (1 mm) is less. Since the hydrolysis reactions are faster with the smaller particles (0.08 mm), more yield is produced in all the components.

Subsequently, a shrinking core model is employed, the particle radius directly affects the particle decomposition. Moreover, all the reactions have happened on the particle surface. Therefore, for a given temperature and a residence time, yields from the hydrolysis of each wood component, as well as the cumulative model (wood), show significant changes in the yields. Moreover, the workup procedure affects bio-oil yields as well as char. However, in the literature, experimental work observed that the particle size of feedstock does not play a significant role[45,46]. This statement means the effect of the particle size of the feedstock on the yields is negligible.

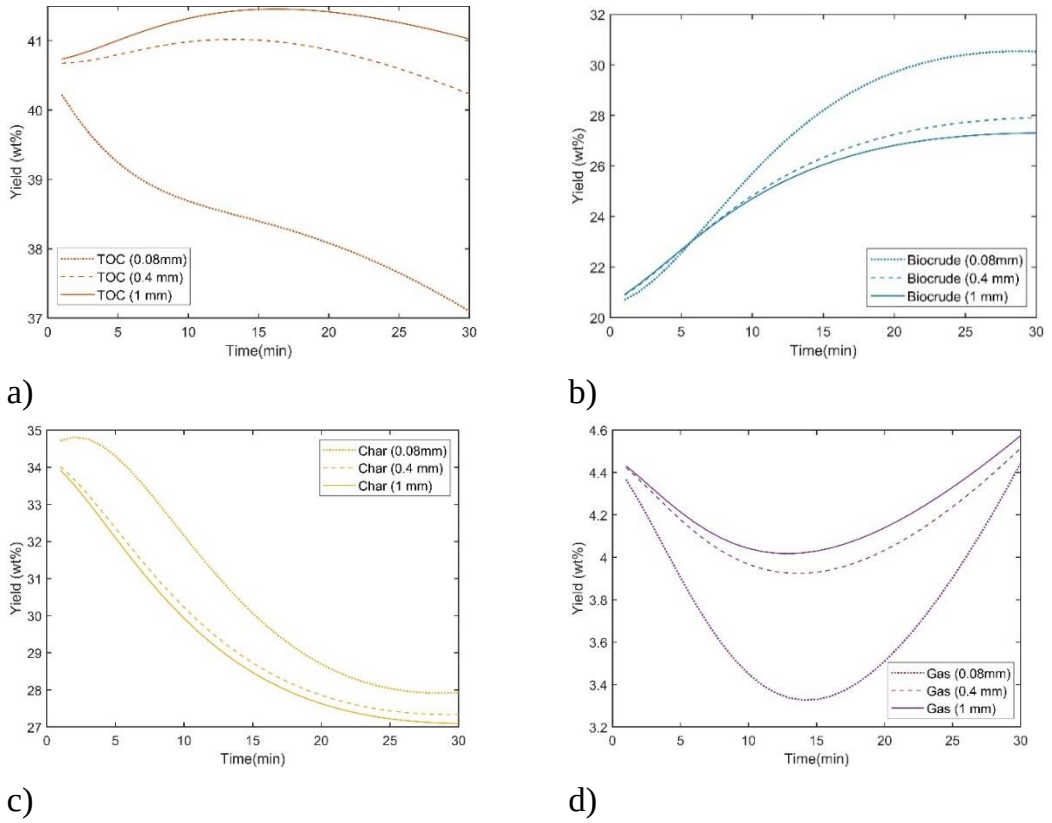

Figure 27: Effect of particle size on hydrolysis of wood a) TOC b) biocrude c) char d) gas

3.2 Validation of the model and product composition

Cellulose, hemicellulose, and lignin hydrolysis are considered separately to model wood hydrolysis as the sum of the hydrolysis effect of those three components. To validate each part of the model, each wood component hydrolysis, and hydrolysis of wood is compared with experimental data from the literature in this section.

For the validation of the cellulose hydrolysis model, kinetic data, and process conditions used by Promdej and Matsumara[29] are used for the developed model. Moreover, the model predictions are shown with the experimental data obtained in their study. As shown in figure 18, the cellulose hydrolysis model has underpredicted the TOC yields while it has overpredicted the char yield. As the size of the cellulose particles is not provided in the literature, a general radius size of 80µm is used for the cellulose particle. Furthermore, different loading conditions, different concentrations, and different reaction routes could affect the differences in the yield components. Promdej and Matsuma-

ra[29] studied the hydrothermal decomposition of glucose, while in this study, cellulose decomposition is studied. Therefore, kinetic data for cellulose and oligosaccharides hydrolysis are obtained from the literature.

Additionally, kinetic data for cellobiose is used to model the oligosaccharides. For the biocrude phase of the cellulose decomposition, kinetic data for 5-HMF is considered. Besides, biocrude from cellulose consists of many chemicals and compounds. Therefore, these can add another error value for the model predictions too. The same applies to lignin and hemicellulose hydrolysis processes.

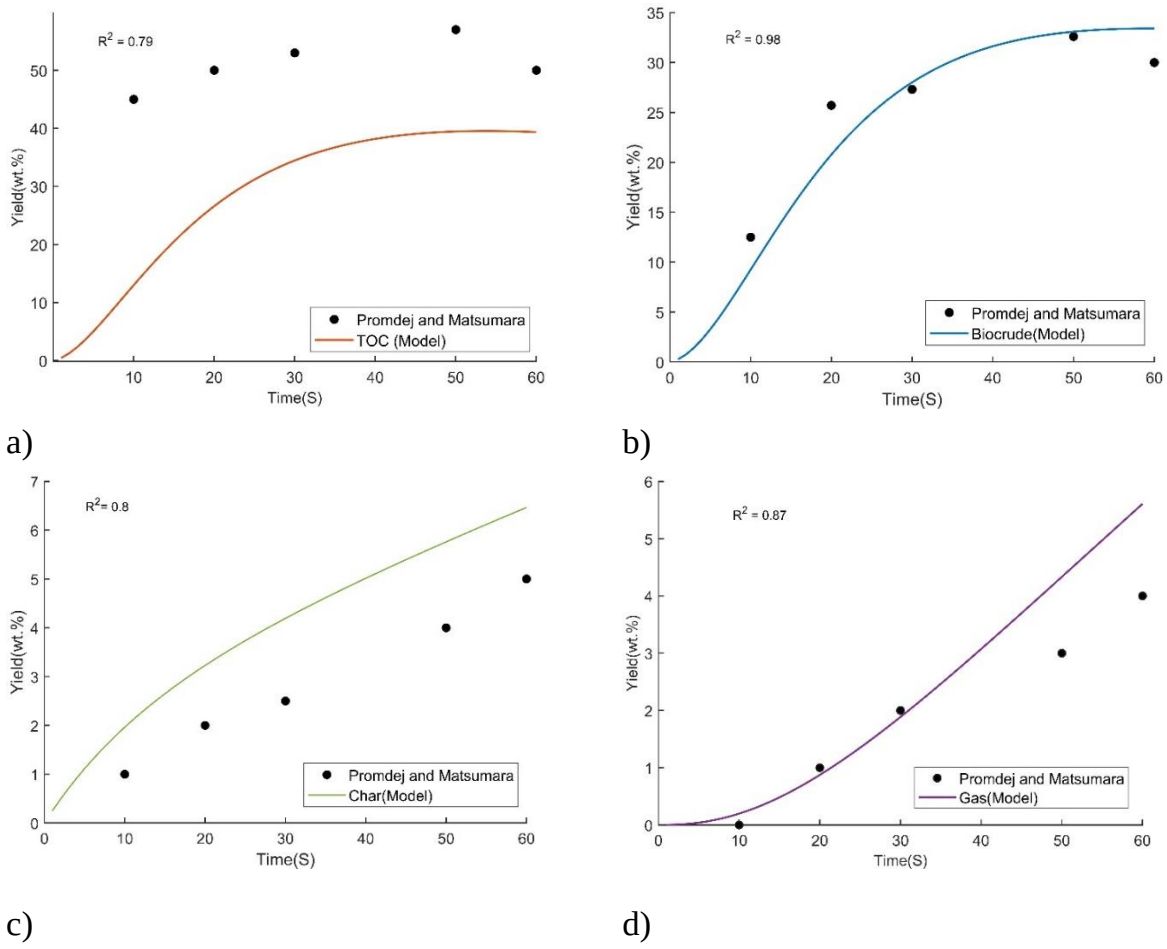

Figure 28:Cellulose hydrolysis model validation using the kinetic data proposed by Promdej and Matsumara [29] *at 573 K. a) TOC b) biocrude c) char d) gas*

To validate the lignin hydrolysis model, experimental work, and kinetic data presented by Yong and Matsumara[9] is used. Below figure 19 illustrates the variations of the different phases. In the lignin model, for the simplification, only TOC, gas, char, and biocrude fractions are used for the validation. Like the cellulose validation, different loading conditions, particle sizes, and different process conditions could make impacts on the differences in the considered compounds.

According to Ye et al. [34], increasing temperatures and residence time help promote the decomposition of Lignin and repolymerization of intermediates to other compounds. Thus, the increase in product yield components with longer residence time can be justified. When the kinetic data from Yong and Matsumara[9] is used, the model predicted yields show a decent fit to the experimental data.

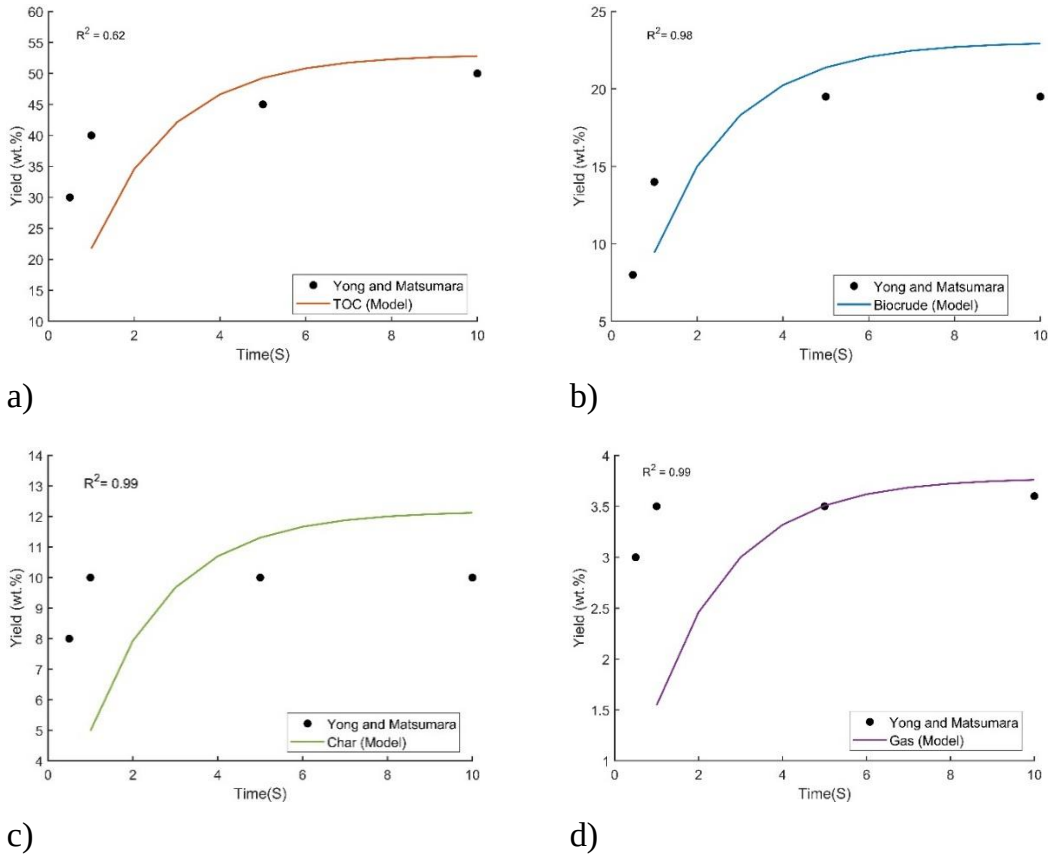

Figure 29: Lignin hydrolysis model validation using the kinetic data proposed by Yong and Matsumara [9] at 573K. a) TOC b) biocrude c) char d) gas

Figure 20 shows the variation of the xylose and biocrude. Due to the lack of detailed literature, and contradictions in the conclusions in the experimental studies, a simplified hemicellulose hydrolysis reaction pathway is followed, and only the decomposition of hemicellulose to xylose and xylose decomposition to biocrude is modelled. Experimental studies by Pinkowska et al. [25] is used for the development of the hemicellulose hydrolysis model. Experimental results from Pronyk and Mazza [13] Gao et al. [47] and Möller and Schröder[26] are used for the validation of the hemicellulose model. Hemicellulose hydrolysis is noted in temperatures from 403K to 500K. With a higher temperature, xylose creation is significantly decreased. Due to this reason, hemicellulose hydrolysis is already finished when the cellulose and lignin hydrolysis is started. Moreover, the hemicellulose hydrolysis temperature range is not considered in this model.

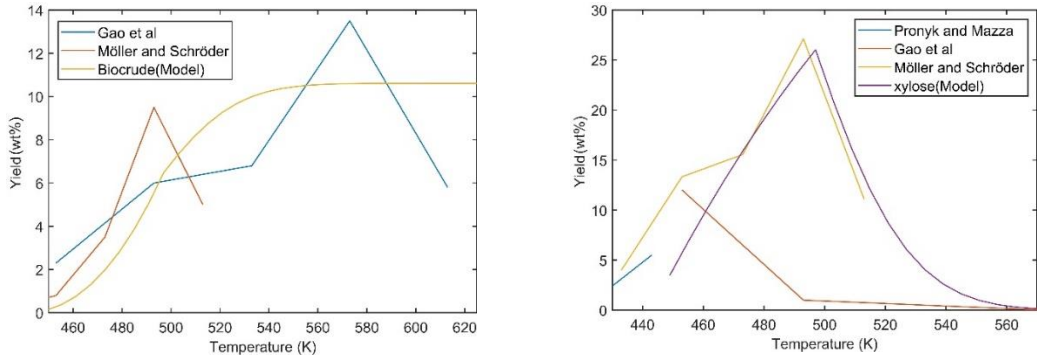

a) b)

Figure 30:Hemicellulose hydrolysis validation a) variation of Biocrude b) variation of xylose

Experimental work from Mosteiro-Romero et al. [3], Sugano et al. [48], Wadrzyk et al. [40], and Qu et al. [41] are used to validate the wood hydrolysis model. The model prediction is based on the cumulative effect of the hydrolysis of three components, while the data from literature are from wood liquefaction. Therefore, thein the validation graphs, the model results, and the actual wood liquefaction data have many differences. For clarity coefficient of determination (R^2) of the model predicted data are calculated and presented with the work done by Sugano et al. [48] since the process conditions and yield calculation method is somewhat similar.

It can be seen that the variation of the wood hydrolysis products follows the path of the cellulose hydrolysis path. Although the biocrude yield prediction can follow the experimental results, char yields are under predicted until 625K. Besides, in their experimental procedure, the sample is heated for a specific time and then kept at a certain temperature to obtain the outputs. Therefore, at the start of the residence time calculation, there are already some hydrolysis outputs developed. Besides, in the model, it is assumed that the reactor is placed in the heater when the heater comes to a specific temperature. Then as soon as the reactor is started heating, the resident time calculation is started. Thus, initially, the hydrolysis products in the system are zero.

Moreover, in most of the results reported, unreacted biomass is considered as solid residue from the start of the study. Therefore, many studies have shown higher solid residue yield at the start of the residence time. When the biomass is decomposed, unreacted biomass has reduced, and the char produced is added into the solid residue component. However, in this model, unreacted biomass is not included in the solid residue (char) calculations.

Furthermore, in the experiments, there is some loss of products due to practical difficulties. Then, it can influence the final yields as well. Moreover, in this model, no inter reactions between hydrolysis products from different wood components are considered. As an example, no reactions are considered between cellulose hydrolysis products and lignin hydrolysis products. It can be the next step of this modeling work.

In the model, cellulose lignin and hemicellulose, percentages are predetermined, and for the validation, those predetermined values are used. However, different wood types have different percentages of Cellulose, Lignin, and hemicellulose[6,49]. It can be the main reason for the difference between the liquefaction results in figure 21 with experimental results.

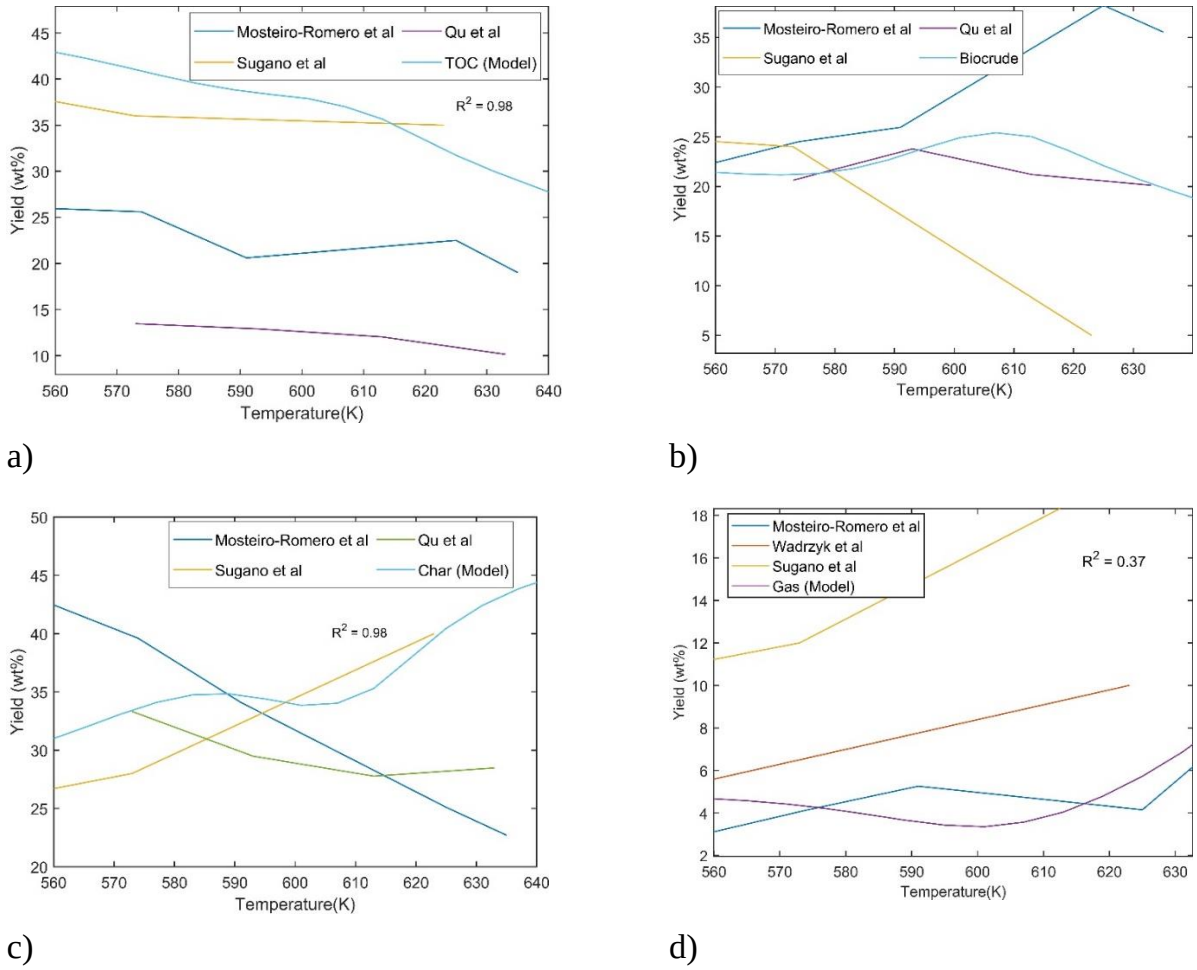

Figure 31:Wood liquefaction validation with 2 K/min heating rate and a particle size of 80µm (Coefficient of determination (R^2) is calculated for experimental results from Sugano et al. [48] *) a) TOC b) biocrude c) char d) gas*

4. Conclusion

In this study, wood hydrolysis is modeled for the subcritical region from 553K to 640K, utilizing Cellulose, Lignin, and hemicellulose hydrolysis using a shrinking core concept. A kinetic model is fitted with the shrinking core model to fit the homogenous reactions in the system. Wood hydrolysis is modeled using the cumulative hydrolysis effect of each wood component.

Hemicellulose hydrolysis occurs around 403K to 500K, and the conversion of hemicellulose into xylose becomes negligible in 553K-640K. Therefore, for further investigations, Hemicellulose hydrolysis is not considered. The model is validated using cellulose, hemicellulose lignin, and wood liquefaction ex-

perimental and model results in the literature. In most of the scenarios, the model shows a reasonable agreement with the available literature. Moreover, the predictions of the model coincide with the literature confirming the reliability of the model. Nevertheless, this model can be developed into a robust model with more inter reactions among the chemicals present in the reaction regime as well to the supercritical region.

At 593K for a 2K/min heating rate and particle size of 0.08 mm, biocrude shows the maximum yield of 26.87% for wood liquefaction. Cellulose and Lignin show maximum char and gas yields at 623K for the same residence time where biocrude and TOC yields show maximum yields at 588K. Lower heating rates initially promote lignin hydrolysis. Thus, for longer residence times, and close to the critical point, the heating rate does not show a visible impact on the lignin hydrolysis, where char and gas yields of cellulose model show a significant increase. Cellulose hydrolysis shows a big impact on the overall wood liquefaction behavior. Char yields of the cellulose hydrolysis are not affected significantly by the heating rates. After 600K, wood liquefaction shows higher char and gas yields of 47% and 20%, respectively, with lower heating rates. For maximum operating temperatures, over 600K TOC and biocrude yields tend to increase the yields. The diameter of the biomass particle has shown a definite impact on the hydrolysis rate of both Cellulose and Lignin.

A limited number of reactions and chemical compounds are used in the model. Furthermore, kinetic data used in the model are found in the literature from various studies under various process conditions. The experimental studies used for validation are operated with various process conditions as well as different workup methods. Therefore, in the validation plots, the model predictions for wood are severely underpredicted or over predicted most of the time. Furthermore, one of the main ideas of developing this model is to observe the difference in the cumulative liquefaction effect of main wood components against actual wood liquefaction. Thus, it is evident that there is an enormous gap between wood liquefaction and modeling wood liquefaction as a cumulative effect of the wood component liquefaction. Since the data used for this model is still too few and bears a high uncertainty in the yields due to the different workup processes, these results should not be used to predict things in a quantitative sense.

Acknowledgment

This study was conducted as part of the Ph.D. research at the Department of Engineering Sciences, funded by the Faculty of Engineering and Science, University of Agder

References

[1] Toor S, Rosendahl L, Rudolf A. Hydrothermal liquefaction of biomass: A review of subcritical water technologies. Energy 2011;36:2328–42. https://doi.org/10.1016/j.energy.2011.03.013.

[2] Barnés MC, de Visser MM, van Rossum G, Kersten SRA, Lange J-P. Liquefaction of wood and its model components. J Anal Appl Pyrolysis 2017;125:136–43. https://doi.org/10.1016/j.jaap.2017.04.008.

[3] Mosteiro-Romero M, Vogel F, Wokaun A. Liquefaction of wood in hot compressed water: Part 1 — Experimental results. Chem Eng Sci 2014;109:111–22. https://doi.org/10.1016/j.ces.2013.12.038.

[4] Shoji D, Kuramochi N, Yui K, Uchida H, Itatani K, Koda S. Visualized Kinetic Aspects of a Wood Block in Sub- and Supercritical Water Oxidation. Ind Eng Chem Res 2006;45:5885–90. https://doi.org/10.1021/ie0604775.

[5] Shoji D, Sugimoto K, Uchida H, Itatani K, Fujie M, Koda S. Visualized Kinetic Aspects of Decomposition of a Wood Block in Sub- and Supercritical Water. Ind Eng Chem Res 2005;44:2975–81. https://doi.org/10.1021/ie040263s.

[6] Zhong C, Wei X. A comparative experimental study on the liquefaction of wood. Energy 2004;29:1731–41. https://doi.org/10.1016/j.energy.2004.03.096.

[7] Mosteiro-Romero M, Vogel F, Wokaun A. Liquefaction of wood in hot compressed water Part 2–Modeling of particle dissolution. Chem Eng Sci 2014;109:220–35. https://doi.org/10.1016/j.ces.2013.12.039.

[8] Yong TL-K, Matsumura Y. Reaction Kinetics of the Lignin Conversion in Supercritical Water. Ind Eng Chem Res 2012;51:11975–88. https://doi.org/10.1021/ie300921d.

[9] Yong TL-K, Matsumura Y. Kinetic Analysis of Lignin Hydrothermal Conversion in Sub- and Supercritical Water. Ind Eng Chem Res 2013;52:5626–39. https://doi.org/10.1021/ie400600x.

[10] Kamio E, Takahashi S, Noda H, Fukuhara C, Okamura T. Effect of heating rate on liquefaction of cellulose by hot compressed water. Chem Eng J 2008;137:328–38. https://doi.org/10.1016/j.cej.2007.05.007.
[11] Kamio E, Sato H, Takahashi S, Noda H, Fukuhara C, Okamura T. Liquefaction kinetics of cellulose treated by hot compressed water under variable temperature conditions. J Mater Sci 2008;43:2179–88. https://doi.org/10.1007/s10853-007-2043-6.
[12] Minowa T, Zhen F, Ogi T. Cellulose decomposition in hot-compressed water with alkali or nickel catalyst. J Supercrit Fluids 1998;13:253–9. https://doi.org/10.1016/S0896-8446(98)00059-X.
[13] Pronyk C, Mazza G. Kinetic Modeling of Hemicellulose Hydrolysis from Triticale Straw in a Pressurized Low Polarity Water Flow-Through Reactor. Ind Eng Chem Res 2010;49:6367–75. https://doi.org/10.1021/ie1003625.
[14] Sasaki M, Adschiri T, Arai K. Kinetics of cellulose conversion at 25 MPa in sub- and supercritical water. AIChE J 2004;50:192–202. https://doi.org/10.1002/aic.10018.
[15] Sasaki M, Kabyemela B, Malaluan R, Hirose S, Takeda N, Adschiri T, et al. Cellulose hydrolysis in subcritical and supercritical water. J Supercrit Fluids 1998;13:261–8. https://doi.org/10.1016/S0896-8446(98)00060-6.
[16] Rogalinski T, Liu K, Albrecht T, Brunner G. Hydrolysis kinetics of biopolymers in subcritical water. J Supercrit Fluids 2008;46:335–41. https://doi.org/10.1016/j.supflu.2007.09.037.
[17] Sasaki M, Fang Z, Fukushima Y, Adschiri T, Arai K. Dissolution and Hydrolysis of Cellulose in Subcritical and Supercritical Water. Ind Eng Chem Res 2000;39:2883–90. https://doi.org/10.1021/ie990690j.
[18] Karagöz S, Bhaskar T, Muto A, Sakata Y. Comparative studies of oil compositions produced from sawdust, rice husk, lignin and cellulose by hydrothermal treatment. Fuel 2005;84:875–84. https://doi.org/10.1016/j.fuel.2005.01.004.
[19] Minowa T, Fang Z, Ogi T, Várhegyi G. Decomposition of Cellulose and Glucose in Hot-Compressed Water under Catalyst-Free Conditions. J Chem Eng Jpn 1998;31:131–4. https://doi.org/10.1252/jcej.31.131.

[20] Kabyemela BM, Adschiri T, Malaluan RM, Arai K. Kinetics of Glucose Epimerization and Decomposition in Subcritical and Supercritical Water. Ind Eng Chem Res 1997;36:1552–8. https://doi.org/10.1021/ie960250h.
[21] Cantero DA, Bermejo MD, Cocero MJ. Kinetic analysis of cellulose depolymerization reactions in near critical water. J Supercrit Fluids 2013;75:48–57. https://doi.org/10.1016/j.supflu.2012.12.013.
[22] Zhang B, Huang H-J, Ramaswamy S. Reaction kinetics of the hydrothermal treatment of lignin. Appl Biochem Biotechnol 2008;147:119–31. https://doi.org/10.1007/s12010-007-8070-6.
[23] Forchheim D, Hornung U, Kruse A, Sutter T. Kinetic Modelling of Hydrothermal Lignin Depolymerisation. Waste Biomass Valorization 2014;5:985–94. https://doi.org/10.1007/s12649-014-9307-6.
[24] Delbecq F, Wang Y, Muralidhara A, El Ouardi K, Marlair G, Len C. Hydrolysis of Hemicellulose and Derivatives—A Review of Recent Advances in the Production of Furfural. Front Chem 2018;6. https://doi.org/10.3389/fchem.2018.00146.
[25] Pińkowska H, Wolak P, Złocińska A. Hydrothermal decomposition of xylan as a model substance for plant biomass waste – Hydrothermolysis in subcritical water. Biomass Bioenergy 2011;35:3902–12. https://doi.org/10.1016/j.biombioe.2011.06.015.
[26] Möller M, Schröder U. Hydrothermal production of furfural from xylose and xylan as model compounds for hemicelluloses. RSC Adv 2013;3:22253–60. https://doi.org/10.1039/C3RA43108H.
[27] Galgano A, Blasi CD. Modeling Wood Degradation by the Unreacted-Core-Shrinking Approximation. Ind Eng Chem Res 2003;42:2101–11. https://doi.org/10.1021/ie020939o.
[28] Laidler KJ. The development of the Arrhenius equation. J Chem Educ 1984;61:494. https://doi.org/10.1021/ed061p494.
[29] Promdej C, Matsumura Y. Temperature Effect on Hydrothermal Decomposition of Glucose in Sub- And Supercritical Water. Ind Eng Chem Res 2011;50:8492–7. https://doi.org/10.1021/ie200298c.
[30] Klingler D, Vogel H. Influence of process parameters on the hydrothermal decomposition and oxidation of glucose in sub- and supercritical water. J Supercrit Fluids 2010;55:259–70. https://doi.org/10.1016/j.supflu.2010.06.004.

[31] Möller M, Harnisch F, Schröder U. Hydrothermal liquefaction of cellulose in subcritical water—the role of crystallinity on the cellulose reactivity. RSC Adv 2013;3:11035–44. https://doi.org/10.1039/C3RA41582A.
[32] Fang Z, Sato T, Smith RL, Inomata H, Arai K, Kozinski JA. Reaction chemistry and phase behavior of lignin in high-temperature and supercritical water. Bioresour Technol 2008;99:3424–30. https://doi.org/10.1016/j.biortech.2007.08.008.
[33] Arturi KR, Strandgaard M, Nielsen RP, Søgaard EG, Maschietti M. Hydrothermal liquefaction of lignin in near-critical water in a new batch reactor: Influence of phenol and temperature. J Supercrit Fluids 2017;123:28–39. https://doi.org/10.1016/j.supflu.2016.12.015.
[34] Ye Y, Zhang Y, Fan J, Chang J. Novel Method for Production of Phenolics by Combining Lignin Extraction with Lignin Depolymerization in Aqueous Ethanol. Ind Eng Chem Res 2012;51:103–10. https://doi.org/10.1021/ie202118d.
[35] Pińkowska H, Wolak P, Złocińska A. Hydrothermal decomposition of alkali lignin in sub- and supercritical water. Chem Eng J 2012;187:410–4. https://doi.org/10.1016/j.cej.2012.01.092.
[36] Marshall HB. The structure and properties of alkali lignin. 1934.
[37] Sauer J, Dahmen N, Hornung U, Schuler J, Kruse A. Hydrothermal Liquefaction of Lignin. J Biomater Nanobiotechnology 2017;8:720–6. https://doi.org/10.4236/jbnb.2017.81007.
[38] de Caprariis B, De Filippis P, Petrullo A, Scarsella M. Hydrothermal liquefaction of biomass: Influence of temperature and biomass composition on the bio-oil production. Fuel 2017;208:618–25. https://doi.org/10.1016/j.fuel.2017.07.054.
[39] Boocock DGB, Sherman KM. Further aspects of powdered poplar wood liquefaction by aqueous pyrolysis. Can J Chem Eng 1985;63:627–33. https://doi.org/10.1002/cjce.5450630415.
[40] Wądrzyk M, Berdel M, Janus R, Brilman DWF. Hydrothermal processing of pine wood: effect of process variables on bio-oil quality and yield. E3S Web Conf 2019;108:02004. https://doi.org/10.1051/e3sconf/201910802004.

[41] Qu Y, Wei X, Zhong C. Experimental study on the direct liquefaction of Cunninghamia lanceolata in water. Energy 2003;28:597–606. https://doi.org/10.1016/S0360-5442(02)00178-0.
[42] Yj Y, J X, Tc L, Zw R. Liquefaction of sawdust for liquid fuel. Fuel Process Technol 1999;60:135–43.
[43] Brand S, Hardi F, Kim J, Suh DJ. Effect of heating rate on biomass liquefaction: Differences between subcritical water and supercritical ethanol. Energy 2014;68:420–7. https://doi.org/10.1016/j.energy.2014.02.086.
[44] Akhtar J, Amin NAS. A review on process conditions for optimum bio-oil yield in hydrothermal liquefaction of biomass. Renew Sustain Energy Rev 2011;15:1615–24. https://doi.org/10.1016/j.rser.2010.11.054.
[45] Yilgin M, Pehlivan D. Poplar wood–water slurry liquefaction in the presence of formic acid catalyst. Energy Convers Manag 2004;45:2687–96. https://doi.org/10.1016/j.enconman.2003.12.010.
[46] Sintamarean IM, Grigoras IF, Jensen CU, Toor SS, Pedersen TH, Rosendahl LA. Two-stage alkaline hydrothermal liquefaction of wood to biocrude in a continuous bench-scale system. Biomass Convers Biorefinery 2017;7:425–35. https://doi.org/10.1007/s13399-017-0247-9.
[47] Gao Y, Wang H, Guo J, Peng P, Zhai M, She D. Hydrothermal degradation of hemicelluloses from triploid poplar in hot compressed water at 180–340 °C. Polym Degrad Stab 2016;126:179–87. https://doi.org/10.1016/j.polymdegradstab.2016.02.003.
[48] Sugano M, Takagi H, Hirano K, Mashimo K. Hydrothermal liquefaction of plantation biomass with two kinds of wastewater from paper industry. J Mater Sci 2008;43:2476–86. https://doi.org/10.1007/s10853-007-2106-8.
[49] Feng S, Yuan Z, Leitch M, Xu CC. Hydrothermal liquefaction of barks into bio-crude – Effects of species and ash content/composition. Fuel 2014;116:214–20. https://doi.org/10.1016/j.fuel.2013.07.096.

Appendix

Developed differential equations

Cellulose compounds (For 530K<T)

$$r_{cel} = -k_{x12} C_{cel}^{\frac{2}{3}} \qquad \text{A 1}$$

$$r_{oligo,c} = 76.7k_{x1}C_{cel}^{\frac{2}{3}} - (k_2 + 3k_3)C_{oligo} \quad \text{A 2}$$

$$r_{mono,c} = 3k_2C_{oligo} - 1.6k_4C_{mono} - k_6C_{TOC,c} \quad \text{A 3}$$

$$r_{MSP,c} = 0.6k_4C_{mono} + 0.03k_3C_{oligo,c} - 1.9k_7C_{toc} - 0.5k_{10}C_{char} \quad \text{A 4}$$

$$r_{char,c} = 40k_{x2}C_{cel}^{\frac{2}{3}} + 7k_{22}C_{TOC,c} + 0.45k_{10}C_{MSP} \quad \text{A 5}$$

$$r_{TOC,C} = 1.4k_6C_{mono} + k_7C_{MSP} - 0.5k_8C_{char,c} - 1.9k_9C_{gas,c} \quad \text{A 6}$$

$$r_{gas,C} = 3.3k_9C_{TOC,c} \quad \text{A 7}$$

Lignin compounds

(For 553K<T<603K)

$$r_{Lig} = -1.5k_{x13}C_L^{\frac{2}{3}} \quad \text{A 8}$$

$$r_{gui,L} = k_{x3}C_L^{\frac{2}{3}} - k_{20}C_{gui,L} - k_{21}C_{gui,L} - k_{22}C_{gui,L} \quad \text{A 9}$$

$$r_{char,L} = 4k_{x4}C_L^{\frac{2}{3}} + 1.5k_{16}C_{Ar} \quad \text{A10}$$

K_{xi} = *Hydrolysis rate constants developed for each hydrolysis reaction using the shrinking core concept*

C_{cel} = *Concentration of Cellulose in the system*

C_{oligo} = *concentration of oligosaccharides in the system*

C_{mono} = *concentration of monosaccharides in the system*

$C_{TOC,c}$ = *Concentration of TOC produced from cellulose hydrolysis in the system*

C_{MSP} = *concentration of biocrude products from cellulose hy drolysis of the phenol in the system*

$C_{gas,L}$ = *concentration of gas produced from lignin hydrolysis of the system*

C_{cat} = *concentration of catechol in the system*

C_{xylose} = *concentration of hemicellulose in the system*

C_{xylose} = *concentration of xylose in the system*

$C_{MSP,h}$ = *concentration of biocrude products from hemicellulose hydrolysis*

Kinetic parameters

Table A 1:List of kinetic parameters from the literature used as starting points for the frequency factors for each reaction in the computational model

Kinetic parameter	*Value*	*Kinetic parameter*	*Value*
$K_{0,1}$	$7.3\times10^{6\ a}$	$K_{0,15}$	$2.15\times10^{3\ e}$
$K_{0,2}$	$6\times10^{7\ b}$	$K_{0,16}$	$1.02\times10^{\ e}$
$K_{0,3}$	$3\times10^{11\ a}$	$K_{0,17}$	$2.44\times10^{\ e}$
$K_{0,4}$	$1.33\times10^{10\ c}$	$K_{0,18}$	$4.47\times10^{\ e}$
$K_{0,5}$	$8\times10^{7\ c}$	$K_{0,19}$	$1.69\times10^{\ e}$
$K_{0,6}$	$5.5\times10^{9\ d}$	$K_{0,20}$	$8.76\times10^{6\ e}$
$K_{0,7}$	$1.39\times10^{9\ c}$	$K_{0,21}$	$5.79\times10^{2\ e}$
$K_{0,8}$	$1.00\times10^{8\ c}$	$K_{0,22}$	$3.91\times10^{3\ e}$
$K_{0,9}$	$2.89\times10^{8\ c}$	$K_{0,23}$	0
$K_{0,10}$	$2.06\times10^{7\ c}$	$K_{0,24}$	0
$K_{0,11}$	$9.18\times10^{2\ e}$	$K_{0,25}$	0
$K_{0,12}$	$1.74\times10^{3\ e}$	$K_{0,26}$	0
$K_{0,13}$	$5.45\times10^{3\ e}$	$K_{0,27}$	$2.59\times10^{6\ f}$
$K_{0,14}$	$3.13\times10^{2\ e}$	$K_{0,28}$	$1.35\times10^{3\ g}$

For all the reactions, a unity reaction order is assumed.

a:- calculated by the data extracted from Sasaki et al.[14,15,17] *and Kamio et al.*[11]

b: - calculated by the data extracted from Kamio et al. [11]

c:- calculated by the data extracted from Promdej and Matsumura[29]

d:- calculated by the data extracted from Cantero et al.[21]

e:- calculated by the data extracted from Yong and Matsumara[9]

f:- calculated by the data extracted from Möller and Schröder[26]

g:- calculated by the data extracted from Mazza and Pronyk[13]

Table A 2:Constant operational conditions used for the calculations

Constant parameter used	Value	Unit
Density of Cellulose	555	mol/m^3
Density of Lignin	560	mol/m^3
Density of hemicellulose	555	mol/m^3
K_a	0.001	m/s
C_b	7000	mol/m^3
$T_{initial}$	553	K
r_0	0.00008	m
R	8.314	J/ (K mol)

Article B

Numerical modeling and validation of hydrothermal liquefaction of a lignin particle for biocrude production. Jayathilake, Madhawa; Rudra, Souman; Rosendahl, Lasse A. Published in Fuel (2021)

The layout has been revised

Numerical modeling and validation of hydrothermal liquefaction of a lignin particle for biocrude production

Madhawa Jayathilake[a], Souman Rudra[a4*], Lasse A. Rosendahl[b]

[a] Department of Engineering Sciences, University of Agder, Jon Lilletuns vei 9, 4879 Grimstad, Norway,
Tel: +47 37233308, Email address: rukshanj@uia.no ,
Tel: +47 37 23 30 36, Email address: souman.rudra@uia.no

[b] Department of Energy Technology, Aalborg University, Pontoppidanstræde 101, 9220, Aalborg, Denmark, E mail address: lar@et.aau.dk

[1*]corresponding author Tel: +47 37 23 30 36,
E mail address: souman.rudra@uia.no

Abstract

Lignin liquefaction process under catalyst-free conditions in a temperature range from 573K to 647K is investigated with this mathematical model. Based on the theoretical understanding of the physical and chemical processes of the liquefaction process in subcritical temperatures, a comprehensive mathematical model for the decomposition of lignin by hydrolysis reaction pathway is developed on the results of a series of batch experiments. The model consists of four main sections. They are liquefaction of lignin particle, oily film, and inorganic (ash) layer formation behavior during the liquefaction, kinetic model to model further liquefaction process of initial products, and the layer model for the intraparticle processes. Hydrolysis of the lignin particle is modeled using the shrinking core concept. The formation of oily film and an inorganic layer around the lignin particle and their behavior is modeled considering water transport through layers, diffusion of products, and dissolution of products in water. Moreover, the layer model is used to obtain surface and center point temperatures of the particle using mass transfer. .The kinetic model consists of ten components and 21 reactions. . Variations of aromatic hydrocarbons and phenolic compounds are given significance. In the experimental study highest biocrude yield of 0.28 w/w_0 is obtained at an operating temperature of 573K. Aromatic hydrocarbons are reduced from 0.23 w/w_0 to 0.145 w/w_0 with the increase of operating temperature from 573K to 623K. For an increase of operating temperature from 573K to 623K, phenol shows an increase from 2.5×10^{-4} w/w_0 to 3×10^{-3} w/w_0. At 573K and with a particle of radius 0.08 mm, oily film and ash layer show a maximum thickness of 2×10^{-12} m and 7.5×10^{-3} m, respectively. Both oily film and ash layer show a faster formation and faster dissolution in water with increasing operating temperature. Finally, the model's liquefaction results are analyzed and validated with the experimental data and the literature data, where it shows a reasonable agreement.

***Keywords*— Lignin, hydrothermal liquefaction**, **numerical modelling**, **shrinking-core, oily film, ash layer, validation.**

1. INTRODUCTION

Lignin is the second most common earthbound biopolymer and the most significant naturally occurring source of aromatic compounds[1]. Lignin is a sig-

nificant by-product of the paper and pulp industry [2]. The amount of lignin extracted in the western hemisphere's pulping process is estimated to be around 50 million tons per year [1]. Despite its relative abundance and colossal potential, lignin is still underutilized, partly due to its complex structure and difficulty breaking down. Lignin consists of three main phenylpropanoid monomers, and it is an irregular aromatic biopolymer[3]. The process of breaking down the complex structure is referred to as depolymerization. Depolymerization can be accomplished using different processes like thermochemical processes and enzymatic and catalytic cracking. The process temperatures range from 373K to 1073K. Depolymerization is performed in both sub and supercritical fluids [4], [5].

Hydrothermal liquefaction (HTL), unlike other thermochemical processes, is usually done at moderate temperatures and shorter residence times at sub and supercritical conditions (T = 523K – 647K and P = 10 – 30 MPa) [6]–[8]**.** Four product streams can be obtained from a typical HTL conversion[9]. The biocrude is considered the most desirable product among them as it can be further upgraded into various chemicals and liquid biofuels. Therefore, recent research on HTL has been centered on improving the yield and quality of biocrude and bio-oil[10].

In recent years, some research has been reported on lignin's hydrothermal liquefaction to obtain different products [5], [11]–[13]. In the hydrothermal liquefaction of lignin to produce phenolic compounds, hydrolysis and cleavage of the ether bond and C-C bond, demethoxylation, alkylation, and condensation reactions occur, and these reactions seem to compete. Alternatively, the aromatic rings are not affected by hydrothermal reactions [14]. The lignin-derived phenolic compounds from the demethoxylation and alkylation will be intensified as the temperature increases. Therefore, due to the different functionalities of phenolic compounds, lignin offers the potential of producing many valuable chemicals [14].

In literature, different methods are used for modeling the liquefaction of lignin. Yong and Matsumara [15] studied lignin decomposition in subcritical conditions and proposed a detailed kinetic reaction scheme. Zhang et al. [16] proposed a two-phase decomposition scheme for kraft lignin liquefaction. Forchheim et al.[17] investigated the phenolic products from lignin hydrothermal depolymerization with a kinetic model. All these models are kinetic

models which handled the liquefaction process. Besides, researchers have been using the shrinking core concept to model wood and cellulose liquefaction [18]–[20]. Further, few researches suggested a possible oily film formation during the liquefaction process of a biomass particle which raises the importance of modeling such an oily film [20], [21].

Despite having much research and many models developed with only kinetic schemes, there is a void in modeling liquefaction as a complete process. Thus, it is scarce to find details on the shrinkage of the particle, mass transfer from the particle, and the temperature behavior inside the particle during the liquefaction process. Furthermore, the formation of oily film and ash layer is yet to be experimentally studied. Therefore, modeling the formation of the oily film and ash layer could clarify the liquefaction behavior and produce better explanations for particle decomposition behaviors at different process conditions. The model presented in this article consists of four main sections. They are liquefaction of lignin particle, oily film, ash layer formation behavior during the liquefaction, kinetic model to model further liquefaction process of initial products, and the layer model for the intraparticle processes. In the proposed model, several aspects such as transport of water to the surface of the particle, diffusion through the ash layer and oily film, adsorption on the particle surface, heterogeneous reaction, desorption of the products from the particle, diffusion of the products through the ash layer, and transport of products back to ambient through the dissolution of products in water are considered. With the layer model, the intraparticle process is modeled. Therefore, the particle's temperature behavior at the particle's surface and the mass transport from the particle to the system are investigated. Besides, the biocrude phase is important as it is considered a mix of six different chemicals (Aromatic hydrocarbons, guaiacol, catechol, phenol, o-cresol, and m-cresol). With this model, each chemical component's variation can be investigated. Therefore, this model gives a better insight into the lignin liquefaction.

2. MATERIALS AND METHOD

2.1. Materials

The lignin feedstock is obtained from Sigma-Aldrich (CAS Number 8068-05-1). It is analyzed by performing both the proximate and ultimate analysis. The proximate analysis is performed with the use of a Nabertherm MORE THAN 30 – 3000^{o}C muffle furnace. The ultimate analysis is also performed for the feedstock using the PerkinElmer 2400 CHNS/O Series II elemental analyzer to determine its elemental composition. The analytical conditions in all the above cases are as follows: 1g of feedstock is used for proximate analysis with the oven temperature at 378K for 24 h to determine the moisture content and the muffle furnace temperature ranging from 523K to 1173K, respectively to determine the ash and volatile matter content. The feedstock sample weights used for the elemental analysis ranged from 0.9 mg to 1.5mg and operated at room temperature. 1g of the sample is used for the calorific test with oxygen as the combustion gas. Ultrapure water is used as the reaction solvent. During the calculations, all the components are normalized to 1 atom 'C' per molecule for simplification. The proximate and ultimate analysis results of the Alkali lignin are illustrated below, Table 1.

Table 7:Proximate and Ultimate Analysis of Alkali lignin

	Proximate Analysis (Wt%)			**Ultimate Analysis (Wt%, d.b)**			
	VM	ASH	FC	C	H	N	O
Current work	73	9.62	17.38	51.5	4.12	0.35	44.03
Literature [22]	72.60 (d.b)	9.50 (d.b)	17.90 (d.b)	49.0	4.4	0	(S & O) 46.6

VM= Volatile matter, FC=Fixed Carbon, d.b= dry base

2.2. Methods

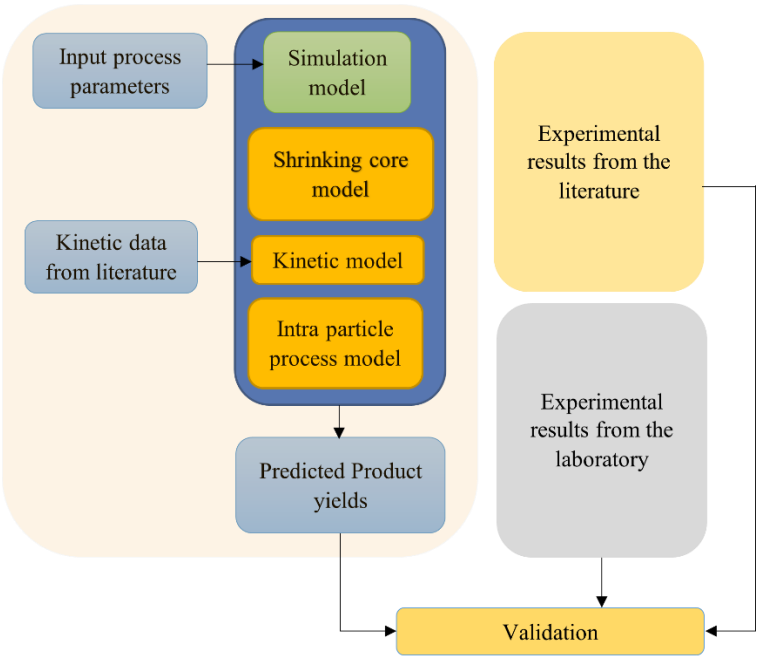

Figure 32:Schematic diagram of the method used for developing the model.

In developing the model, the shrinking core model is developed and connected with the heterogeneous reactions to model the particle decomposition through hydrolysis. Afterwards, the formation of oily film and the inorganic (ash) layer is modeled. As the next step, the kinetic model is developed to model the further decomposition, polymerization, and rearrangement reactions. For the kinetic model, data is taken from the literature. As the next step, the layer model is developed and merged with the rest of the model to study the temperature behavior on the particle. Once the model is fully developed, model predictions are graphed along with laboratory's experimental data and data from the literature for validation. Figure 1 shows a schematic diagram of the method used to develop the model.

2.2.2. Experimental procedure

The experimental study is carried out only to validate the results from the proposed model. Therefore, only the biocrude yields are quantified for validation purposes. The liquefaction experiment is performed in a steel tubular reactor from the HIP, with an internal volume of 24 ml. A feed slurry of 16ml is fed into the reactor, with a feedstock/water ratio of 1:9 maintained for all experi-

mental runs. Therefore, in each sample, 1.6g of lignin is mixed with 14.4 ml of ultrapure water. A dead volume of 8ml is maintained throughout all the runs. The reactor is sealed and purged with nitrogen to displace the air inside. The reactor is heated in a fluidized sand bath, suspended inside the sand bath with a shaft connected to the electric motor, for shaking the reactor during the test. The reactor is heated until the reaction temperature is attained. Then the temperature is kept for residence times ranging between 10 and 20 mins. Same residence times are used for reaction temperatures between 573K and 623K at the sub-critical condition. At the end of each reaction, the reactor is taken out and put into the water at room temperature at once and kept for 30mins. The gaseous products are vented out and later calculated by mass balance. Acetone is used to extract the liquid and solid products, and the reactor is washed three times to ensure complete removal of the product. The collected solid (biochar) is washed further with acetone and water to ensure the complete removal of residual acetone and bio-crude. Then the char is oven-dried at 378K for 24 hours to quantify the biochar yield. The bio-crude and residual water content are separated from the acetone with a rotary evaporator by evaporating acetone at 335K. Figure 2 below shows the extraction process of each output from the liquefaction process.

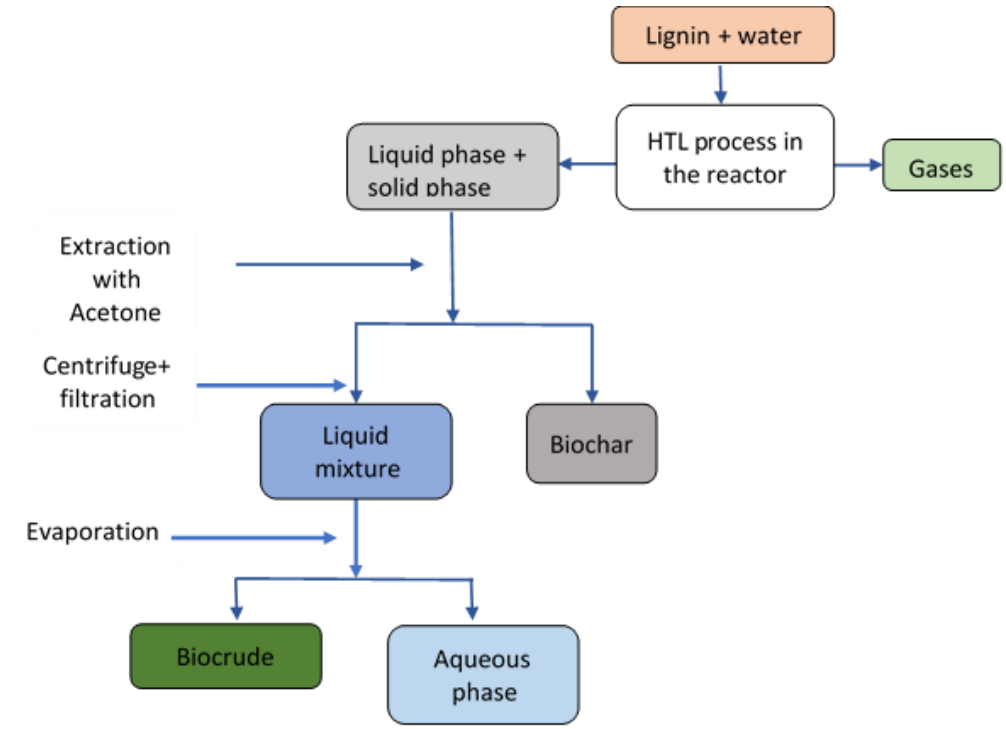

Figure 33:Process Flow Diagram for the HTL experiment and separation techniques used.

All experimental tests are carried out under similar conditions and in quadruples to ensure repeatability of the results. According to Eq 1 below, the yields of biocrude and char obtained from the experimental study are calculated based on the lignin's carbon content.

$$Product\ yield = \frac{Carbon\ available\ in\ product}{Initial\ Carbon\ available\ in\ the\ input\ lignin} \qquad \text{Eq 1}$$

2.2.1. Method of modeling

2.2.1.1. Shrinking core approach and hydrolysis modeling

Frequently, model compounds are abundantly used for the kinetic models of hydrolysis studies[15], [16], [18], [19], [23]–[28]. The proposed model is influenced by a model developed for wood liquefaction and is a continuation of that work [18].

In the proposed model, lignin hydrolysis is modeled using a shrinking core system. The decomposition of the lignin particle is assumed to be only in the radial direction. Figure 3 below shows a graphical model of the assumed shrinking core concept used for the proposed model[18].

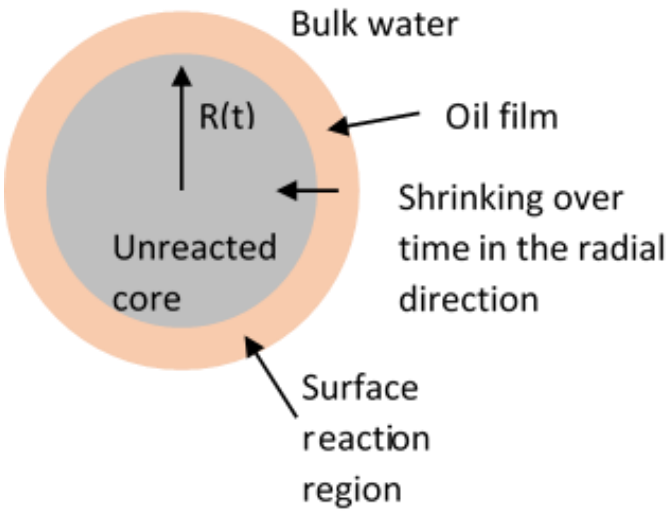

Figure 34:Shrinking core model assumed for the hydrolysis of the lignin particle of model components submerged in water.

The decomposition of the lignin particle creates an oily film around the particle surface. Besides, the ash produced by the decomposition of the particle forms a layer as well. Therefore, the approach of water monomers to the lignin particle as well as diffusion of biocrude produced in the initial hydrolysis reactions are affected. Therefore, this model discusses the formation, behavior, and impact of those two layers around the particle.

2.2.1.2. Decomposition of the lignin particle

The considered lignin particle system with a fully developed ash layer and the oily film is shown in figure 4. Hydrolysis of the lignin particle is determined by the developed reaction rate constant. The lignin particle's overall decomposition is a cumulative effect of each hydrolysis compound and occurs in the radial direction. The water monomer's diffusion through the aqueous film surrounding the lignin particle is modeled using water's mass transfer (when no oily film is present) from Kamio et al.[19]. The derivation of the decomposition of the lignin particle according to the shrinking core model is presented in section 1and from eq1 to eq 27 in the supplementary document.

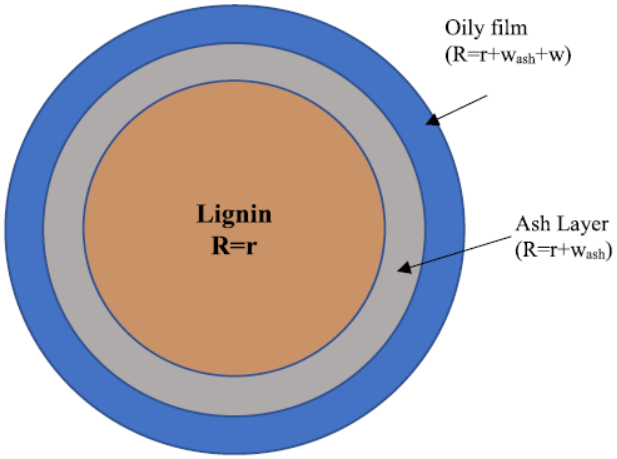

Figure 35:Liginin particle system considered in the model.

Each chemical component's theoretical values are calculated using differential equations using the backward Euler method. From the differential equations, the variation of each chemical compound's concentrations is obtained in mol/m^3. Then, each chemical compound or resultant phase is presented as a percentage of the total input.

2.2.1.3. Layer model for intra-particle process modeling.

In this paper, a layer model is implemented to study the intra-particle transport and sub-processes of the thermally thick lignin particle. Although the ash layer thickness and oily film thickness are small (10^{-7}mm and 10^{-12} mm, respectively), all the three layers present in the previous section are considered here. The lignin component is regarded as a single homogenous particle. The layer model is influenced by the work done by Mehrabian et al., 2012[29]. Figure 5 shows the layer model used in the proposed model.

The layer model treats the three layers in one dimension. This simplification is done to avoid model complexities. For the modeling purpose, it is assumed the particle boundary conditions are homogeneous, and all the points at a certain distance from the surface at a radial direction have the same conversion rates and temperatures[30].

As the conversion starts, the mass and thickness of the two layers in the particle are changed. Since the lignin particle started decomposing, the oily film will change its thickness according to the diffusion of water to the lignin particle surface, rate of hydrolysis, and dilution of the oily film in water. Along with this, the boundaries are moving towards the center of the particle as well. Therefore, the density and the particle size may change during the thermal conversion of the particle.

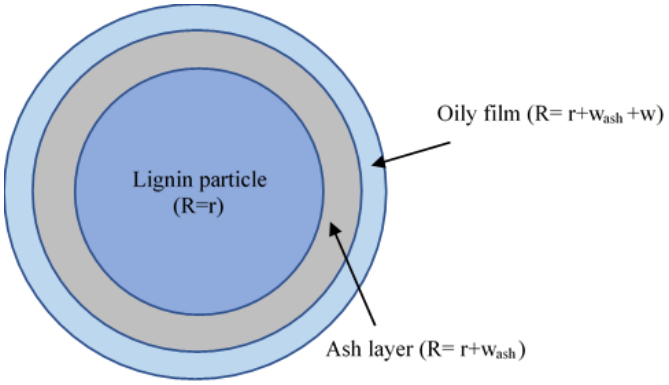

Figure 36:Layer model considered for the intraparticle process.

The derivation of the equations related to the layer model is presented in section 2 and from eq 28 to eq 35 the supplementary document.

2.2.1.4. Kinetic model for lignin liquefaction

The lignin liquefaction model is a continuation of the previous work by the authors[18]. Figure 6 shows the used reaction pathway of hydrolysis and the decomposition of lignin during the liquefaction process. For the lignin hydrolysis model, required kinetic parameters are taken from the literature[15]–[17], [31], [32]. In the supplementary document eq 36 to eq 46 in section 3 show the reactions incorporated in the lignin liquefaction model.

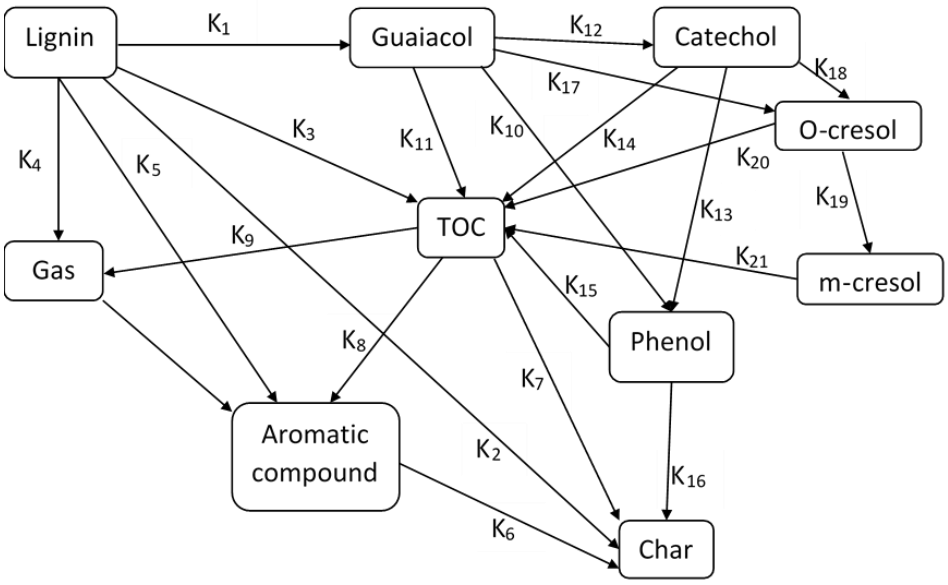

Figure 37:Reaction pathways of lignin in hydrothermal conditions.

Table 8:Reaction type of each reaction used in the lignin liquefaction model.

Reaction type	*Kinetic parameters*
Hydrolysis	K_1, K_3, K_4, K_5
Dehydration	K_2
Polymerization	K_6, K_7, K_{16}
Decomposition	K_8 , K_{10} , K_{11} , K_{12} , K_{13} , K_{14} , K_{15} , K_{17} , K_{18} , K_{19} , K_{20}, K_{21}
Gasification	K_9
Rearrangement	K_{17}

The set of chemical reaction used for the kinetic model is presented in the supplementary document.

To acquire the results presented in this section, differential equations developed in the mathematical model are solved and discretized in MATLAB R2019b.

2.2.1.5. General assumptions and simplifications

The lignin particle is deemed as a spherical particle with a given radius. It is submerged in a vast water volume, which is much larger than the particle's radius. Hence the dilution of the hydrolysis products is assumed to be infinite at a given distance from the particle center. Moreover, it is assumed that there is always enough water to perform all the required hydrolysis reactions. The particle decomposition is assumed only in the radial direction. Some of the thermophysical properties are presumed to be constant throughout the process as well. (All the constant and temperature dependent thermophysical properties are mentioned in the Appendix.) Particle is assumed to be homogenous in properties and composition. Only ash is amassed around the particle, and then the oily film around the ash layer is assumed.

Hydrolysis reactions of lignin occur only on the surface of the particle at the given time. Nevertheless, for simplification, primary char is considered a direct degradation product of lignin and stays within the system and does not partake in any secondary reactions. Nevertheless, the composition of the particle is not changed with time or with the hydrolysis reaction. The particle decomposition is dependent only on the lignin left in the particle and the concentration of water at the particle surface. Lignin is partially soluble in water[33]. Besides in this model it is assumed that the whole lignin particle is available to react with water.

A simplified elemental balance is used for the model using an approximation for oxygen and hydrogen balance in the model compounds. Therefore, only Carbon balance is given importance due to the calculations' simplification. Only CO_2 is considered the main contributor to the gas phase.

Furthermore, due to the lack of literature, especially on the heating and fast reaction kinetics, some of the kinetic data is modified and fit to reaction equations to obtain the literature's yield values. It could be a possible reason for some of the over predictions and under predictions in the model. The layer model assumes that the oily film's outer surface has the same temperature as the surrounding water. The developed model calculations assumed no losses during the extraction process, which is a regular occurrence in an experimental procedure.

3. Results and discussion

3.1. Model predictions

In this section, different model predictions are demonstrated. First, the biocrude component variation with different variables is presented. Then oily film and ash layer behavior is illustrated and then followed by the layer model predictions.

3.1.1. Biocrude component variation

Figure 7 shows the impact of temperature variation on biocrude components. Temperature values of 573K, 603K, and 623K are applied to examine the effect of temperature on the biocrude component yields. Generally lignin is hydrolyzed quickly and decomposes into various products[1], [12], [15], [17]. According to figure 7, aromatic hydrocarbons, guaiacol, and m-cresol produce reduced yields with increased temperatures while phenol levels go up. Aromatic hydrocarbons represent benzene, toluene, and naphthalene, which are nonphenolic aromatic compounds. Higher yields of aromatic hydrocarbons at lower temperatures can be due to ionic reactions rather than free radical reactions [15].

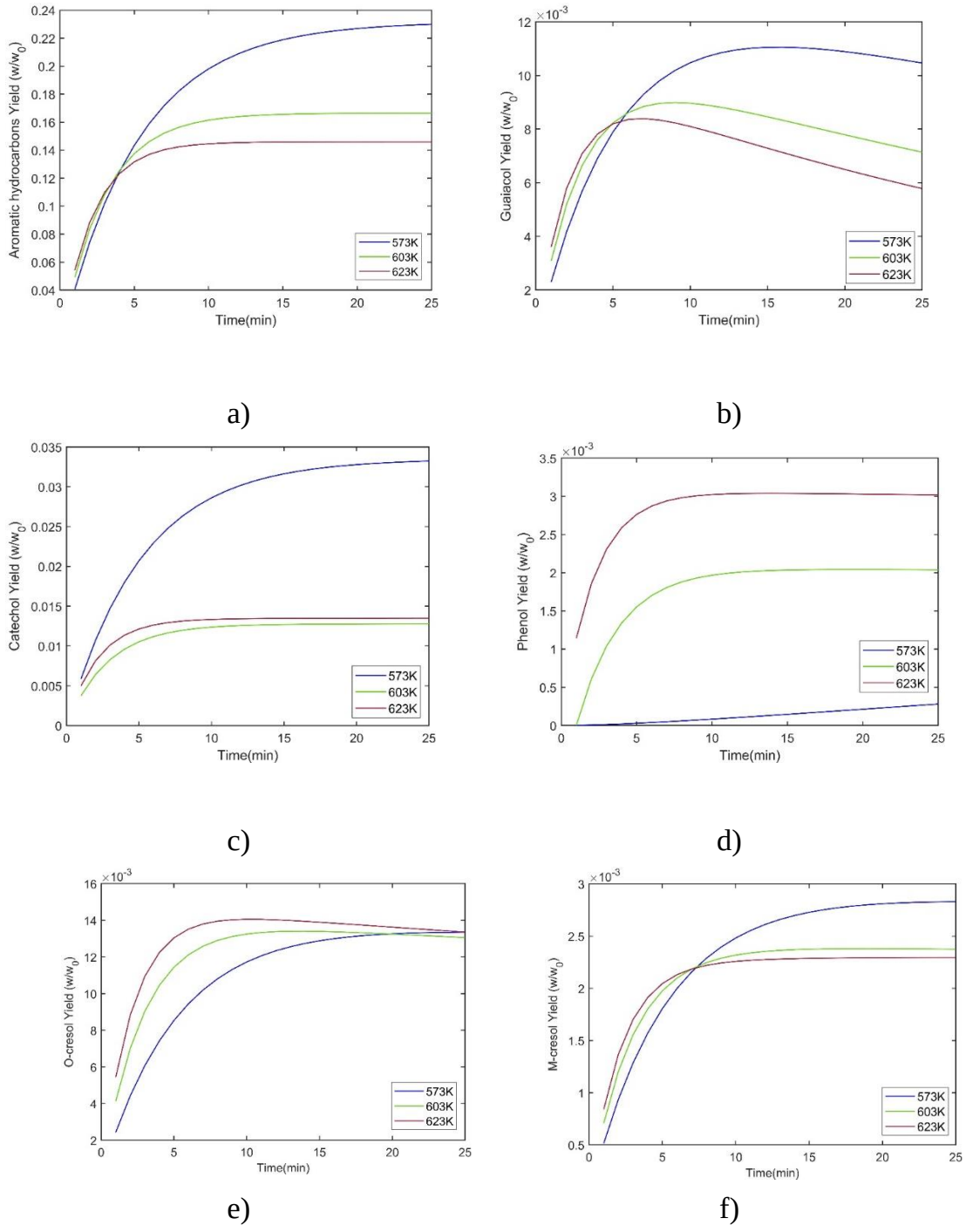

Figure 38:Effect of temperature on production of components of biocrude at 573K, 603K and 623K with a lignin particle radius of 0.08 mm a) Aromatic hydrocarbons b) Guaiacol c) Catechol d) Phenol e) O-cresol f) M-cresol

Meanwhile, catechol yield decreases in yields with 603K and then increases its yield with 623K. A similar variation of catechol is observed by Yong and Matsumara [15] as well. Most of the components show a decrease in the yields

with increasing temperature. The reason could be improved secondary reactions with a higher ionic water product and decomposition or repolymerization of these chemicals into char. Specially guaiacol is an intermedia degradation component in the lignin decomposition process[2]. With the increase of temperature and residence time, guaiacol decreases in the system, mainly due to its high reactivity and decomposition into catechol and phenols[32]. Since the bond energy of the aliphatic $C-O$ bond is lesser than the aromatic $C-O$ bond it is prone to be more reactive[15].

Moreover, the high ionic product and dielectric constant of water could impact the fast decomposition of guaiacol into phenol. Similar variation is shown by both guaiacol and catechol. Guaiacol is the main structure of softwood lignin. Catechol, o-cresol, and phenol are not present in natural lignin and are only produced by the secondary decomposition or hydrolysis of guaiacol [2], [15], [34]–[36]. Therefore, the variation of catechol, o-cresol, and phenol is heavily impacted by guaiacol in the system. Similar behavior of phenol and guaiacol is observed by Pińkowska et al.2012, [17], [32].In addition, Forchheim et al. 2014 reported that the catechol, phenols, and stable intermediates are produced through the reactive intermediates, which is similar to guaiacol in this study[16]. M-cresol is a direct derivate from o-cresol where m-cresol is possibly created through alkyl rearrangement [34].

According to figure 7, with all the considered chemicals except guaiacol, yields tend to stay approximately constant with longer residence times for all the considered temperatures. Understandably, guaiacol shows a decrease with the longer residence time where it shows a maximum of $11 \times 10^{-3} w/w_0$ at 15 min residence time. With this observation, it can be determined that any factor resulting in a higher yield of monomers such as temperature (553K-643K) or longer residence times helps both repolymerization and depolymerization[3]. Therefore, for guaiacol and catechol to decrease and phenol to increase simultaneously, can be supported. The phenol's behavior with temperatures can be justified by the observations from Forchheim et al.2014[16].

The particle size diminution reasoning is to have a better specific area of biomass to the liquefaction medium. Nonetheless, access to the fine particles can be difficult at times, and the behavior of the yields with bigger particles can be of interest. However, as, change of particle radius makes a low impact on

yields, subcritical water is a proper heat transfer medium [37]. For this study, three different particle radii sizes (0.08mm, 0.4 mm, and 0.8 mm) are used. Figure 8 shows the variation of biocrude component variation with different particle radius.

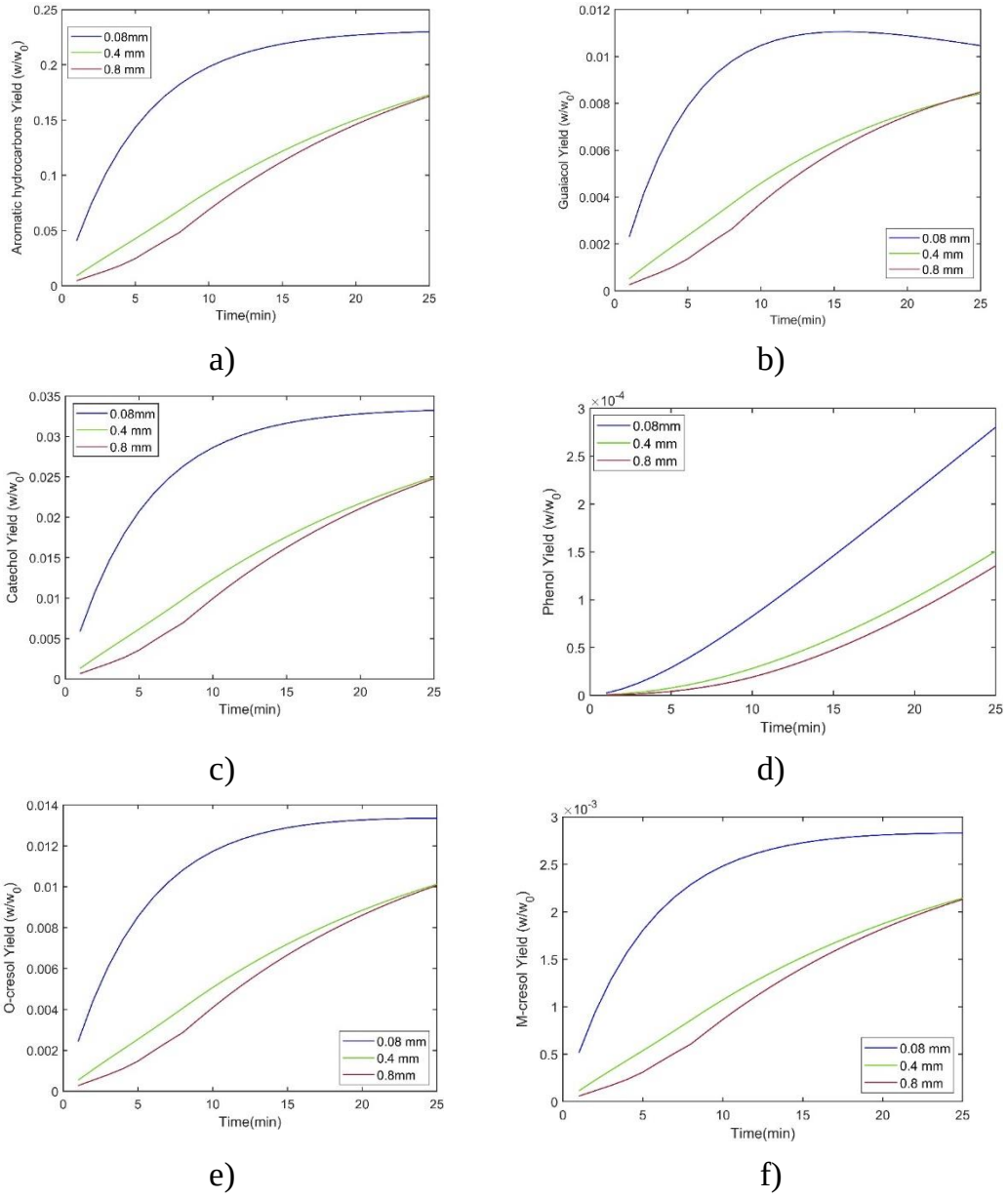

Figure 39: Effect of particle size on the production of components of biocrude with lignin particle radius of 0.08mm, 0.4mm, and 0.8mm at 573K a) Aromatic hydrocarbons b) Guaiacol c) Catechol d) Phenol e) O-cresol f) M-cresol

Figure 9 below shows the decomposition of lignin particles with different particle radius. With a bigger particle radius, lignin shows a reduced decomposi-

tion rate. Therefore, with figure 9, the above fact of reduced production of biocrude components with increasing radius is supported by observing the lignin's slower decomposition.

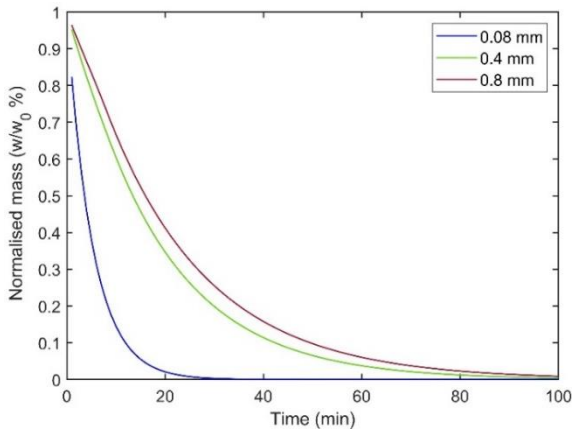

Figure 40: Lignin decomposition with different particle radius of 0.08mm, 0.4mm and 0.8mm at 573K

Three different heating rates (1 K/min, 3 K/min, and 5 K/min) are applied to the model to analyze the heating rate's impact on the biocrude components. Figure 10 below shows the yield variation of the products with different heating rates in a temperature range of 573 K to 640K.

With 1 K/min heating rate , is used the particle stay longer at lower temperatures and thus the reactions can also occur at these lower temperatures. However, this behavior does not mean that the lignin particle has faster decomposition. Besides, a decomposition at lower temperatures due to the longer residence time at these temperatures. According to figure 10, Lignin does not significantly change yields with the heating rate variation. Except for the phenol production, other biocrude component yields are not significantly changed by the heating rate. Besides, at 640K, phenol production is reduced to $3 \times 10^{-4} w/w_0$ from $1.75 \times 10^{-3} w/w_0$ when the heating rate is grown from 1K/min to 5 K/min. Ultimately when the temperature value reaches 640K (the critical point is at 647 K), product yields have become more stable except for guaiacol and phenol. This can be mainly due to the further decomposition of guaiacol to phenol. Nevertheless, the impact of the heating rate at short resi-

dence times is evident. Therefore, the impact of heating rates on both the initial kinetics of lignin decomposition and decomposition of guaiacol can be observed from these results. This brings out the importance of the heating rate on the fast liquefaction concept. Akhtar and Amin, 2011[37] hinted at the reasoning behind higher char yields with higher heating rates due to the secondary reactions' dominance. Eq 38, Eq 39, and Eq 46 in supplementary document showcase those reactions where higher heating rates promote higher char yields instead of producing biocrude. In a previous work by the authors and Akhtar and Amin, 2011[37], this fact is supported by illustrating the increase of char yield and a decrease of biocrude yield with the higher heating rate.

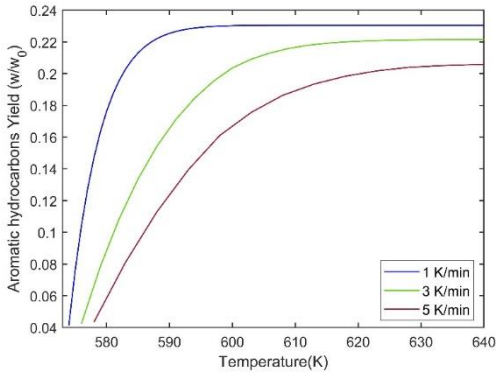

a)

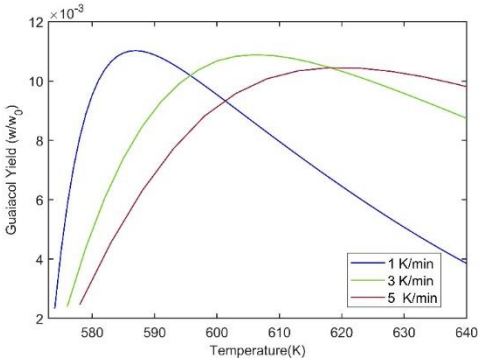

b)

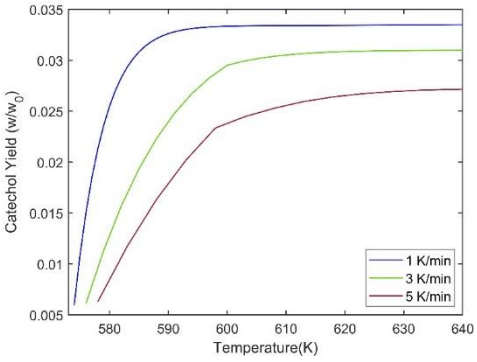

c)

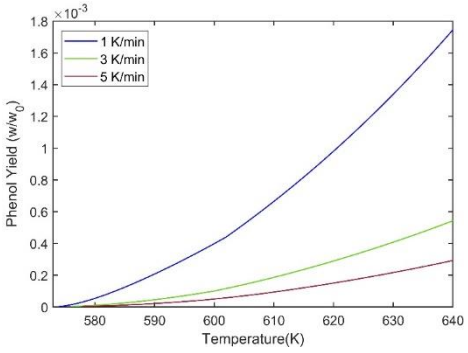

d)

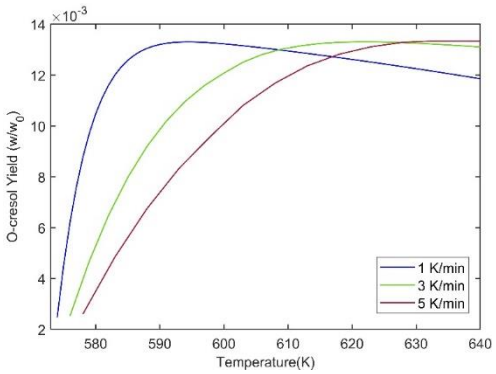

e)

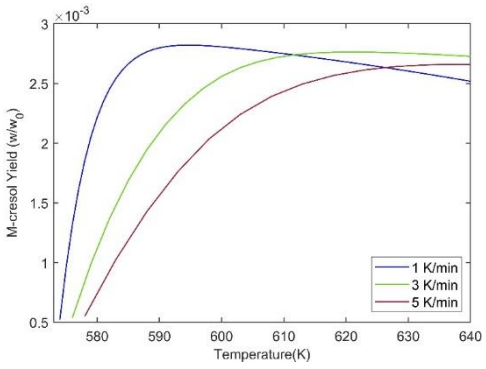

f)

Figure 41:Effect of heating rate on production of components of biocrude with a lignin particle radius of 0.08mm a) Aromatic hydrocarbons b) Guaiacol c) Catechol d) Phenol e) O-cresol f) M-cresol

3.1 .2. Oily film and ash layer behavior

The behavior of oily film and the ash layer with different operating temperatures is shown in below figure 11. According to figure 11, the oily film and ash layer have the maximum thicknesses after the reactions are started. This can be due to the initial fast decomposition of lignin. As soon as the particle is submerged in the water, no oily film or ash layer exists. Therefore, there is no resistance for water to reach the lignin particle surface. Nevertheless, with the reactions progress, the oily film and ash layer are formed, and the water monomer's movement to the particle surface is impeded. As time increases, both the oily film and ash layer come to equilibrium and dissolve into the system.

However, according to figure 11, oily film thickness increases dramatically with higher operating temperatures while it dissolves quickly. The rapid increase of the oily film can be justified by the initial rapid growth of aromatic hydrocarbons with higher temperatures. In another way, the oily film's behavior might have an impact on the product yields too. Similarly, with the ash layer, the initial rapid increase could be due to the fast initial hydrolysis of lignin under unobstructed water monomer arrival to the particle surface. Both the oily film and the ash layer are relatively thinner with lower temperatures, which helps both water and the products quickly diffuse through them. More

water is gone through to the lignin particle surface, which allows hydrolysis to happen.

Moreover, thinner oily film and ash layer could allow guaiacol to quickly come out to the water to complete the secondary decomposition and produce more secondary products. With higher operating temperatures, due to the rapid increase of the oily film and the ash layer, water diffusion is hampered, leading to reduced lignin's initial hydrolysis. Potentially, this could have an impact on reduced yields of biocrude at higher operating temperatures. Therefore, a further study of the formation of oily film and the ash layer can be significant. Dissolution of the ash layer is dependent on the oily film thickness as well.

According to figure 11b and figure 12b, the ash layer's thickness is much higher than the oily film. Therefore, ash layer formation might have a more significant impact on the liquefaction.

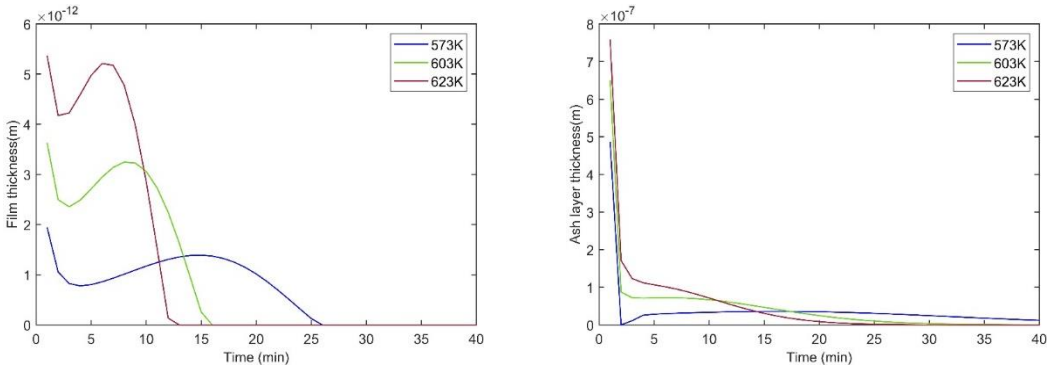

a) b)

Figure 42:Impact of temperature on oily film and ash layer formation with a lignin particle radius of 0.08mm at 573K, 603K, and 623K a) Oily film b) Ash layer

Below, figure 12 shows the oily film's behavior and the ash layer with different heating rates. Oily film and the ash layer show a thicker formation with higher heating rates. When the biocrude phase behavior is compared with this, it might create hints on the possible impact of oily film and ash layer thicknesses on the biocrude components' yields. Thicker oily film and ash layers could obstruct water monomers' arrival to the particle surface and the diffusion of guaiacol to the water medium.

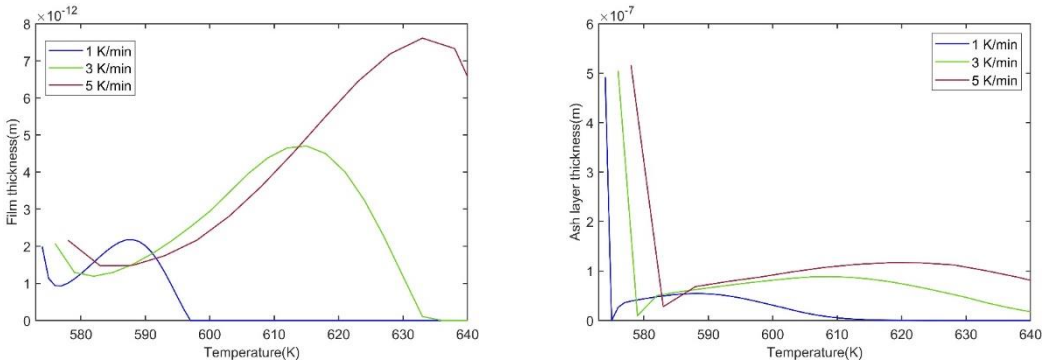

a) b)

Figure 43: Impact of heating rate on oily film and ash layer formation with heating rates of 1K/min, 3K/min and 5K/min with a lignin particle radius of 0.08mm a) Oily film b) Ash layer

When a particle radius is of the power of 10^{-5} m is utilized, the oily film thickness and ash layer thickness are of the power of 10^{-12} m and 10^{-7} m, respectively. Hence, there might not be a significant impact of oily film and ash layer thickness on the liquefaction. Therefore, the actual impact of the thickness of the oily film and ash layer is yet to be tested experimentally. Furthermore, benzene is used as the model compound for the oily film, and the actual dissolution properties of essential chemicals present in biocrude can be much different from the values used here. Likewise, the properties used for ash are taken from lignin ash. Besides, ash's actual behavior and dissolution properties in the liquefaction conditions can differ from those used for the model. Moreover, these aspects are difficult to study experimentally. Therefore, the oily film and ash layer's actual dissolution properties can be much different from what is observed here.

3.1 .3. Intraparticle behavior during liquefaction

Figure 13 shows the particle center temperature and particle surface temperature during the liquefaction process. A slower thermal conductivity or an increase of ash layer thickness could lead to higher resistance against the heat transfer, and as a result, a decrease in the particle center temperature is visible. As shown in Fig. 14, the lignin mass loss is consistent. The water monomer diffusion rate primarily controls the hydrolysis rate. With lignin mass is lost

with hydrolysis, the available surface area decreases due to the decreasing particle radius. The reduction of surface area could lead to reduced mass transfer. However, the particle temperature increases gradually.

Once the lignin is wholly consumed, the ash layer should be cooled rapidly towards the water phase temperature. Nevertheless, simultaneously the ash layer dissolves in the water too. In theory, due to particle heat-up and endothermic evaporation, the particle's temperature should be slightly lower than the surrounding temperature at the beginning. It is also assumed that the particle surface gets to the surrounding water temperature at once.

When volatile components start to release, the exothermic reactions around the particle increase the surface temperature. The slight rise in the surface temperatures from the surrounding water temperature in figure 13 explains it. Therefore during hydrolysis, the particle surface temperature increases and heats the gas phase by convective heat transfer.

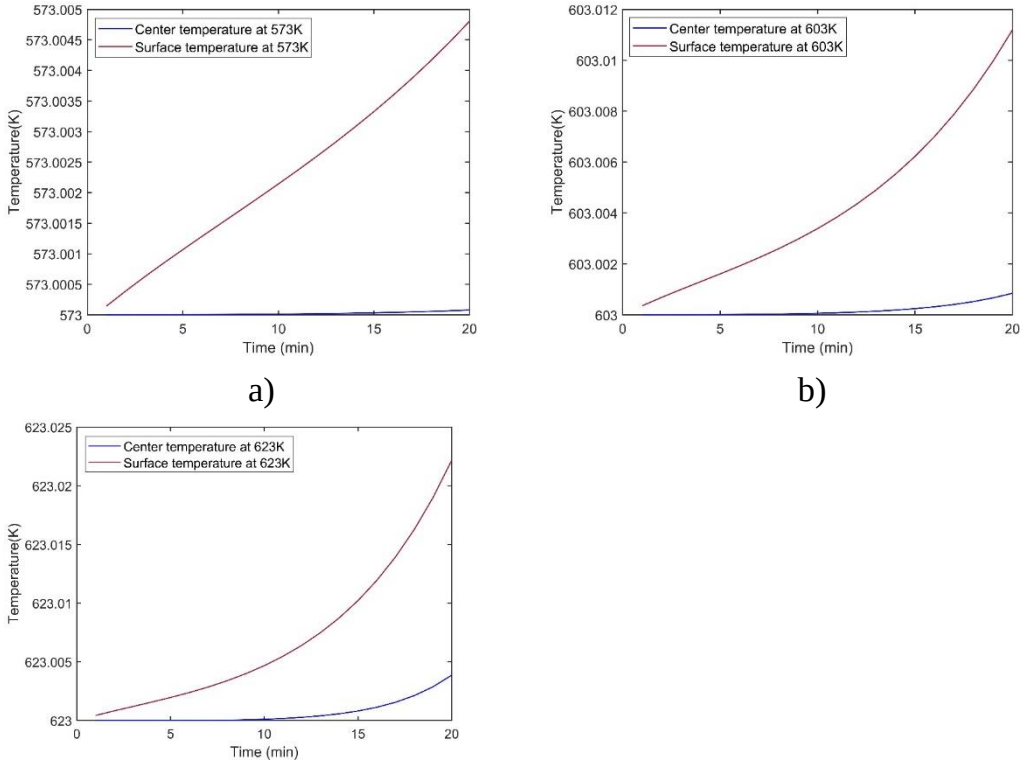

Figure 44: particle temperature profiles at different temperatures with a lignin particle radius of 0.08mm a) 573K, b) 603K, c) 623K.

The layer model calculates the mass and energy sources that are used in the species governing equations. The considered species calculations obtain few factors which are applied as boundary conditions for the layer model. These parameters are temperature, species concentrations, and available water concentration at each boundary. Furthermore, the species concentrations and the temperature around the particle are time-dependent and directly affected by the species generated by the lignin conversion through the hydrolysis process.
Model predictions show a slight increase in the particle center temperature and the surface during the hydrolysis process. The reason could be an exothermic reaction during the hydrolysis and decomposition of lignin[2], creating new stable bonds than in the lignin structure. Moreover, the further repolymerization of exothermic reactions at the particle surface could cause an increased particle surface temperature.

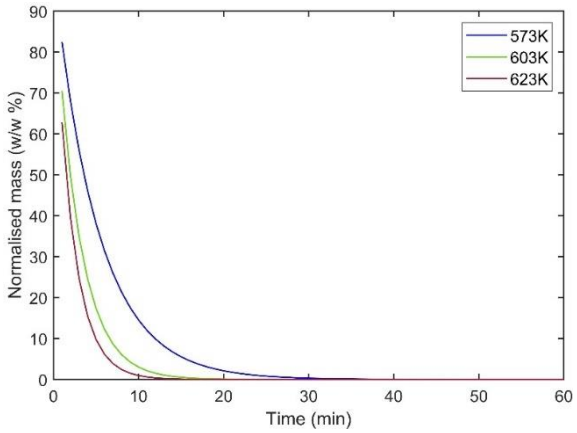

Figure 45:Normalized mass profile at different temperatures of 573K, 603K, and 623K with a lignin particle radius of 0.08mm

Subsequently, the hydrolysis rate of lignin, which is exponentially dependent on temperature, is responsible for the particle mass loss rate. Moreover, the empirical constants and data for the hydrolysis rate are obtained under certain process conditions. Therefore, any changes in these conditions might impact the validity of the hydrolysis rates, mass loss, and the calculated temperature values.
This model assumes that the char formed from the dehydration (Eq 37 in the supplementary document) stays within the particle without taking part in the reactions. Therefore, even when the lignin is completely hydrolyzed, the mod-

el particle is still available. Hence the particle center temperature is kept calculating, and it does not show any difference after the total hydrolysis of lignin. That explains the model still has space to improve in the future.

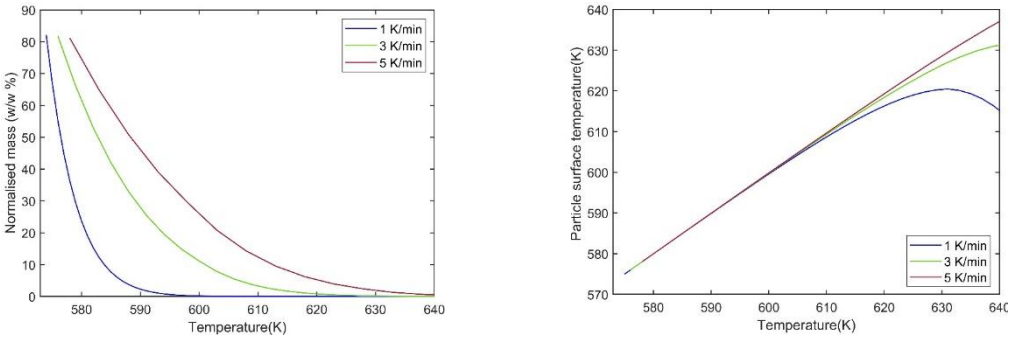

a) b)

Figure 46: Normalized mass profiles and particle surface temperature at different heating rates with heating rates of 1K/min, 3K/min and 5K/min with a lignin particle radius of 0.08mm a) Normalized mass profile b) Particle surface temperature

Although the lignin layer disappears, due to the non-reactive char availability inside the ash layer, the model senses a particle's availability. Therefore, until the ash layer is fully dissolved, the particle consists of char and behaves as a regular lignin particle and shows the same effect on the temperature variation. The particle mass predicted by the model decreases faster with higher temperatures (Figure 14) and slower heating rates (Figure 15a). These values are calculated solely on the empirical constants and developed differential equations. Due to the unavailability of experimental data on these parameters, it is difficult to determine whether these predictions are correct. Nevertheless, according to figure 15b, the particle surface temperature starts going down after coming to a maximum value with different heating rates. The reason can be the full dissolution of the ash layer after the complete hydrolysis of lignin. When the ash layer is fully dissolved, char that remained inside the ash layer released into the system. Then the particle does not exist anymore.

3.2. Validation

Validation of this model is done in two steps. First, the model's overall biocrude yield predictions are validated using the experimental study data from the lab-scale HTL reactor at the University of Agder, Norway. For the experiments, 573K, 603K, and 623K temperatures are considered, and the yield values are reported below in figure16.

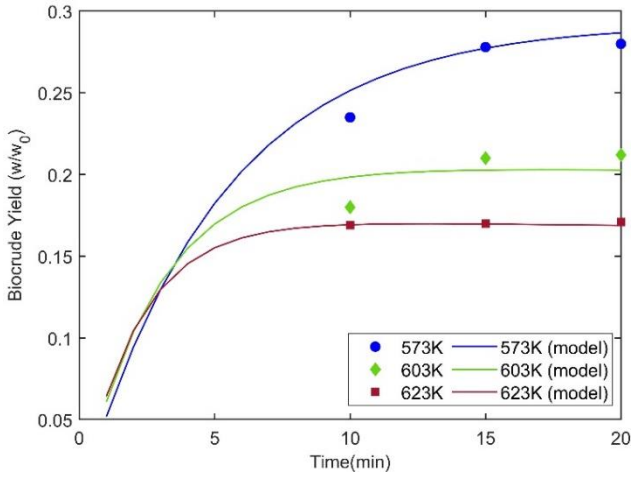

Figure 47:Lignin Liquefaction model validation Biocrude at 573K, 603K and 623K

According to the experimental data and model predictions, when the operating temperature increased, it has reduced the biocrude yield. This could be due to the promotion of the repolymerization reactions, which would yield more char in the secondary reactions[15], [32]. Moreover, when the operating temperature increases and goes close to the critical point, the process goes towards hydrothermal gasification, where it produces more gas [15], [17]. According to Ye et al.2012 [31], increased operating temperature and residence time promote further decomposition of lignin where it helps further repolymerization. This could ultimately result in overall biocrude yield reduction [15], [32].

The second validation step is done using the experimental data, kinetic data, and process conditions used by Yong and Matsumara [15]. In this step, the main components of the biocrude phase considered in this work are validated. Therefore, the kinetic data and the process conditions from Yong and Matsumara [15] are used as inputs for the model, and predictions from the model are

graphed along with the experimental values and model predictions obtained in their work. The validation plots are shown in figure 17. In their work, 603K is not considered as an experimental operating temperature. Therefore, 603K is not considered for the validation plots.

Ever Since the particle size of the lignin used by Yong and Matsumara [15] is not reported, a general radius size of 80µm is used for the lignin particle. Different concentrations, loading conditions, different reaction routes, and kinetics could affect yield values. In most of the validation plots model predicted data shows a deviation from the initial experimental data, taken below two seconds residence time. This could be due to the unavailability of precise initial kinetic data to feed the model. Besides, in the proposed model, the particle decomposition mechanism is given attention. Therefore, the temperature variation in the particle, oily film, and ash layer behavior and the mass transfer from the particle impact the deviations from the experimental results. Furthermore, during the modeling process only benzene is used as the model compound for the oily film. Properties of ash used for the model might not be the same as the liquefaction conditions. Thus, these factors can be vital in matching the experimental results exactly. Nevertheless, With the increase of residence time, the model data shows an excellent agreement with the experimental data.

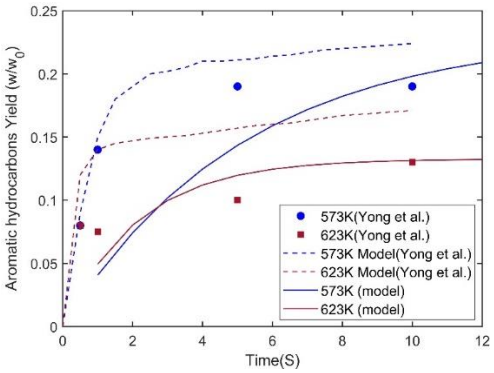

a)

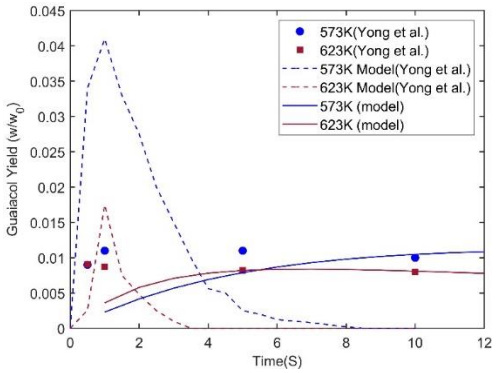

b)

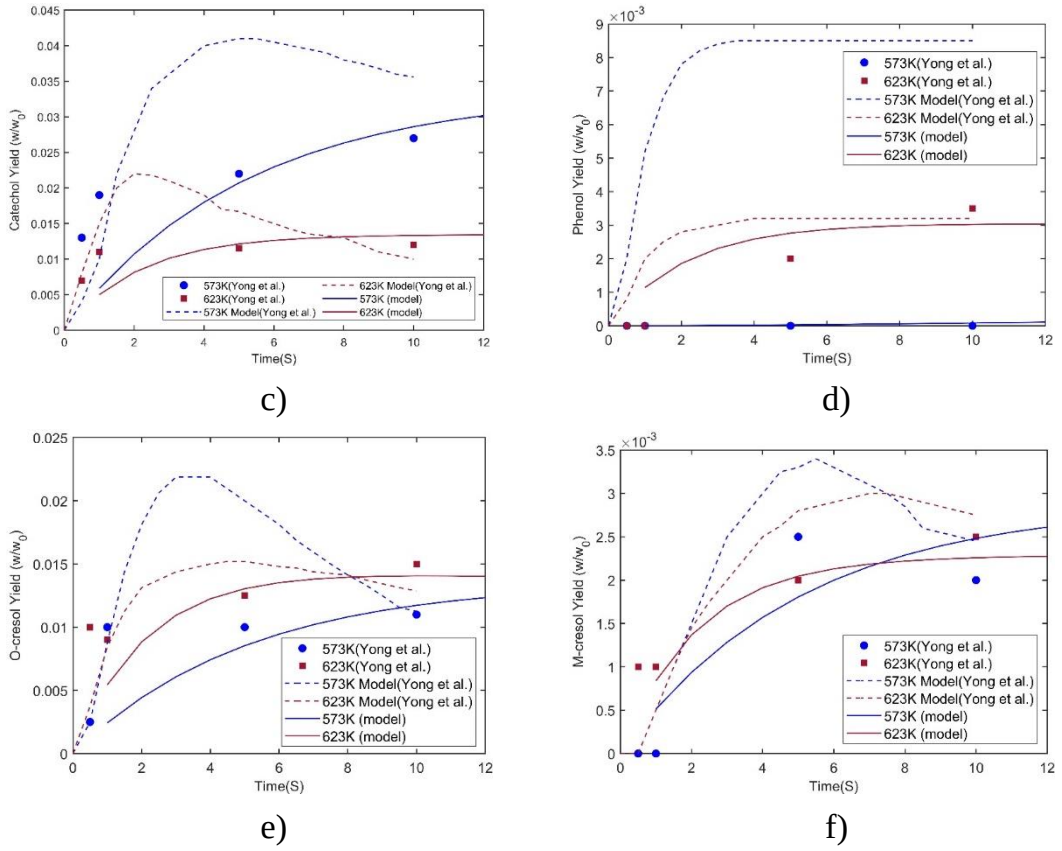

Figure 48: Biocrude phase validation a) Aromatic hydrocarbons b) Guaiacol c) Catechol d) Phenol e) O-cresol f) M-cresol

4. Conclusion

The model is validated using lignin, experimental liquefaction data obtained at the University of Agder, and literature. The predictions of the model agree with the literature showing reliability.

At 573K with a particle size of 0.08 mm, aromatic hydrocarbons show the maximum yield of 0.23 w/w_0. Slower heating rates have produced better yields with all the chemical components. For longer residence times and close to the critical point, heating rates reduce the yields. Oily film and ash layer shows a similar formation process and similar behavior at different process conditions.

Some of the model input values can differ from actual liquefaction conditions and could change the actual results. Since the availability of data used for this

model is limited and bears a high uncertainty in the yields due to the different workup processes, it is better not to obtain results in a quantitative sense. The behavior of the oily film and ash layer is not experimentally tested. Therefore, more experimental studies are required to validate some of the results obtained. In this article, only subcritical temperatures are considered. When the temperatures are shifted to the supercritical region, the ionic product of water, as well as the kinetic parameters change dramatically. Therefore, modeling the same scenario in supercritical conditions needs a separate study.

Acknowledgment

This study was conducted as part of the Ph.D. research at the Department of Engineering Sciences, funded by the Faculty of Engineering and Science, University of Agder

References

[1] K. R. Arturi, M. Strandgaard, R. P. Nielsen, E. G. Søgaard, and M. Maschietti, "Hydrothermal liquefaction of lignin in near-critical water in a new batch reactor: Influence of phenol and temperature," *J. Supercrit. Fluids*, vol. 123, pp. 28–39, May 2017, doi: 10.1016/j.supflu.2016.12.015.

[2] M. Brebu and C. Vasile, "THERMAL DEGRADATION OF LIGNIN – A REVIEW," *Cellul. Chem. Technol.*, vol. 44, no. 9, pp. 353–363, 2010.

[3] E. I. Kozliak *et al.*, "Thermal Liquefaction of Lignin to Aromatics: Efficiency, Selectivity, and Product Analysis," *ACS Sustain. Chem. Eng.*, vol. 4, no. 10, pp. 5106–5122, Oct. 2016, doi: 10.1021/acssuschemeng.6b01046.

[4] J. Becker and C. Wittmann, "A field of dreams: Lignin valorization into chemicals, materials, fuels, and health-care products," *Biotechnol. Adv.*, vol. 37, no. 6, p. 107360, Nov. 2019, doi: 10.1016/j.biotechadv.2019.02.016.

[5] M. Fache, B. Boutevin, and S. Caillol, "Vanillin Production from Lignin and Its Use as a Renewable Chemical," *ACS Sustain. Chem. Eng.*, vol. 4, no. 1, pp. 35–46, Jan. 2016, doi: 10.1021/acssuschemeng.5b01344.

[6] D. C. Elliott, P. Biller, A. B. Ross, A. J. Schmidt, and S. B. Jones, “Hydrothermal liquefaction of biomass: Developments from batch to continuous process,” *Bioresour. Technol.*, vol. 178, pp. 147–156, Feb. 2015, doi: 10.1016/j.biortech.2014.09.132.

[7] D. Castello, T. H. Pedersen, and L. A. Rosendahl, “Continuous Hydrothermal Liquefaction of Biomass: A Critical Review,” *Energies*, vol. 11, no. 11, Art. no. 11, Nov. 2018, doi: 10.3390/en11113165.

[8] S. Rudra and M. Jayathilake, “Hydrothermal Liquefaction of Biomass for Biofuel Production,” in *Reference Module in Earth Systems and Environmental Sciences*, Elsevier, 2021. doi: 10.1016/B978-0-12-819727-1.00043-1.

[9] B. de Caprariis, P. De Filippis, A. Petrullo, and M. Scarsella, “Hydrothermal liquefaction of biomass: Influence of temperature and biomass composition on the bio-oil production,” *Fuel*, vol. 208, pp. 618–625, Nov. 2017, doi: 10.1016/j.fuel.2017.07.054.

[10] J. Yang, Q. (Sophia) He, K. Corscadden, H. Niu, J. Lin, and T. Astatkie, “Advanced models for the prediction of product yield in hydrothermal liquefaction via a mixture design of biomass model components coupled with process variables,” *Appl. Energy*, vol. 233–234, pp. 906–915, Jan. 2019, doi: 10.1016/j.apenergy.2018.10.035.

[11] M. Y. Lui, B. Chan, A. K. L. Yuen, A. F. Masters, A. Montoya, and T. Maschmeyer, “Unravelling Some of the Key Transformations in the Hydrothermal Liquefaction of Lignin,” *ChemSusChem*, vol. 10, no. 10, pp. 2140–2144, 2017, doi: 10.1002/cssc.201700528.

[12] J. Sauer, N. Dahmen, U. Hornung, J. Schuler, and A. Kruse, “Hydrothermal Liquefaction of Lignin,” *J. Biomater. Nanobiotechnology*, vol. 8, no. 1, pp. 720–726, Jan. 2017, doi: 10.4236/jbnb.2017.81007.

[13] S. Kang, X. Li, J. Fan, and J. Chang, “Classified Separation of Lignin Hydrothermal Liquefied Products,” *Ind. Eng. Chem. Res.*, vol. 50, no. 19, pp. 11288–11296, Oct. 2011, doi: 10.1021/ie2011356.

[14] S. Kang, X. Li, J. Fan, and J. Chang, “Hydrothermal conversion of lignin: A review,” *Renew. Sustain. Energy Rev.*, vol. 27, no. C, pp. 546–558, 2013.

[15] T. L.-K. Yong and Y. Matsumura, “Kinetic Analysis of Lignin Hydrothermal Conversion in Sub- and Supercritical Water,” *Ind. Eng. Chem. Res.*, vol. 52, no. 16, pp. 5626–5639, Apr. 2013, doi: 10.1021/ie400600x.

[16] B. Zhang, H.-J. Huang, and S. Ramaswamy, “Reaction kinetics of the hydrothermal treatment of lignin,” *Appl. Biochem. Biotechnol.*, vol. 147, no. 1–3, pp. 119–131, Mar. 2008, doi: 10.1007/s12010-007-8070-6.

[17] D. Forchheim, U. Hornung, A. Kruse, and T. Sutter, “Kinetic Modelling of Hydrothermal Lignin Depolymerisation,” *Waste Biomass Valorization*, vol. 5, no. 6, pp. 985–994, Dec. 2014, doi: 10.1007/s12649-014-9307-6.

[18] M. Jayathilake, S. Rudra, and L. A. Rosendahl, “Hydrothermal liquefaction of wood using a modified multistage shrinking-core model,” *Fuel*, vol. 280, p. 118616, Nov. 2020, doi: 10.1016/j.fuel.2020.118616.

[19] E. Kamio, H. Sato, S. Takahashi, H. Noda, C. Fukuhara, and T. Okamura, “Liquefaction kinetics of cellulose treated by hot compressed water under variable temperature conditions,” *J. Mater. Sci.*, vol. 43, no. 7, pp. 2179–2188, Apr. 2008, doi: 10.1007/s10853-007-2043-6.

[20] M. Mosteiro-Romero, F. Vogel, and A. Wokaun, “Liquefaction of wood in hot compressed water Part 2–Modeling of particle dissolution,” *Chem. Eng. Sci.*, vol. 109, pp. 220–235, Apr. 2014, doi: 10.1016/j.ces.2013.12.039.

[21] F. Vogel, “Catalytic Conversion of High-Moisture Biomass to Synthetic Natural Gas in Supercritical Water,” in *Handbook of Green Chemistry*, American Cancer Society, 2010, pp. 281–324. doi: 10.1002/9783527628698.hgc024.

[22] C. ShuNa, C. Wilks, Y. ZhongShun, M. Leitch, and X. ChunBao, “Hydrothermal degradation of alkali lignin to bio-phenolic compounds in sub/supercritical ethanol and water-ethanol co-solvent.,” *Polym. Degrad. Stab.*, vol. 97, no. 6, pp. 839–848, 2012.

[23] E. Kamio, S. Takahashi, H. Noda, C. Fukuhara, and T. Okamura, “Effect of heating rate on liquefaction of cellulose by hot compressed water,” *Chem. Eng. J.*, vol. 137, no. 2, pp. 328–338, Apr. 2008, doi: 10.1016/j.cej.2007.05.007.

[24] H. Pińkowska, P. Wolak, and A. Złocińska, “Hydrothermal decomposition of xylan as a model substance for plant biomass waste – Hydrother-

molysis in subcritical water," *Biomass Bioenergy*, vol. 35, no. 9, pp. 3902–3912, Oct. 2011, doi: 10.1016/j.biombioe.2011.06.015.

[25] C. Pronyk and G. Mazza, "Kinetic Modeling of Hemicellulose Hydrolysis from Triticale Straw in a Pressurized Low Polarity Water Flow-Through Reactor," *Ind. Eng. Chem. Res.*, vol. 49, no. 14, pp. 6367–6375, Jul. 2010, doi: 10.1021/ie1003625.

[26] D. Shoji, N. Kuramochi, K. Yui, H. Uchida, K. Itatani, and S. Koda, "Visualized Kinetic Aspects of a Wood Block in Sub- and Supercritical Water Oxidation," *Ind. Eng. Chem. Res.*, vol. 45, no. 17, pp. 5885–5890, Aug. 2006, doi: 10.1021/ie0604775.

[27] D. Shoji, K. Sugimoto, H. Uchida, K. Itatani, M. Fujie, and S. Koda, "Visualized Kinetic Aspects of Decomposition of a Wood Block in Sub- and Supercritical Water," *Ind. Eng. Chem. Res.*, vol. 44, no. 9, pp. 2975–2981, Apr. 2005, doi: 10.1021/ie040263s.

[28] T. L.-K. Yong and Y. Matsumura, "Reaction Kinetics of the Lignin Conversion in Supercritical Water," *Ind. Eng. Chem. Res.*, vol. 51, no. 37, pp. 11975–11988, Sep. 2012, doi: 10.1021/ie300921d.

[29] R. Mehrabian *et al.*, "A CFD model for thermal conversion of thermally thick biomass particles," *Fuel Process. Technol.*, vol. 95, pp. 96–108, Mar. 2012, doi: 10.1016/j.fuproc.2011.11.021.

[30] H. Thunman, B. Leckner, F. Niklasson, and F. Johnsson, "Combustion of wood particles—a particle model for eulerian calculations," *Combust. Flame*, vol. 129, no. 1, pp. 30–46, Apr. 2002, doi: 10.1016/S0010-2180(01)00371-6.

[31] Y. Ye, Y. Zhang, J. Fan, and J. Chang, "Novel Method for Production of Phenolics by Combining Lignin Extraction with Lignin Depolymerization in Aqueous Ethanol," *Ind. Eng. Chem. Res.*, vol. 51, no. 1, pp. 103–110, Jan. 2012, doi: 10.1021/ie202118d.

[32] H. Pińkowska, P. Wolak, and A. Złocińska, "Hydrothermal decomposition of alkali lignin in sub- and supercritical water," *Chem. Eng. J.*, vol. 187, pp. 410–414, Apr. 2012, doi: 10.1016/j.cej.2012.01.092.

[33] M. Jayathilake, S. Rudra, N. Akhtar, and A. A. Christy, "Characterization and Evaluation of Hydrothermal Liquefaction Char from Alkali Lignin in Subcritical Temperatures," *Materials*, vol. 14, no. 11, Art. no. 11, Jan. 2021, doi: 10.3390/ma14113024.

[34] Wahyudiono, M. Sasaki, and M. Goto, “Thermal decomposition of guaiacol in sub- and supercritical water and its kinetic analysis,” *J. Mater. Cycles Waste Manag.*, vol. 13, no. 1, pp. 68–79, Feb. 2011, doi: 10.1007/s10163-010-0309-6.

[35] M. Kleinert and T. Barth, “Phenols from Lignin,” *Chem. Eng. Technol.*, vol. 31, no. 5, pp. 736–745, 2008, doi: https://doi.org/10.1002/ceat.200800073.

[36] J. R. Lawson and M. T. Klein, “Influence of water on guaiacol pyrolysis,” *Ind. Eng. Chem. Fundam.*, vol. 24, no. 2, pp. 203–208, May 1985, doi: 10.1021/i100018a012.

[37] J. Akhtar and N. A. S. Amin, “A review on process conditions for optimum bio-oil yield in hydrothermal liquefaction of biomass,” *Renew. Sustain. Energy Rev.*, vol. 15, no. 3, pp. 1615–1624, Apr. 2011, doi: 10.1016/j.rser.2010.11.054.

[38] D. Bergström *et al.*, “Effects of raw material particle size distribution on the characteristics of Scots pine sawdust fuel pellets,” *Fuel Process. Technol.*, vol. 89, no. 12, pp. 1324–1329, Dec. 2008, doi: 10.1016/j.fuproc.2008.06.001.

[39] M. G. Grønli, *A theoretical and experimental study of the thermal degradation of biomass*. 1996. Accessed: Dec. 18, 2020. [Online]. Available: https://ntnuopen.ntnu.no/ntnu-xmlui/handle/11250/228108

[40] N. I. Gorbunova, V. A. Grigoriev, V. M. Simonov, and V. A. Shipova, “Heat capacity of liquid benzene and hexafluorobenzene at atmospheric pressure,” *Int. J. Thermophys.*, vol. 3, no. 1, pp. 1–15, Mar. 1982, doi: 10.1007/BF00503954.

[41] H. Lu, “Experimental and Modeling Investigations of Biomass Particle Combustion,” *Theses Diss.*, Aug. 2006, [Online]. Available: https://scholarsarchive.byu.edu/etd/778

[42] M. L. V. Ramires, F. J. Vieira dos Santos, U. V. Mardolcar, and C. A. N. de Castro, “The thermal conductivity of benzene and toluene,” *Int. J. Thermophys.*, vol. 10, no. 5, pp. 1005–1011, Sep. 1989, doi: 10.1007/BF00503169.

[43] Y. Furutani, Y. Dohara, S. Kudo, J. Hayashi, and K. Norinaga, “Theoretical Study on the Kinetics of Thermal Decomposition of Guaiacol and

Catechol," *J. Phys. Chem. A*, vol. 121, no. 44, pp. 8495–8503, Nov. 2017, doi: 10.1021/acs.jpca.7b08112.

Glossary

C_{lig} = Concentration of lignin in the system
M_w = Mass transfer rate of the water monomer
r = Radial position of the lignin particle
k_A = Mass transfer coefficient
C_B = Bulk water monomer concentration
C_S = Water concentration at the surface.
M_B = Mass transfer through hydrolysis at the surface of each model compound
k_H = Hydrolysis rate constant
r_d = Decomposition rate of the lignin particle
k_x = Rate coefficient of lignin decomposition
$k_{i,t}$ = Calculated rate constant
$k_{o,i}$ = Frequency factor
E_a = Activation energy for each component
$\sqrt{k_W}$ = Impact of the ionic product of water.
w_{Ash} = Thickness of the ash layer
w = Thickness of the oily film
C_{S1} = Water concentration in between oily film and the ash layer
k_M = Mass transfer coefficient through the oily film.
k_{Diff} = Diffusion coefficient of the oily film
k_B = Boltzmann's constant,
T = Temperature (K)
r_{H_2O} = Radius of the water molecule
μ_{Oil} = Viscosity of the oily film
k_{M_ash} = Mass transfer coefficient through the ash layer
m_{oil} = Mass of the oily film at a given time
ρ_{oil} = Density of the oily film
r_{oil} = Rate of formation of the oily film
$r_{dissolve}$ = Rate of dissolution of the oily film in water

k_{M2} = Mass transfer coefficient to the water from the oily film

k_{Diff1} = Diffusivity of oily film to water

m_{ash} = Mass of the ash layer at a given time

ρ_{ash} = Density of the ash

k_{L_i} = Thermal conductivity of the layer

Δx_{Li} = Ratio of the area of the boundary to half of the layer thickness

c_p = Specific heat capacity

ΔH_f° = Standard enthalpy of formation

H = Specific enthalpy

A. Appendix

$$C_{sat}(T) = \frac{x_{oil}\ M_{oil}}{\frac{(1-x_{oil})M_{water}}{\rho_{water}} + \frac{x_{oil}\ M_{oil}}{\rho_{oil}}} \quad \text{Eq A.1}$$

$$ln(x_{oil}) = -170.04018 + \frac{6922.912}{T} + 24.398795\ ln\ (T) \quad \text{Eq A.2}$$

Table A 3: Parameters and constants used.

Density			
Lignin	560	Kgm^{-3}	
Ash	300	Kgm^{-3}	[38]
Char	200	Kgm^{-3}	[38]

Heat capacity			
Lignin (wood)	1500+T	$JKg^{-1}K^{-1}$	[39]
Ash	$420+2.09T+6.85\times10^{-4}T^2$	$JKg^{-1}K^{-1}$	[39]
Char	$420+2.09T+6.85\times10^{-4}T^2$	$JKg^{-1}K^{-1}$	[39]
Biocrude (Benzene)	$1.5194-1.299\times10-3T+6.927\times10^{-6}T^2$	$JKg^{-1}K^{-1}$	[40]

Thermal conductivity	Value

Lignin	$0.056+2.6\times10^{-4}T$	$Wm^{-1}K^{-1}$	[41]
Ash	1.2	$Wm^{-1}K^{-1}$	[41]
Char	0.071	$Wm^{-1}K^{-1}$	[41]
Biocrude (Benzene)	$0.22598-2.8744\times10^{-4}T$	$Wm^{-1}K^{-1}$	[42]

Constant parameters		
K_a	0.001	m/s
C_b	7000	mol/m^3
$T_{initial}$	553	K
r_0	0.00008	m
R	8.314	J/ (K mol)

Table A 4:List of kinetic parameters

Kinetic parameter	Value
$K_{0,1}$	9.18×10^2 [15],[29],[35]
$K_{0,2}$	1.74×10^3 [15]
$K_{0,3}$	5.45×10^3 [15]
$K_{0,4}$	3.13×10^2 [15] ,[17]
$K_{0,5}$	2.15×10^3 [15]
$K_{0,6}$	1.02×10 [15]
$K_{0,7}$	2.44×10 [15]
$K_{0,8}$	4.47×10 [15]
$K_{0,9}$	1.69×10 [15]
$K_{0,10}$	8.76×10^6 [17],[32]
$K_{0,11}$	5.79×10^2 [15]
$K_{0,12}$	3.91×10^3 [15],[17],[32]
$K_{0,13}$	1.97×10^2 [17],[32],[43]
$K_{0,14}$	$2.71x10^{-2}$ [17]
$K_{0,15}$	0 [15],[17]
$K_{0,16}$	0 [15],[17]

$K_{0,17}$	2.83×10^{3} [15],[17]
$K_{0,18}$	2.57×10^{2} [15],[17]
$K_{0,19}$	8.92×10^{2} [15],[17],[32]
$K_{0,20}$	8.19×10^{2} [15]
$K_{0,21}$	5.77×10^{3} [15]

Supplementary document for : Numerical modeling and validation of hydrothermal liquefaction of a lignin particle for biocrude production

Madhawa Jayathilake[a], Souman Rudra[a5*], Lasse A. Rosendahl[b]

[a] Department of Engineering Sciences, University of Agder, Jon Lilletuns vei 9, 4879 Grimstad, Norway,
Tel: +47 37233308, Email address: rukshanj@uia.no
Tel: +47 37 23 30 36, Email address: souman.rudra@uia.no

[b] Department of Energy Technology, Aalborg University, Pontoppidanstræde 101, 9220, Aalborg, Denmark, E mail address: lar@et.aau.dk

1. Decomposition of the lignin particle

The considered lignin particle system with a fully developed ash layer and the oily film is shown in figure 3.

Hydrolysis of the lignin particle is determined by the developed reaction rate constant. The lignin particle's overall decomposition is a cumulative effect of each hydrolysis compound and occurs in the radial direction. The water monomer's diffusion through the aqueous film surrounding the lignin particle is modeled using water's mass transfer (when no oily film is present) from Kamio et al.[18]

[1*]corresponding author Tel: +47 37 23 30 36,
E mail address: souman.rudra@uia.no

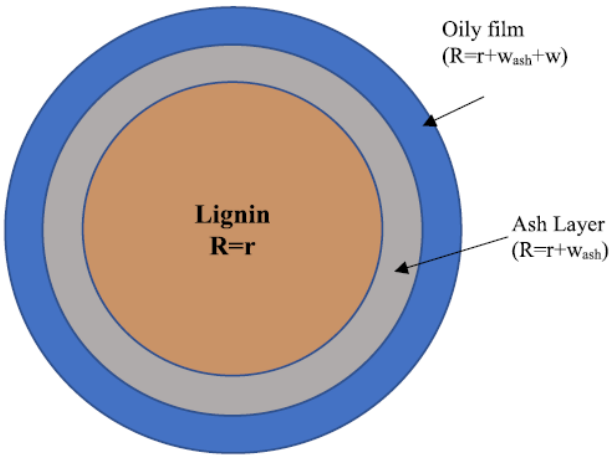

Figure 49:Liginn particle system considered in the model.

$$M_w = 4\pi r^2 k_A (C_B - C_S) \quad \text{Eq 1}$$

Where M_w is the mass transfer rate of the water monomer, r is the radial position of the lignin particle, k_A is the mass transfer coefficient, C_B represents the bulk water monomer concentration, and C_S is the water concentration at the surface.

Hydrolysis of the lignin particle is expressed below, where M_B is the mass transfer through hydrolysis at the surface of each model compound, and k_H is the hydrolysis rate constant [18].

$$M_B = 4\pi r^2 k_H C_S \quad \text{Eq 2}$$

The decomposition rate of lignin particle can be written as following [17]:,

$$r_d = -k_x C_{lig}^{\frac{2}{3}} \quad \text{Eq 3}$$

Where i = 1,2,3

Here, r_d is the decomposition rate of the lignin particle, k_x is the rate coefficient of lignin decomposition, and C_{lig} is the concentration of lignin in the system. Therefore from [17],

$$k_x = \frac{3C_B C_{lig\ i,0}^{\frac{1}{3}}}{r_0 \beta \rho (\frac{1}{k_A} + \frac{1}{k_H})} \quad \text{Eq 4}$$

Where ρ represents the density of lignin.

All the rate constants are changed with temperature. Since the temperature is changed during the process, the Arrhenius equation can be used to calculate the changing rate constants. Moreover, liquefaction kinetics in the sub and supercritical conditions depend on water's ionic product and the ionic product of water is dependent on the temperature [24], [25]. Therefore. Ionic product of water is added to the equation.

$$k_{i,t} = k_{0,i}\, e^{\frac{-E_a}{RT}} \sqrt{k_W} \quad \text{Eq 5}$$

Where, $k_{i,t}$ is the calculated rate constant, $k_{o,i}$ is the frequency factor, R is the mass-specific gas constant, T is the temperature and, E_a is the activation energy for each component. Arrhenius law can be applied to all the reactions since the rate constants are changed with temperature. $\sqrt{k_W}$ represents the impact of the ionic product of water in the Arrhenius equation.

In the liquefaction process, the lignin's ash component can be formed as another layer around the lignin particle. Therefore, in this model, a limiting factor for the lignin particle's convertible part is introduced. Such a limiting factor is presented by Hu et al. 2007 [27] to consider the wood's convertible part for pyrolysis models as well as by Mosteiro-Romero [19] in a liquefaction model. Following that concept, a factor is introduced such as follows,

$$k_{con} = \frac{m_0 - m_{(t)}}{m_0 - m_{ash}} \quad \text{Eq 6}$$

Where, m_0 is the initial weight of lignin, $m_{(t)}$ is the weight of the sample at a given time t, and m_{ash} is the ash weight in the sample.

Moreover, the diffusion of water to the particle surface is limited by the ash layer formation. After adding the limiting factor, the liquefaction of the lignin particle is limited by the factor introduced above in equation Eq 6. Then overall decomposition of the lignin particle is modified as follows.

$$r_d = -k_x k_{con} C_{lig}^{\frac{2}{3}} \quad \text{Eq 7}$$

Decomposition of the lignin particle depends on the water's concentration on the surface of the particle and the unreacted lignin remaining in the system. When the oily film and ash layer are formed around the lignin particle, the water concentration on the lignin particle's surface depends on the water diffused through the oily film and ash layer. Therefore, when an oily film of thickness $'w'$ and an ash layer of thickness $'w_{Ash}'$ are formed, decomposition of the lignin particle depends on the formation of the oily film and ash layer, diffusion of water through the formed layers, and the dissolution of the oily film in water.

According to Eq 4 and Eq 7, when the oily film is not present, decomposition of the lignin particle can be written as

$$r_d = -\frac{3C_B C_{lig\ i,0}^{\frac{1}{3}}}{r_0 \beta \rho (\frac{1}{k_A}+\frac{1}{k_H})} k_{con} C_{lig}^{\frac{2}{3}} \quad \text{Eq 8}$$

When the oily film is present, if the water concentration at the lignin particle surface is C_S, then.

$$k_x = \frac{3C_s C_{lig\ i,0}^{\frac{1}{3}}}{r_0 \beta \rho (\frac{1}{k_A}+\frac{1}{k_H})} \quad \text{Eq 9}$$

Therefore, by Eq 8 and Eq 9,

$$r_d = -\frac{3C_S C_{lig\,i,0}^{\frac{1}{3}}}{r_0 \beta \rho (\frac{1}{k_A}+\frac{1}{k_H})} k_{con}\, C_{lig}^{\frac{2}{3}} \quad \text{Eq 10}$$

In the presence of the oily film and ash layer, the decomposition of the lignin particle depends on the concentration of water (C_S) on the particle surface and water consumption by the hydrolysis reaction on the particle surface.
The rate of water diffusion through the oily film when the ash layer is present can be written as follows in Eq 11. The modeling of the oily film is influenced by the method used [19].

$$r_{diffusion} = 4\pi(r + w_{Ash} + w)^2 k_M (C_B - C_{S1}) \quad \text{Eq 11}$$

Where $(r + w_{Ash} + w)$ is the radius of the oily film, C_{S1} is the water concentration in between oily film and the ash layer, and k_M is the mass transfer coefficient through the oily film. If the ash layer is not formed, then the oily film radius becomes $(r + w)$.

$$k_M = \frac{k_{Diff}}{w} \quad \text{Eq 12}$$

k_{Diff} represent the diffusion coefficient of the oily film, which is calculated by the Stokes-Einstein equation.

$$k_{Diff} = \frac{k_B T}{6\pi r_{H_2O} \mu_{Oil}} \quad \text{Eq 13}$$

Where, k_B is the Boltzmann's constant, T is the temperature (K), r_{H_2O} is the radius of the water molecule and μ_{Oil} is the viscosity of the oily film.

The rate of diffusion of water through the ash layer can be written as follows in Eq 14.

$$r_{diffusion\_ash} = 4\pi(r + w_{Ash})^2 k_{M\_ash} (C_{S1} - C_S) \quad \text{Eq 14}$$

Where $(r + w_{Ash})$ is the radius of the ash layer, and C_S is the water concentration at the surface of the lignin particle. k_{M_ash} is the mass transfer coefficient

through the ash layer, which depends on the ash layer's diffusion coefficient. (Calculated by Fick's law). The rate of change of water concentration at the particle surface can be written according to the formations of oily film and ash layer. There are four different scenarios considered as follows.

$$\frac{dC_S}{dt} = rate\ wate\ of\ water\ diffusion\ through\ the\ ash\ layer - rate\ of\ water\ consumed\ by\ the\ hydrolysis \quad \text{Eq 15}$$

Therefore, when

$$w > 0\ and\ w_{Ash} = 0\ ;\ \frac{dC_S}{dt} = 4\pi(r+w)^2 k_M (C_B - C_S) - 4\pi r^2 k_H C_S k_{con} \quad \text{Eq 16}$$

$$w > 0\ and\ w_{Ash} > 0\ ;\ \frac{dC_S}{dt} = r_{diffusion\_ash} - 4\pi r^2 k_H C_S k_{con} \quad \text{Eq 17}$$

$$w = 0\ and\ w_{Ash} > 0\ ;\ \frac{dC_S}{dt} = 4\pi(r+w_{Ash})^2 k_{M\_ash} (C_B - C_S) - 4\pi r^2 k_H C_S k_{con} \quad \text{Eq 18}$$

$$w = 0\ and\ w_{Ash} = 0;\ \frac{dC_S}{dt} = -4\pi r^2 k_H C_S k_{con} \quad \text{Eq 19}$$

The undissolved volume of the oily film at a given time (V_{oil})can be written as below in Eq 20,

$$V_{oil} = \frac{4}{3}(\pi(r + w_{Ash} + w)^3 - (r + w_{Ash})^3) = \frac{m_{oil}}{\rho_{oil}} \quad \text{Eq 20}$$

Here, m_{oil} is the mass of the oily film at a given time and ρ_{oil} is the density of the oily film.

When both sides are differentiated and rearranged,

$$\frac{dw}{dt} = \frac{1}{4\pi\rho_{oil}}\left(\frac{1}{r+w_{Ash}+w}\right)^2 . \frac{dm_{oil}}{dt} - \left[1 - \left(\frac{r+w_{Ash}}{r+w_{Ash}+w}\right)^2\right]\left[\frac{dr}{dt} + \frac{dw_{Ash}}{dt}\right]$$

Eq 21

The rate of change of mass of the oily film equals the difference in the formation and the dissolution of the oily film,

$$\frac{dm_{oil}}{dt} = r_{oil} - r_{dissolve}$$ Eq 22

Here, r_{oil} is the rate of formation of the oily film and $r_{dissolve}$ is the rate of dissolution of the oily film in water.
From Fick's first law,

$$r_{dissolve} = k_{M2}\ 4\pi(r + w_{Ash} + w)^2\ (C_{Sat} - C_{\infty})$$ Eq 23

k_{M2} is the mass transfer coefficient to the water from the oily film. Here C_{∞} is assumed to be zero with the assumption that the hydrolysis products' solubility is equal to their concentration at the oily film's surface. Moreover, at some distance, the dissolution of the hydrolysis products in water is infinite.

$$k_{M2} = \frac{k_{Diff_1}}{r+w_{Ash}+w}$$ Eq 24

The diffusivity of oily film to water (k_{Diff_1}) is calculated by the Stokes-Einstein equation. Using the same method used in Eq 20, the ash layer volume can be written in Eq 25 below.

$$V_{ash} = \frac{4}{3}(\pi(r + w_{Ash})^3 - (r)^3) = \frac{m_{ash}}{\rho_{ash}}$$ Eq 25

Here, m_{ash} is the mass of the ash layer at a given time and ρ_{ash} is the density of the ash. When both sides are differentiated and rearranged,

$$\frac{dw_{Ash}}{dt} = \frac{1}{4\pi\rho_{ash}}\left(\frac{1}{r+w_{Ash}}\right)^2 . \frac{dm_{ash}}{dt} - \left[1 - \left(\frac{r}{r+w_{Ash}}\right)^2\right]\left[\frac{dr}{dt}\right]$$ Eq 26

The radius of the lignin particle at each time can be calculated by the following Eq 27.

$$r(t) = \sqrt[3]{\frac{3m_{lig}}{4\pi.\rho_{lig}}} \quad \text{Eq 27}$$

Each chemical component's theoretical values are calculated using differential equations using the backward Euler method. From the differential equations, the variation of each chemical compound's concentrations is obtained in *mol/m*^{3}. Then, each chemical compound or resultant phase is presented as a percentage of the total input.

2. Layer model for intra-particle process modeling.

In this paper, a layer model is implemented to study the intra-particle transport and sub-processes of the thermally thick lignin particle. Although the ash layer thickness and oily film thickness are small (10^{-7}mm and 10^{-12} mm respectively), all the three layers present in the previous section are considered here. The lignin component is regarded as a single homogenous particle. The layer model is influenced by the work done by Mehrabian et al., 2012[28]. Figure 4 shows the layer model used in the proposed model.

The layer model treats the three layers in one dimension. This simplification is done to avoid model complexities. For the modeling purpose, it is assumed the particle boundary conditions are homogeneous, and all the points at a certain distance from the surface at a radial direction have the same conversion rates and temperatures[29].

As the conversion starts, the mass and thickness of the two layers in the particle are changed. Since the lignin particle started decomposing, the oily film will change its thickness according to the diffusion of water to the lignin particle surface, rate of hydrolysis, and dilution of the oily film in water. Along with this, the boundaries are moving towards the center of the particle as well. Therefore the density and the particle size may change during the thermal conversion of the particle.

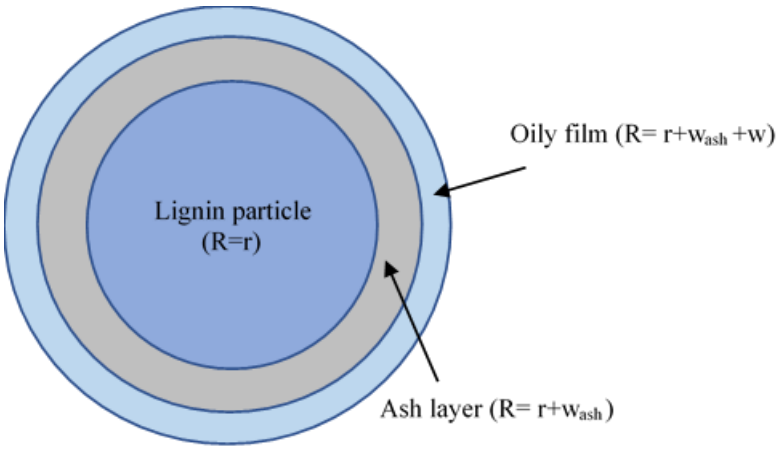

Figure 50:Layer model considered for the intra particle process.

For the particle, thermal energy conversion is expressed in the following Eq 28.

$$\frac{\partial}{\partial t}\rho H = -\nabla.\rho v H - \nabla.q \qquad \text{Eq 28}$$

Where, $\frac{\partial}{\partial t}\rho H$ is the accumulation rate of enthalpy per unit volume, $\nabla.\rho v H$ represents enthalpy change by advection per unit volume, and $\nabla.q$ is the conductive heat transfer per unit volume.

The thermal energy per unit volume is replaced by the thermal energy per each layer for simplification. Then the energy equation can be written as follows in Eq 29

$$\frac{\partial}{\partial t}\sum_c m_i H_i = \sum_{c=in}\dot{m}_{in}H_{in} - \sum_{c=out}\dot{m}_{out}H_{out} + k_{L_i}\Delta x_{0Li}\left(T_{B(i-1)} - T_{Li}\right) - k_{L_i}\Delta x_{1Li}\left(T_{Li} - T_{Bi}\right) \qquad \text{Eq 29}$$

Where, $m_i H_i$ are the multiplication of mass and specific enthalpy of each component present in the layer i, $\dot{m}_{in}H_{in}$ is the multiplication of mass flow rate and specific enthalpy respectively of each component at the boundary, k_{L_i} is the thermal conductivity of layer i, Δx_{0Li} is the ratio of the area of the boundary $B(i-1)$ to half of the layer i thickness, and Δx_{1Li} is the ratio of the boundary Bi to half of the layer i thickness. Moreover T_{Li} andT_{Bi} are tempera-

tures of the center of layer i and the temperature at the boundary Bi, respectively. (Since three layers are considered here, $i = 1,2,3$)

The conservation of mass for each layer can be written as follows in Eq 30,

$$\frac{\partial}{\partial t}\sum_c m_i = \sum_{in} \dot{m}_{Bi-1} - \sum_{out} \dot{m}_{Bi} \qquad \text{Eq 30}$$

In addition to that, from the specific heat at constant pressure,

$$dH = c_p dT \qquad \text{Eq 31}$$

From Eq 29, Eq 30 and Eq 31, below Eq 32 can be obtained.

$$\sum_c m_i c_i \frac{dT_i}{dt} = \sum_{in}\left[\dot{m}_{Bi-1}(H_{B(i-1)} - H_i)\right] - \sum_{out}[\dot{m}_{Bi}(H_i - H_{Bi})] + k_{L_i}\Delta x_{0Li}\left(T_{B(i-1)} - T_{Li}\right) - k_{L_i}\Delta x_{1Li}\left(T_{Li} - T_{Bi}\right)$$

Eq 32

Enthalpy of each component at every boundary and every layer is calculated by the following Eq 33,

$$H_i(T) = \Delta H_f^\circ + \int_{T_{ref}}^{T} c_p dT \qquad \text{Eq 33}$$

Here, ΔH_f° represent the Standard enthalpy of formation and c_p represents specific heat capacity.
By using the energy balance for each boundary, the boundary temperatures are calculated.

$$k_{L_i}\Delta x_{1Li}\left(T_{Li} - T_{Bi}\right) - k_{L_{i+1}}\Delta x_{0Li+1}\left(T_{Bi} - T_{L(i+1)}\right) = \sum_{c=in} \dot{m}_{Bi} H_{Bi} - \sum_{c=out} \dot{m}_{Bi} H_{Bi} \qquad \text{Eq 34}$$

In the model, the reactions are happening on the particle surface. Therefore, the same components which enter a specific boundary might not leave the boundary. A resultant component could leave instead. The right-hand side of Eq 34 may represent the enthalpy difference of products and reactants of the

reactions. The mass flow rate of each component is dependent on the reaction rates $(r)_i$ and stoichiometry (η_i) of each reaction.

$$\dot{m}_{Bi} = \sum_{c=out} r_i \eta_i \qquad \text{Eq 35}$$

In this regard, the mass flow rates of each component can be calculated by the differential equations developed using the shrinking core concept in section 2.2.1.2

3. Kinetic model for lignin liquefaction

The lignin liquefaction model is a continuation of the previous work by the authors[17]. Figure 5 shows the used reaction pathway of hydrolysis and the decomposition of lignin during the liquefaction process. For the lignin hydrolysis model, required kinetic parameters are taken from the literature[14]–[16], [30], [31]. The below equations from Eq 36 to Eq 46 show the reactions incorporated in the lignin liquefaction model.

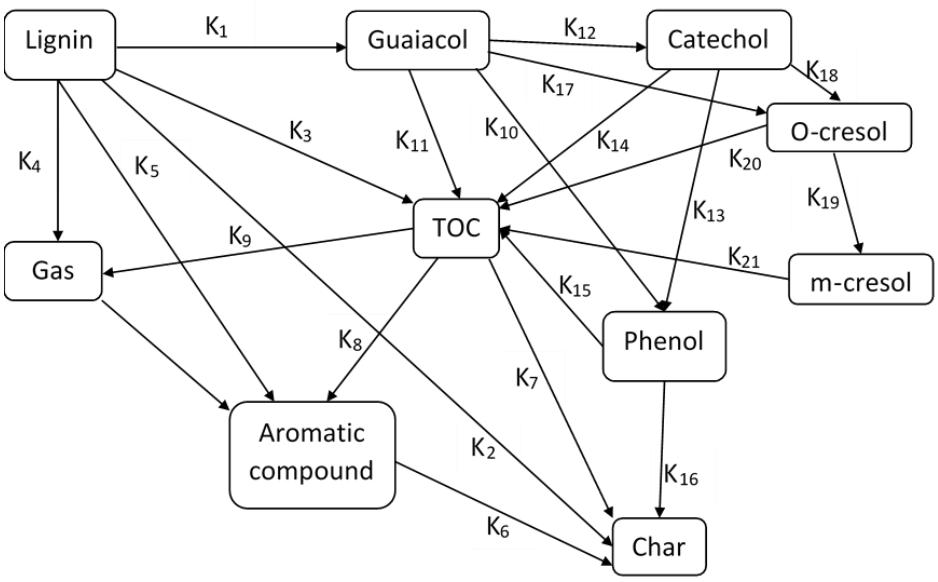

Figure 51:Reaction pathways of lignin in hydrothermal conditions.

Table 9:Reaction type of each reaction used in the lignin liquefaction model.

Reaction type	*Kinetic parameters*
Hydrolysis	K_1, K_3, K_4, K_5
Dehydration	K_2
Polymerization	K_6, K_7, K_{16}
Decomposition	K_8 , K_{10} , K_{11} , K_{12} , K_{13} , K_{14} , K_{15} , K_{17} , K_{18} , K_{19} , K_{20} , K_{21}
Gasification	K_9
Rearrangement	K_{17}

$$Lignin + c_1H_2O \xrightarrow{k_i} d_1guaiacol + d_2Aromatics + d_3TOC + d_4CO_2 \quad \text{Eq 36}$$

$$Lignin \xrightarrow{k_i} d_5\ char + H_2O \quad \text{Eq 37}$$

$$Aromatics \xrightarrow{k_i} d_6\ char \quad \text{Eq 38}$$

$$TOC \xrightarrow{k_i} d_7 char \quad \text{Eq 39}$$

$$TOC \xrightarrow{k_i} d_8 Aromatics + d_9 CO_2 \quad \text{Eq 40}$$

$$Guaiacol \xrightarrow{k_i} d_{10}Phenol + d_{11}TOC + d_{12}Catechol + d_{13}O - cresol \quad \text{Eq 41}$$

$$Catechol \xrightarrow{k_i} d_{14}Phenol + d_{15}TOC + d_{16}O - cresol \quad \text{Eq 42}$$

$$O - cresol \xrightarrow{k_i} d_{17}M - cresol + d_{18}TOC \quad \text{Eq 43}$$

$$M - cresol \xrightarrow{k_i} d_{19}TOC \quad \text{Eq 44}$$

$$Phenol \xrightarrow{k_i} d_{20}TOC \quad \text{Eq 45}$$

$$Phenol \xrightarrow{k_i} d_{21}Char \quad \text{Eq 46}$$

c_i is the stoichiometry value for water for each hydrolysis reaction (where *i=1,2, 3, 4*)
d_i is the stoichiometry value for the output of each reaction (where *i=1,2, 3,…,21*)

To acquire the results presented in this section, differential equations developed in the mathematical model are solved and discretized in MATLAB R2019b.

Article C

Characterization and evaluation of char from hydrothermal liquefaction of alkali lignin in subcritical temperatures. Madhawa Jayathilake, Souman Rudra, Naureen Akhtar, Alfred A. Christy, Published in Materials (2021)

The layout has been revised

Characterization and Evaluation of Hydrothermal Liquefaction Char from Alkali Lignin in Subcritical Temperatures

Madhawa Jayathilake [1], Souman Rudra [1,*], Naureen Akhtar [1] and Alfred Antony Christy [2]

[1] Department of Engineering and science, Faculty of Engineering Sciences, University of Agder, 4879, Grimstad, Norway; madhawa.jayathilake@uia.no (M.J.); naureen.akhtar@uia.no (N.A.)

[2] Department of Natural Science, University of Agder, 4630 Kristiansand, Norway; alfred.christy@uia.no

* Correspondence: souman.rudra@uia.no; Tel.: +47-37233036

Abstract:

An evaluation of hydrothermal liquefaction (HTL) char is investigated in this work. Morphological studies, N_2 adsorption behavior, FTIR analysis, thermal behavior, and elemental composition are studied. The HTL char yield showed an increase with higher operating temperatures. It increased from 11.02% to 33% when the temperature increased from 573 K to 623 K. At lower temperatures, the residence time showed an impact on the yield, while close to the critical point, residence time became less impactful. Elemental analysis showed that both higher operating temperatures and longer residence times increased the nitrogen content of the chars from 0.32% to 0.51%. FTIR analysis suggested the char became more aromatic with the higher temperatures. The aliphatic groups present diminished drastically with the increasing temperature. Residence time did not show a significant impact as much as the temperature when considering the functional group elimination. An increase in operating temperatures and residence times produced thermally stable chars. HTL char produced at the lowest operating temperature and showed both the highest surface area and pore volume. When temperature and residence time increase, more polyaromatic char is produced due to carbonization.

Keywords: lignin; HTL char; FTIR; SEM; TGA; carbonization; pores

---

1. Introduction

Numerous research groups study hydrochar from the hydrothermal carbonization (HTC) process. The morphological surface and chemical characteristics of that char have been investigated profusely. Besides, comprehensive studies on char from the hydrothermal liquefaction (HTL) process are sparse. HTL produces comparably less char yield than HTC. Nevertheless, with a small yield, the char from HTL can be utilized for a valuable purpose. Limited studies have suggested that hydrothermal char can help produce porous carbon [1]. Besides, hydrochar-based porous carbon can be an effective material in agriculture [2]. Porous carbon produced from hydrochar can be used as carbon storage in fields. Further, hydrochar and biochar's (pyrolysis char) diverse

abilities in the nitrogen cycling process were studied recently [3]. Notably, activated char can be used as an adsorbent for organic pollutants [4].

Lignin makes itself a valuable resource, being the second most common earthbound biopolymer available and the most significant naturally occurring source of aromatic compounds [5]. As a significant by-product of the paper and pulp industry, lignin is mainly used by paper mills to fuel energy recovery [6].

Hydrochar from HTC has been investigated thoroughly in recent studies. Falco et al. showed the strikingly different behavior of different chars from HTC of cellulose and glucose, where cellulose-derived char illustrated properties close to pyrolysis char [7]. Leng et al. investigated the hydrochar behavior of sewage sludge liquefaction with a morphological study and a study on the oxygen-containing functional group in char. Although the surface area and pore volume were low, oxygen-containing functional groups were high in char [8]. After that, their studies found that the rice husk-derived biochar was effective on Malachite green (MG) removal from the aqueous phase [9]. An illustrative study by Zhu et al. showed a positive correlation between the elemental compositions and the porous carbon's porosity.

Furthermore, the authors observed that lower maximum temperatures and retention times lead to high porosity porous carbon [1]. Wahyudiono et al. observed that the functional group distribution of char from lignin changes drastically during decomposition in near supercritical water [10]. The impact of increasing temperature on the repolymerization of decomposed products from lignin was unearthed by Pinkowska et al. [11]. Char produced by the hydrothermal carbonization of cellulose, xylose, and lignin were studied by Kang et al., where the chars' carbon content was mainly investigated [12]. Moreover, many studies have been carried out to study the decomposition of lignin in organic solvents [13–16].

Despite the considerable work on the HTL of lignin, most of studies have only focused on the liquid phase from the output. Focusing on the char may give insight into the decomposition pathways and possible ways to utilize the char as a helpful precursor for other value-added products, such as soil stabilizers for agricultural purposes and porous carbon production as well as anode production. Subsequently, pyrolysis char and hydrochar from HTC are widely studied, and the behavior and evolution of pyrolysis char and HTC char are

widely accessible [1,17,18]. Besides, due to the different chemistry in the process and the complex reactions and degradation mechanisms, HTL char could offer different properties than pyrolysis and HTC char.

Char is a by-product of HTL, where in most of the studies, the bio-crude product is given importance [19]. The motivation to study char extensively is to investigate the possibility of using HTL char effectively. It could be either in porous carbon production, as a fertilizer for agricultural purposes, or using it as a carbon capture material. Nevertheless, this study focuses on evaluating HTL char properties and characteristics with different operating temperatures and residence times. This study investigates the morphological, surface, thermal, and chemical characteristics of lignin derived HTL char. The functional groups present in char are studied with Fourier transform infrared spectroscopy (FTIR), where the structural and surface behavior is studied with scanning electron microscopy (SEM). The thermal behavior of char is studied with thermogravimetric (TGA) analysis, and the nitrogen adsorption/desorption method is used to determine the surface and pore distribution of char. The chars are produced with different HTL operating temperatures and residence times to study and understand the different char-derived attributes with varying process parameters.

2. Materials and Methods

2.1. Material

Being obtained from Sigma Aldrich Co.,Oslo, Norway, the lignin used in this study was alkali lignin with a low sulfonate content and an average molecular weight of 10 kg/mole. In total, 16 mL of slurry was fed into the reactor. The lignin and water weight ratio was 1:9, which was maintained for all feedstock samples. All the analysis instruments used in the study are mentioned in the Section 2.3 characterization.

2.2. Experimental Procedure

Experiments were carried out in a 24 mL tubular steel reactor from Graco High-Pressure Equipment Inc. (HiP, pennsylvania, United States). A dead volume of 8 mL was kept in all the experiments to hold space for produced gasses and expansions. The reactor was purged with N_2 to check for leakages and emit the air after the reactor was sealed. A fluidized sandbath was used to heat the reactor, while an external shaking mechanism connected to a frequen-

cy controller was deployed to shake the reactor during the reactions. In this study, three temperature values and three residence times were used. The temperatures used were 573 K, 603 K, and 623 K, while the residence times used ranged 10 min, 15 min, and 20 min. Therefore, every temperature value was studied with three residence times. For the experiments' consistency, every experiment was repeated five times, and average values were used for analysis and are recorded below in Table 1. According to Table 1, each char sample's carbon content stayed very similar regardless of the operating temperature or the residence time.

Table 1. Ultimate analysis results of the experimental samples (wt.% dry ash-free).

Sample	C	H	N	O
Lignin	51.500 ± 0.102	4.120 ± 0.021	0.350 ± 0.031	44.030 ± 0.154
Char 1 (573 K—10 min)	61.125 ± 0.315	4.780 ± 0.02	0.325 ± 0.075	33.770 ± 0.070
Char 2 (573 K—15 min)	63.105 ± 0.295	4.455 ± 0.045	0.346 ± 0.061	32.094 ± 0.279
Char 3 (573 K—20 min)	61.800 ± 0.160	4.140 ± 0.010	0.453 ± 0.024	33.607 ± 0.126
Char 4 (603 K—10 min)	63.930 ± 0.210	4.125 ± 0.025	0.368 ± 0.022	31.577 ± 0.163
Char 5 (603 K—15 min)	63.845 ± 0.005	3.875 ± 0.065	0.503 ± 0.015	31.777 ± 0.075
Char 6 (603 K—20 min)	63.710 ± 0.172	3.759 ± 0.032	0.517 ± 0.017	32.014 ± 0.221
Char 7 (623 K—10 min)	63.625 ± 0.105	3.770 ± 0.022	0.407 ± 0.013	32.198 ± 0.112
Char 8 (623 K—15 min)	58.920 ± 0.930	3.395 ± 0.015	0.461 ± 0.021	37.224 ± 0.966
Char 9 (623 K—20 min)	63.380 ± 0.165	3.590 ± 0.014	0.512 ± 0.018	32.518 ± 0.197

After the desired residence time and the reactor were dismantled from the shaker and cooled with cold water for 30 min, acetone was used to extract the liquid and solid products from the reactor. The reactor was then washed with acetone four times after every experiment to ensure all the products were extracted. Furthermore, the solution was filtered, and the solid product was separated. To ensure that the solid and liquid phases were appropriately separated,

solid residue (char phase) was again washed with acetone and filtered. Then, the char phase was weighted and dried at 378 K for 24 h before quantifying. A simple process diagram of the char separation and extraction from the HTL output is shown in Figure 1.

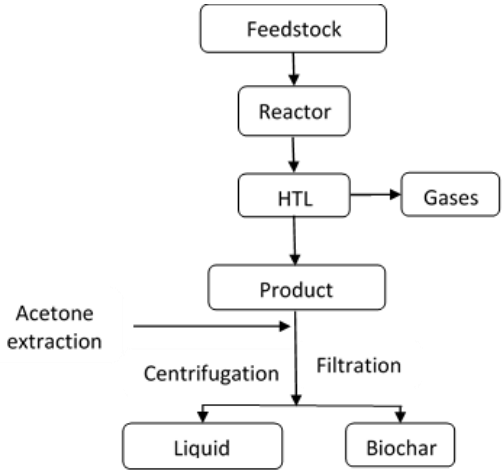

Figure 1. Char separation and extraction method.

In this article, char yield denotes the amount of recovered solid residue after HTL, based on Equation (1) [20].

$$Char\ yield\ (\%) = \frac{Char\ recoverd\ after\ the\ heat\ treatment\ (g)}{Initial\ amount\ of\ lignin\ used\ for\ the\ experiment\ (g)} \times 100\% \quad (1)$$

2.3. Characterization

Several different analytical tools and methods were used in this study to determine the char's different properties and behaviors.

According to ISO standard procedures, the lignin's proximate analysis was performed using a muffle furnace LT 40/11/P330 (Nabertherm, Lilienthal, Germany). A PerkinElmer 2400 CHNS/O Series II elemental analyzer (PerkinElmer Waltham, MA, United States) was used for the ultimate analysis. Oxygen as calculated by the difference of the other elements, where sulphur content was assumed to be negligible, although it is present in very low percentages in lignin. EN 15148 was applied to measure the volatile matter. In the

elemental analysis, 1–1.5 mg of sample weight was used in all the test cases where samples were weighted in an Sn capsule and then placed in the elemental analyzer. Calorific tests were carried out using an IKA C6000 global standard-type bomb calorimeter (IKA®-Werke GmbH & Co. KG, Staufen, Germany) according to the DIN 51900–1 standard test for solid and liquid fuels. For the morphological study, scanning electron microscope (SEM) images of the samples were obtained by using a JSM-7200F scanning electron microscope (JEOL,Tokyo, Japan).

Thermogravimetric analysis of the feedstock and the char samples was carried out using a Mettler-Toledo Thermal Analyzer (TGA, Mettler-Toledo,Columbus, Ohio, United States). Mainly, the TGA and derivative thermogravimetry (DTG) graphs were used in this study to analyze the thermal behavior of char. The temperature was raised from 303 to 1273 K with a heating rate of 20 K/min with nitrogen as the purging gas with a constant flow rate of 25 mL/min. The mass loss in the sample was calculated using Equarion (3).

$$Mass\ loss\ (\%) = Initial\ mass\ (\%) - Final\ mass\ (\%) \qquad (2)$$

The sample's infrared spectrum was measured using a Perkin Elmer FTIR spectrometer (Perkin-Elmer Ltd., Cambridge, UK) equipped with a nitrogen-cooled mercury-cadmium-telluride detector. Each dried sample dispersed in KBr as a 10% mixture was placed in a sample cup of a Perkin Elmer diffuse reflectance accessory, and the surface of the sample was carefully leveled flat. The spectrum of finely ground KBr was used as the background. The spectrum was measured in the range 4000–600 cm^{-1}, and a total of 32 scans were made at a resolution of 4 cm^{-1}. The resulting average reflectance spectrum was then transformed into the Kubelka–Munk format and saved as the final spectrum.

N_2 adsorption isotherms of hydrochar were determined at 77 K (Nova-Touch, Quantachrome,Boynton Beach, Florida, USA). The Brunauer–Emmett–Teller (BET) model was used to calculate the surface area [21]. Pore volume was evaluated with the quenched solid density functional theory (QSDFT), using the calculation model for slits and cylindrical pores on the adsorption branch [22]. Before each measurement of surface area and porosity, samples were degassed at 423 K for 6 h. The total pore volume was defined from the amount of N_2 adsorbed at a p/p_0 value of 0.99.

3. Results and Discussion

3.1. Char yield

At 573 K char, the yield showed 11.02% w/w_0, 11.06%w/w_0, and 12% w/w_0 at 10 min, 15 min, and 20 min residence times, respectively. When the operating temperature was increased to 603 K, the char yield showed a rapid increase to 31% w/w_0, followed by a rise to 33.05 % w/w_0 at 15 min residence time and then to 34% w/w_0 at 20 min residence time. At 623 K for all the residence times, the char yield stayed around 33% w/w_0. According to Table 1, with increasing temperatures and longer residence times, the nitrogen content of the chars increased. Therefore, for all three operating temperature values, the longest residence time reported the highest amount of nitrogen in the char. Similar behavior of nitrogen content has been observed with hydrochar produced by HTC process [1].

Further, an increase in operating temperature also increased the char's nitrogen content, where it showed the complete opposite to pyrolysis char, which showed a reduction in nitrogen content with the increasing operating temperature [23]. Other research that carried out the hydrothermal degradation of lignin has observed the same trend: the lowest solid yield is obtained at the lowest operating temperature, and then the yield is increased with the increase of the operating temperature [24–26]. Besides, in some studies, the residence times used are relatively different from the current study. The relatively low yield at 573 K could be due to the promotion of hydrolysis and a decomposition reaction at lower temperatures than the repolymerization or rearrangement reactions. The relatively high yields at 603 K and 623 K can be attributed to the promotion of repolymerization and rearrangement reactions. Repolymerization reactions become prominent with the higher operating temperatures and longer residence times, leading to the higher char yield at higher temperatures [25,26]. With the increasing temperatures, free radicals from the broken ether bonds could pair with other carbon atoms and create more rigid bonds towards cleavage, which would create char-like structures [27]. Below, Table 2 shows the char yield obtained at different temperatures and residence times.

Table 2. Char yields at different operating temperatures and residence times.

Sample	Char 1	Char 2	Char 3	Char 4	Char 5	Char 6	Char 7	Char 8	Char 9
Yield (w/w_0 %)	11.02 ± 0.3	11.06 ± 0.15	12.00 ± 0.21	31.00 ± 0.4	33.05 ± 0.23	34.00 ± 0.16	33.03 ± 0.11	33.03 ± 0.16	33.05 ± 0.22

3.2. FTIR Analysis

The normalized FTIR spectra of the chars are shown in Figure 2. All the char samples obtained at different operating temperatures and residence times were analyzed, and the FTIR spectrums were obtained. In general, from the color and the spectra, it was apparent that the samples contain very little aliphatic content. The minor aliphatic character appearing in the low-temperature samples seemed to disappear at a high-temperature treatment. The aliphatic content also reduced in the samples treated at longer residence times.

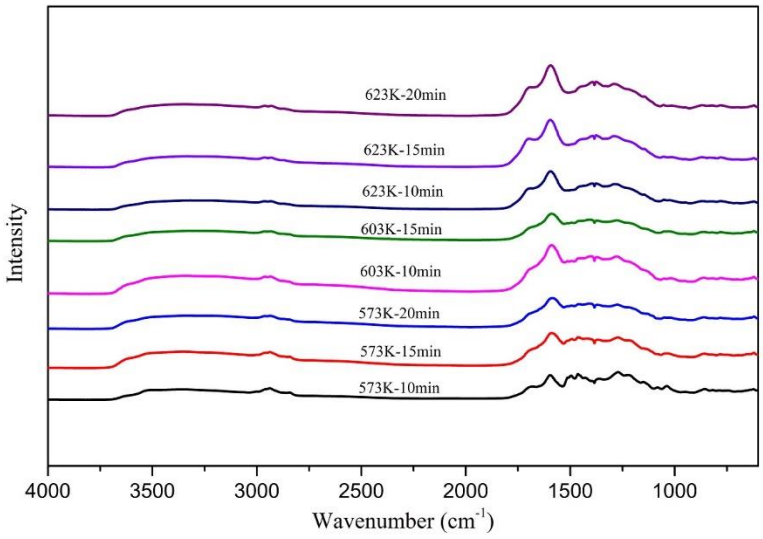

Figure 2. FTIR spectra of the chars.

Figure 3 below illustrates a closer look at the FTIR spectrum from the char sample obtained at 573 K and 10 min residence time, produced at the lowest temperature and the shortest residence time among all the samples. The fingerprint in the region 2000–600 cm^{-1} mainly arises from the condensed products containing O, N, and sulfur compounds of lignin used in the experiments.

The area under the region 3000–2850 cm^{-1} is an indication of the aliphatic content.

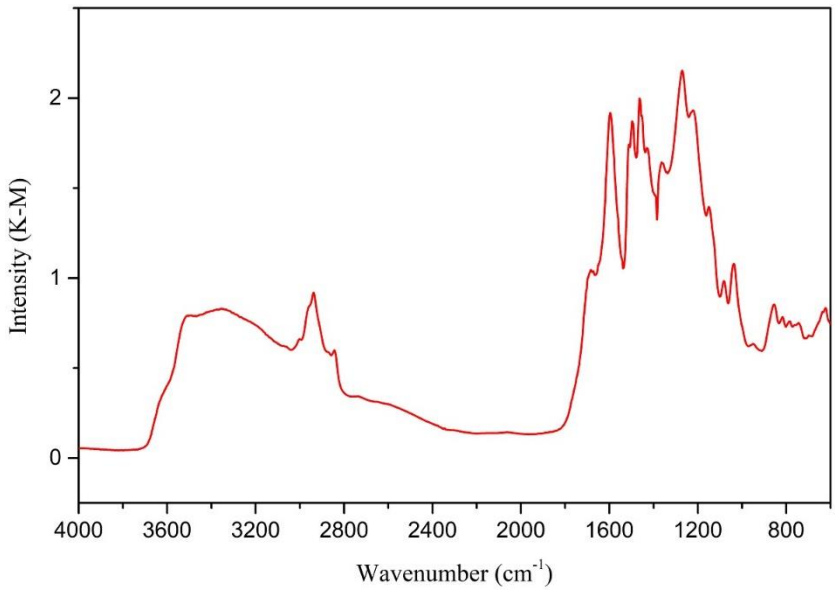

Figure 3. FTIR spectra and the available peaks of char from 573 K and 10 min residence time.

The FTIR spectra intensity variation reflects the variety of different functional groups as the temperature and residence time increase [28]. Figure 4a below shows the normalized FTIR spectra of the chars obtained with a residence time of 10 min at different temperatures of 573 K, 603 K, and 623 K, where Figure 4b shows the normalized FTIR spectra of the chars obtained at different residence times at 573 K.

The spectrum of char produced at 573 K with a 10 min residence time shows bands corresponding to aliphatic and aromatic -OH (3415 cm^{-1}), aromatic ring modes (1595 cm^{-1} and 1140 cm^{-1}), carbonyl group (1684 cm^{-1}), aliphatic -CH_3 (2944 cm^{-1}) and CH_2 groups (1453 cm^{-1}), symmetric -CH_3 stretching of the methoxyl groups (2851 cm^{-1}), and symmetric -CH_3 stretching (1035 cm^{-1}) and C-H in Syringyl, Guaiacyl (857 cm^{-1} and 807 cm^{-1}, respectively), as well as the nitro compounds (1353 cm^{-1}) [29].

As temperature and residence time increase, the depth of aliphatic -CH_3 (2944 cm^{-1}), the symmetric -CH_3 stretching of the methoxyl groups (2851 cm^{-1}), -CH_3 and CH_2 groups (1453 cm^{-1}), and the symmetric -CH_3 stretching (1035 cm^{-1}) [10,17], all decreased rapidly. This indicates how the polar func-

tional groups decrease with increasing operating temperature and increasing residence time [30]. These groups are reduced to produce an aromatic char [10,17]. Such aromatic rings would result in producing fused aromatic rings after losing oxygen and hydrogen. Therefore, the increasing temperatures and the longer residence times promote fused ring production, resulting in more char. Although the aliphatic groups were eliminated from the chars produced at higher temperatures, many studies have shown that those aliphatic groups can be found in the liquid phase [11,25].

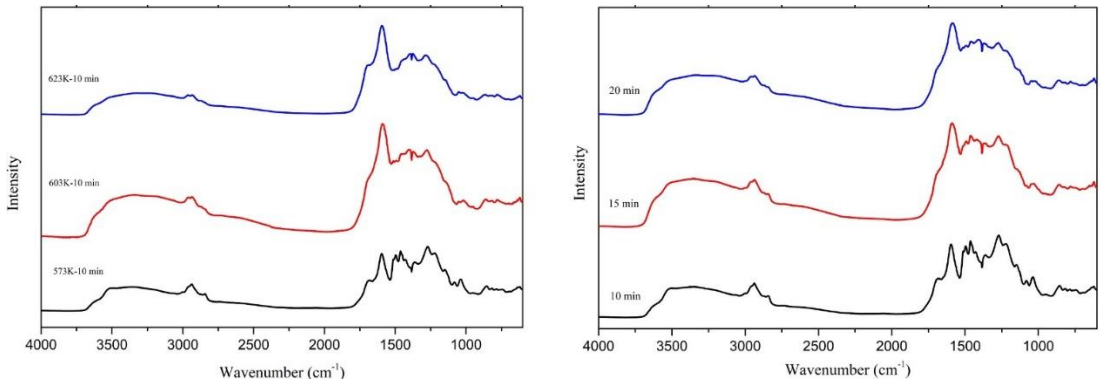

(a) (b)

Figure 4. FTIR spectra of chars from (**a**) different temperatures with a 10 min residence time (**b**) different residence times at 573 K.

The peaks corresponding to Syringyl, Guaiacyl C-O (1272 cm^{-1})[31], which are characteristic of softwood lignin, started to diminish clearly. At 623 K and with longer residence times, most groups decreased. Subsequently, pyrolysis char and HTC char still presented some of the groups at 623 K [17,18]. Meanwhile, the small amount of aromatic and aliphatic OH (3415 cm^{-1}) was seen to vanish with the increasing operating temperature. This can be mainly credited to the improvement of the dehydration reaction [32]. The band at 1595 cm^{-1} [10,17], corresponding to the aromatic ring and carbonyl group (1684 cm^{-1}), seemed to be increasing drastically with the increase of operating temperature. This means the C-C and C-H bonds are consumed throughout the hydrothermal liquefaction process. Although the aromatic ring (1595 cm^{-1}) increased with the longer residence time, it was not as significant as the operating temperature.

Meanwhile, the carbonyl group (1684 cm^{-1}) seemed to decrease with the longer residence time. A possible reason for this observation could be reduced carbonyl group consumption, C-C, and C-H bonds with the longer residence time. Further, the nitro compounds (1353 cm^{-1}) were observed to increase slightly with the increase of both the operating temperature and residence time. This can be attributed to the increase of nitrogen content in the char samples.

O-containing functional groups in char can be used to measure using char as an adsorptive material. When the O-containing functional groups are enhanced, biochar has shown improved heavy metal sorption ability [33,34]. Although aromatic ring and carbonyl groups are increased with the increase of operating temperature, aromatic and aliphatic OH and Guaiacyl C-O are significantly decreased. Therefore, for particular purposes such as heavy metal sorption, optimum operating parameters should be used to obtain the maximum possible O-containing functional groups.

The longer residence times cannot help consuming C=C and C-H bonds effectively as the temperature does. Because of the dealkylation reaction, CH_3 and CH_2 groups are primarily removed from the chars, and this reaction could be more influenced by the operating temperature than the residence time. The fact that the aromatic ring keeps growing with the increasing operating temperatures and residence times means that an increase of fused aromatic rings is further observed. The chars' aromatic nature increases with the rise in operating temperature monitored with pyrolysis char and hydrochar from hydrothermal carbonization [12,17,35].

The spectrum depicts a vanishing of the small aliphatic content with the residence time increase. Nevertheless, the reduction of the peak relating to the aliphatic content is slower with the residence time increase than the operating temperature increase. Therefore, both higher operating temperatures and longer residence times result in removing the aliphatic content from the chars in HTL. However, the impact of the operating temperature is more significant in removing the chars' aliphatic groups than the residence time.

Monomeric radicals can be created by splitting weak bonds in the lower operating temperatures. The produced radicals can potentially create new radicals by attracting hydrogen to form monomeric phenolic compounds. When the operating temperature is further increased, C-C bonds can also be broken

to create phenolic monomeric compounds. Meanwhile, these phenolic compounds can be polymerized and potentially produce more char as well. With the residence time increase, polymerization is further supported, and more char is made. When the operating temperature is further increased and comes close to the critical point, more fused aromatic rings could also be produced. In this study, the longest residence time used was 20 min. Besides, even at 623 K, increasing residence time did not significantly increase the char yield. Therefore, the impact of residence time on producing phenolic monomeric compounds and generating more char with polymerization must be studied further with longer residence times. Hydrothermal char could have certain advantages over pyrolysis char, such as easy decomposition, easy feedstock preparation, abundant functional group availability, and the possibility of coating pre-formed nanostructures with carbonaceous shells [36].

3.3. Thermal Stability of Char

Char residues are studied for their thermal stability in an N_2 atmosphere with a 20 K/min heating rate. Mass loss (TGA) curves of the lignin and chars are shown in Figure 5.

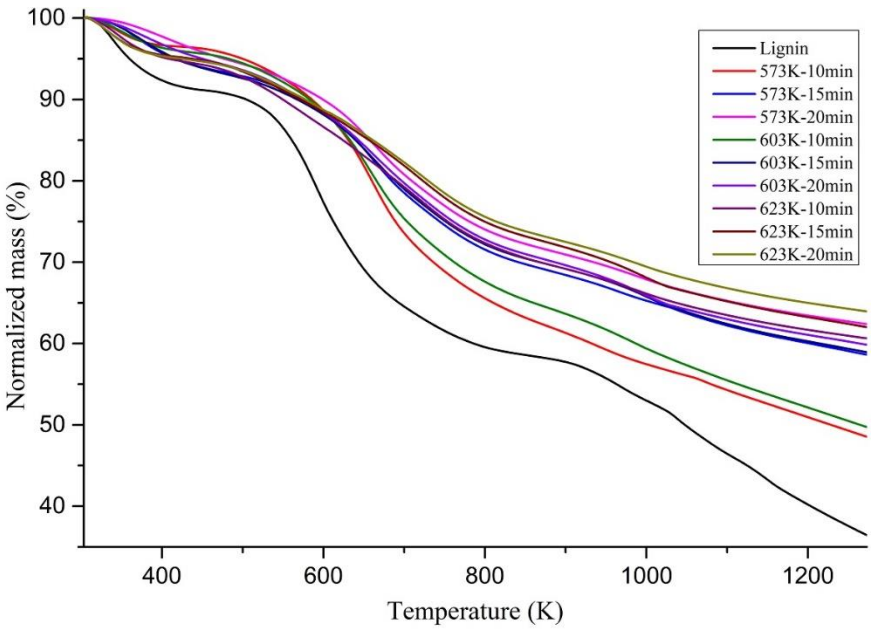

Figure 5. TG curves of lignin and the chars at 20 C/min heating rate under N_2.

According to Figure 5, the chars from hydrothermal liquefaction are further heated and decomposed until temperatures reach up to 1273 K. A mass loss due to water vaporization can be observed around 373 K. Chars obtained at lower operating temperatures decomposed earlier. Furthermore, at the same operating temperature, chars produced from longer residence times took longer to decompose than the chars produced at shorter residence times, which should be attached to the remaining active functional groups. This can be supported by the FTIR results shown in Section 3.2, which clearly showed the decrease of the availability of aliphatic functional groups and the increase of aromatic functional groups in chars produced with increasing operating temperatures and increasing residence times.

At 1273 K, the remaining solid residue percentage increased with the hydrothermal liquefaction operating temperature of chars, extending from 36.47% of the original lignin to 63.95% of the char prepared with 623 K and 20 min residence time. This observation indicated that more thermally stable structures are established at higher hydrothermal liquefaction operating temperatures and longer residence times. Similar behavior has been shown in pyrolysis char from lignin as well [37]. Below, Figure 6 shows the mass lost from each char sample at 1273 K as a percentage. It also presents a clear connection between the operating temperature, residence time, and the remaining solid residue. For each hydrothermal liquefaction operating temperature, the char produced with the shortest residence time showed the highest percentage mass loss. In contrast, the longest residence time showed the most negligible percentage mass loss.

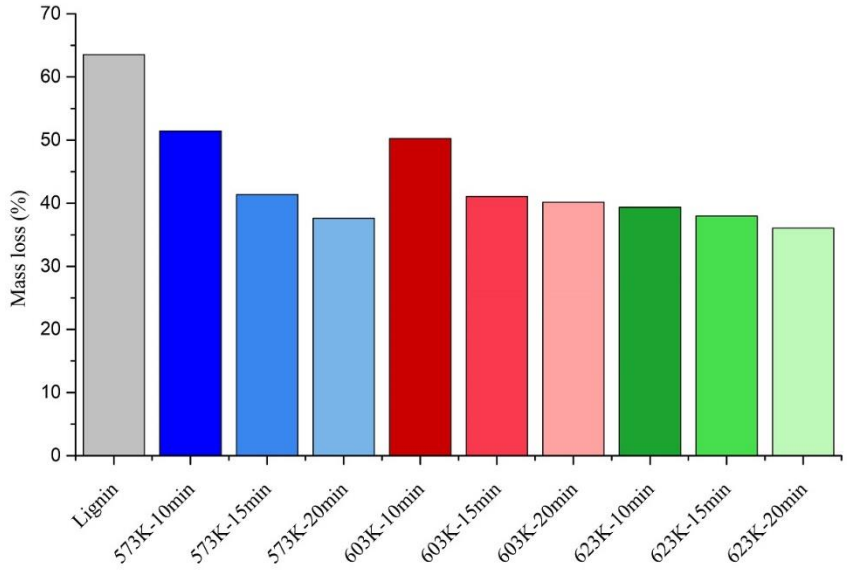

Figure 6. Mass loss of lignin and the HTL chars.

Chars produced with lower operating temperatures and shorter residence times could have more volatiles in them and weaker bonds in the chemicals in them. That could be a possible reason for the higher mass loss percentage. When FTIR analysis conclusions are taken into consideration, the chars become more aromatic with increasing temperature and residence time. Thus, the stability of the chars could go up with stronger bonds in the aromatic rings. Therefore, creating more stable structures with higher operating temperatures and longer residence times is a finding that can be drawn from this study.

Mass loss rate (DTG) curves of the lignin and chars are shown in Figure 7. According to the DTG graphs illustrated in Figure 7, the maximum mass loss peak was reduced and moved towards higher temperatures with the increasing HTL operating temperatures and residence time. This indicates that the chars produced at higher temperatures and residence times took longer to decompose and decomposed at higher temperatures due to more thermally stable structures.

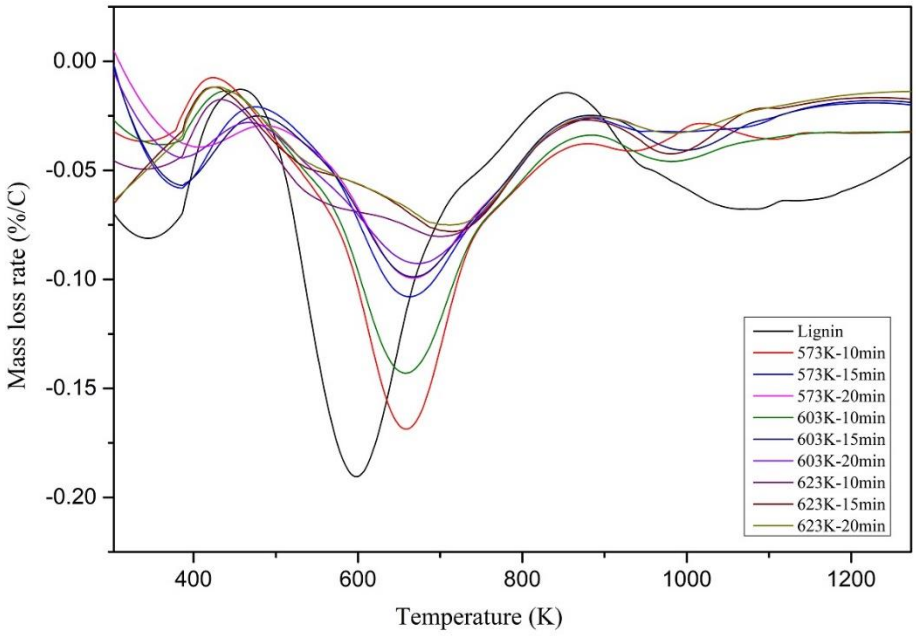

Figure 7. DTG curves of lignin and the chars at 20 C/min under N_2.

The mass loss peak observed from 300 K to 420 K could be due to the moisture loss and the low boiling organic compounds loss. This is a widespread phenomenon with hydrochar. The maximum mass loss peak observed from 500 K to 800 K could be due to the carboxylation and cleavage of methoxyl groups. Moreover, the height of the mass loss peak was considerably reduced towards the higher HTL operating temperatures. This could explain the elimination of the methoxyl groups from the chars produced at higher HTL operating temperatures and longer residence times. Secondary reforming reactions of aromatic carbon skeletons could be the primary source for the evolution after 750 K.

Biochar interacts with soil fractions in different ways, and such interactions determine the influences on soil fractions by biochar [38]. Since the properties of biochar or HTL char are determined by the process conditions and feedstock properties, the influence on soil directly depends on how the char is produced. Biochar could positively and negatively impact soil, such as water-holding capacity, surface area, and bulk density [38]. Since HTL char and biochar chemistry are similar, these facts can also be actual with HTL char. Moreover, more stable char can be helpful from a climate mitigation point of view and regarding agronomic effects [39]. Further, with HTL char,

higher operating temperatures and residence times produced more stable chars while also having higher nitrogen content. Therefore, chars produced at higher operating conditions and residence times could be beneficial in soil.

3.4. Adsorption of N_2 at 77 K

The surface area, pore size distribution, and pore volume are the main factors that can explain the chars' solid internal structure. The Brunauer–Emmett–Teller (BET) surface area and the density functional theory (DFT) pore volume of different chars obtained by hydrothermal liquefaction are shown in Table 3. For the N_2 adsorption studies, chars produced at a residence time of 10 min at 573 K, 603 K, and 623 K temperatures are used.

Table 3. Surface area and pore volume variation at different operating temperatures at 10 min residence time.

Sample	Surface Area (m^2/g)	DFT Pore Volume (cm^3/g)
573 K—10 min	5.82	0.0158
603 K—10 min	1.77471	0.0065
623 K—10 min	2.65	0.0045

Below, Figure 8 shows the behavior of the Brunauer–Emmett–Teller surface areas and the quenched solid density functional theory (QSDFT) pore volume of different chars with their respective carbon contents in the chars. The lowest operating temperature produced the highest pore volume and surface area, where the pore volume shrunk with the increasing HTL operating temperature of the chars. The surface area showed the behavior of inverse dependability to the carbon content of the sample. Nevertheless, this behavior must be further investigated to observe a strong relationship between the surface area and the sample's carbon content.

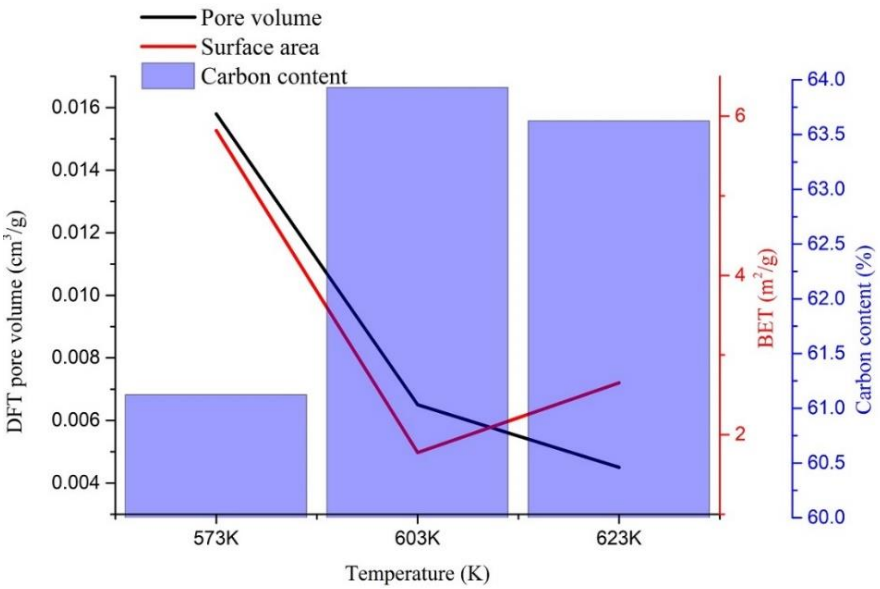

Figure 8. Relationship of carbon content surface area and the pore volume.

The chars produced at 573 K showed both the highest surface area value and the highest pore volume value. The surface area of HTL char produced at 573 K (5.82 m^2/g) was considerably higher than of the lignin pyrolysis char (about 0.5 m^2/g) and pyrolysis char from wood (2.39 m^2/g) produced at the same temperature [17,40]. At 603 K, both pyrolysis char (about 2 m^2/g) and HTL char (1.77 m^2/g) showed similar surface area values, whereas the HTL char produced at 623 K (2.65 m^2/g) showed a lesser value than the pyrolysis char (about 5 m^2/g) produced at the same temperature [17]. Nevertheless, the surface area of both HTL and pyrolysis-derived char ranged in the same values. The chars' surface area exciting behavior reduced the surface area at 603 K and increased it at 623 K.

Pore volumes between 1.45 and 32.7 nm diameter were calculated by the QSDFT adsorption method. The maximum pore volume of 0.0158 cm^3/g was observed with char produced at 573 K, whereas the lowest value of 0.0045 cm^3/g was observed with the char produced at 623 K. Similar pore volume variation was observed with hydrochar produced by hydrothermal carbonization (HTC) [1]. Nevertheless, the pore volume of pyrolysis char from wood at 573 K was smaller (0.00256 cm^3/g) than the values reported here [40]. Since the hydrochar (from HTC process)-based porous carbon inherits its parent material properties, the HTL char produced at 573 K may produce porous char

with the highest porosity [1]. Nevertheless, to investigate the behavior of porous carbon from HTL, porous carbon produced from HTL must be further investigated with different activator kinds. The adsorbed volume distribution against micropore radius and adsorbed volume distribution against relative pressure for all three temperatures are shown in Figure 9a,b, respectively.

Chars obtained at 573 K and 623 K showed a wide range of pore diameter distribution from 1.45 nm to 32.7 nm, whereas the chars produced at 603 K were limited to a pore distribution from around 9 nm to 29 nm. The adsorption volume of chars produced at 573 K and 623 K were observed to be 2.04×10^{-4} to 1.01×10^{-4} $cm^3/(g.\ nm)$ and 1.19×10^{-4} to 6.74×10^{-6} $cm^3/(g.\ nm)$, respectively, whereas for char produced at 603 K, the adsorption volume was between 1.08×10^{-4} to 8.85×10^{-6} $cm^3/(g.\ nm)$. No pores over 30 nm were observed with the char produced at 603 K. Nonetheless, all the samples showed an incomplete pore distribution close to the most minor pore size limit. Although the pores' distribution was a bit more complicated with the three different char samples, more conclusions could be drawn from the following section's morphological analysis.

According to Figure 9b, in the low relative pressure region from 0.2 to 0.8, a slight increment in the adsorption volume was observed with all the samples indicating the mesopores' existence with a broad distribution. Meanwhile, a sudden increase was noted in the relative pressure region from 0.8 to 1.0, showing a small microporosity of chars produced at all three temperatures [35,41]. Overall, char produced at 573 K showed a greater porosity.

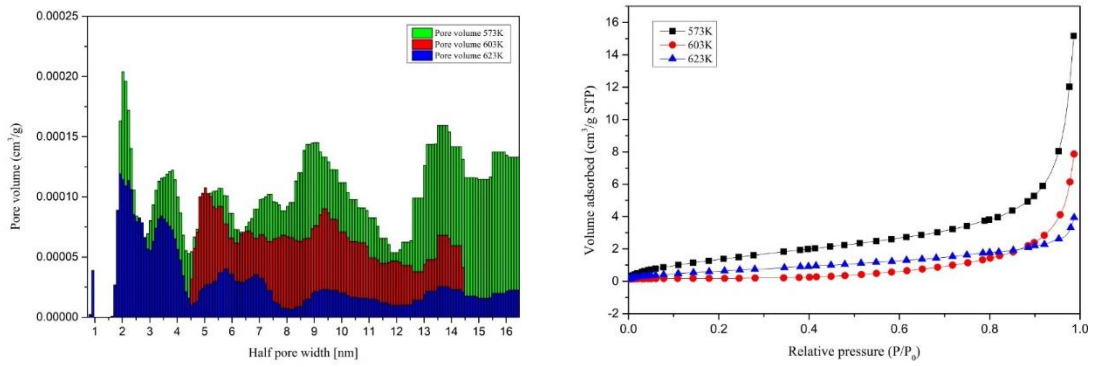

(**a**) (**b**)

Figure 9. Adsorbed volume distribution (**a**) against micropore radius and (**b**) against relative pressure.

In the HTL temperatures, volatiles are formed due to the strong decompositions. These volatiles could initiate the char structure's pores when cooled if they are not scattered to the water medium. Higher temperatures might be capable of diffusing the volatiles faster. Therefore, the pores are not created abundantly. Moreover, the chars produced at 603 K had a higher carbon content and might have stacked better than the other chars produced at different temperatures. This could be a possible reason for the low surface area at 603 K. However, chars produced at 573 K showed the highest surface area, which can be attributed to the higher amount of volatile matter production during the liquefaction. This fact was ultimately proven by the char produced at 573 K having the highest pore volume among all three samples. At high temperatures, pores can be shrunk, resulting in macropores collapses [35]. Another explanation could be that due to further carbonization, pores could be melted, fused, combined, collapsed, or filled up by material around the pores [42]. This can be a possible reason behind the lower pore volumes of chars produced at higher temperatures. Due to the small pore sizes, CO_2 adsorption is preferred over N_2 adsorption for porosity and surface area analysis of HTC char. Therefore, the same basis could be applied to HTL char as well [36].

HTL char can be used for many applications, including HTL char-based catalysts, biochar-supported metal catalysts, and the availability of high surface functional groups as carbon storage to reduce fertilizers' use in agricultural farms. Activated production for anode production for battery technology is also a possibility. Due to the high porosity, char produced at 573 K can be a good precursor for porous carbon production since it boasts considerably higher porosity to biochar produced at the same temperature.

3.5. SEM Analysis

Scanning electron microscope (SEM) images of the char sample obtained at 573 K are shown in Figure 10.

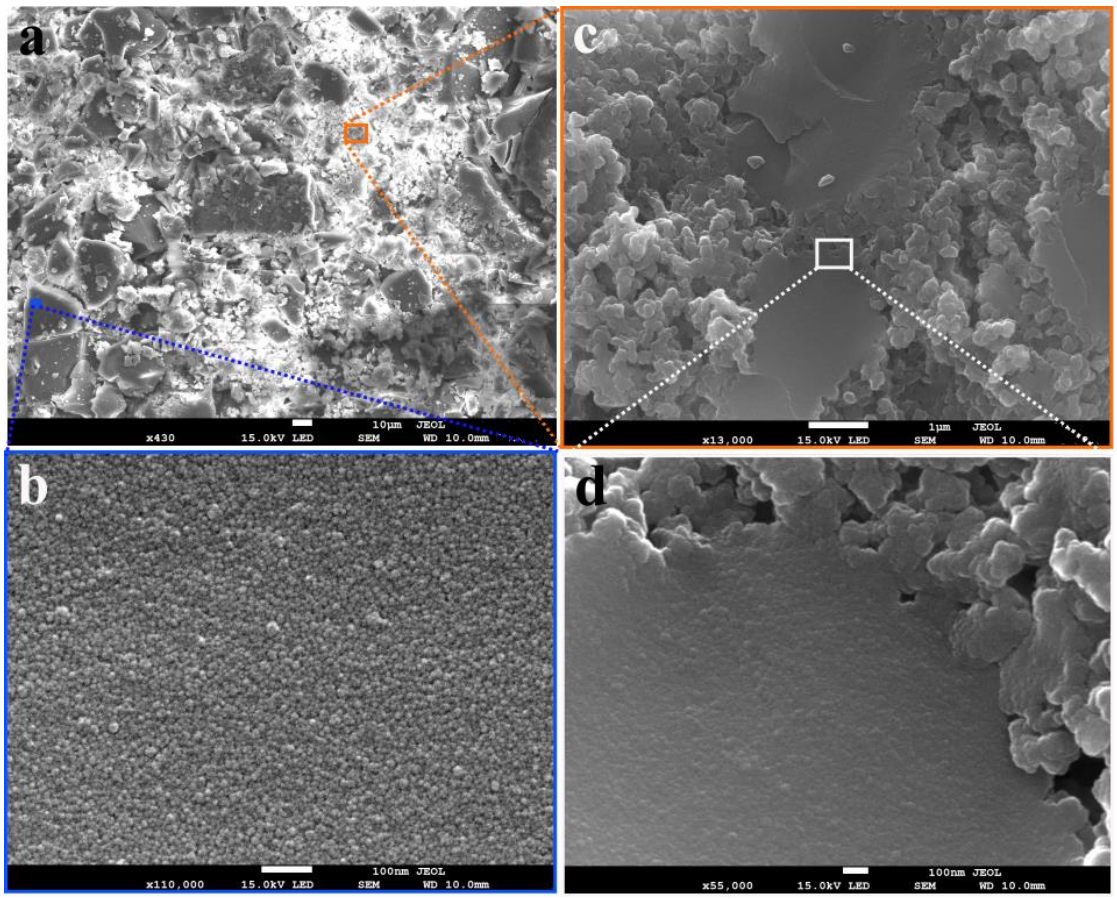

Figure 10. (**a**) SEM image taken at low magnification for the char produced at 573 K and 10 min residence time; (**b**) high magnification (×110000) image of the area indicated as blue color small square in part (a); (**c**) high magnification (×13000) image of the area indicated as orange color small square in part (a); (**d**) high magnification (×55000) image of the area indicated by a white color square in part (c).

As shown in Figure 10a, a significant part of the char sample formed at 573 K consists of large particles (>10 um) with a smooth surface. A high-resolution SEM image showed the spores distributed all over the surface of these particles (Figure 10b). However, a small portion of the char sample showed smaller particles with a rough surface, where many vesicles adhered to the surface could be seen (Figure 10c). During char formation, lignin particles soften, melt, fuse, and release volatile materials [42]. The emission of volatile materials leads to the formation of open pores, consequently increasing the surface area. However, vesicles are often formed and adhere to the surface if

volatiles are not completely diffused out [43]. This may result in pore blockage and, consequently, a reduced surface area.

At low operational temperatures (<603 K), the hydrothermal char is reported to exhibit minimum vesicle formation compared to the pyrolysis char, and this inhibition is suggested to be due to the permeation of water into the pores [43]. This is also consistent with the N_2 adsorption studies presented in the previous section. A significantly higher surface area and pore volume were observed compared to the pyrolysis char.

Hydrothermal char produced at 603 K showed most of the phase with small particles with a large number of vesicles adhered to the surface. A small number of larger particles with a relatively smooth surface was also present (Figure 11).

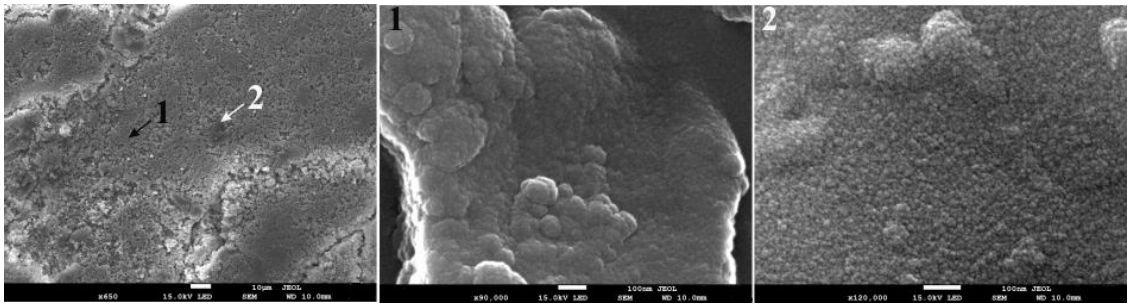

Figure 11. SEM images of the char produced at 603 K and 10 min residence time. High magnification images of the regions marked as 1 and 2 are displayed in the middle and the right panel respectively.

High-resolution images showed the presence of pores on the surface of these particles. An increase in vesicle formation with the rise in operation temperature could be due to the strengthening of the degradation process and intense release of gaseous materials that did not entirely diffuse out and subsequently condensed during the cooling process. A further increase of the temperature to 623 K assists the release of gaseous materials to some extent so that volatiles have sufficient energy to escape the lignin matrix timely [43]. This is evident from the SEM image in Figure 12 (left panel), where the larger particles with a smoother surface are observed to increase. These particles have minimal vesicles and a large density of open pores. This is consistent

with the N_2 adsorption results, where an increase in the char's surface area was observed when the operation temperature increased from 603 K to 623 K.

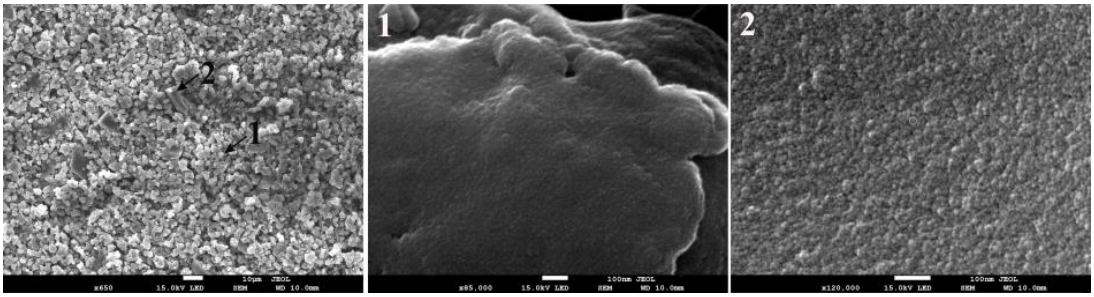

Figure 12. SEM images of the char produced at 623 K and 10 min residence time. High magnification images of the regions marked as 1 and 2 are displayed in the middle and the right panel respectively.

3.6. Proposed Formation Pathway of Lignin Char at Hydrothermal Conditions

Lignin might not fully dissolve in water when the operating temperature is below 650 K [16]. Being a phenolic polymer, undissolved lignin can become polyaromatic char through solid–solid conversion [12]. Dissolved lignin can take part in hydrolysis reactions and produce phenolics in the process, which can be a main conversion route in this process. These phenolics can further polymerize and produce secondary char with aromatic properties. Additionally, polymerization can take place on the surface of the undissolved lignin as well. In low temperatures, lignin can be partially hydrolyzed because of the high bond energy.

Further, due to high ionic product and dielectric constant of water, ionic reactions are the most likely to happen. Mainly because of the hydrolysis reactions and possible free radical reactions, phenolic compounds can be produced [25,44]. In the FTIR analysis, the chars produced at 573 K showed relatively higher carbonyl, CH_3, CH_2, and OH groups. When the residence time and temperature are further increased, phenolic compounds such as guaiacol can be produced due to C-C bonds' cleavage [25]. Nevertheless, guaiacol is an intermediate during the lignin liquefaction process and converts into catechol and phenols with increased temperature and residence time [6,11]. Furthermore, these phenolic compounds, such as guaiacol, can further polymerize and

produce more char as well [25]. Around 573 K, guaiacol has shown the maximum production, and with the temperature increased, the production rate has gone down [25,44]. This could be a possible reason for the high surface area, the pore volume observed in N_2 adsorption, and the chars' SEM analysis. Besides, around 603 K, vesicles are often and abundantly formed because of the high degradation and fast and intense release of volatiles.

Nevertheless, the vesicles adhere to the surface when the volatiles are not completely diffused out. These closed vesicles create smooth surfaces. Thus, the surface area can be decreased at 603 K and then increased at 623 K since the pores are opened up due to the uncovering of vesicles.

The increase of peaks corresponding to the aromatic ring (1595 cm^{-1}) and carbonyl (1684 cm^{-1}) with the increasing temperature show the aromatization or the fusion of the chars' ring structures. Further, the consumption of C-C and C-H bonds is also portrayed by increasing those peaks. When the temperature is around 603 K the CH_3, and the CH_2 groups start eliminating, the char has shown a more aromatic nature already. With the further incrementation of the temperature and residence time, fused ring structures can be formed by carbonizing the aromatic rings. Most of the functional groups except aromatic groups are expelled from the chars at this moment. Close to the critical point, radical reactions become dominant and more influential than ionic reactions due to the property change of water [25]. Because of the medium's high radical nature, the phenolic radicals could depolymerize and contribute to the char phase. At this temperature, most of the volatiles may be emitted, and only a smaller amount of volatiles is available to leave the structure and create pores. This could be a possible reason for chars produced at 623 K showing the least pore volume and showing a significantly smaller surface area value than the chars produced at 573 K. Furthermore, the peaks corresponding to nitro compounds (1353 cm^{-1}) show the increase of nitrogen compounds with the increase of the operating temperature and residence time. This could be mainly due to the aromatization process in the char [29]. With the results found and the literature data, a possible reaction mechanism for char formation from lignin HTL is illustrated in Figure 13.

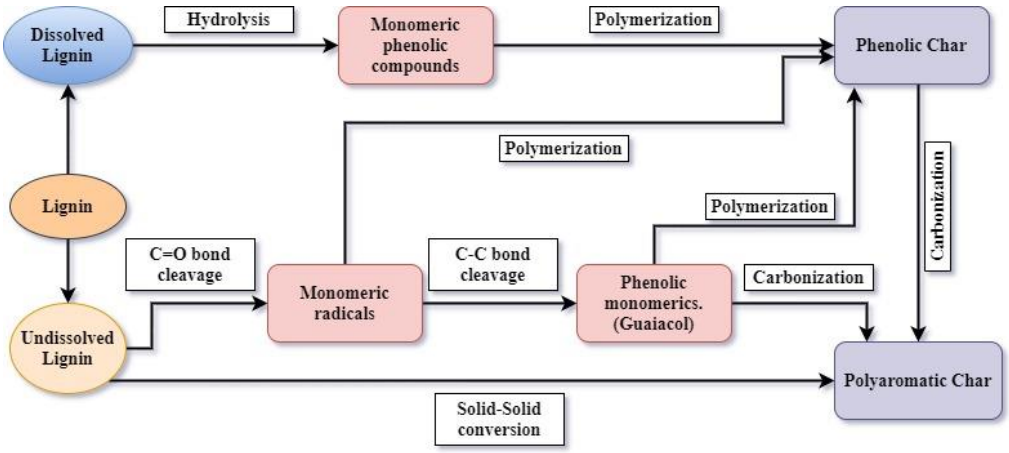

Figure 13. Reaction mechanism for char formation from lignin HTL.

4. Conclusions

HTL chars produced from lignin at 573 K, 603 K, and 623 K and residence times of 10 min, 15 min, and 20 min were studied. Both increasing operating temperature and residence time resulted in a positive impact on the nitrogen content of the chars.

The aromatic ring and the carbonyl group were strengthened drastically with increased operating temperature, and chars became more aromatic, while aliphatic groups were observed to vanish. Although the impact was considerably low, the same trend could be seen with the residence time too. Nevertheless, the carbonyl group showed contradictive behavior with temperature and residence time, where it showed an increase with increasing operating temperature, while a decrease was observed with the longer residence times.

With the increasing temperature, the pore volume decreased at all the operating temperatures, where the surface area showed the minimum at 603 K. According to the SEM analysis, the char sample formed at 573 K consists of large particles (>10 um) with a smooth surface. A high-resolution SEM image showed the presence of pores distributed all over the surface of these particles. Possibly because of the permeation of water into the pores at 603 K, minimum vesicle formation was exhibited by the char, compared to the pyrolysis char. Besides, at 623 K, the vesicles seemed to be opened and increased the surface area slightly.

Higher operating temperatures and longer residence times produced more thermally stable chars, where the residence time substantially impacted the

thermal stability of chars produced at 573 K. At lower temperatures, the cleavage of the weak bonds can be seen, where polymerization was observed at higher temperatures and longer residence times. Carbonization is the main process of creating char. Longer residence times helped create more polyaromatic rings by assisting further carbonization.

Author Contributions Conceptualization, M.J.; methodology, M.J. and S.R.; formal analysis, M.J.; investigation, M.J., S.R., N.A. and A.A.C.; resources, M.J.; data curation, M.J.; writing—original draft preparation, M.J.; writing—review and editing, M.J., S.R., N.A. and A.A.C.; visualization, M.J., N.A. and A.A.C.; supervision, S.R.; project administration, S.R.; funding acquisition, S.R. All authors have read and agreed to the published version of the manuscript.

Funding: This study was conducted as part of the Ph.D. research at the Department of Engineering Sciences, funded by the Faculty of Engineering and Science, University of Agder.

Institutional Review Board Statement: Not applicable.

Informed Consent Statement: Not applicable.

Data Availability Statement: Data available on request due to the privacy. The data presented in this study is available on request from the corresponding author. The data are not publicly available due to ongoing research.

Acknowledgments: The authors would like to thank Giulia Ravenni from the Technical University of Denmark for assisting with char sample analysis and J.A. Godwin for the contribution at the initial phase of the experiments.

Conflicts of Interest: The authors declare no conflict of interest.

References

1. Zhu, X.; Liu, Y.; Qian, F.; Zhou, C.; Zhang, S.; Chen, J. Role of Hydrochar Properties on the Porosity of Hydrochar-based Porous Carbon for Their Sustainable Application. *ACS Sustain. Chem. Eng.* **2015**, *3*, 833–840, doi:10.1021/acssuschemeng.5b00153.
2. Okoro, O.V.; Sun, Z. The characterisation of biochar and biocrude products of the hydrothermal liquefaction of raw digestate biomass. *Biomass Convers. Biorefinery* **2020**, doi:10.1007/s13399-020-00672-7.

3. Clough, T.J.; Condron, L.M. Biochar and the Nitrogen Cycle: Introduction. *J. Environ. Qual.* **2010**, *39*, 1218–1223, doi:10.2134/jeq2010.0204.
4. Arun, J.; Varshini, P.; Prithvinath, P.K.; Priyadarshini, V.; Gopinath, K.P. Enrichment of bio-oil after hydrothermal liquefaction (HTL) of microalgae C. vulgaris grown in wastewater: Bio-char and post HTL wastewater utilization studies. *Bioresour. Technol.* **2018**, *261*, 182–187, doi:10.1016/j.biortech.2018.04.029.
5. Arturi, K.R.; Strandgaard, M.; Nielsen, R.P.; Søgaard, E.G.; Maschietti, M. Hydrothermal liquefaction of lignin in near-critical water in a new batch reactor: Influence of phenol and temperature. *J. Supercrit. Fluids* **2017**, *123*, 28–39, doi:10.1016/j.supflu.2016.12.015.
6. Brebu, M.; Vasile, C. Thermal degradation of lignin—A review. *Cellul. Chem. Technol.* **2010**, *44*, 353–363.
7. Falco, C.; Baccile, N.; Titirici, M.-M. Morphological and structural differences between glucose, cellulose and lignocellulosic biomass derived hydrothermal carbons. *Green Chem.* **2011**, *13*, 3273–3281, doi:10.1039/C1GC15742F.
8. Leng, L.; Yuan, X.; Huang, H.; Shao, J.; Wang, H.; Chen, X.; Zeng, G. Bio-char derived from sewage sludge by liquefaction: Characterization and application for dye adsorption. *Appl. Surf. Sci.* **2015**, *346*, 223–231, doi:10.1016/j.apsusc.2015.04.014.
9. Leng, L.; Yuan, X.; Zeng, G.; Shao, J.; Chen, X.; Wu, Z.; Wang, H.; Peng, X. Surface characterization of rice husk bio-char produced by liquefaction and application for cationic dye (Malachite green) adsorption. *Fuel* **2015**, *155*, 77–85, doi:10.1016/j.fuel.2015.04.019.
10. Wahyudiono; Sasaki, M.; Goto, M. Recovery of phenolic compounds through the decomposition of lignin in near and supercritical water. *Chem. Eng. Process. Process Intensif.* **2008**, *47*, 1609–1619, doi:10.1016/j.cep.2007.09.001.
11. Pińkowska, H.; Wolak, P.; Złocińska, A. Hydrothermal decomposition of alkali lignin in sub- and supercritical water. *Chem. Eng. J.* **2012**, *187*, 410–414, doi:10.1016/j.cej.2012.01.092.
12. Kang, S.; Li, X.; Fan, J.; Chang, J. Characterization of Hydrochars Produced by Hydrothermal Carbonization of Lignin, Cellulose, d-Xylose,

and Wood Meal. *Ind. Eng. Chem. Res.* **2012**, *51*, 9023–9031, doi:10.1021/ie300565d.

13. Cheng, S.; Wilks, C.; Yuan, Z.; Leitch, M.; Xu, C. (Charles) Hydrothermal degradation of alkali lignin to bio-phenolic compounds in sub/supercritical ethanol and water–ethanol co-solvent. *Polym. Degrad. Stab.* **2012**, *97*, 839–848, doi:10.1016/j.polymdegradstab.2012.03.044.
14. Kleinert, M.; Barth, T. Phenols from Lignin. *Chem. Eng. Technol.* **2008**, *31*, 736–745, doi:10.1002/ceat.200800073.
15. Fang, Z.; Sato, T.; Smith, R.L.; Inomata, H.; Arai, K.; Kozinski, J.A. Reaction chemistry and phase behavior of lignin in high-temperature and supercritical water. *Bioresour. Technol.* **2008**, *99*, 3424–3430, doi:10.1016/j.biortech.2007.08.008.
16. Sharma, R.K.; Wooten, J.B.; Baliga, V.L.; Lin, X.; Geoffrey Chan, W.; Hajaligol, M.R. Characterization of chars from pyrolysis of lignin. *Fuel* **2004**, *83*, 1469–1482, doi:10.1016/j.fuel.2003.11.015.
17. Rutherford, D.W.; Wershaw, R.L.; Rostad, C.E.; Kelly, C.N. Effect of formation conditions on biochars: Compositional and structural properties of cellulose, lignin, and pine biochars. *Biomass Bioenergy* **2012**, *46*, 693–701, doi:10.1016/j.biombioe.2012.06.026.
18. Rudra, S.; Jayathilake, M. Hydrothermal Liquefaction of Biomass for Biofuel Production. In *Reference Module in Earth Systems and Environmental Sciences*; Elsevier: Amsterdam, The Netherlands, 2021; ISBN 978-0-12-409548-9, doi:10.1016/B978-0-12-819727-1.00043-1.
19. Wikberg, H.; Ohra-aho, T.; Pileidis, F.; Titirici, M.-M. Structural and Morphological Changes in Kraft Lignin during Hydrothermal Carbonization. *ACS Sustain. Chem. Eng.* **2015**, *3*, 2737–2745, doi:10.1021/acssuschemeng.5b00925.
20. Brunauer, S.; Emmett, P.H.; Teller, E. Adsorption of Gases in Multimolecular Layers. *J. Am. Chem. Soc.* **1938**, *60*, 309–319, doi:10.1021/ja01269a023.
21. Neimark, A.V.; Lin, Y.; Ravikovitch, P.I.; Thommes, M. Quenched solid density functional theory and pore size analysis of micro-mesoporous carbons. *Carbon* **2009**, *47*, 1617–1628, doi:10.1016/j.carbon.2009.01.050.

22. Chatterjee, R.; Sajjadi, B.; Chen, W.-Y.; Mattern, D.L.; Hammer, N.; Raman, V.; Dorris, A. Effect of Pyrolysis Temperature on Physico-Chemical Properties and Acoustic-Based Amination of Biochar for Efficient CO2 Adsorption. *Front. Energy Res.* **2020**, *8*, doi:10.3389/fenrg.2020.00085.
23. Ye, Y.; Fan, J.; Chang, J. Effect of reaction conditions on hydrothermal degradation of cornstalk lignin. *J. Anal. Appl. Pyrolysis* **2012**, *94*, 190–195, doi:10.1016/j.jaap.2011.12.005.
24. Yong, T.L.-K.; Matsumura, Y. Kinetic Analysis of Lignin Hydrothermal Conversion in Sub- and Supercritical Water. *Ind. Eng. Chem. Res.* **2013**, *52*, 5626–5639, doi:10.1021/ie400600x.
25. Zhang, B.; Huang, H.-J.; Ramaswamy, S. Reaction kinetics of the hydrothermal treatment of lignin. *Appl. Biochem. Biotechnol.* **2008**, *147*, 119–131, doi:10.1007/s12010-007-8070-6.
26. Kozliak, E.I.; Kubátová, A.; Artemyeva, A.A.; Nagel, E.; Zhang, C.; Rajappagowda, R.B.; Smirnova, A.L. Thermal Liquefaction of Lignin to Aromatics: Efficiency, Selectivity, and Product Analysis. *ACS Sustain. Chem. Eng.* **2016**, *4*, 5106–5122, doi:10.1021/acssuschemeng.6b01046.
27. *Methods in Lignin Chemistry*; Lin, S.Y., Dence, C.W., Eds.; Springer Series in Wood Science; Springer: Berlin/Heidelberg, Germnay, 1992; ISBN 978-3-642-74067-1, doi:10.1007/978-3-642-74065-7.
28. Shrestha, A.; Acharya, B.; Farooque, A.A. Study of hydrochar and process water from hydrothermal carbonization of sea lettuce. *Renew. Energy* **2021**, *163*, 589–598, doi:10.1016/j.renene.2020.08.133.
29. Zhou, L.; Liu, Y.; Liu, S.; Yin, Y.; Zeng, G.; Tan, X.; Hu, X.; Hu, X.; Jiang, L.; Ding, Y.; et al. Investigation of the adsorption-reduction mechanisms of hexavalent chromium by ramie biochars of different pyrolytic temperatures. *Bioresour. Technol.* **2016**, *218*, 351–359, doi:10.1016/j.biortech.2016.06.102.
30. Tejado, A.; Peña, C.; Labidi, J.; Echeverria, J.M.; Mondragon, I. Physico-chemical characterization of lignins from different sources for use in phenol–formaldehyde resin synthesis. *Bioresour. Technol.* **2007**, *98*, 1655–1663, doi:10.1016/j.biortech.2006.05.042.

31. Chen, Y.; Yang, H.; Wang, X.; Zhang, S.; Chen, H. Biomass-based pyrolytic polygeneration system on cotton stalk pyrolysis: Influence of temperature. *Bioresour. Technol.* **2012**, *107*, 411–418, doi:10.1016/j.biortech.2011.10.074.
32. Liu, Z.; Zhang, F.-S. Removal of lead from water using biochars prepared from hydrothermal liquefaction of biomass. *J. Hazard. Mater.* **2009**, *167*, 933–939, doi:10.1016/j.jhazmat.2009.01.085.
33. Chen, Z.; Ma, L.; Li, S.; Geng, J.; Song, Q.; Liu, J.; Wang, C.; Wang, H.; Li, J.; Qin, Z.; et al. Simple approach to carboxyl-rich materials through low-temperature heat treatment of hydrothermal carbon in air. *Appl. Surf. Sci.* **2011**, *257*, 8686–8691, doi:10.1016/j.apsusc.2011.05.048.
34. Chen, W.; Shi, S.; Nguyen, T.; Chen, M.; Zhou, X. Effect of Temperature on the Evolution of Physical Structure and Chemical Properties of Bio-char Derived from Co-pyrolysis of Lignin with High-Density Polyethylene. *BioResources* **2016**, *11*, 3923–3936.
35. Cheng, F.; Li, X. Preparation and Application of Biochar-Based Catalysts for Biofuel Production. *Catalysts* **2018**, *8*, 346, doi:10.3390/catal8090346.
36. Zhang, C.; Shao, Y.; Zhang, L.; Zhang, S.; Westerhof, R.J.M.; Liu, Q.; Jia, P.; Li, Q.; Wang, Y.; Hu, X. Impacts of temperature on evolution of char structure during pyrolysis of lignin. *Sci. Total Environ.* **2020**, *699*, 134381, doi:10.1016/j.scitotenv.2019.134381.
37. Tomczyk, A.; Sokołowska, Z.; Boguta, P. Biochar physicochemical properties: Pyrolysis temperature and feedstock kind effects. *Rev. Environ. Sci. Biotechnol.* **2020**, *19*, 191–215, doi:10.1007/s11157-020-09523-3.
38. Enders, A.; Hanley, K.; Whitman, T.; Joseph, S.; Lehmann, J. Characterization of biochars to evaluate recalcitrance and agronomic performance. *Bioresour. Technol.* **2012**, *114*, 644–653, doi:10.1016/j.biortech.2012.03.022.
39. Zhao, S.-X.; Ta, N.; Wang, X.-D. Effect of Temperature on the Structural and Physicochemical Properties of Biochar with Apple Tree Branches as Feedstock Material. *Energies* **2017**, *10*, 1293, doi:10.3390/en10091293.

40. Mohan, D.; Kumar, H.; Sarswat, A.; Alexandre-Franco, M.; Pittman, C.U. Cadmium and lead remediation using magnetic oak wood and oak bark fast pyrolysis bio-chars. *Chem. Eng. J.* **2014**, *236*, 513–528, doi:10.1016/j.cej.2013.09.057.
41. Zubbri, N.A.; Mohamed, A.R.; Kamiuchi, N.; Mohammadi, M. Enhancement of CO2 adsorption on biochar sorbent modified by metal incorporation. *Environ. Sci. Pollut. Res.* **2020**, *27*, 11809–11829, doi:10.1007/s11356-020-07734-3.
42. Hu, J.; Shen, D.; Wu, S.; Zhang, H.; Xiao, R. Effect of temperature on structure evolution in char from hydrothermal degradation of lignin. *J. Anal. Appl. Pyrolysis* **2014**, *106*, 118–124, doi:10.1016/j.jaap.2014.01.008.
43. Jayathilake, M.; Rudra, S.; Rosendahl, L.A. Hydrothermal liquefaction of wood using a modified multistage shrinking-core model. *Fuel* **2020**, *280*, 118616, doi:10.1016/j.fuel.2020.118616.

Article D

Jayathilake KGRM, Rudra S, Christy AA. Effect of co-liquefaction of lignin and laminaria saccharina on optimization of bio-oil yield (2021). Published in Energy Conversion and Management: X (2021)

The layout has been revised

Effect of co-liquefaction of lignin and laminaria saccharina on optimization of bio-oil yield

KGRM Jayathilake[a], S. Rudra[b1] , A.A. Christy[c]

a: Faculty of Engineering Sciences, Department of Engineering and science, Universitetet I Agder, Grimstad, Norway, madhawa.jayathilake@uia.no ,+47 37233308, +47 94435703

b: Associate Professor, Department of Engineering and Science, Faculty of Engineering Sciences, Universitetet I Agder, Grimstad, Norway, souman.rudra@uia.no, +47-37233036

c: Professor, Department of Natural Science, University of Agder, 4630 Kristiansand, Norway

[1] corresponding author Tel: +47 37 23 30 36,

E mail address: souman.rudra@uia.no

Abstract

Hydrothermal liquefaction (HTL) is a valuable technology to convert and use wet biomass feedstocks. Lignin, waste from the paper industry and the main component of lignocellulosic biomass, is co-liquefied with laminaria saccharina, a commonly available seaweed in Norway. The aim is to conduct statistical analysis and investigate the possibility of increasing bio-oil yield while lowering the char yield through a synergistic effect. The bio-oil and char yields are measured with different operating temperatures, residence times, and blending ratios (mass ratio of laminaria saccharina to the total mass) to find out the optimized process conditions for better outputs statistically. Response surface methodology (RSM) with a Box Behnken design methodology is used to optimize the liquefaction yields of laminaria saccharina, lignin, and the different blends of the two biomasses. The results explicitly revealed that the biomass blend's optimal bio-oil and char yields are 0.2513 (w/w_0) and 0.1791 (w/w_0) respectively at 573K, 20 min with the blending mass ratio of 0.2. The synergistic effects on the bio-oil yield are detected at comparatively severe reaction conditions. According to the RSM, residence time does not affect bio-oil and char yields as much as the operating temperature and the blending ratio.

Nevertheless, temperature, residence time, and blending ratio have different impacts on the functional groups. The temperature increase has helped increase the alcohol and phenolic compounds production while the residence time consumes the C-O bonds. The increase of laminaria saccharina mass ratio in the feedstock has improved the phenolic compounds, long-chain aliphatic hydrocarbons, carboxylic acids, ketones, aldehydes, and esters in the bio-oils. Co-liqueafctio has produces bio-oil with significantly lower N content than from bio-oil produced from laminaria saccharina liquefaction.

***Keywords*— Co-liquefaction; Laminaria saccharina; Lignin; Synergistic effect; statistical analysis**

1. Introduction

The fast surge in energy requirements and environmental-related issues encourage the interest of many in renewable energy sources [1,2]. Among many renewable energy sources, biomass is one of the most crucial of these resources. Biomasses are a product of solar energy and an inexpensive, clean, and sustainable energy source. Many raw materials such as lignocelluloses and

waste from industries, animals, and households are included in biomass[1]. Biomass meets about 10–14% of the world's energy demand[1].

Among many thermochemical conversion methods, the hydrothermal liquefaction (HTL) process is one of the promising conversion techniques in transforming biomass into value-added products such as biocrude and chemicals. In this process, solid bio-polymeric structures are transformed to new compounds through depolymerization and isomerization reactions by high temperature (493–653 K) and pressure (5–25 MPa)[3–5]. Through HTL, biomass is converted into liquid products with high energy content. The process is performed under both subcritical and supercritical conditions, and bio-oil is obtained, which is an organic liquid as the primary output[6,7].

Lignin is a valuable renewable resource for producing bio-oil or biofuel with hydrothermal liquefaction process as the only natural source of aromatic compounds [8,9]. Lignin is a morphologically amorphous structure as hemicellulose. Nevertheless, it has a low solubility resembling cellulose and reinforces the plant cell wall[2]. Due to the multiple bonds in the small units in the structure, lignin is the most resistive biopolymer to biological degradation. Moreover, lignin boasts a high level of energy value due to its phenol compounds[10]. Due to lignin being a significant by-product of the paper and pulp industry, paper mills mainly use it for energy recovery [11]. Further, lignin is underutilized since such high amounts of lignin produced from industries are not well utilized. Mainly, lignin-based research focuses on value-added chemicals [12] and high-performance materials[13,14] production. Nevertheless, lignin is studied as a source for biofuel production and other different products through HTL [9,15–21]. Yields from lignin liquefaction directly depend on the composition and the structure of the feedstock [22]. The lignin-derived phenolic compounds production is strengthened as the temperature rises. Thus, due to the diverse functionalities of phenolic compounds, lignin presents the possibility of generating numerous valuable chemicals in subcritical and supercritical conditions [15,16,23]. Char and the bio-oil from lignin showed contradictive behavior with the increase of temperature, whereas char demonstrated an increase with the increasing temperature [16]. Further, lignin showed the ability to produce bifunctional aromatic molecules [9]. In contrast, alkali lignin with comparatively high molecular weight preceded the production of

phenolic compounds such as guaiacol, catechol, phenol, o-cresol, m-cresol, and p-cresols [18].

On the contrary, macroalgae are generally an excellent sustainable, renewable, and inexpensive resource for biofuels and chemicals due to their high conversion rate, flexibility, and environmental friendliness[24–28]. Numerous studies show that macroalgae are capable of producing comparably high bio-oil yields[24]. Macroalgae produce high bio-oil yields when it has high lipid content. The major drawback of using macroalgae is bio-oil's high nitrogen content when the macroalgae boast high protein content[28]. Some studies showed that liquefaction is not suitable as a sole conversion of macroalgae to bio-oil due to lower conversion rates[29].

Nevertheless, bio-oil and char phases from laminaria saccharina liquefaction show a contradictive behavior to lignin where the increase of temperature shows an increase in the bio-oil production and a decrease in char production at the same time [24]. Therefore, the co-liquefaction of lignin and laminaria saccharina is worth studying since the mix of these two feedstocks could produce a better feedstock mix to obtain better bio-oil yields while having less char yield. In addition, HTL of lignin produces relatively high amounts of char than seaweed in general[28].

Co-liquefaction of macroalgae and lignocellulosic feedstocks have not been studied extensively. As mentioned above, the char phase and bio-oil phase behavior directions of lignocellulosic feedstocks and macroalgae are different. Therefore, the mix of these feedstocks could create a better feedstock for bio-oil production. Co-liquefaction of poplar and spirulina produced a noticeably different char phase from the char produced from individual feedstocks, where it showed reduced repolymerization of phenolics and a substantial number of different pyrroles [30]. Co-liquefaction of lignin with Spirulina platensis showed a clear improvement of bio-oil yield than of the bio-oil yield from lignin where the co-liquefaction has improved the quality of the bio-oil as well[31]. Therefore, the co-liquefaction of macroalgae with lignocellulosic or even with lignin has shown a glimpse of the good results it can produce.

The motivation of this study is to use laminaria saccharina as a co-feedstock and lignin in HTL for energy-dense liquid fuel production in an optimized way. Lignin generally produces less char and better bio-oil yields at lower operating temperatures[5,16], where laminaria saccharina behaves otherwise

[24]. In the liquefaction process, char is a by-product, and it contains a considerable amount of carbon [32]. Nonetheless, with more space for repolymerization, more char can be produced by the process [32,33]. When the liquefaction reactions are concerned, less bio-oil production is noticeable when more char is produced, mainly due to repolymerization[3,5]. Therefore, the idea behind using these two feedstocks is to find a particular blend of feedstocks that produces more bio-oil and a lesser amount of char than lignin. Although used as sole feedstock in different studies, these feedstocks have not been descriptively studied for co-liquefaction [16,22,24]. Optimization of the products from co-liquefaction can be performed to determine the possibility of producing better bio-oil yields. In general, response surface methodology (RSM) is abundantly used to optimize responses dependent on several independent variables [31,34–37]. In that case, RSM can be used effectively in optimizing the bio-oil yield in this study. Therefore RSM is implemented to design the experimental setup, verify the model, and perform the surface analysis. The FTIR analysis is used to analyze the functional groups of the bio-oil. Therefore, the functional groups are studied to overview the quality of the different bio-oils from different blends. Moreover, elemental analysis of the bio-oil is performed to investigate the carbon and nitrogen contents. Furthermore, the operating parameters are optimized to obtain the best bio-oil yield and lowest char yield of HTL of laminaria saccharina, lignin, and blended feedstocks. Furthermore, the synergistic effect of using laminaria saccharina in the co-liquefaction is studied to investigate the actual impact of co-liquefaction on these two feedstocks. Therefore, it is possible to understand from which feedstock the actual impact of having an increased bio-oil yield and lower char yields.

2. **Method**

2.1. Material

Laminaria saccharina is obtained from Lerøy Ocean Harvest, Norway (produced 05.2019 from rongøy island close to Bergen Norway 60.5083°N 4.9175°E). Then the seaweed is washed with fresh water and air-dried before making it a powder of particle size less than 250 microns. Alkali lignin with a low sulfonate content is obtained from Sigma Aldrich Co., Norway. Both feedstocks are dried at 378K overnight before the experiments. In all experiments, a feed slurry of 16ml is fed to the reactor where a 1:9 feedstock/water

weight ratio is maintained. Ultrapure water is used as the reaction solvent in all cases. The proximate and ultimate analysis data of laminaria saccharina and lignin are shown in Table 1.

Table 10:Characterization of lignin and laminaria saccharina

	Proximate Analysis (Wt%)			**Ultimate Analysis (Wt%, Ash free)**			
	VM	ASH	FC	C	H	N	O
Alkali Lignin	73	9.62	17.38	51.5	4.12	0.35	44.03
Laminaria Saccharina	69.11	16.84	14.05	47.18	6.19	3.61	43.02

2.2. Experimental procedure

Experimental procedure and extraction of products from HTL of lignin and laminaria saccharina are carried out as mentioned elsewhere in our previous articles[5,32]. A steel reactor with a 24 ml dead volume is used for the experiments, and 16 ml of feedstock slurry is used for all the experiments. For the co-liquefaction experiments, the feedstock to water ratio is kept at 1:9 at all cases where seaweed to total weight ratio (blending ratio) is varied as 0.2, 0.4, and 0.6. For the consistency of the experiments, every experiment is repeated four times, and average values are taken. Once the reactor is filled with the feedstock slurry and tightened, check for leakages using N_2. The reactor is then placed in a heated sandbath using a rod. The rod is connected to a motor to obtain a reciprocating movement to ensure the proper mixing of the reactants during the liquefaction experiments. After the desired residence time at desired operating temperature, the reactor is cooled in cold water for 30 minutes before extracting the resultant. A schematic figure of the experimental setup is shown below in figure 1.

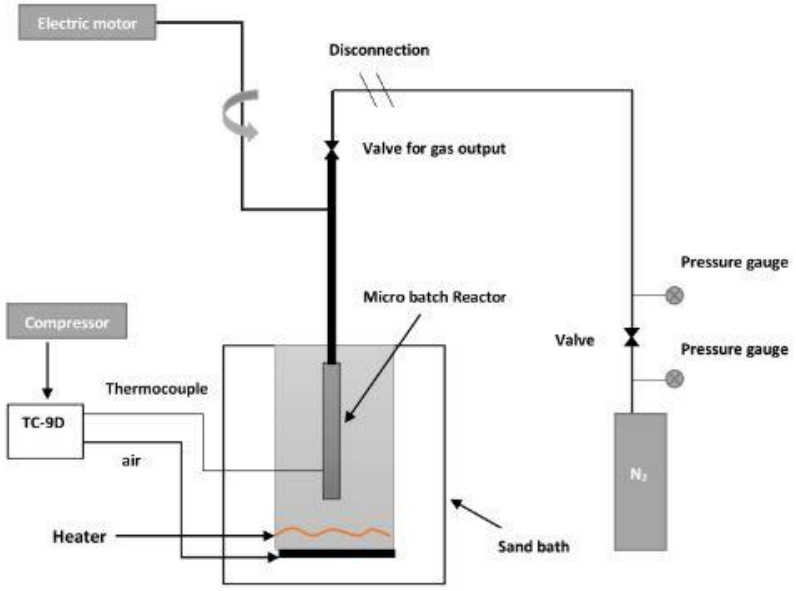

Figure 52:Schematic diagram of the experimental setup(adapted from[28])

The term blending ratio is explained below in eq 1.

$$Blending\ ratio\ = \frac{Weight\ of\ seaweed}{Total\ weight\ of\ feedstock} \qquad \text{Eq 1}$$

2.3. Characterization

The proximate analysis of the feedstocks is performed using a muffle furnace LT 40/11/P330 (Nabertherm, Germany) according to the procedure EN 14775 (by a standard ash test at 550 °C) and EN 15148 for the ash content and the volatile matters respectively. The elemental analysis is carried out using a PerkinElmer 2400 CHNS/O Series II elemental analyzer, following EN 15104:2011, where Oxygen is calculated by difference and Sulphur is assumed as negligible.

The thick liquid samples from the experiments were analyzed using a PerkinElmer Spectrum One FT-IR spectrometer equipped with a Harrick single reflectance attenuated total internal reflectance (ATR) accessory and liquid nitrogen cooled MCT detector. Each of the samples was placed on the ATR crystal using a blunt glass rod. The sample was spread on the crystal, and the sample's spectrum was measured in the range of 4000- 600 cm^{-1}. The background was measured with the ATR crystal before the application of the sample. A total of 32 scans at a resolution of 4 cm-1 were made on each sample.

The infrared spectra in absorbance format were used in the comparison of the functional groups in the samples.

The bio-oil yield, char yield, and synergistic effect (SE)[31] are calculated using Eq. (2), (3), and (4), as shown below:

$$Bio-oil\ \ yield(wt\%) = \frac{Mass\ of\ biocrude\ recoverd\ after\ the\ extraction\ (g)}{Initial\ amount\ of\ lfeedstock\ used\ for\ the\ experiment\ (g)} \times 100\% \quad \text{Eq 2}$$

$$Char\ yield\ (wt\%) = \frac{Mass\ of\ char\ recoverd\ after\ the\ extraction\ (g)}{Initial\ amount\ of\ feedstock\ used\ for\ the\ experiment\ (g)} \times 100\% \quad \text{Eq 3}$$

$$SE = Y_{mixed} - (X_{L.Saccharina} \times Y_{L.Saccharina} + (1 - X_{L.Saccharina}) \times Y_{Lignin}) \quad \text{Eq 4}$$

Where Y_{mixed} is the co-liquefied bio-oil yield, $X_{L.Saccharina}s$ is the mass content of *laminaria saccharina* in the blended feedstock, $Y_{L.Saccharina}$ and Y_{Lignin} are the bio-oil yields of *laminaria saccharina* and *lignin*, respectively. Therefore, the term $(X_{L.Saccharina} \times Y_{L.Saccharina} + (1 - X_{L.Saccharina}) \times Y_{Lignin})$ in Eq 3 delivers the theoretical bio-oil yield of co-liquefaction.

2.4. Design of experiments

The response surface methodology with Box Behnken Design (BBD) is used to evaluate the impacts of HTL operating temperature(X_1), residence time (X_2), and feedstock blending ratio (X_3) on bio-oil yield (Y_1) and char yield (Y_2) from co-liquefaction of lignin and laminaria saccharina. BBD is a statistical optimization method with three factors and three levels of design. It comprises a duplicated center point and a set of points sitting on the center of each edge of the multidimensional cube that distinguishes the space of significance. BBD is applied due to the demonstrated higher efficiency than the three-level complete factorial design and the central composite design methods, respectively[36,38]. The factors are optimized using DOE (Design of Experiment) software-Minitab 17.1.0. According to the principles of BBD, factors, levels, and responses and the experimental scheme are defined. In this study, the tem-

perature range of 573K-633K, residence time from 10-20 min, and laminaria saccharina blending ratio from 0.2 to 0.6 are used to investigate the synergetic effect. The same operating parameter range is used to investigate the bio-oil and char yields of lignin and laminaria saccharina hydrothermal liquefaction. A polynomial quadratic equation (Eq 5) is fitted to correlate the connection between the selected variables and the responses.

$$Y = a_0 + \sum_{i=1}^{4} a_i X_i + \sum_{i=1}^{4} a_{ii} X_i^2 + \sum_{i=1}^{4} \sum_{i=j} a_{ij} X_i X_j + \varepsilon \qquad \text{Eq 5}$$

Where Y is the measured response value related to each factor level combination, a_0 is the intercept coefficient, a_i, a_{ii}, and a_{ij} are the regression coefficients calculated from the obtained experimental values of Y, X_i, and X_j are the levels of independent variables, and ε represents the model's error.

The RSM is performed in three different scenarios. First, the behavior of bio-oil yield and char yield of lignin against the operating temperature and residence time is performed. Then the same method is followed with laminaria saccharina. These two studies are performed with only two independent variables. After that, the co-liquefaction of two feedstocks is studied with the variation of operating temperature, residence time, and the blending ratio. Every independent variable is set into three levels in all the studies, like +1, 0, and −1, corresponding to the minimum, medium, and maximum levels. The levels of all process factors are presumed based on results obtained from preliminary tests. The independent variables, along with their coded values, are shown in Table 2.

Table 11:Independant factors used in the experimental design and their levels

Independent factors	Levels		
	-1	0	1
Operating temperature (X_1)	573K	603K	633K
Residence time (X_2)	10min	15min	20min
Blending ratio (X_3)	0.2	0.4	0.6

When it comes to statistical analysis, using the correct type of statistical test is vital. If a wrong statistical test is used, there is a possibility of either type 1 or type 2 error[39]. Type 1 error is the opposite of the type 2 error, where the likelihood of occurring type 2 error increases when it is tried to avoid type 1 error. Further, when two or more two groups of data, it requires an analysis of variance (ANOVA). It allows comparing means of several distributions with different significance levels and avoiding having errors[39]. In this study, ANOVA is performed with the Minitab 17.1.0 software (UK) to examine the statistical significance of the regression coefficients by using the Fisher's F-test with a confidence level of 95%. Particularly, p-values smaller than 0.05 ($\leq$0.05) prove that the model values are significant and closer to the actual experimental results, while higher P values could be due to noise in the produced data. The appropriateness of the quadratic models is estimated based on the lack of fit test, coefficient of determination (R^2), and the adjusted coefficient of determination (R^2_{adj}). Specifically, the precision of the experimental data is determined by $R^{2,}$ while the R^2_{adj} values verify the deviation of data predicted from the proposed models. High discrepancies between R^2 and R^2_{adj} values could be due to the non-significant model terms[40].

Moreover, to perform the lack of fit test, the variability of the actual model residuals is compared to the variability of observations at replicate settings of the factors [36,38]. A model is statistically significant at a 95% confidence level, only if the lack of fit test has a p-value higher than 0.05 ($p \geq 0.05$). Furthermore, the contour plots and the surface plots for evaluating the impacts of different factors are generated using the Quadratic models.

3. Results and Discussion

In this section, the results are presented and discussed. The parameter optimization of lignin, laminaria saccharina, and the blended feedstocks are illustrated. Then the synergistic effect and the bio-oil and char characterization are presented.

3.1. Liquefaction yield results of lignin and laminaria saccharina

The operating parameters of HTL of lignin and laminaria saccharina are optimized. The operating conditions used for the experiments are 573K-633K and 10-20 min residence time. The variation of bio-oil yields and char yields of

lignin and laminaria saccharina is shown below in figure 2 and figure 3 separately. The maximum bio-oil yield of lignin and laminaria saccharina is 0.38 w/w_0 at 603K and 15 min, and 0.295 w/w_0 at 633K and 10 min, respectively. Therefore, the reported maximum bio-oil yield of lignin is higher than that of laminaria saccharina.

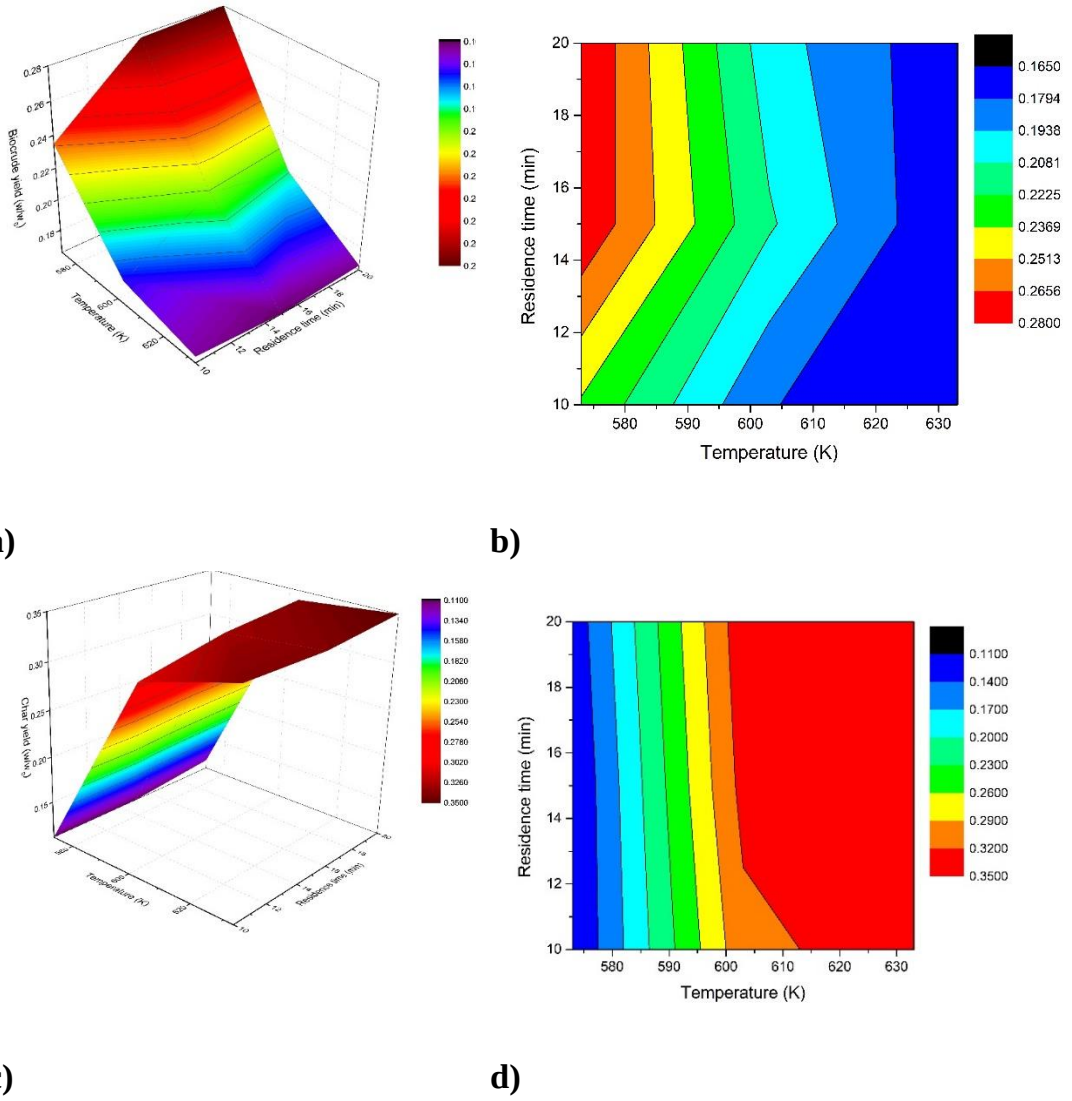

Figure 53:Effect of reaction temperature and residence time of HTL of lignin on a)bio-oil yield (3D surface plot) b) bio-oil yield (contour plot), c) char yield(3D surface plot) d) char yield (contour plot)

For lignin HTL the bio-oil yield first increased and then decreased as the temperature rose and reached the maximum at 603K. At 633K, the bio-oil yield slightly changed and almost stayed constant throughout all the residence times. When the operating temperature increases, the bio-oil yield of lignin

decreases while the char yield shows a clear increment. Although the char yield is highly dependent on the operating temperature, the effect of the residence time on the char yield seems to be negligible. Above and beyond, the bio-oil component is consists of many valuable chemicals, where the variation of each component is different, and the different behaviors need to be investigated*[5]*. The lignin HTL product consists of many phenolic compounds, suitable precursors or intermediates for synthesizing many binders, pharmaceutical products, and polymers*[5,41,42]*.

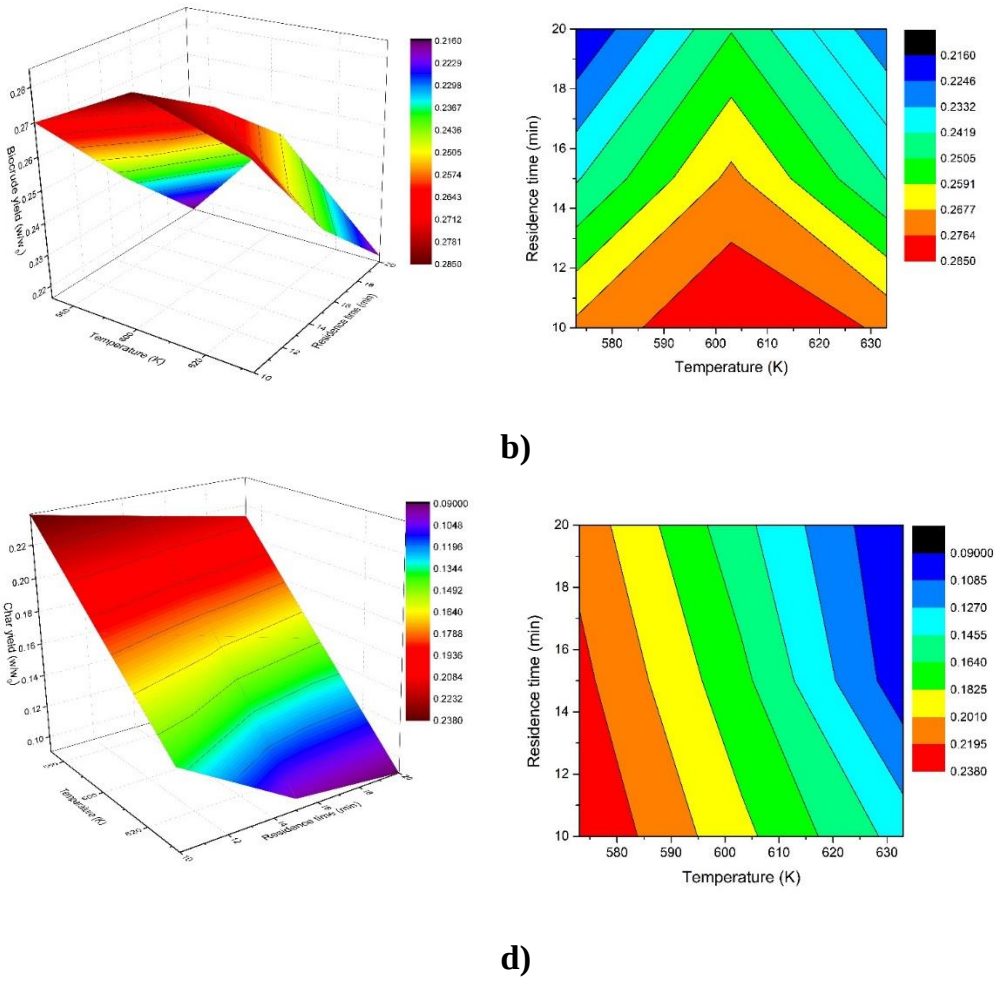

Figure 54: Effect of reaction temperature and residence time of HTL of laminaria saccharina on a) bio-oil yield (3D surface plot) b) bio-oil yield (contour plot) c) char yield (3D surface plot) d) char yield (contour plot)

Intriguingly, the bio-oil yield from laminaria saccharina showed a maximum at 603K, whereas the char yield maximized at 573K. The bio-oil yield is consistently reduced when the operating temperature is too high or when the reac-

tion time is too long. Besides, both bio-oil and char yields show a decrease in the yields with increasing residence times at all temperatures.

3.2. **Parameter optimization of individual feedstocks**

According to the CCD model, for the study on HTL of lignin and laminaria saccharina individually, nine experimental points are used with each feedstock, with triplicate centre points to estimate the pure error. The Minitab 17.1.0 software (Minitab Ltd., Coventry, UK) selected the nine experimental points to minimize the bias and are shown in Table 3, along with the observed responses.

Table 12:Randomized runs selected for lignin and laminaria saccharina HTL.

	Independent variables		Lignin		Laminaria saccharina	
Run	Temperature (K) (X_1)	Residence time(min) (X_2)	Bio-oil yield(w/w_0) (Y_1)	Char yield(w/w_0) (Y_2)	Bio-oil yield(w/w_0) (Y_1)	Char yield(w/w_0) (Y_2)
1	573	10	0.235	0.11	0.270	0.237
2	633	10	0.169	0.34	0.275	0.138
3	573	20	0.280	0.12	0.216	0.213
4	633	20	0.168	0.35	0.218	0.090
5	573	15	0.278	0.11	0.241	0.225
6	633	15	0.165	0.34	0.242	0.097
7	603	10	0.180	0.31	0.285	0.188
8	603	20	0.200	0.34	0.250	0.151
9	603	15	0.210	0.33	0.270	0.169

According to table 3, 9 random runs of each feedstock are used in the DOE method. For both feedstocks, the operating temperatures of 573K-633K and residence times of 10min-20min are used. The variation of each feedstock's bio-oil and char yields hinted that the results are a combined effect of temperature and time rather than a single-valued function. Since the data groups are

scattered, and the consistency of the bio-oil yield (or char yield) vs. single factor is difficult to be observed, the bio-oil and char yields are fitted using the statistical model. The rationale of the fitting is not only to find the optimum values of the bio-oil and char yields but also to identify the predictability of the bio-oil and char yields as a function of the operating parameters.

The p-value of each table indicates the value of significance, which is the vital testimony used to decide whether the used model is appropriate. The P-value of both the "Models" is less than 0.0001, which means they are significant. The P-value corresponding to "Lack of Fit" is higher than 0.05, which denotes not the significance of the "lack of fit." These observations show that the experimental error at the center points of the models is within an acceptable range, where the relevant results are realistic. In addition, for both models, the P-value of the temperature for bio-oil and char yields is smaller than 0.05, which is significant. This revealed that temperature is the most significant factor concerning bio-oil and char yields of lignin HTL. The residence time's P-values on each yield are observed to be 0.0004, which is somewhat insignificant, indicating the residence time has a slightly lesser effect on the bio-oil and char yields. These findings are in line with the conclusions made in our previous works [5,28,32,42]. It is also confirmed that the temperature is the most critical operating parameter affecting the HTL of lignin suggested by many other articles.

Using the DOE method, operating parameters can be optimized by fitting the bio-oil and char yield of Laminaria saccharina HTL within 573K-633K and 10-20 min based on the cubic model. Liquefaction results of laminaria saccharina showed a maximum at 603K, where the char yields show a reduction with the temperature increase.

The bio-oil yield increased as the temperature increased from 573K to 603K. Both bio-oil and char yields are reduced with the residence time increased from 10 min to 20min. The maximum bio-oil yield (0.285 w/w_0) is achieved at 603K and 10 min. However, the bio-oil yield from Laminaria saccharina started to decline when the temperature and residence time exceeded a particular critical value. For example, the bio-oil yield is reduced to $0.275 w/w_0$ when the temperature is 633K and the residence time is 10 min. According to the literature, when the temperature is too high or the reaction time is too long, the bio-

oil dehydration increases, the oxygen content is reduced, and the bio-oil yield is also reduced accordingly[24].

Nevertheless, bio-oil quality is improved due to the decrease in oxygen content[24,31]. The bio-oil yield from HTL of laminaria saccharina is visually seen as a function of reaction temperature and residence time. The response surface method can obtain the results under the conditions that have not been included in the experiment to compare with the previous experimental analysis. Below table 4 illustrates the optimum bio-oil yields and the optimum operating parameters obtained because of the response surface method.

Table 13: The optimized bio-oil yield of HTL of lignin and laminaria saccharina based on the DOE

Feedstock	Residence time (min)	Temperature (K)	Oil yield (w/w_0)
Lignin	17.27	573	0.2801
Laminaria Saccharina	10	627.55	0.2782

3.3. **Parameter optimization of blended feedstocks**

For the study on the co-liquefaction, 15 experiments are performed with triplicate center points to estimate the pure error. The randomized runs selected from the software are shown below in Table 5. The quadratic equations used in the bio-oil and char yield optimization models are shown below in eq 6 and eq 7, respectively.

$$Bio\text{-}oil = -5.599 + 0.02048\ X_1 + 0.01677\ X_2 - 1.530\ X_3 - 0.000018\ X_1^2 + 0.000006\ X_2^2 - 0.1929\ X_3^2 - 0.000025\ X_1 * X_2 + 0.003042\ X_1 * X_3 - 0.00721\ X_2 * X_3 \quad \text{Eq 6}$$

$$Char = -22.58 + 0.0713\ X_1 + 0.0342\ X_2 + 4.672\ X_3 - 0.000056\ X_1^2 - 0.000453\ X_2^2 - 0.082\ X_3^2 - 0.000028\ X_1 * X_2 - 0.00755\ X_1 * X_3 - 0.01396\ X_2 * X_3 \quad \text{Eq 7}$$

Table 14:Randomized runs selected for co-liquefaction of lignin and laminaria saccharina.

	Independent variables			Co-liquefaction			
Run	Temper-ature (K) (X_1)	Resi-dence time(min) (X_2)	Blend-ing ratio (X_3)	Bio-oil yield(w/w_0) (Y_1) Experi-mental	Bio-oil yield(w/w_0) (Y_1) Predict-ed	Char yield(w/w_0) (Y_2) Experi-mental	Char yield(w/w_0) (Y_2) Predict-ed
1	633	15	0.6	0.226	0.2287	0.175	0.1603
2	573	10	0.4	0.242	0.2460	0.188	0.1900
3	603	15	0.4	0.244	0.2426	0.274	0.2690
4	603	15	0.4	0.241	0.2426	0.262	0.2690
5	633	15	0.2	0.179	0.1754	0.302	0.3139
6	603	10	0.2	0.220	0.2241	0.297	0.2799
7	633	20	0.4	0.204	0.2053	0.219	0.2168
8	603	20	0.6	0.236	0.2322	0.183	0.2009
9	573	15	0.6	0.222	0.2242	0.220	0.2080
10	603	15	0.4	0.243	0.2426	0.271	0.2690
11	573	15	0.2	0.248	0.2462	0.165	0.1803
12	603	10	0.6	0.257	0.2533	0.235	0.2449
13	603	20	0.2	0.227	0.2301	0.302	0.2918
14	633	10	0.4	0.219	0.2173	0.236	0.2412
15	573	20	0.4	0.241	0.2429	0.188	0.1822

The individual feedstock HTL results showed that the maximum bio-oil yield of laminaria saccharina is noted near 603K and 10 min, and the maximum bio-oil yield of lignin HTL is found close to 603K and 15 min. Therefore, based on the findings of the HTL of laminaria saccharina and lignin, the operating parameter ranges for the co-liquefaction are chosen as reaction temperature (573K-633k), residence time, (10-20 min), and laminaria saccharina mass ratio (0.2-0.6). When these 15 sets of experiments are observed, the maximum bio-oil yield of 0.257 w/w_0 is noted at 603K, the residence time of 10 min, and the blending ratio of 0.6. This yield is much higher than that of lignin (0.18 w/w_0)

and slightly lesser than that of laminaria saccharina (0.285 w/w_0) under the same operating conditions.

The ANOVA results of the response surface Box Behnken model for blended feedstocks are shown in Table 6. The "Model" p-values for both bio-oil and char yields are less than 0.05 and proved to be significant. Model verification of "Lack of Fit" for both models is not significant, as their p-values are higher than 0.05, which indicates that the value error close to the center point of the model is satisfactory, and the model is credible. Furthermore, in both models, the p-value related to the temperature and the laminaria saccharina blending ratio is less than 0.05, indicating that the above two operating conditions significantly affect the bio-oil and char yields. Subsequently, this suggests that these two parameters ought to be optimized favorably. Nevertheless, the effect of residence time on bio-oil and char yield is not statistically significant.

According to Table 6 below, F-values are equal to 119.28, 6.86, and 34.57 for temperature, residence time, and blending ratio, respectively. These results indicate that the quadratic regression models are significant ($p < 0.05$) for temperature and blending ratio. Additionally, the appropriateness of the BBD method is exhibited by high R^2 values obtained for all the considered responses (R^2=0.985 and 0.947 for Y_1, and Y_2, respectively). Due to the three-level independent variables, the quadratic models adapted for the study comprise additional terms. Therefore, the adjusted coefficient of determination (R^2_{adj}) is more effective in checking the level of fit since it is less responsive to the degrees of freedom [40]. Both R^2_{adj} values are over 0.85 and close to R^2 values, proving the precision of the used models.

There could be a statistical effect from the residence time. Nevertheless, it could be too small, or the sample size is too small for a conclusion. A high 'p' value means noise in the produced data or too much variability with the residence time. Therefore, residence time might have a negligible effect that cannot be detected by the statistical model, or the variability upon the residence time is too much where the used sample size is not enough to detect that. A similar scenario has been observed with other feedstocks in other studies as well[31].

Table 15: ANOVA for response surface quadratic model based on bio-oil yield and char yield from the blended Feedstocks

Source	DF	Bio-oil yield			Char yield		
		F-Value	P-Value		F-Value	P-Value	Source
Model	9	36.56	<0.0001	significant	9.98	0.01	significant
Temperature	1	119.28	<0.0001	significant	10.77	0.022	significant
Residence time	1	6.86	0.057		1.51	0.273	
Ratio	1	34.57	0.002	significant	23.21	0.005	significant
Square	3	23.5	0.002		9.25	0.018	
Temperature*Temperature	1	60.19	0.001	significant	27.13	0.003	significant
Residence time*Residence time	1	0.01	0.942		1.39	0.292	
Ratio*Ratio	1	13.49	0.014	significant	0.12	0.747	
2-Way Interaction	3	32.59	0.001		8.84	0.019	
Temperature*Residence time	1	3.34	0.127		0.2	0.673	
Temperature*Ratio	1	81.69	<0.0001	significant	24.05	0.004	significant
Residence time*Ratio	1	12.75	0.016	significant	2.28	0.191	

				cant			
Lack-of-Fit	3	12.78	0.073	not sig-nifi-cant	13.93	0.068	not signifi-cant
		Adj SS	Adj MS		Adj SS	Adj MS	
Pure error	2	0.000 004	0.0000 02		0.000 078	0.000 039	
		$R^2 = 0.985, R^2_{adj} = 0.958$			$R^2 = 0.947, \quad R^2_{adj} = 0.852$		

Adj SS = Adjusted sum of squares; Adj MS = Adjusted mean square

The three-dimensional response surface plots related to bio-oil and char yields within 573K-633K, 10-20 min, and the laminaria saccharina blending ratio of 0.2-0.6 are shown in figure 4. Figure 4(a) and figure 4(b) illustrate the yield distributions of bio-oil and char yields, respectively when the blending ratio is fixed at 0.4. The bio-oil yield rose initially and then diminished with the temperature increase, reaching the maximum value around 603K. Char yield displays an increase with the operating temperature increase and then shows a maximum in the temperature range of 600K-620K before lowering its value with the further increase of residence time.

According to figure 4(c) and figure 4(d), when the residence time is held at 15min, with the increasing temperature, both bio-oil and char yields show an increase and illustrate a maximum of around 600K started diminishing. After that, the diminishing trend continued throughout all the residence times. Meanwhile, the bio-oil yield almost shows a linear increment with the increase of the blending ratio, and a maximum value is not noticed within the capacity of inspection from Fig. 4(c), while the char yield shows a maximum around the 0.4 blending ratio before started going down in value towards 0.6 blending ratio.

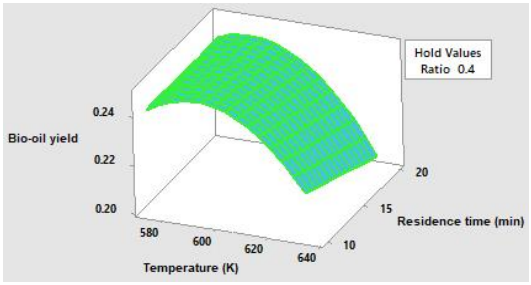

a)

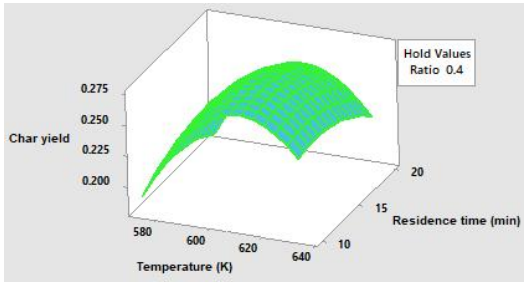

b)

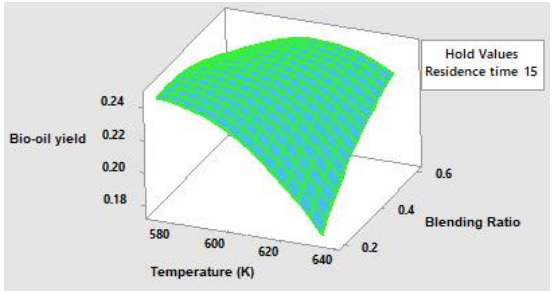

c)

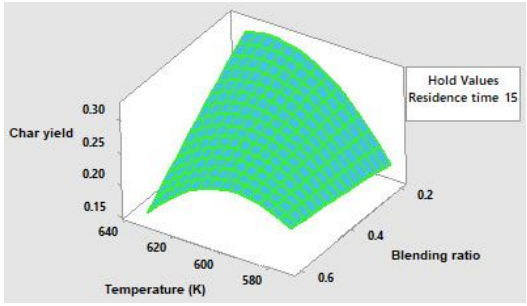

d)

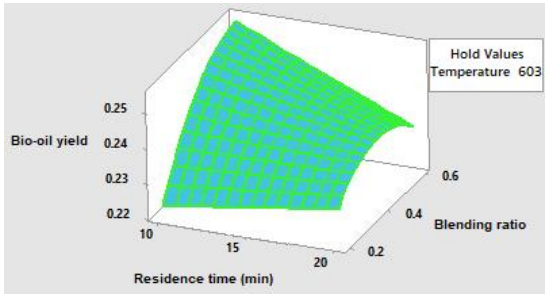

e)

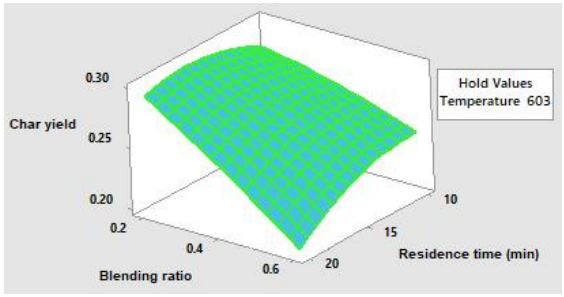

f)

Figure 55: bio-oil yield (w/w_0) and char yield(w/w_0) distribution of HTL of blended feedstocks : (a) bio-oil yield at fixed blending ratio =0.4; (b) char yield at fixed blending ratio =0.4 (c) bio-oil yield fixed reaction residence time =15 min;(d) char yield fixed reaction residence time =15 min (e) bio-oil yield at fixed reaction temperature = 603K (f) char yield at fixed reaction temperature = 603K

According to figure 4(e) and figure 4(f), both the yields of bio-oil and char show a decrease in the yield values with the increase of the residence time. Longer residence times help reduce the bio-oil yield and increase char yield mainly due to repolymerization reactions[5,16,43]. Nevertheless, in this case, the char yield reduction could be the influence of the seaweed. Laminaria saccharina showed a reduction of the char yield with longer residence time, ac-

cording to figure 3(c) and the literature[24]. It can be seen that with the increase of laminaria saccharina blending ratio, the outputs inherit more properties from laminaria saccharina liquefaction. Bio-oil yield illustrates a maximum around 0.4 blending ratio while the char yield comes to its lowest value around 0.6 blending ratio value.

Three mass ratio values (X_3=0.2, 0.4, and 0.6) are used for the investigations to study the influence of different blending ratios on the distribution of the bio-oil and char yields of the co-liquefaction. The results are presented in Figure 5. At the 0.2 blending ratio value, bio-oil displayed a gradual reduction of the yields with the increase of operating temperature for all the residence time values used, while the char yield increased with temperature. At this blending ratio, the impact of lignin is more prominent, and similar behaviors are reported with lignin liquefaction in the literature [5,16,21]. According to figure 5(c) and figure 5(d), when the blending ratio increases to 0.4 value, the bio-oil, and char yields show maximums close to 590K and 600K, respectively, before decreasing values with an increase in temperature.

Following the same trend as the previous case, the bio-oil and char yields show maximums of their yields close to 610K when the blending ratio increases to 0.6. Figures 5(e) and 5(f) respectively show the bio-oil and char yields variation. It also learned that with the increase of the blending ratio, higher operating temperature and longer residence time are essential for reaching the maximum bio-oil and char yields. According to Figures 5(a), 5(c), and 5(e), the bio-oil yield is higher while the laminaria saccharina weight ratio is maximum. It is observed that the highest bio-oil yield of 0.2625 w/w_0 is achieved, at 603K, with a laminaria saccharina blending ratio of 0.6. This pattern can be explained by the reaction mechanisms involved in the process. Lignin generally produces more char with higher operating temperatures and longer residence times with polymerizations. Lignin produced more polyaromatic char by polymerizing aromatic chars produced by phenolic monomers [32,33]. This process reduced the amount of lignin-derived bio-oil that remained in the system [32].

Meanwhile, laminaria saccharina produced more phenol and ketone fractions when the temperature was increased [24]. Similar behavior is observed with other seaweed types as well [44]. Therefore, the higher blending ratio of laminaria saccharina has caused a higher bio-oil yield. This equilibrium of bio-oil

production from both feedstocks could result in the behavior shown in figure 5 below.

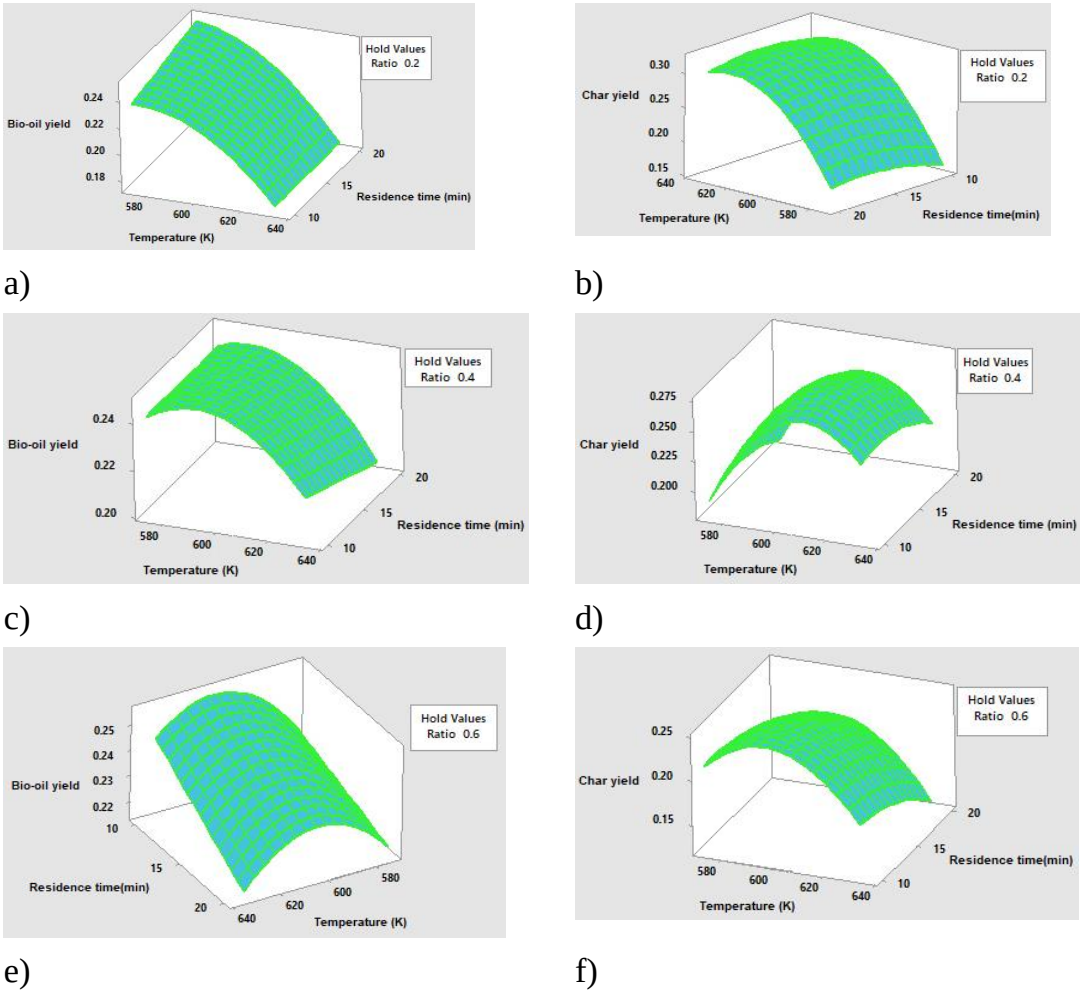

Figure 56: bio-oil yield (w/w_0) and char yield (w/w_0) distribution of HTL of blended feedstocks at different blending ratios : (a) bio-oil yield at fixed blending ratio =0.2; (b) char yield at fixed blending ratio =0.2 (c) bio-oil yield at fixed blending ratio =0.4;(d) char yield at fixed blending ratio =0.4 (e) bio-oil yield at fixed blending ratio =0.6 (f) char yield at fixed blending ratio =0.6

3.4. **Optimization of responses using the desirability function approach**

In the HTL process, relatively high bio-oil yield and low char yield are desired since bio-oil is the preferred output of the process. Therefore, the process needs to be optimized to achieve the highest possible bio-oil yield and lowest

possible char yield. Multi-response optimization is helpful in these types of scenarios [34–36]. Nevertheless, the optimization of both responses under the constant process conditions is challenging since their areas of interest are different. Therefore, Multi-response optimization is applied to assess the conditions on the three independent factors that simultaneously control the optimal responses' optimal values. Therefore, Derringer's desirability function-based method is utilized to solve the multiple response optimization[45]. This method transforms each response (Y_i) to a dimensionless function called the individual desirability function (d_i). d_i is ranges from 0 to 1, which is from the lowest to the highest desirability[36,46]. In a most desirable scenario (Y_i is at its desired value) value of d_i can be found as 1, or else, d_i=0 (the least desired scenario).

During the optimization process, the aim is to maximize the D value. Theoretically, the D value equals one when all required responses achieve the desired output and equals zero when one response is outside the specified range of values. In this study, the goal of the optimization process is to achieve maximum bio-oil yield while minimizing the char yield. The Minitab 17 software does the optimization, and the proposed optimal conditions are described in figure 6.

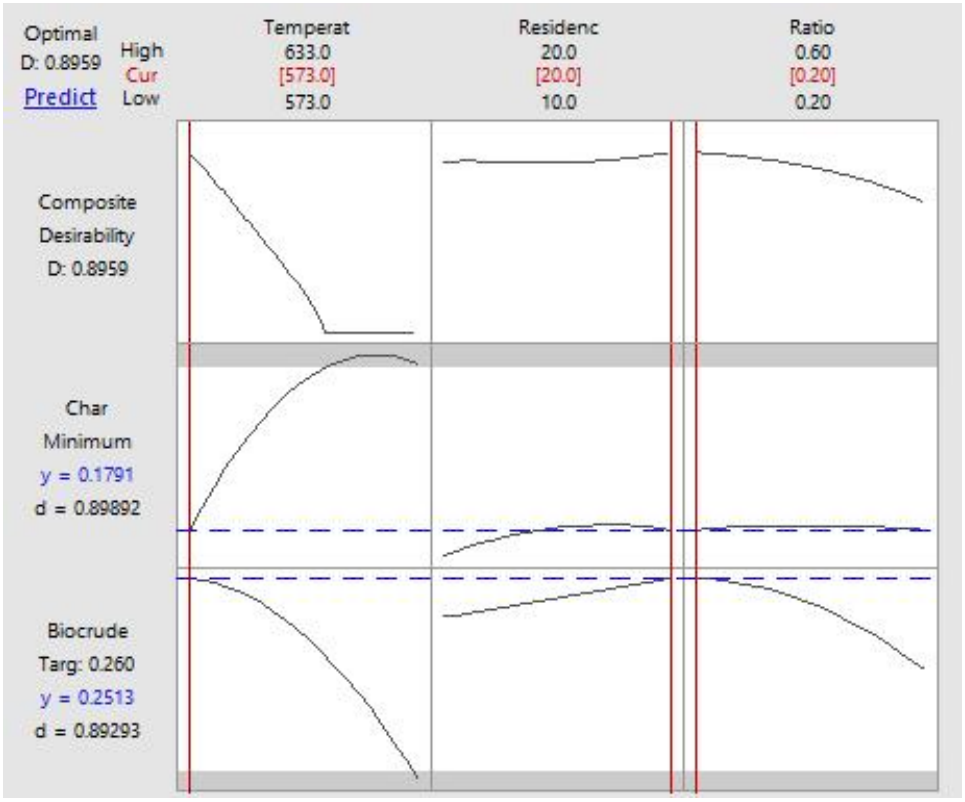

Figure 57:Plots for simultaneous optimization of operating variables (Temperature, residence time, and blending ratio)

According to Derringer's desirability function approach, the optimum process conditions are the temperature of 573K, the residence time of 20min, and the blending ratio of 0.2. Under the optimum process conditions, the predicted bio-oil yield and char yield are 0.2513w/w_0 and 0.1791w/w_0, respectively. The composite desirability value turned out to be close to 1 (0.8959), which proved that good results are accomplished for all responses. Subsequently, new liquefaction tests with the predicted values of the independent variables are performed to investigate the validity of the optimization procedure. Table 7 shows that the observed values are close to predicted and within acceptable predicted error ranges.

Table 16:The predicted and the experimental values of the responses under the optimum process conditions.

Response	Predicted value (w/w_0)	Experimental value	Deviation
Bio-oil yield	0.2513	0.26 ± 0.03	3.34%
Char yield	0.1791	0.19 ± 0.07	5.73%

3.5. Synergistic effect

Synergistic effect (SE) is defined as in Eq. (3) section 2.3. The principle of SE is to find the difference by comparing the actual and the theoretical yields of co-liquefaction. The bio-oil yields obtained at 45 different operating conditions are chosen for the SE analysis. Lignin, laminaria saccharina, and their different mixtures with the blending ratio of 0.2, 0.4, and 0.6 are used, creating five different feedstocks in total. The liquefactions are carried out at nine different conditions. A total of 45 different sets of bio-oil yield result data are registered in Table 8.

Table 17:The Bio-oil yield of various feedstocks under various typical operating conditions

Blending ratio	Temperature (K), Residence time (min)								
	573,10	573,15	573,20	603,10	603,15	603,20	633,10	633,15	633,20
0	0.235	0.278	0.280	0.180	0.210	0.200	0.169	0.165	0.168
0.2	0.231	0.248	0.261	0.220	0.218	0.227	0.189	0.179	0.196
0.4	0.242	0.233	0.232	0.240	0.244	0.233	0.219	0.210	0.204
0.6	0.251	0.222	0.219	0.257	0.263	0.236	0.250	0.226	0.213
1	0.270	0.241	0.216	0.285	0.270	0.250	0.275	0.242	0.218

The computed SE values are shown below in table 9, where the apparent differences are seen between the actual and theoretical bio-oil yields. The differences are relatively significant at the lowest temperature and with more laminaria saccharina. The most substantial negative synergistic effect of 0.034 w/w_0 can be seen with 573K,15min residence time, and 0.6 blending ratio.

Nevertheless, as the operating temperature and residence time increased and the blending ratio of laminaria saccharina is increased, the repressive effect became weaker, and a positive synergistic effect appeared. The bio-oil yield with a blending ratio of 0.2 and an operating temperature of 603K and 10 min residence time was higher than the theoretical bio-oil yield value at the same operating conditions, demonstrating a positive synergistic effect with 0.019 w/w_0. Even Though this was not significant, this positive synergistic effect did appear on the results according to the eq. (3). Furthermore, according to the SE values shown in table 9, the synergistic enhanced effect continues to be reinforced as the temperature, residence time, and blending ratio of laminaria saccharina further increases. This clearly emphasized the positive impact of increasing the bio-oil yield. Similar SE has been observed in other studies as well [31]. This shows that at milder conditions, the co-liquefaction has a repressive effect on the bio-oil yield. In similar studies, co-liquefaction of protein and alkaline lignin showed no improvement in the bio-oil yield [34,47].

Table 18:Synergistic effect (SE) of the bio-oil yield of blended feedstocks under various typical

Blending ratio	Temperature (K), Residence time (min)								
	573,10	573,15	573,20	603,10	603,15	603,20	633,10	633,15	633,20
0.2	-0.011	-0.023	-0.006	0.019	-0.005	0.017	-0.001	-0.001	0.018
0.4	-0.007	-0.031	-0.023	0.018	0.010	0.013	0.007	0.014	0.016
0.6	-0.005	-0.034	-0.023	0.014	0.017	0.006	0.017	0.015	0.015

Furthermore, co-liquefaction of alkaline lignin and soybean oil reported a repressive effect on the bio-oil yield as well [34,48]**.** Nevertheless, co-liquefaction endorsed the required reactions to produce bio-oil in more harsh reaction conditions. Therefore, bio-oil yield is improved to a certain extent, where high temperature and long residence time boosted the synergistic effect. Nonetheless**,** literature reported a positive synergetic effect on bio-oil yield with co-liquefaction of Spirulina platensis with cellulose [35].

In addition, the HTL products of laminaria saccharina, lignin, feedstock mixtures with blending ratios 0.2, 0.4, and 0.6 at 603K and 20 min are selected for mass equilibrium analysis. As shown in figure 7 below, laminaria saccharina displayed the highest bio-oil yield while lignin showed the lowest at the considered conditions.

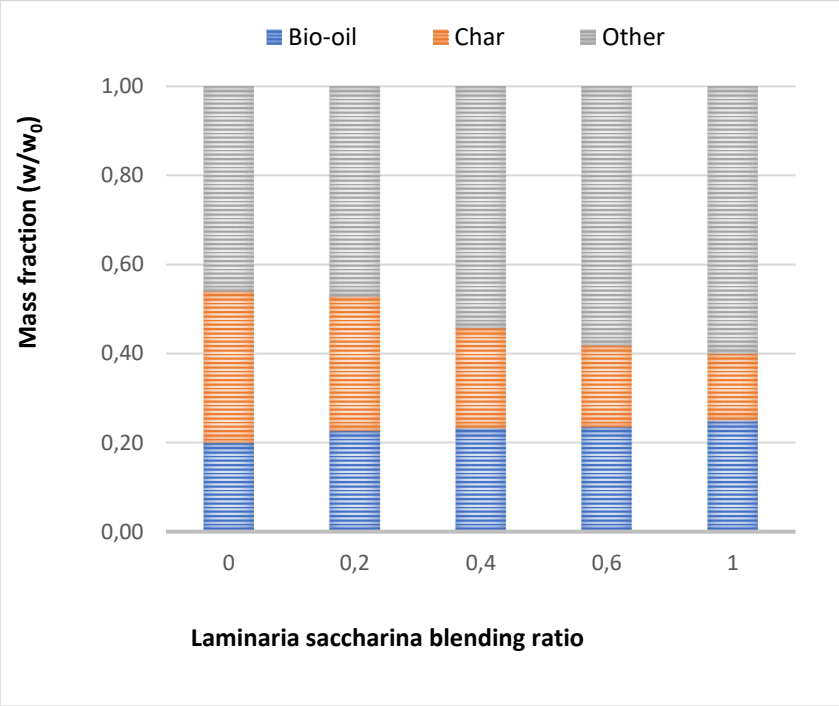

Figure 58:Mass yield balance of different feedstocks at 603K, and 20min

The aqueous and gas phases accounted for a considerable mass ratio from the resultants of the liquefaction process. Mainly, the gas phase consisted of CO, CO2, and a small amount of CH3. The aqueous phase can be reused for slurry making or agricultural purposes due to its high nitrogen content [49]. Nevertheless, the gas and aqueous phases are neither analyzed nor further studied in this study mainly because the focus was on bio-oil and char yield.

All the feedstocks made of blending mixtures showed a synergistic effect on the bio-oil yield. This observation supported the idea of the ability of co-liquefaction to encourage the production of bio-oil under more harsh process conditions. The char yield of lignin was much more significant than what laminaria saccharina produced. Besides, the solid residue yield is gradually decreased when the blending ratio is increased. However, co-liquefaction has imposed a negative synergetic effect on the char yield (-0.00064 at 0.2 blend-

ing ratio, -0.0394 at 0.4 blending ratio, and -0.04324 at 0.6 blending ratio), suggesting that the co-liquefaction resulted in a reduction of solid residue. Although the composition of bio-oil does not show a significant variation, N content of the bio-oil from co-liquefaction is significantly lower than to bio-oil from laminaria saccharina[24].

3.6. FTIR analysis of the bio-oil

Figure 8 demonstrates a closer look at the FTIR spectrum from the bio-oil sample obtained at 573 K, 10 min residence time, and 0.2 blending ratio. This bio-oil sample is delivered at the lowest temperature, the smallest blending ratio, and with the shortest residence time among all the operating conditions. According to figure 8, the wavenumbers between 3000cm^{-1} and 3600cm^{-1} and between 1000cm^{-1} and 1750cm^{-1} showed significant peaks that correspond to functional groups such as C-H, C=C C–O bonds, C=O bonds, and O–H bonds. These functional groups proved the availability of phenols, alcohols, aromatics, and acids in the bio-oil [32].

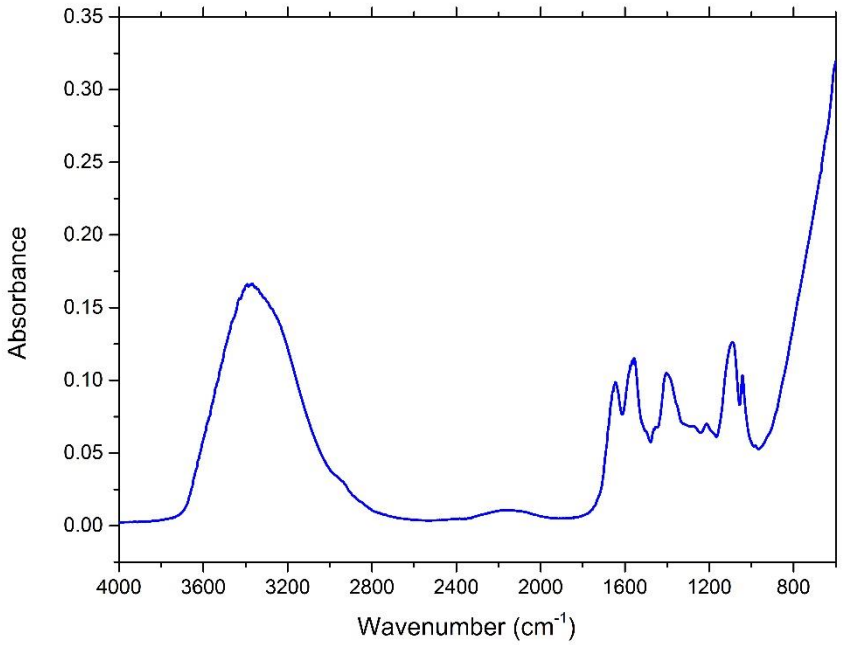

Figure 59:The available peaks of the FTIR spectra of bio-oil obtained at 573 K, 10 min residence time, and 0.2 blending ratio.

The broad and intense absorption peak around 3380 cm^{-1} corresponds to the N–H /O–H stretching of amino and hydroxyl group compounds (water, fatty acid amides, phenols, and N-containing heterocyclic compounds)[50]. Absorbance peaks at 1650cm^{-1} and 1540cm^{-1} signify the C=O group stretching vibration, consistent with a substantial quantity of carboxylic acids, ketones, aldehydes, and esters triglyceride [50,51]. Then the peak found at 1395 cm^{-1} is coincided with the C–H stretching of $–CH_2$ and $-CH_3$ groups that indicated the existence of long-chain aliphatic hydrocarbons [52]. The absorption peaks presented in the range of 1280cm^{-1} and 1050 cm^{-1} mark the C–O stretching vibrations, indicating the presence of phenolic and alcohol compounds [50,53]. Furthermore, the developing peak presented from 850 cm^{-1} to 600 cm^{-1} showed aromatic compounds and corresponding alternate derivatives [50]. The normalized FTIR spectra of the bio-oils are shown in Figure 9. Bio-oil samples obtained at different temperatures and residence times with the same blending ratio are analyzed, and the FTIR spectrums are obtained analysis.

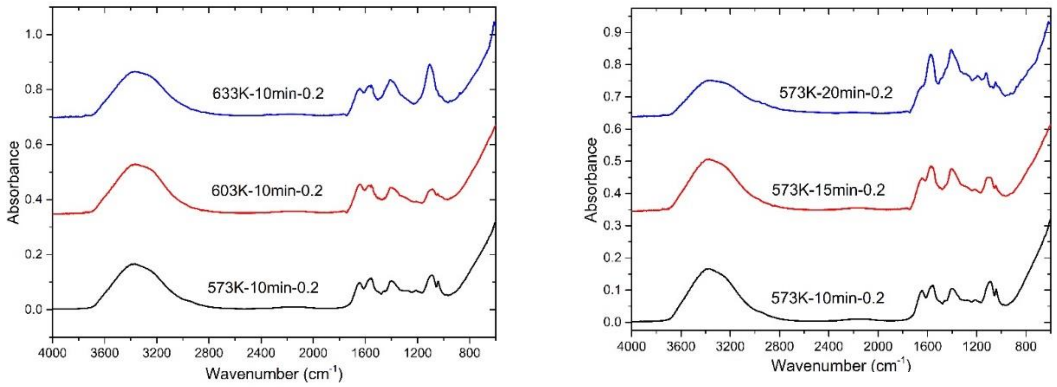

a) b)

Figure 60: FTIR spectra of bio-oils from (a) different temperatures with a 10 min residence time and 0.2 blending ratio (b) different residence times at 573 K and a blending ratio of 0.2.

As the operating temperature and residence time change, the variation of FTIR spectra intensity signified the diversity of different functional groups [32]. Figure 9(a) showed the normalized FTIR spectra of the bio-oil obtained with a residence time of 10 min and blending ratio 0.2 at different temperatures of 573 K, 603 K, and 633 K, where figure 9(b) showed the normalized FTIR

spectra of the bio-oils obtained at different residence times at 573 K and blending ratio of 0.2.

According to figure 9(a), when the operating temperature increases, the peak at band 1402cm^{-1} and 1083cm^{-1} peaks are improved significantly while the other peaks are kept constant. Therefore, the temperature increase has produced more compounds consisting of C-H bonds and probably the C-O bonds. Furthermore, also the temperature increase has affected in production of more alcohols and phenolic compounds. Nevertheless, residence time increase has shown even more significant impacts on the bio-oil components.

The reduction of the peak at 3380 cm^{-1} hinted at reducing compounds like water, fatty acid amides, phenols, and N-containing heterocyclic compounds. The main reason could be breaking the carbohydrates and the proteins available in the unreacted macroalgae (laminaria saccharina)[51]. The reduction of peak 1640cm^{-1} means the esters such as triglyceride are reacted, where the increase of residence time has supported the process. The consumption of C-O bonds available in the bio-oil is indicated by the peak's reductions at 1280cm^{-1} and 1030 cm^{-1}. The development of peaks at 1560cm^{-1} and 1395cm^{-1} explains the increase of C=O bonds and the $–CH_2$ and $-CH_3$ groups representing the long-chain aliphatic hydrocarbons. Therefore, the residence time has resulted in consuming C-O bonds while producing new C=O bonds.

According to the statistical analysis in section 3.3, the residence time did not impact the bio-oil yield significantly, while the temperature highly influenced the bio-oil yield. Nevertheless, under the FTIR analysis, both the operating temperature and residence time have played a significant role in shaping the chemical composition of the bio-oil yield.

Figure 10 below illustrates the variation of functional groups in the bio-oil with the feedstock's blending ratio.

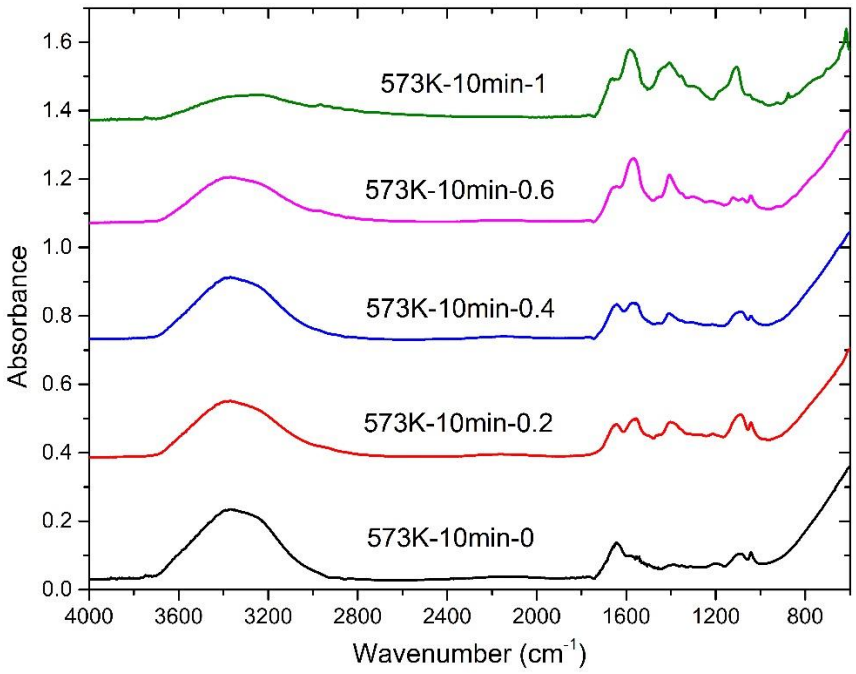

Figure 61: FTIR spectra of bio-oils from different blending ratios at 573K and with a 10 min residence time

In this study, when the blending ratio is zero, feedstock includes 100% lignin, whereas when the blending ratio is one, feedstock includes 100% laminaria saccharina. According to figure 10, when the blending ratio has increased, the peak at 3380 cm^{-1} shows a gradual decline, reducing water, fatty acid amides, phenols, and N-containing heterocyclic compounds from the system. Most importantly, the introduction of laminaria saccharina has dramatically improved the peak at 1560cm^{-1}, 1395$cm^{-1,}$ and 1050$cm^{-1,}$ which corresponds to the C=O bonds, C-H bonds, and the C-O bonds. This proves that the co-liquefaction of the feedstocks would produce more phenolic compounds, long-chain aliphatic hydrocarbons, carboxylic acids, ketones, aldehydes, and esters.

4. **Conclusions**

Co-liquefaction of lignin and laminaria saccharina is statistically studied using RSM for enriching the bio-oil yield while having a minimized char yield. In addition, the synergistic effect of co-liquefaction is investigated. The bio-oil yield and char yield of the liquefaction process are used as the responses to be optimized. The models used showed an excellent fit to the data, and it is

proved by lack of fit test 'F value' and 'p value' determination. The goodness of fit (R^2) values for both bio-oil and char yield regression models are highly significant, 0.985 and0.947, respectively.

After the statistical analysis, it was found out that the bio-oil yield mainly depends on the temperature and blending ratio. Residence time has shown less impact on bio-oil and char yields. A positive synergetic effect is observed in more harsh process conditions and laminaria saccharina rich environments. Furthermore, the co-liquefaction has shown a negative synergetic effect on the char yield. 573K, 20 min residence time, and 0.2 blending ratio proved the optimum process conditions. At the optimum point, the bio-oil yield of 0.2513 w/w_0 with a minimum char yield of 0.1791w/w_0 is produced. Corresponding to the FTIR results, temperature increase helped increase the alcohols and phenolic compounds production when longer residence times consume the C-O bonds more. Co-liquefaction of the feedstocks helped improve the bio-oil composition by helping produce more phenolic compounds, long-chain aliphatic hydrocarbons, carboxylic acids, ketones aldehydes, and esters. Finally, the co-liquefaction has produced bio-oil with a significantly lower N content than a bio-oil from laminara saccharina.

Acknowledgment

The authors would like to thank Mr. Harald Sveier of Lerøy ocean harvest for lending seaweed for the research, Dr. Odin Kvam, Mr. Steve Shading, and Mr. Johan Olav Brakestad from the University of Agder for their assistance in the laboratory. This study was conducted as part of the Ph.D. research at the Department of Engineering Sciences, funded by the Faculty of Engineering and Science, University of Agder.

References

[1] Durak H, Genel S. Catalytic hydrothermal liquefaction of lactuca scariola with a heterogeneous catalyst: The investigation of temperature, reaction time and synergistic effect of catalysts. Bioresour Technol 2020;309:123375. https://doi.org/10.1016/j.biortech.2020.123375.

[2] Çolak U, Durak H, Genel S. Hydrothermal liquefaction of Syrian mesquite (Prosopis farcta): Effects of operating parameters on product yields and characterization by different analysis methods. J Supercrit Fluids 2018;140:53–61. https://doi.org/10.1016/j.supflu.2018.05.027.

[3] Castello D, Pedersen TH, Rosendahl LA. Continuous Hydrothermal Liquefaction of Biomass: A Critical Review. Energies 2018;11:3165. https://doi.org/10.3390/en11113165.

[4] Elliott DC, Biller P, Ross AB, Schmidt AJ, Jones SB. Hydrothermal liquefaction of biomass: Developments from batch to continuous process. Bioresour Technol 2015;178:147–56. https://doi.org/10.1016/j.biortech.2014.09.132.

[5] Jayathilake M, Rudra S, Rosendahl LA. Numerical modeling and validation of hydrothermal liquefaction of a lignin particle for biocrude production. Fuel 2021;305:121498. https://doi.org/10.1016/j.fuel.2021.121498.

[6] Jasiūnas L, Pedersen TH, Toor SS, Rosendahl LA. Biocrude production via supercritical hydrothermal co-liquefaction of spent mushroom compost and aspen wood sawdust. Renew Energy 2017;111:392–8. https://doi.org/10.1016/j.renene.2017.04.019.

[7] Toor S, Rosendahl L, Rudolf A. Hydrothermal liquefaction of biomass: A review of subcritical water technologies. Energy 2011;36:2328–42. https://doi.org/10.1016/j.energy.2011.03.013.

[8] Arturi KR, Strandgaard M, Nielsen RP, Søgaard EG, Maschietti M. Hydrothermal liquefaction of lignin in near-critical water in a new batch reactor: Influence of phenol and temperature. J Supercrit Fluids 2017;123:28–39. https://doi.org/10.1016/j.supflu.2016.12.015.

[9] Sauer J, Dahmen N, Hornung U, Schuler J, Kruse A. Hydrothermal Liquefaction of Lignin. J Biomater Nanobiotechnology 2017;8:720–6. https://doi.org/10.4236/jbnb.2017.81007.

[10] Gollakota ARK, Kishore N, Gu S. A review on hydrothermal liquefaction of biomass. Renew Sustain Energy Rev 2018;81:1378–92. https://doi.org/10.1016/j.rser.2017.05.178.

[11] Brebu M, Vasile C. THERMAL DEGRADATION OF LIGNIN – A REVIEW. Cellul Chem Technol 2010;44:353–63.

[12] Stewart D. Lignin as a base material for materials applications: Chemistry, application and economics. Ind Crops Prod 2008;27:202–7. https://doi.org/10.1016/j.indcrop.2007.07.008.

[13] Thakur VK, Thakur MK, Raghavan P, Kessler MR. Progress in Green Polymer Composites from Lignin for Multifunctional Applications: A Review. ACS Sustain Chem Eng 2014;2:1072–92. https://doi.org/10.1021/sc500087z.

[14] Kadla JF, Kubo S, Venditti RA, Gilbert RD, Compere AL, Griffith W. Lignin-based carbon fibers for composite fiber applications. Carbon 2002;40:2913–20. https://doi.org/10.1016/S0008-6223(02)00248-8.

[15] Yong TL-K, Matsumura Y. Reaction Kinetics of the Lignin Conversion in Supercritical Water. Ind Eng Chem Res 2012;51:11975–88. https://doi.org/10.1021/ie300921d.

[16] Yong TL-K, Matsumura Y. Kinetic Analysis of Lignin Hydrothermal Conversion in Sub- and Supercritical Water. Ind Eng Chem Res 2013;52:5626–39. https://doi.org/10.1021/ie400600x.

[17] Breunig M, Gebhart P, Hornung U, Kruse A, Dinjus E. Direct liquefaction of lignin and lignin rich biomasses by heterogenic catalytic hydrogenolysis. Biomass Bioenergy 2018;111:352–60. https://doi.org/10.1016/j.biombioe.2017.06.001.

[18] Pińkowska H, Wolak P, Złocińska A. Hydrothermal decomposition of alkali lignin in sub- and supercritical water. Chem Eng J 2012;187:410–4. https://doi.org/10.1016/j.cej.2012.01.092.

[19] Fache M, Boutevin B, Caillol S. Vanillin Production from Lignin and Its Use as a Renewable Chemical. ACS Sustain Chem Eng 2016;4:35–46. https://doi.org/10.1021/acssuschemeng.5b01344.

[20] Lui MY, Chan B, Yuen AKL, Masters AF, Montoya A, Maschmeyer T. Unravelling Some of the Key Transformations in the Hydrothermal Liquefaction of Lignin. ChemSusChem 2017;10:2140–4. https://doi.org/10.1002/cssc.201700528.

[21] Kang S, Li X, Fan J, Chang J. Classified Separation of Lignin Hydrothermal Liquefied Products. Ind Eng Chem Res 2011;50:11288–96. https://doi.org/10.1021/ie2011356.

[22] Zhang B, Huang H-J, Ramaswamy S. Reaction kinetics of the hydrothermal treatment of lignin. Appl Biochem Biotechnol 2008;147:119–31. https://doi.org/10.1007/s12010-007-8070-6.

[23] Kang S, Li X, Fan J, Chang J. Hydrothermal conversion of lignin: A review. Renew Sustain Energy Rev 2013;27:546–58.

[24] Anastasakis K, Ross AB. Hydrothermal liquefaction of the brown macroalga Laminaria saccharina: effect of reaction conditions on product distribution and composition. Bioresour Technol 2011;102:4876–83. https://doi.org/10.1016/j.biortech.2011.01.031.

[25] Aresta M, Dibenedetto A, Barberio G. Utilization of macro-algae for enhanced CO2 fixation and biofuels production: Development of a computing software for an LCA study. Fuel Process Technol 2005;86:1679–93. https://doi.org/10.1016/j.fuproc.2005.01.016.

[26] Elliott DC, Hart TR, Neuenschwander GG, Rotness LJ, Roesijadi G, Zacher AH, et al. Hydrothermal Processing of Macroalgal Feedstocks in Continuous-Flow Reactors. ACS Sustain Chem Eng 2014;2:207–15. https://doi.org/10.1021/sc400251p.

[27] Parsa M, Jalilzadeh H, Pazoki M, Ghasemzadeh R, Abduli M. Hydrothermal liquefaction of Gracilaria gracilis and Cladophora glomerata macro-algae for biocrude production. Bioresour Technol 2018;250:26–34. https://doi.org/10.1016/j.biortech.2017.10.059.

[28] Rudra S, Jayathilake M. Hydrothermal Liquefaction of Biomass for Biofuel Production. Ref. Module Earth Syst. Environ. Sci., Elsevier; 2021. https://doi.org/10.1016/B978-0-12-819727-1.00043-1.

[29] López Barreiro D, Beck M, Hornung U, Ronsse F, Kruse A, Prins W. Suitability of hydrothermal liquefaction as a conversion route to produce biofuels from macroalgae. Algal Res 2015;11:234–41. https://doi.org/10.1016/j.algal.2015.06.023.

[30] Madsen RB, Jensen MM, Glasius M. Qualitative characterization of solid residue from hydrothermal liquefaction of biomass using thermochemolysis and stepwise pyrolysis-gas chromatography-mass spectrometry. Sustain Energy Fuels 2017;1:2110–9. https://doi.org/10.1039/C7SE00357A.

[31] He Z, Wang B, Zhang B, Feng H, Kandasamy S, Chen H. Synergistic effect of hydrothermal Co-liquefaction of Spirulina platensis and Lignin:

Optimization of operating parameters by response surface methodology. Energy 2020;201:117550. https://doi.org/10.1016/j.energy.2020.117550.

[32] Jayathilake M, Rudra S, Akhtar N, Christy AA. Characterization and Evaluation of Hydrothermal Liquefaction Char from Alkali Lignin in Subcritical Temperatures. Materials 2021;14:3024. https://doi.org/10.3390/ma14113024.

[33] Chen W, Shi S, Nguyen T, Chen M, Zhou X. Effect of Temperature on the Evolution of Physical Structure and Chemical Properties of Bio-char Derived from Co-pyrolysis of Lignin with High-Density Polyethylene. BioResources 2016;11:3923–36.

[34] Lu J, Liu Z, Zhang Y, Savage PE. Synergistic and Antagonistic Interactions during Hydrothermal Liquefaction of Soybean Oil, Soy Protein, Cellulose, Xylose, and Lignin. ACS Sustain Chem Eng 2018;6:14501–9. https://doi.org/10.1021/acssuschemeng.8b03156.

[35] Feng H, He Z, Zhang B, Chen H, Wang Q, Kandasamy S. Synergistic bio-oil production from hydrothermal co-liquefaction of Spirulina platensis and α-Cellulose. Energy 2019;174:1283–91. https://doi.org/10.1016/j.energy.2019.02.079.

[36] Riva L, Nielsen HK, Skreiberg Ø, Wang L, Bartocci P, Barbanera M, et al. Analysis of optimal temperature, pressure and binder quantity for the production of biocarbon pellet to be used as a substitute for coke. Appl Energy 2019;256:113933. https://doi.org/10.1016/j.apenergy.2019.113933.

[37] Liu J, Chen P, Yao W, Wang J, Wang L, Deng L, et al. Subcritical water extraction of betulinic acid from birch bark. Ind Crops Prod 2015;74:557–65. https://doi.org/10.1016/j.indcrop.2015.05.064.

[38] Ferreira SLC, Bruns RE, Ferreira HS, Matos GD, David JM, Brandão GC, et al. Box-Behnken design: An alternative for the optimization of analytical methods. Anal Chim Acta 2007;597:179–86. https://doi.org/10.1016/j.aca.2007.07.011.

[39] Scott I, Mazhindu D. Statistics for Health Care Professionals. 1 Oliver's Yard, 55 City Road, London England EC1Y 1SP United Kingdom: SAGE Publications, Ltd; 2005. https://doi.org/10.4135/9781849209960.

[40] Nasouri K, Bahrambeygi H, Rabbi A, Shoushtari AM, Kaflou A. Modeling and optimization of electrospun PAN nanofiber diameter using re-

sponse surface methodology and artificial neural networks. J Appl Polym Sci 2012;126:127–35. https://doi.org/10.1002/app.36726.

[41] Amen-Chen C, Pakdel H, Roy C. Separation of phenols from Eucalyptus wood tar. Biomass Bioenergy 1997;13:25–37. https://doi.org/10.1016/S0961-9534(97)00021-4.

[42] Jayathilake M, Rudra S, Rosendahl LA. Hydrothermal liquefaction of wood using a modified multistage shrinking-core model. Fuel 2020;280:118616. https://doi.org/10.1016/j.fuel.2020.118616.

[43] Minowa T, Sawayama S. A novel microalgal system for energy production with nitrogen cycling. Fuel 1999;78:1213–5. https://doi.org/10.1016/S0016-2361(99)00047-2.

[44] Zhou D, Zhang S, Fu H, Chen J. Liquefaction of Macroalgae Enteromorpha prolifera in Sub-/Supercritical Alcohols: Direct Production of Ester Compounds. Energy Fuels 2012;26:2342–51. https://doi.org/10.1021/ef201966w.

[45] Derringer G, Suich R. Simultaneous optimization of several response variables. J Qual Technol 1980;12:214–9.

[46] Kim K-J, Lin DKJ. Simultaneous optimization of mechanical properties of steel by maximizing exponential desirability functions. J R Stat Soc Ser C Appl Stat 2000;49:311–25. https://doi.org/10.1111/1467-9876.00194.

[47] Yang J, He Q (Sophia), Niu H, Corscadden K, Astatkie T. Hydrothermal liquefaction of biomass model components for product yield prediction and reaction pathways exploration. Appl Energy 2018;228:1618–28. https://doi.org/10.1016/j.apenergy.2018.06.142.

[48] Yang J, He Q (Sophia), Corscadden K, Niu H, Lin J, Astatkie T. Advanced models for the prediction of product yield in hydrothermal liquefaction via a mixture design of biomass model components coupled with process variables. Appl Energy 2019;233–234:906–15. https://doi.org/10.1016/j.apenergy.2018.10.035.

[49] Biller P, Ross AB, Skill SC, Lea-Langton A, Balasundaram B, Hall C, et al. Nutrient recycling of aqueous phase for microalgae cultivation from the hydrothermal liquefaction process. Algal Res 2012;1:70–6. https://doi.org/10.1016/j.algal.2012.02.002.

[50] Mishra S, Mohanty K. Co-HTL of domestic sewage sludge and wastewater treatment derived microalgal biomass – An integrated biorefinery approach for sustainable biocrude production. Energy Convers Manag 2020;204:112312. https://doi.org/10.1016/j.enconman.2019.112312.

[51] Jin B, Duan P, Xu Y, Wang F, Fan Y. Co-liquefaction of micro- and macroalgae in subcritical water. Bioresour Technol 2013;149:103–10. https://doi.org/10.1016/j.biortech.2013.09.045.

[52] Li R, Ma Z, Yang T, Li B, Wei L, Sun Y. Sub–supercritical liquefaction of municipal wet sewage sludge to produce bio-oil: Effect of different organic–water mixed solvents. J Supercrit Fluids 2018;138:115–23. https://doi.org/10.1016/j.supflu.2018.04.011.

[53] Zhang B, Feng H, He Z, Wang S, Chen H. Bio-oil production from hydrothermal liquefaction of ultrasonic pre-treated Spirulina platensis. Energy Convers Manag 2018;159:204–12. https://doi.org/10.1016/j.enconman.2017.12.100.

Co-liquefaction of lignin and laminaria saccharina on optimization of bio-oil yield

Supplementary document

Figure 1(a) and figure1(b) show the normalized FTIR spectra of the bio-oil obtained with a residence time of 10 min and blending ratio 0.4
and 0.6 respectively at different temperatures of 573 K, 603 K, and 633 K

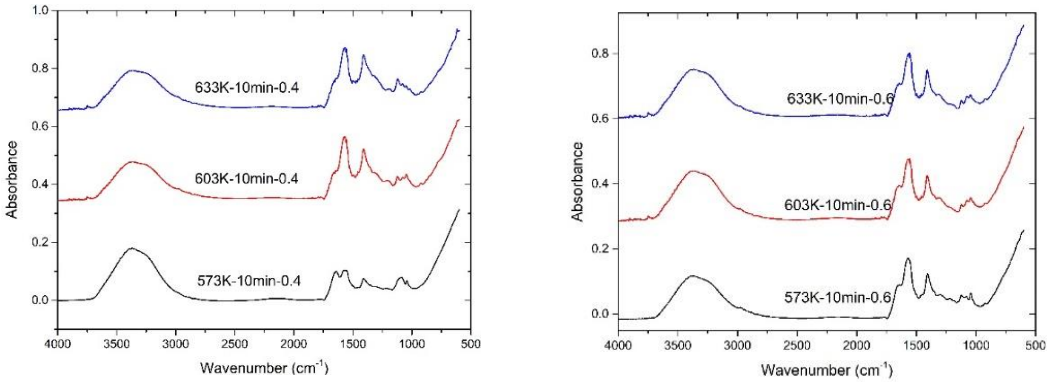

a) **b)**

Figure 62: FTIR spectra of bio-oils from (a) different temperatures with a 10 min residence time and with a) 0.4 blending ratio (b) 0.6blending ratio

Figure 2 and figure 3 below illustrates the variation of functional groups in the bio-oil with the variation of the blending ratio of the feedstock at 603K and 633K respectively

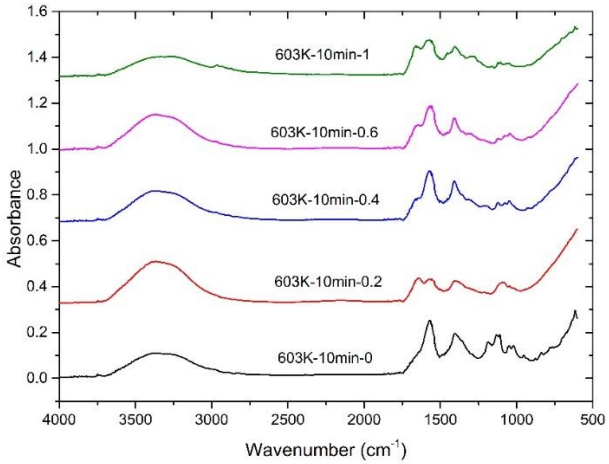

Figure 63:FTIR spectra of bio-oils from different blending ratios at 603K and with a 10 min residence time

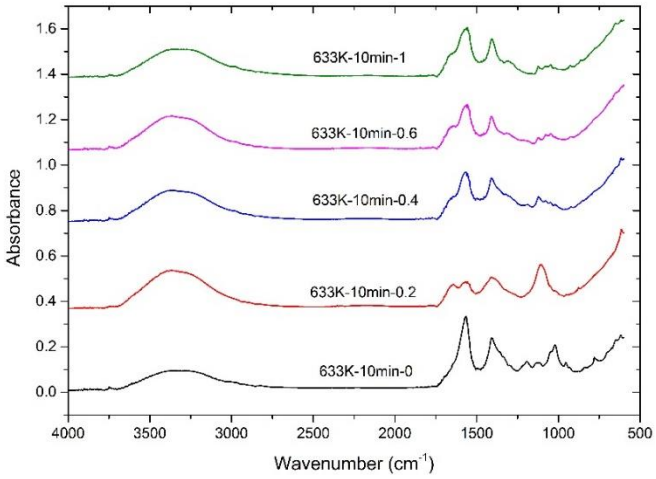

Figure 64:FTIR spectra of bio-oils from different blending ratios at 633K and with a 10 min residence time